

JSCSEN 77(5)569–715(2012)

ISSN 1820-7421 (Online)

Journal of the Serbian Chemical Society

ersion
lectronic

Society
115th
Anniversary
1897 - 2012

VOLUME 77

No 5

BELGRADE 2012

Available on line at



www.shd.org.rs/JSCS/

The full search of JSCS
is available through

DOAJ DIRECTORY OF
OPEN ACCESS
JOURNALS
www.doaj.org

Штампање ове свеске је суфинансирао ЛУКОИЛ Србија АД



Publication of this issue is financially co-supported by LUKOIL Srbija AD





CONTENTS

Organic Chemistry

- S. Ž. Drmanić, J. B. Nikolić and B. Ž. Jovanović: Effects of solvent and structure on the reactivity of 2-substituted nicotinic acids with diazodiphenylmethane in aprotic solvents..... 569
- H. Liu, X. Lv, L. Zhou, R. Yin and X. Wang: Preparation of 2-heteroatom substituted-4-oxo-4-arylbutanoates via thio- and aza-Michael addition..... 581
- M. Malhotra, M. Arora, A. Samad, K. Sahu, P. Phogat and A. Deep: Synthesis and evaluation of some novel derivatives of 2-propoxybenzylideneisonicotinohydrazide for their potential antimicrobial activity..... 589
- P. Samadhiya, R. Sharma, S. K. Srivastava and S. D. Srivastava: Synthesis of 2-oxo-azetidine derivatives of 2-aminothiazole and their biological activity..... 599

Biochemistry and Biotechnology

- G. Miljuš, M. Petrović and O. Nedić: Isolation of complexes formed between insulin-like growth factor-binding protein-3 and transferrin from human serum..... 607
- D. Gođevac, Lj. Vujisić, I. Vučković, Vl. Vajs, M. Soković, P. D. Marin and V. Tešević: Composition and antimicrobial activity of the essential oil from *Galatella linosyris* (L.) Rchb. f. (Asteraceae)..... 619

Inorganic Chemistry

- N. Pal Singh and A. Srivastava: Physico-chemical and biological studies of Cu(II), Co(II) and Ni(II) complexes of an N₄ coordinating ligand derived from the Schiff base of diacetyl with ethylenediamine and benzoic acid..... 627

Theoretical Chemistry

- M. Adimi, M. Salimi, M. Nekoei, E. Pourbasheer and A. Beheshti: A quantitative structure–activity relationship study on histamine receptor antagonists using the genetic algorithm–multi-parameter linear regression method..... 639

Electrochemistry

- G. Orhan and G. G. Gezgin: Effect of electrolysis parameters on the morphologies of copper powders obtained at high current densities..... 651

Analytical Chemistry

- R. Pavlović, P. A. Biondi, L. M. Chiesa, N. Trutić, M. Abramović and E. Santaniello: Different behaviour of 3-nitrotyrosine and tyrosine toward perfluorinated reagents suitable for the one-step preparation of volatile derivatives..... 667

Polymers

- B. Tamami, R. Heiran and E. R. Montazer: Modified polyacrylamide-supported chlorochromate as a new polymeric oxidizing agent..... 685

Materials

- M. B. Radoičić, Z. V. Šaponjić, M. T. Marinović-Cincović, S. P. Ahrenkiel, N. M. Bibić and J. M. Nedeljković: The influence of shaped TiO₂ nanofillers on the thermal properties of poly(vinyl alcohol)..... 699
- Errata..... 715

Published by the Serbian Chemical Society
Karnegijeva 4/III, 11000 Belgrade, Serbia
Printed by the Faculty of Technology and Metallurgy
Karnegijeva 4, P.O. Box 35-03, 11120 Belgrade, Serbia



J. Serb. Chem. Soc. 77 (5) 569–579 (2012)
JSCS–4290

Effects of solvent and structure on the reactivity of 2-substituted nicotinic acids with diazodiphenylmethane in aprotic solvents

SAŠA Ž. DRMANIĆ^{1*#}, JASMINA B. NIKOLIĆ^{1#} and BRATISLAV Ž. JOVANOVIĆ^{2#}

¹Department of Organic Chemistry, Faculty of Technology and Metallurgy, University of Belgrade, Karnegijeva 4, P. O. Box 3503, 11121 Belgrade, Serbia and ²Institute of Chemistry, Technology and Metallurgy, University of Belgrade, Njegoševa 12, Belgrade, Serbia

(Received 23 February, revised 5 March 2012)

Abstract: The rate constants for the reactions of diazodiphenylmethane (DDM) with 2-substituted nicotinic acids in nine aprotic solvents at 30 °C were determined. The obtained second order rate constants in aprotic solvents were correlated using the Kamlet–Taft solvatochromic equation in the complete form: $\log k = \log k_0 + s\pi^* + a\alpha + b\beta$. The correlations of the kinetic data were realized by means of multiple linear regression analysis. The obtained results were analyzed in terms of the initial and the transition state of the reaction and compared with previously determined kinetic data for nicotinic acid. The signs of the equation coefficients (*s*, *a* and *b*) are in agreement with the reaction mechanism and the influence of the solvent on the reaction rate is discussed based on the correlation results. The mode of the transmission of the substituent effect is discussed in light of the contribution of solute–solvent interaction to the reactivity of the acid. The substituent effect was additionally analyzed by the Hammett equation, $\log k = \rho\sigma + \log k_0$.

Keywords: pyridinecarboxylic acids; diazodiphenylmethane; reaction rate constants; solvatochromic parameters; aprotic solvents.

INTRODUCTION

The relationship between the structure of carboxylic acids and their reactivity with diazodiphenylmethane (DDM) has been studied by many authors, with particular regard to the influence of the solvent.^{1–5} Related to previous studies^{6–10} of the chemical behavior of pyridinecarboxylic acid, the reactivity of 2-substituted nicotinic acids with the following substituents Cl (chloro), OH (hydroxy), CH₃ (methyl), Br (bromo) and SH (mercapto) was studied in its reaction

* Corresponding author. E-mail: drmana@tmf.bg.ac.rs

Serbian Chemical Society member.

doi: 10.2298/JSC120223019D

with DDM. The kinetics of the reaction of these carboxylic acids with DDM was investigated in a series of aprotic solvents.

Kamlet *et al.*³ established that the effect of a solvent on the reaction rate should be given in terms of the following properties: *i*) the behavior of a solvent as a dielectric facilitating the separation of opposite charges in the transition state, *ii*) the ability of a solvent to donate a proton in a solvent-to-solute hydrogen bond and thus stabilize the carboxylate anion in the transition state and *iii*) the ability of a solvent to donate an electron pair and therefore to stabilize the initial carboxylic acid, through a hydrogen bond between the carboxylic proton and the solvent electron pair. These properties are connected through Eq. (1):

$$\log k = A_0 + s\pi^* + a\alpha + b\beta \quad (1)$$

The parameter π^* is an appropriate measure of the first property, while the second and the third properties are governed by the effects of the solvent acidity and basicity, quantitatively expressed by the parameters α and β , respectively. The linear solvation energy relationship (LSER) of the solvent parameters is used to correlate and predict a wide variety of solvent effects, as well as to provide an analysis in terms of knowledge and theoretical concepts of molecular structural effects.³ Such a correlation indicates the existence of both specific and non-specific solute-solvent interactions in the studied reaction.

The reactivity of the investigated acids with DDM in relationship to the electronic substituent effects was also studied using the Hammett equation (linear free energy relationship – LFER) of the type:

$$\log k = \rho\sigma + \log k_0 \quad (2)$$

where ρ is a reaction constant reflecting the sensitivity of the rate constant to the substituent effect, and σ is the substituent constant, a measure of the electronic effect of a substituent. The analysis of the contribution of electronic substituent effects showed that these effects have a definite influence on the reactivity of the investigated acids.

EXPERIMENTAL

Materials

The acids were commercial samples of *p.a.* quality, used without further purification. Diazodiphenylmethane was prepared by the Smith and Howard method.¹¹ A stock solution of 0.06 mol dm⁻³ was stored in a refrigerator and diluted before use. The solvents were purified as described in the literature.¹² All the solvents used for the kinetic studies were examined by GC and no impurities were detected.

Kinetic measurements

The rate constants, k , for the reactions of the investigated acids with DDM were determined as reported previously by the spectroscopic method of Roberts and co-workers¹³ using a Shimadzu 1700A spectrophotometer. The optical density measurements were performed at 525 nm with 1.0 cm cells at 30±0.05 °C. Three to five measurements were made

with each acid and in every case, the individual second-order rate constants agreed within 3 % of the mean.

RESULTS AND DISCUSSION

The mechanism of the reaction between carboxylic acids and DDM, in both protic and aprotic solvents is known to involve the rate-determining proton transfer from the acids to DDM, and the formation of a diphenylmethanediazonium carboxylate ion-pair (Fig. 1).^{14–21} Chapman *et al.*²² established that the solvent effects are best interpreted in the form of the contributions of the initial and transition state to specific (α and β) and non-specific (π^*) solvent–solute interactions (Fig. 1).

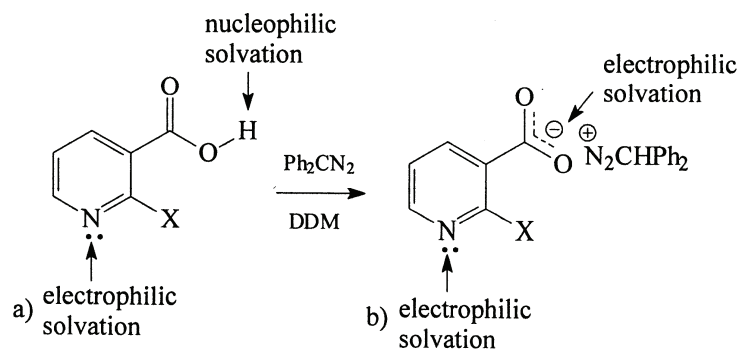


Fig. 1. The mode of the solvent effects in 2-substituted nicotinic acids in a) the initial state and b) the transition state.

The reaction rate constants (as $\log k$) for the reaction of the examined acids with DDM in the applied solvent set are given in Table I.

TABLE I. Logarithm of the second order rate constants ($k / \text{dm}^3 \text{mol}^{-1} \text{min}^{-1}$) for the reaction of 2-substituted nicotinic acids with DDM at 30 °C in aprotic solvents

Solvent/substituent	H ¹⁰	2-Cl	2-OH	2-CH ₃	2-Br	2-SH
Dimethyl sulfoxide	-0.678	0.005	-0.030	-0.611	0.006	-0.044
<i>N,N</i> -Dimethylacetamide	-0.940	-0.259	-0.201	-0.851	-0.240	-0.131
<i>N</i> -Methylpyrrolidone	-0.921	-0.131	0.139	-0.796	-0.138	-0.121
<i>N,N</i> -Dimethylformamide	-0.611	-0.014	0.171	-0.480	-0.016	0.196
<i>N</i> -Methylformamide	-0.027	0.103	-0.354	0.242	0.111	0.378
Acetophenone	0.714	1.343	- ^a	0.751	1.373	1.231
Acetone	0.190	0.451	-	0.524	0.506	0.719
Ethyl benzoate	0.528	1.088	-	0.860	1.082	0.895
Isobutyl methyl ketone	0.143	0.606	-	0.313	0.651	0.751

^aInsoluble

The results from Table I show that the influence of a solvent on the reactivity is rather complex, due to the many types of solvent to solute interactions: dipolarity/polarizability, π^* , proton-donor, α (HBD), and proton-acceptor, β (HBA), effects. Considering the reaction mechanism, it is obvious that polar solvents accelerate the reaction by stabilizing the ion-pair in the transition state. However, their other properties have to be taken into consideration. Solvents of high polarity and of high HBA capability cause a significant decrease in the reaction rate by stabilizing the carboxylic hydrogen in the ground state before commencement of the reaction. For example, the reaction rate constant in dimethyl sulfoxide was lower than in acetophenone – both solvents are of similar polarity, 1.00 and 0.90, respectively, but dimethyl sulfoxide has a higher proton-acceptor ability (0.75) than acetophenone (0.49), and hence the reaction was slower in dimethyl sulfoxide.

Generally, the results of the kinetic studies show that reactions of all acids with DDM are of second order, which was confirmed by the high correlation coefficients, R , which were in the range 0.938–0.990. The exception was 2-hydroxynicotinic acid, which was, because the R -value was only 0.817, excluded from the calculation.

Solvent–reactivity relationship

In order to explain the obtained kinetic results based on the polarity, acidity and basicity of the solvent, the $\log k$ values were correlated with the solvatochromic parameters π^* , α and β using the solvatochromic Eq. (1). The correlation of the kinetic data was realized by means of multiple regression analysis, which was very useful in separating and quantifying the solvent effect on the examined reaction.

The correlation results are presented in the following equations.

Nicotinic acid:

$$\log k = 0.82 + (2.45 \pm 0.85)\pi^* + (1.72 \pm 0.32)\alpha - (5.18 \pm 0.63)\beta$$

$$R = 0.977, s = 0.17, n = 9$$

2-Chloronicotinic acid:

$$\log k = 0.70 + (3.12 \pm 1.23)\pi^* + (0.78 \pm 0.46)\alpha - (4.90 \pm 0.91)\beta$$

$$R = 0.938, s = 0.25, n = 9$$

2-Methylnicotinic acid:

$$\log k = 1.50 + (1.91 \pm 0.60)\pi^* + (1.99 \pm 0.22)\alpha - (5.30 \pm 0.44)\beta$$

$$R = 0.990, s = 0.12, n = 9$$

2-Bromonicotinic acid:

$$\log k = 0.81 + (3.03 \pm 1.21)\pi^* + (0.80 \pm 0.45)\alpha - (4.93 \pm 0.89)\beta$$

$$R = 0.942, s = 0.24, n = 9$$

2-Mercaptonicotinic acid:

$$\log k = 1.31 + (1.79 \pm 0.92)\pi^* + (1.03 \pm 0.35)\alpha - (3.99 \pm 0.68)\beta$$

$$R = 0.955, s = 0.18, n = 9$$

The values for π^* , α and β (Table II) were taken from the literature.²³ Here, the correlation results for nicotinic acid are also given for comparison.

TABLE II. Solvent parameters

Solvent	π^*	α	β
Dimethyl sulfoxide	1.00	0.00	0.75
<i>N,N</i> -Dimethylacetamide	0.88	0.00	0.76
<i>N</i> -Methylpyrrolidone	0.92	0.00	0.77
<i>N,N</i> -Dimethylformamide	0.88	0.00	0.69
<i>N</i> -Methylformamide	0.90	0.62	0.80
Acetophenone	0.90	0.04	0.49
Acetone	0.71	0.08	0.43
Ethyl benzoate	0.74	0.00	0.41
Isobutyl methyl ketone	0.65	0.02	0.48

The correlation equations obtained for all the examined acids confirmed the reaction mechanism described above, as the solvent polarity and its proton-donor (HBD) activity increase the reaction rate constant, and the proton-acceptor (HBA) ability decreases it. It could be noticed that the HBA effect is the most prominent effect in this solvent set.

From the values of regression coefficients (s , a and b), the contribution of each parameter to the reactivity of the investigated compounds on a percentage basis was calculated and the results are listed in Table III.

TABLE III. Percentage contribution of the Kamlet–Taft solvatochromic parameters for the reactivity of the investigated acids in aprotic solvents

Acid	$P_{\pi^*} / \%$	$P_{\alpha} / \%$	$P_{\beta} / \%$
H	26	18	56
2-Cl	35	9	56
2-CH ₃	22	20	58
2-Br	35	9	56
2-SH	26	15	59

It could be noticed that in the case of the electron withdrawing substituents, the values for the HBD parameter (α) were lower than for the unsubstituted acid and for the acid with the electron-donor substituent (CH₃). The negative inductive effect of the electron-acceptor substituents additionally stabilizes the carboxylic anion and hence, the HBD solvent effect is less involved.

The results from Table III, lead to the following conclusions:

a) The rate of the reaction is mostly influenced by the rate-decreasing HBA parameter, as its percentage prevails over the other two rate-increasing parameters.

b) The non-specific interaction have higher influence (higher percentage value) than HBA on the reaction rate in all cases, meaning that the classical or non-specific solute–solvent interactions dominate in the transition state and increase the reaction rate.

When the obtained correlation results were compared with the previously published results for the corresponding 6-substituted nicotinic acids,¹⁰ it was found that the solvent effect disposition was similar considering the dominant HBA effect. However, the percentage values for the non-specific and the HBD interactions were different, as the proton-donor ability had a larger influence on the 6-substituted acids. This can be explained by the strong negative inductive effect of the majority of substituents, which is considerably stronger in the C-2 position, as it is next to the reactive center, than in C-6 position of the ring, with three atoms separating them. Comparing the reaction rate constants for both types of nicotinic acid, it can be noticed that the 2-substituted acids generally react faster, due to the additional stabilization of the anion in the transition state by the negative inductive substituent effect. The fact that the only examined acid with an electron-donor substituent, the methyl group, also reacts faster when it is in the 2-position can be explained by the steric effect of the substituent which twists the carboxylic group out of the plane of the ring and makes it more approachable for the other reactant, the DDM molecule. The higher value of the HBD coefficient (α) shows that electron-donor support from the solvent is necessary to a larger extent in this case, as there is no negative inductive substituent effect to stabilize the transition state. The inductive effect of the substituents in C-2 position, which is in fact based on their electronegativity, is additionally proved by HBD coefficient value for the 2-mercaptonicotinic acid: sulfur is less electronegative than chlorine or bromine, and this compound has a higher α coefficient than the other two acids, but somewhat lower than the unsubstituted and the methyl-substituted acid.

The outlier found in 2-hydroxynicotinic acid with its earlier mentioned unsuccessful correlation also draws attention. 6-Hydroxynicotinic acid, unlike 2-hydroxynicotinic acid, gave a successful correlation in the same solvents, with the expected signs of the arithmetic coefficients.

6-Hydroxynicotinic acid:¹⁰

$$\log k = -1.92 + (2.37 \pm 0.36)\pi^* + (1.99 \pm 0.09)\alpha - (2.20 \pm 0.51)\beta$$

$$R = 0.982, s = 0.26, n = 5$$

Due to the ability of forming strong hydrogen bonds between oxygen and hydrogen of both the carboxylic and the hydroxyl group, both compounds are

insoluble in many solvents; however, a set of five solvents in which both dissolved was found, and this set of solvents was used in this study.

The exception of the unsuccessful correlation for the 2-hydroxynicotinic acid could be explained by its specific structure. As can be seen in Fig. 2, this compound forms a strong intramolecular hydrogen bond, enhanced by the positive resonance effect of the hydroxyl group, which significantly decreases its reactivity in the anionic form. When the carboxylic proton leaves the molecule, the strong hydrogen bond is formed between the carboxylic group and the hydroxylic proton, preventing the anion from further reacting.

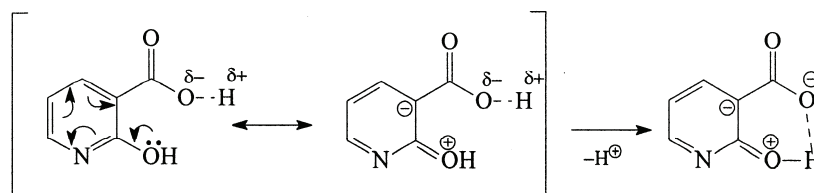


Fig. 2. The resonance effect of a hydroxyl group as substituent at C-2 and the formation of an intramolecular hydrogen bond.

Contrary to this, in case of 6-OH-nicotinic acid, there is a possibility of forming intermolecular hydrogen bonds (Fig. 3) which, as can be concluded from the successful Kamlet-Taft equation, do not interfere significantly with its reactivity in the examined reaction.

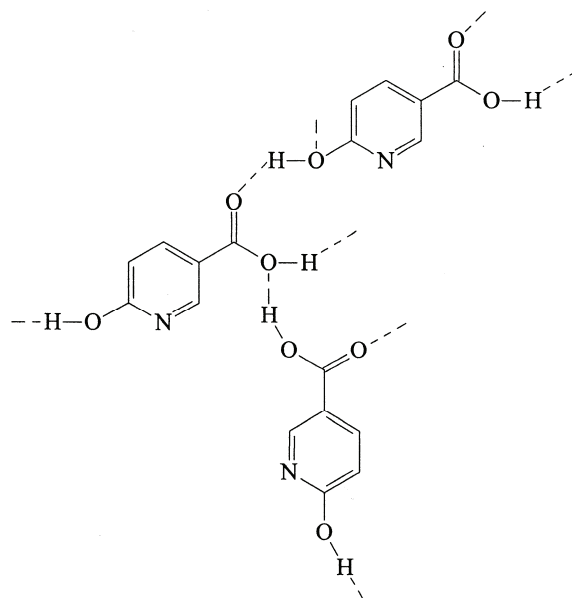


Fig. 3. Intermolecular hydrogen bonds of 6-hydroxynicotinic acid.

It could be concluded that, due to the complex possibilities of the formation of intramolecular hydrogen bonds, 2-hydroxynicotinic acid is not an appropriate compound for the investigation of the reaction mechanism of carboxylic acids with DDM and the effect of the solvent on it; neither can it be analyzed by the Kamlet–Taft equation.

None of the other examined 2-substituted nicotinic acids possesses the ability to form such an intramolecular hydrogen bond, except 2-mercaptopyridonic acid. However, it is obvious that in this case, the strength of the hydrogen bond was not sufficient to influence the reactivity of the compound as it behaved similarly to the other examined compounds in their reaction with DDM.

Structure–reactivity relationship

The relationship between the molecular structure and chemical reactivity gives additional insight into the electronic effect of substituents and the influence of solvent on the electronic distribution in the initial and transition states. Here, the most successful correlations obtained using the Hammett Equation (2) are given:

Dimethyl sulfoxide:

$$\log k = -0.33 + (1.57 \pm 0.13)\sigma_p$$
$$R = 0.992, s = 0.04, n = 4$$

N,N-Dimethylacetamide:

$$\log k = -0.54 + (1.59 \pm 0.44)\sigma_p$$
$$R = 0.931, s = 0.14, n = 4$$

N-Methylpyrrolidone:

$$\log k = -0.48 + (1.71 \pm 0.27)\sigma_p$$
$$R = 0.976, s = 0.09, n = 4$$

Acetophenone:

$$\log k = 1.00 + (1.51 \pm 0.05)\sigma_p$$
$$R = 0.999, s = 0.015, n = 4$$

The values for the σ_p constant were taken from the literature.²⁴

2-Hydroxynicotinic and nicotinic acid had to be excluded from the calculations in order to obtain a successful correlation. From the values of the obtained reaction constants, it could be concluded that the reaction is significantly susceptible to substituent effects. Furthermore, the positive reaction constant confirms that a negative charge is formed during the reaction. All four solvents are of similar properties, high polarity/polarizability and HBA ability and, as could be expected, the examined compounds behaved similarly in them, judging by the similar values of the reaction constants. The high sensitivity of the reaction constant to solvent effects in aprotic dipolar solvents may be explained by the

fact that at high relative permittivity of the surrounding solvent molecules, the energy necessary to bring about charge separation in the transition state is relatively small, which causes higher susceptibility to the electronic substituent effect.

CONCLUSIONS

The overall solvent effects on the reactivity of carboxylic acids in their reaction with DDM are complicate because of intertwined interactions between the solvent, and the reacting acid molecules. The results of the present investigation show that these solvent effects could be generally quantified by use of the Kamlet–Taft equation in the case of 2-substituted nicotinic acids. The quantitative separation of these effects into individual contributions in the initial and transition states showed the domination of the proton acceptor solvent effect. The low contribution of the proton donor solvent effect in the case of acids with electron-acceptor substituents can be explained by the negative inductive effects of these substituents, which draw the excess negative charge in the transition state and make the carboxylic anion more stable. The exception of the failed correlation for 2-hydroxynicotinic can be explained by the existence of the strong intramolecular hydrogen bond that this compound can form. In addition, the higher reaction rates for the 2-substituted nicotinic acids than for the previously investigated 6-substituted nicotinic acids confirm the electronic substituent influence, which is much more prominent in the C-2 position. In the case of 2-methylnicotinic acid, the positive inductive effect of the methyl group decreases the reaction rate, which is contrary to the steric effect. Actually, the steric effect twists the carboxylic group out and facilitates the approach of a DDM molecule, the consequence of which is an increase of the reaction rate.

Additional insight into the electronic effect of the substituents was given by the use of the Hammett equation, which showed that examined compounds behave similarly in solvents of similar properties, judging by the similar values of the reaction constants.

Considering the values of the reaction constants, it could be noticed that the negative charge increased in the transition state, which also confirms the discussed mechanism of the examined reaction. Furthermore, the same values indicate that the reaction is also considerably susceptible to the effects of substituents.

Acknowledgements. The authors are grateful to the Ministry of Education and Science of the Republic of Serbia for financial support (Project No. 172013).

ИЗВОД

ЕФЕКТИ СТРУКТУРЕ И РАСТВОРАЧА НА РЕАКТИВНОСТ 2-СУСПИТУИСАНИХ НИКОТИНСКИХ КИСЕЛИНА СА ДИАЗОДИФЕНИЛМЕТАНОМ У АПРОТИЧНИМ РАСТВОРАЧИМА

САША Ж. ДРМАНИЋ¹, ЈАСМИНА Б. НИКОЛИЋ¹ и БРАТИСЛАВ Ж. ЈОВАНОВИЋ²¹Каџедра за орџанску хемију, Технолошко–металурџиџи факултетџи, Универзитетџи у Беоџраду, џ. џр. 3503, Карнеџијева 4, 11120 Беоџрад и ²Институтџи за хемију, технологију и металурџију, Универзитетџи у Беоџраду, Њеџошева 12, Беоџрад

Константе брзине за реакцију диазодифенилметана (DDM) са 2-супституисаним никотинским киселинама у девет аprotичних растварача су одређене на 30 °C. Добијене константе брзине за реакцију другог реда су корелисане Камлет–Тафтовом тоталном солватохромном једначином у облику: $\log k = \log k_0 + s\pi^* + a\alpha + b\beta$. Корелација кинетичких података извршена је вишеструком линеарном регресионом анализом. Добијени резултати су анализирани у односу на основно и прелазно стање и упоређени са раније одређеним вредностима за несупституисану киселину. Знаци испред коефицијената у једначини су у складу са претпостављеним механизмом реакције. Дискутован је пренос ефеката супституената на реакциони центар узимајући у обзир допринос ефеката растварача на реактивност испитиваних једињења. Ефекат супституената је додатно анализиран Хаметовом једначином: $\log k = \rho\sigma + \log k_0$.

(Примљено 23. фебруара, ревидирано 5. марта 2012)

REFERENCES

1. M. H. Aslam, A. G. Burden, N. B. Chapman, J. Shorter, *J. Chem. Soc. Perkin Trans. 2* (1981) 500
2. N. B. Chapman, D. J. Newman, J. Shorter, *J. Chem. Soc., B* (1976) 847
3. M. Kamlet, J. Abboud, R. W. Taft, in *Progress in Physical Organic Chemistry*, Vol. 13, S. G. Kohen, A. Streitwieser, R. W. Taft, Eds., Wiley, New York, 1981, p. 485
4. D. Mather, J. Shorter, *J. Chem. Soc. Perkin Trans. 2* (1983) 1179
5. N. B. Chapman, J. R. Lee, J. Shorter, *J. Chem. Soc., B* (1969) 769
6. B. Jovanović, S. Drmanić, M. Mišić-Vuković, *J. Chem. Res.* (1998) 2581 (M); 554 (S)
7. S. Drmanić, B. Jovanović, M. Mišić-Vuković, *J. Serb. Chem. Soc.* **65** (2000) 481
8. A. Marinković, S. Drmanić, B. Jovanović, M. M. Mišić-Vuković, *J. Serb. Chem. Soc.* (2005) 557
9. S. Drmanić, B. Jovanović, A. Marinković, M. Mišić-Vuković, *J. Serb. Chem. Soc.* **68** (2003) 515
10. S. Drmanić, A. Marinković, B. Jovanović, *J. Serb. Chem. Soc.* **74** (2009) 1359
11. L. I. Smith, K. L. Howard, *Org. Synth. Coll.* **3** (1955) 351
12. W. L. F. Armarego, C. L. L. Chai, *Purification of laboratory chemicals*, Elsevier Science, Burlington, USA, 2003
13. J. D. Roberts, E. A. McElhill, R. Armstrong, *J. Am. Chem. Soc.* **71** (1949) 2923
14. A. Buckley, N. B. Chapman, M. R. J. Dack, J. Shorter, H. M. Wall, *J. Chem. Soc., B* (1968) 631
15. B. Ž. Jovanović, A. D. Marinković, Ž. Vitnik, I. O. Juranić, *J. Serb. Chem. Soc.* **72** (2007) 1191
16. J. B. Nikolić, G. S. Ušćumlić, *J. Serb. Chem. Soc.* **72** (2007) 1217
17. A. Buckley, N. B. Chapman, J. Shorter, *J. Chem. Soc., B* (1969) 195

18. N. B. Chapman, M. R. J. Dack, D. J. Newman, J. Shorter, R. Wilkinson, *J. Chem. Soc. Perkin Trans. 2* (1974) 962
19. K. Bowden, A. Buckley, N. B. Chapman, J. Shorter, *J. Chem. Soc.* (1964) 3380
20. R. A. More O'Ferrall, W. K. Kwok, S. I. Miller, *J. Am. Chem. Soc.* **86** (1964) 5553
21. B. Jovanović, I. Juranić, M. Mišić-Vuković, D. Brkić, Ž. Vitnik, *J. Chem. Res. (S)* (2000) 506
22. N. B. Chapman, D. J. Newman, J. Shorter, H. M. Wall, *J. Chem. Soc. Perkin Trans. 2* (1976) 847
23. Y. Marcus, *Chem. Soc. Rev.* (1993) 409
24. D. H. McDaniel, H. C. Brown, *J. Org. Chem.* **23** (1958) 420.



J. Serb. Chem. Soc. 77 (5) 581–588 (2012)
JSCS–4291

Preparation of 2-heteroatom substituted-4-oxo-4-arylbutanoates via thio- and aza-Michael addition

HUILI LIU, XIN LV*, LIEJIN ZHOU, RUIFENG YIN and XIAOXIA WANG*

*Zhejiang Key Laboratory for Reactive Chemistry on Solid Surfaces, College of Chemistry and
Life Sciences, Zhejiang Normal University, Jinhua 321004, P. R. China*

(Received 25 July, revised 11 November 2011)

Abstract: Efficient regioselective conjugate additions of thiophenols and benzotriazole to 4-aryl-4-oxobut-2-enoates were achieved under mild conditions. Thus, a variety of 2-(arylthio)-4-oxo-4-arylbutanoates and 2-benzotriazolyl-4-oxo-4-arylbutanoates were conveniently synthesized in good to excellent yields.

Keywords: Michael addition; thiophenol; benzotriazole; 4-aryl-4-oxobut-2-enoate.

INTRODUCTION

4-Aryl-4-oxobut-2-enoates, which can be readily prepared from low-cost and readily available materials,^{1,2} have aroused great interest because of their biological activity and applications in the field of synthetic chemistry.^{3–6} The conjugate addition using 4-aryl-4-oxobut-2-enoates as Michael acceptors has received significant attention since the adducts are usually multi-functional compounds and are potentially synthetically or medicinally valuable. The addition of amino acids to 4-aryl-4-oxobut-2-enoates (γ -oxo- γ -phenylbutyrate) could produce useful intermediates for the synthesis of angiotensin-converting enzyme (ACE) inhibitors.^{7,8} Indoles underwent conjugate addition to 4-aryl-4-oxobut-2-enoates, forming a C–C bond, catalyzed by a Lewis acid.⁹ The facile Michael addition of other C-nucleophiles, such as active methylene compounds to 4-aryl-4-oxobut-2-enoates was also reported.¹⁰

In our recent program focused on the selective reduction of 2-heteroatom-substituted carbonyl compounds, some 2-heteroatom-substituted 4-oxo-4-arylbutanoates were required. Although thio-Michael addition has been intensively studied,^{11–19} only a few unusual approaches to certain specific 2-arylthio-4-oxo-4-arylbutanoates have been reported. Yoshimatsu *et al.* found that scandium(III) triflate ($\text{Sc}(\text{OTf})_3$), *i.e.*, scandium(III) trifluoromethanesulfonate, could facilitate the reaction between trimethyl((1-phenylvinyl)oxy)silane and ethyl 2-fluoro-2-

*Corresponding authors. E-mail: lvxin@zjnu.cn (X. Lv); wangxiaoxia@zjnu.cn (X. Wang)
doi: 10.2298/JSC110526202L

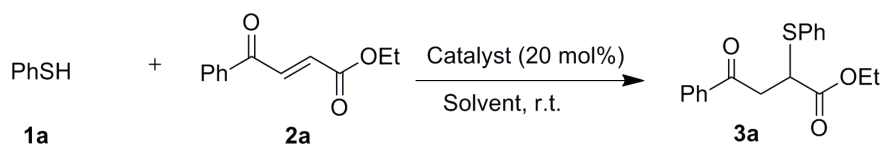
-(phenylthio)acetate to afford ethyl 4-oxo-4-phenyl-2-(phenylthio)butanoate.^{20,21} Mukaiyama *et al.* reported that methyl 4-oxo-4-phenyl-2-(phenylthio)butanoate was synthesized in low yield (23 %) *via* Sn(OTf)₂-promoted rearrangement of a β -keto sulfoxide.²² In addition, methyl 4-oxo-4-aryl-2-(arylthio)butanoates could be prepared from the substitution between α -chloro- α -phenylthio ketone and silyl enol ethers.^{23,24} Nevertheless, the above methods might suffer from special substrates, expensive (or special) catalysts, low efficiency, and/or harsh conditions.

On the other hand, to the best of our knowledge, a method for the synthesis of 2-benzotriazolyl-4-oxo-4-arylbutanoates is unknown. Although a variety of 2-heterocycle (C–N bond) substituted 4-oxo-4-arylbutanoates could be synthesized *via* 1,8-diazabicyclo[5.4.0]undec-7-ene (DBU) catalyzed redox isomerization of ethyl 4-aryl-4-hydroxybut-2-ynoate, followed by aza-Michael addition of *N*-containing heterocyclic compounds to the isomerized product, unfortunately the reaction of benzotriazole failed and the desired 2-benzotriazolyl-4-oxo-4-arylbutanoates could not be obtained.²⁵

Herein, the preparations of 2-(arylthio)-4-oxo-4-arylbutanoates and 2-benzotriazolyl-4-oxo-4-arylbutanoates *via* regioselective conjugate addition of thiophenol and benzotriazole to 4-aryl-4-oxobut-2-enoates are reported.

RESULTS AND DISCUSSION

This investigation focused first on the catalytic conjugate addition of thiophenols to 4-aryl-4-oxobut-2-enoates. The conjugate addition between thiophenol **1a** and ethyl 4-phenyl-4-oxobut-2-enoate **2a** was employed as a model reaction. It is of interest that all the examined bases (DBU, 1,4-diazabicyclo[2.2.2]octane (DABCO), triethylamine (TEA), pyridine (PyH) and K₂CO₃) led to the formation of the desired **3a** (Scheme 1, Table I). Among them, TEA proved to be the most efficient (Table I, entry 3). Furthermore, screening of the solvents showed that in CH₂Cl₂ an excellent yield of **3a** was obtained (Table I, entry 7). Therefore, CH₂Cl₂ was chosen as the most suitable solvent.



Scheme 1. The catalytic conjugate addition of thiophenol to ethyl 4-phenyl-4-oxobut-2-enoate.

With the optimized conditions in hand, various 4-aryl-4-oxobut-2-enoates were employed as the substrates to test the generality of the reaction (Scheme 2). The results are given in Table II.

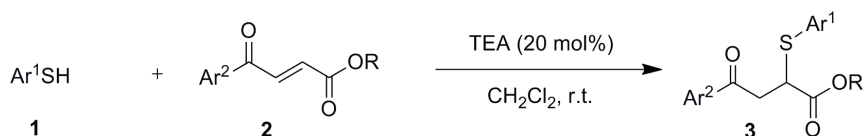
Generally, aryls with electron-donating groups and electron-withdrawing group at the 4-position of substrate **2** exerted little influence on the efficiency of

the reaction (entries 3, 5, 7, 8 and 10, Table III). Exceptionally, 2-furyl caused the corresponding substrate **2** to react more slowly and afforded a lower yield (entry 6). The more nucleophilic *p*-methoxythiophenol was also employed, and the desired product was smoothly obtained in a shorter reaction time (entry 7).

TABLE I. The catalytic conjugate addition of thiophenol to ethyl 4-phenyl-4-oxobut-2-enoate under different conditions

Entry	Catalyst ^a	Solvent	Yield, % ^{b,c}
1	DBU	THF	76
2	DABCO	THF	65
3	TEA	THF	82
4	PyH	THF	49
5	K ₂ CO ₃	THF	37
6	TEA	EtOH	57
7	TEA	CH ₂ Cl ₂	90
8	TEA	PhMe	52

^aCatalyst loading: 20 mol %; ^bthe runs were performed at room temperature for 6 h; ^cisolated yields



Scheme 2. The catalytic conjugate addition of thiophenols to 4-aryl-4-oxobut-2-enoates.

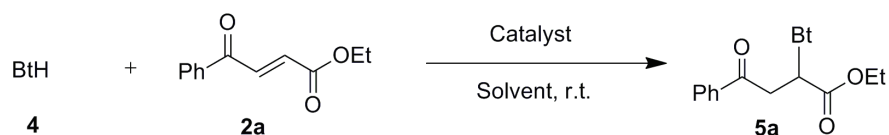
TABLE II. TEA promoted conjugate addition of thiophenols to 4-aryl-4-oxobut-2-enoates (reaction conditions: thiophenol **1** (1 mmol), 4-aryl-4-oxobut-2-enoate **2** (1 mmol), CH₂Cl₂ (10 mL), TEA (0.2 mmol, 20 mol %), room temperature)

Entry	Ar ¹	Ar ²	R	Product	Time, h	Yield, % ^a
1			Et	3a	6	90
2			Et	3b	6	95
3			Et	3c	6	89
4			CH ₂ Ph	3d	6	93
5			Et	3e	6	92
6			Et	3f	8	62
7			Et	3g	4	88

^aIsolated yields

With the successful preparation of 2-(arylthio)-4-oxo-4-arylbutanoates, the conjugate addition between 1*H*-benzotriazole (BtH) and 4-aryl-4-oxobut-2-enoates was then explored.

Since BtH is also weakly acidic, the above base-catalyzed conditions for thio-Michael addition was tentatively applied to the aza-Michael addition. However, the reaction of BtH (**4**) and ethyl 4-phenyl-4-oxobut-2-enoate (**2a**) under the above optimized conditions, afforded **5a** in only 53 % yield (Scheme 3) (Table III, entry 1). Other bases, such as DBU, DABCO, PyH, cyclohexylamine, and K₂CO₃ were also tested, but the yield could not be improved (Table III, entries 2–6).



Scheme 3. The catalytic conjugate addition of BtH to ethyl 4-phenyl-4-oxobut-2-enoate.

TABLE III. The catalytic conjugate addition of BtH to ethyl 4-phenyl-4-oxobut-2-enoate under different conditions

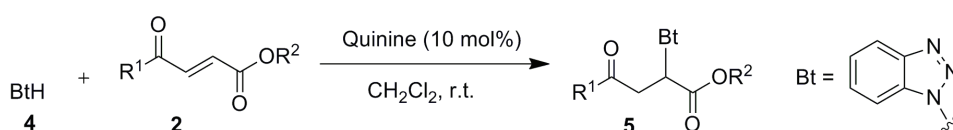
Entry	Catalyst ^a	Solvent	Yield, % ^{b,c}
1	TEA	CH ₂ Cl ₂	53
2	DBU	CH ₂ Cl ₂	47
3	DABCO	CH ₂ Cl ₂	20
4	PyH	CH ₂ Cl ₂	33
5	Cyclohexylamine	CH ₂ Cl ₂	46
6	K ₂ CO ₃	CH ₂ Cl ₂	35
7	Quinine	CH ₂ Cl ₂	93
8	Quinine	THF	73
9	Quinine	PhMe	51
10	Quinine	CH ₂ Cl ₂	92 ^d
11	Quinine	CH ₂ Cl ₂	80 ^e

^aCatalyst loading: 20 mol %; ^bthe runs were performed at r.t. for 24 h; ^cisolated yields; ^dcatalyst loading: 10 mol %; ^ecatalyst loading: 5 mol %

In light of the fact that quinine could promote many Michael additions due to its special bi-functional structure,^{26–30} it was introduced as a base catalyst for the addition of BtH with **2a**. Encouragingly, the yield of **5a** increased to 93 % yield with quinine as the catalyst (Table III, entry 7). Other solvents were also screened. THF and toluene seemed to be inferior to CH₂Cl₂ (entries 8–10). Reducing the amount of the catalyst to 10 mol % had hardly any influence on the efficiency (entry 10). However, the yield sharply decreased when the amount of the catalyst was reduced to 5 mol % (entry 11).

Therefore, the conjugate addition of BtH to various substituted 4-oxobut-2-enoates was performed at room temperature in CH₂Cl₂ with 10 mol % of qui-

nine as the catalyst (Scheme 4). The results are summarized in Table IV. With regard to the substituents on the aryl in substrate **2**, the electron properties seemed to only slightly affect the efficiency of the reactions and good to excellent yield of product **5** could be isolated (Table IV, entries 1–6). The substrate with 2-furyl substitution afforded a lower yield (entry 7). An alkyl substituted substrate was also tried and moderate yield of the desired adduct was obtained (entry 8).



Scheme 4. The catalytic conjugate addition of BtH to 4-phenyl-4-oxobut-2-enoates.

TABLE IV. Quinine promoted conjugate addition of BtH to 4-aryl-4-oxobut-2-enoates (reaction conditions: thiophenol **1** (1 mmol), 4-aryl-4-oxobut-2-enoate **2** (1 mmol), in CH_2Cl_2 (10 mL) with TEA (0.2 mmol, 20 mol %) as catalyst, stirred at room temperature)

Entry	R ¹	R ²	Product	Yield, % ^a
1		Et	5a	92
2		Et	5b	90
3		CH ₂ Ph	5c	80
4		CH ₂ Ph	5d	88
5		Et	5e	83
6		Et	5f	90
7		Et	5g	57
8	Me	Et	5h	62

^aIsolated yields

A plausible mechanism of this quinine catalyzed aza-Michael addition was proposed (Fig. 1). The hydroxyl on the quinine could form a hydrogen bond with the γ -carbonyl of the 4-aryl-4-oxobut-2-enoate, and the tertiary nitrogen of quinine acts as a base, which deprotonates the BtH to give a benzotriazole anion (Bt^-). The combination of these factors could double-activate the aza-Michael addition, thereby making the reaction highly efficient.

It is noteworthy that the above catalytic conjugate reactions exhibited complete regioselectivity. The *S*- and *N*- nucleophiles selectively attacked the β -po-

sition of the ketone carbonyl. In addition, no product resulting from addition to the β -position of the ester carbonyl was observed under the employed catalytic conditions. Furthermore, attacks of *S*- and *N*- nucleophiles on the carbonyls were not observed.

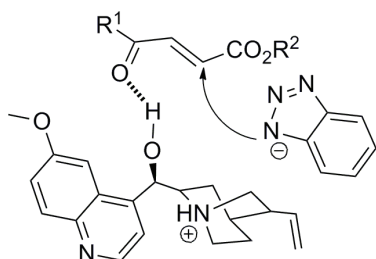


Fig. 1. Proposed mechanism for the conjugate addition between BtH and 4-aryl-4-oxobut-2-enoate.

Thiophenol was more nucleophilic towards 4-aryl-4-oxobut-2-enoate than BtH. Thus, by employing simple TEA as the base catalyst, thiophenol underwent efficient regioselective thio-Michael addition and 2-arylthio-4-oxo-4-arylbutanoates were prepared in good to excellent yields. Using quinine as the catalyst, the regioselective aza-Michael addition between BtH and 4-aryl-4-oxobut-2-enoate proceeded efficiently and afforded the desired 2-benzotriazolyl-4-oxo-4-arylbutanoates in satisfactory yields.

EXPERIMENTAL

Reagents were commercially available and used without further purification unless otherwise indicated. 4-Aryl-4-oxobut-2-enoic acid,³¹ and the corresponding esters **2** were prepared according to literature procedures.³² TLC was performed on silica gel plates with F-254 indicator; viewing was by UV light (254 nm). Flash column chromatography was performed on silica gel (200–300 mesh), using ethyl acetate/petroleum ether mixtures as eluents. The ¹H- and ¹³C-NMR spectra were recorded on a Bruker Avance 400 MHz spectrometer with CDCl₃ as the solvent and TMS as the internal standard. The elemental analyses were recorded on a Varian-ELIII elemental analyzer. The HRMS spectra were obtained on a Bruker APEXIII 7.0 Tesla FTMS.

General procedure for the conjugation of thiophenols 1 to 4-aryl-4-oxobut-2-enoates 2.

Synthesis of compounds 3

To a solution of 4-aryl-4-oxobut-2-enoate **2** (1 mmol) and thiophenol **1** (1 mmol) in CH₂Cl₂ (10 mL) was added TEA (0.20 mmol, 20 mol %) at room temperature. The mixture was stirred at room temperature and monitored by TLC. After the starting material **2** had been completely consumed, the solvent was evaporated under vacuum and the residue purified by flash column chromatography on silica gel to give the desired product **3**.

General procedure for the conjugation of BtH 4 to 4-aryl-4-oxobut-2-enoates 2. Synthesis of compounds 5

To a solution of 4-aryl-4-oxobut-2-enoate **2** (1.0 mmol) and BtH **4** (1.0 mmol) in CH₂Cl₂ (10 mL) was added quinine (0.1 mmol, 10 mol %). The mixture was stirred at room temperature and monitored by TLC. After the starting material **2** had been completely consumed, the

reaction was quenched by aq. HCl. The mixture was extracted with ethyl acetate. The combined organic layers were washed with aq. Na₂CO₃ and then with saturated NaCl. The obtained organic layer was dried over anhydrous Na₂SO₄. After the solvent had been evaporated under vacuum, the residue was purified by flash column chromatography on silica gel to give the desired product **5**.

CONCLUSIONS

In summary, efficient and facile conjugate addition reactions of thiophenols and benzotriazole to various 4-aryl-4-oxobut-2-enoates were developed. The obtained multi-functionalized adducts might be valuable for synthetic or pharmaceutical utilization. The addition reactions proceeded with complete regioselectivity and tolerated various substituents. The readily available materials, simplicity of the procedure, high efficiency, and potentially valuable adducts make the method convenient and useful to synthetic chemists.

SUPPLEMENTARY MATERIAL

Spectral data of the products are available electronically from <http://www.shd.org.rs/JSCS/>, or from the corresponding author on request.

Acknowledgement. This work was financially supported by the National Natural Science Foundation of China (No. 20802070).

ИЗВОД

СИНТЕЗА 2-ХЕТЕРОАТОМ-СУПСТИТУИСАНИХ 4-ОКСО-4-АРИЛБУТАНОАТА ТИО- И АЗА-МАЈКЛОВОМ АДИЦИЈОМ

HUILI LIU, XIN LV, LIEJIN ZHOU, RUIFENG YIN и XIAOXIA WANG

Zhejiang Key Laboratory for Reactive Chemistry on Solid Surfaces, College of Chemistry and Life Sciences, Zhejiang Normal University, Jinhua 321004, P R China

Развијен је ефикасан поступак региоселективне коњуговане адиције тиофенола и бензотриазола, под благим реакционим условима, при чему су добијени 4-арил-4-оксобут-2-еноати. Овим поступком добијени су различити 2-(арилтио)-4-оксо-4-арилбутаноати и 2-бензотриазол-4-оксо-4-арилбутаноати у добром до одличном приносу.

(Примљено 25. јула, ревидирано 11. новембра 2011)

REFERENCES

1. J. P. Sonye, K. Koide, *J. Org. Chem.* **71** (2006) 6254
2. K. Onoue, T. Shintou, C. S. Zhang, I. Itoh, *Chem. Lett.* **35** (2006) 22
3. M. Yamada, N. Nagashima, J. Hasegawa, S. Takahashi, *Tetrahedron Lett.* **49** (1998) 9019
4. C. S. Chien, T. Kawasaki, M. Sakamoto, Y. Tamura, Y. Kita, *Chem. Pharm. Bull.* **33** (1985) 2743
5. G. Blay, I. Fernandez, A. Monleon, M. C. Munoz, J. R. Pedro, C. Vila, *Adv. Synth. Catal.* **351** (2009), 2433.
6. M. Bianchi, F. Barzagli, United States Patent 4 500 731, 1985
7. M. Yamada, N. Nagashima, J. Hasegawa, S. Takahashi, *Tetrahedron Lett.* **39** (1998) 9019

8. M. Knollmuller, M. Ferencic, P. Gartner, U. Girreser, M. Klinge, L. Gaischin, K. Me-reiter, C. R. Noe, *Monatsh. Chem.* **130** (1999) 769
9. X. X. Wang, Y. H. Zhang, X. H. Xiao, X. S. Li, *Chem. Lett.* **37** (2008) 1284
10. X. Lv, Y. H. Zhang, L. J. Zhou, X. X. Wang, *J. Serb. Chem. Soc.* **76** (2011) 947 and refe-rences cited therein
11. W. X. Guo, G. S. Lv, J. X. Chen, W. X. Gao, J. C. Ding, H. Y. Wu, *Tetrahedron* **66** (2010) 2297
12. G. Sharma, R. Kumar, A. K. Chakraborti, *Tetrahedron Lett.* **49** (2008) 4272
13. S. Hussain, S. K. Bharadwaj, M. K. Chaudhuri, H. Kalita, *Eur. J. Org. Chem.* (2007) 374
14. C. M. Chu, S. Gao, M. N. V. Sastry, C. W. Kuo, C. W. Lu, J. T. Liu, C. F. Yao, *Tetra-hedron* **63** (2007) 1863
15. G. L. Khatik, G. Sharma, R. Kumar, A. K. Chakraborti, *Tetrahedron* **63** (2007) 1200
16. C. M. Chu, W. J. Huang, C. W. Lu, P. Wu, J. T. Liu, C. F. Yao, *Tetrahedron Lett.* **47** (2006) 7375
17. M. Kumarraja, K. Pitchumani, *J. Mol. Catal., A* **256** (2006) 138
18. H. Firouzabadi, N. Iranpoor, A. A. Jafari, *Adv. Synth. Catal.* **347** (2005) 655
19. N. Srivastava, B. K. Banik, *J. Org. Chem.* **68** (2003) 2109
20. K. Gotoh, T. Yamamoto, M. Yoshimatsu, *Chem. Pharm. Bull.* **54** (2006) 1611
21. M. Yoshimatsu, M. Kawamoto, K. Gotoh, *Eur. J. Org. Chem.* (2005) 2884
22. M. Shimizu, T. Akiyama, T. Mukaiyama, *Chem. Lett.* (1984) 1531
23. I. Fleming, J. Iqbal, *Tetrahedron Lett.* **24** (1983) 327
24. T. V. Lee, J. O. Okonkwo, *Tetrahedron Lett.* **24** (1983) 323
25. X. Han, *Tetrahedron Lett.* **48** (2007) 2845
26. A. Scettri, A. Massa, L. Palombi, R. Villano, M. R. Acocella, *Tetrahedron: Asymmetry* **19** (2008) 2149
27. Y. N. Xuan, S. Z. Nie, L. T. Dong, J. M. Zhang, M. Yan, *Org. Lett.* **11** (2009) 1583
28. Y. F. Cai, L. Li, M. X. Luo, K. F. Yang, G. Q. Lai, J. X. Jiang, L. W. Xu, *Chirality* **23** (2011) 397
29. A. Russo, A. Perfetto, A. Lattanzi, *Adv. Synth. Catal.* **351** (2009) 3067
30. G. Bartoli, M. Bosco, A. Carlone, A. Cavalli, M. Locatelli, A. Mazzanti, P. Ricci, L. Sambri, P. Melchiorre, *Angew. Chem. Int. Ed. Engl.* **45** (2006) 4966
31. M. Bianchi, F. Barzaghi, United States Patent 4 473 583, 1984
32. S. T. Kobe, Y. U. Takasago, Y. Yanagida, T. O. Kobe, K. W. Akashi, United States Pa-tent 4 994 600, 1991.



SUPPLEMENTARY MATERIAL TO
**Preparation of 2-heteroatom substituted-4-oxo-4-arylbutanoates
via thio- and aza-Michael addition**

HUILI LIU, XIN LV*, LIEJIN ZHOU, RUIFENG YIN and XIAOXIA WANG*

Zhejiang Key Laboratory for Reactive Chemistry on Solid Surfaces, College of Chemistry and
Life Sciences, Zhejiang Normal University, Jinhua 321004, P. R. China

J. Serb. Chem. Soc. 77 (5) (2012) 581–588

SPECTRAL DATA FOR THE PRODUCTS

The structural elucidations of the products were based on their spectral (^1H -NMR, ^{13}C -NMR, elemental analysis, and mass) data as given below.

Ethyl 4-oxo-4-phenyl-2-(phenylthio)butanoate (3a).^{1,2} Yield: 90 %; white solid; m.p. 46–48 °C (oil)³¹; ^1H -NMR (400 MHz, CDCl_3 , δ / ppm): 7.93 (2H, *m*), 7.58–7.53 (3H, *m*), 7.46 (2H, *t*, $J = 8.0$ Hz), 7.36–7.33 (3H, *m*), 4.24 (1H, *dd*, $J_1 = 4.4$ Hz, $J_2 = 10.2$ Hz), 4.14 (2H, *q*, $J = 7.2$ Hz), 3.71 (1H, *dd*, $J_1 = 10.2$ Hz, $J_2 = 18.0$ Hz), 3.39 (1H, *dd*, $J_1 = 4.4$ Hz, $J_2 = 18.0$ Hz), 1.18 (3H, *t*, $J = 7.2$ Hz); ^{13}C -NMR (100 MHz, CDCl_3 , δ / ppm): 196.9, 171.7, 136.1, 133.8, 133.6, 132.4, 129.1, 128.7, 128.6, 128.1, 61.4, 45.2, 40.9, 14.0.

Ethyl 4-(3,4-dimethylphenyl)-4-oxo-2-(phenylthio)butanoate (3b). New compound. Yield: 95 %; white solid; m.p. 63–65 °C; Anal. Calcd. for $\text{C}_{20}\text{H}_{22}\text{O}_3\text{S}$: C, 70.15; H, 6.48 %. Found: C, 70.32; H, 6.45 %; ^1H -NMR (400 MHz, CDCl_3 , δ / ppm): 7.70 (1H, *s*), 7.67 (1H, *d*, $J = 7.6$ Hz), 7.55–7.52 (2H, *m*), 7.35–7.32 (3H, *m*), 7.20 (1H, *d*, $J = 7.6$ Hz), 4.25 (1H, *dd*, $J_1 = 4.4$ Hz, $J_2 = 10.2$ Hz), 4.13 (2H, *q*, $J = 6.8$ Hz), 3.66 (1H, *dd*, $J_1 = 10.2$ Hz, $J_2 = 18.0$ Hz), 3.36 (1H, *dd*, $J_1 = 4.4$ Hz, $J_2 = 18.0$ Hz), 2.37 (3H, *s*), 2.30 (3H, *s*), 1.17 (3H, *t*, $J = 6.8$ Hz); ^{13}C -NMR (100 MHz, CDCl_3 , δ / ppm): 196.7, 171.8, 143.2, 137.1, 134.1, 133.6, 132.6, 129.9, 129.2, 129.0, 128.4, 125.9, 61.4, 45.4, 40.7, 20.1, 19.8, 14.0; MS (ESI): m/z 365 $[\text{M} + \text{Na}]^+$.

Ethyl 4-(4-chlorophenyl)-4-oxo-2-(phenylthio)butanoate (3c). New compound. Yield: 89 %; white solid; m.p. 80–82 °C; Anal. Calcd. for $\text{C}_{18}\text{H}_{17}\text{ClO}_3\text{S}$: C, 61.97; H, 4.91 %. Found: C, 61.72; H, 4.94 %; ^1H -NMR (400 MHz, CDCl_3 , δ / ppm): 7.87 (2H, *d*, $J = 8.8$ Hz), 7.54–7.52 (2H, *m*), 7.43 (2H, *d*, $J = 8.8$ Hz), 7.35–7.33 (3H, *m*), 4.22 (1H, *dd*, $J_1 = 4.4$ Hz, $J_2 = 10.0$ Hz), 4.14 (2H, *q*, $J = 7.2$

* Corresponding authors. E-mail: lvxin@zjnu.cn (X. Lv); wangxiaoxia@zjnu.cn (X. X. Wang)

Hz), 3.66 (1H, *dd*, $J_1 = 10.0$ Hz, $J_2 = 18.0$ Hz), 3.34 (1H, *dd*, $J_1 = 4.4$ Hz, $J_2 = 18.0$ Hz), 1.18 (3H, *t*, $J = 7.2$ Hz); ^{13}C -NMR (100 MHz, CDCl_3 , δ / ppm): 195.7, 171.6, 140.0, 134.4, 133.8, 132.3, 129.5, 129.1, 129.0, 128.6, 61.5, 45.1, 40.8, 14.0; MS (ESI): m/z 371 (^{35}Cl), 373.0 (^{37}Cl) [$\text{M} + \text{Na}$] $^+$.

Benzyl 4-(4-chlorophenyl)-4-oxo-2-(phenylthio)butanoate (3d). New compound. Yield: 93 %; white solid; m.p. 87–89 °C; ^1H -NMR (400 MHz, CDCl_3 , δ / ppm): 7.86 (2H, *d*, $J = 8.4$ Hz), 7.43 (4H, *d*, $J = 8.4$ Hz), 7.33–7.26 (8H, *m*), 5.13 (2H, *dd*, $J_1 = 12.4$ Hz, $J_2 = 27.2$ Hz), 4.29 (1H, *dd*, $J_1 = 4.4$ Hz, $J_2 = 10.0$ Hz), 3.66 (1H, *dd*, $J_1 = 10.0$ Hz, $J_2 = 18.0$ Hz), 3.36 (1H, *dd*, $J_1 = 4.4$ Hz, $J_2 = 18.0$ Hz); ^{13}C -NMR (100 MHz, CDCl_3 , δ / ppm): 195.6, 171.4, 140.1, 135.4, 134.4, 133.9, 132.0, 129.5, 129.1, 129.0, 128.7, 128.5, 128.3, 128.2, 67.2, 45.1, 40.8; MS (ESI): m/z 433 (^{35}Cl), 435 (^{37}Cl) [$\text{M} + \text{Na}$] $^+$; HRMS (ESI): Calcd. for $\text{C}_{23}\text{H}_{19}\text{ClO}_3\text{S}$ [$\text{M} + \text{Na}$] $^+$: 433.0636. Found: 433.0656.

Ethyl 4-(naphthalen-2-yl)-4-oxo-2-(phenylthio)butanoate (3e). New compound. Yield: 92 %; white solid; m.p. 126–128 °C; ^1H -NMR (400 MHz, CDCl_3 , δ / ppm): 8.45 (1H, *s*), 8.00–7.98 (2H, *m*), 7.89–7.86 (2H, *m*), 7.62–7.54 (4H, *m*), 7.36–7.34 (3H, *m*), 4.33 (1H, *dd*, $J_1 = 4.8$, $J_2 = 9.6$ Hz), 4.16 (2H, *q*, $J = 7.2$ Hz), 3.85 (1H, *dd*, $J_1 = 9.6$ Hz, $J_2 = 18.0$ Hz), 3.53 (1H, *dd*, $J_1 = 4.8$ Hz, $J_2 = 18.0$ Hz), 1.20 (3H, *t*, $J = 7.2$ Hz); ^{13}C -NMR (100 MHz, CDCl_3 , δ / ppm): 196.8, 171.7, 135.8, 133.7, 133.5, 132.6, 132.5, 130.0, 129.7, 129.1, 128.7, 128.6, 128.5, 127.8, 126.9, 123.7, 61.4, 45.4, 40.9, 14.0; MS (ESI): m/z 387 [$\text{M} + \text{Na}$] $^+$; HRMS (ESI): Calcd. for $\text{C}_{22}\text{H}_{20}\text{O}_3\text{S}$ [$\text{M} + \text{Na}$] $^+$: 387.1025, Found: 387.1023.

Ethyl 4-(furan-2-yl)-4-oxo-2-(phenylthio)butanoate (3f). New compound. Yield: 52 %; yellow viscous oil; Anal. Calcd. for $\text{C}_{22}\text{H}_{20}\text{O}_3\text{S}$: C, 63.14; H, 5.30 %. Found: C, 62.99; H, 5.33 %; ^1H -NMR (400 MHz, CDCl_3 , δ / ppm): 7.58–7.57 (1H, *m*), 7.53–7.51 (2H, *m*), 7.34–7.32 (3H, *m*), 7.20 (1H, *d*, $J = 3.6$ Hz), 6.53 (1H, *dd*, $J_1 = 2.0$ Hz, $J_2 = 3.6$ Hz), 4.22 (1H, *dd*, $J_1 = 4.8$ Hz, $J_2 = 9.6$ Hz), 4.13 (2H, *q*, $J = 7.2$ Hz), 3.53 (1H, *dd*, $J_1 = 9.6$ Hz, $J_2 = 17.6$ Hz), 3.26 (1H, *dd*, $J_1 = 4.8$ Hz, $J_2 = 17.6$ Hz), 1.17 (3H, *t*, $J = 7.2$ Hz); ^{13}C -NMR (100 MHz, CDCl_3 , δ / ppm): 185.7, 171.5, 152.1, 146.7, 133.8, 132.3, 129.0, 128.6, 117.6, 112.4, 61.5, 44.9, 40.4, 14.0; MS (ESI): m/z 327 [$\text{M} + \text{Na}$] $^+$.

Ethyl 2-((4-methoxyphenyl)thio)-4-oxo-4-phenylbutanoate (3g). New compound. Yield: 88 %; yellow solid; m.p. 58–60 °C; Anal. Calcd. for $\text{C}_{19}\text{H}_{20}\text{O}_4\text{S}$: C, 66.26; H, 5.85 %. Found: C, 66.40; H, 5.82 %; ^1H -NMR (400 MHz, CDCl_3 , δ / ppm): 7.92–7.90 (2H, *m*), 7.58–7.54 (1H, *m*), 7.47–7.43 (4H, *m*), 6.86 (2H, *d*, $J = 8.8$ Hz), 4.14 (2H, *q*, $J = 7.2$ Hz), 4.09 (1H, *dd*, $J_1 = 4.4$ Hz, $J_2 = 10.0$ Hz), 3.80 (3H, *s*), 3.62 (1H, *dd*, $J_1 = 10.0$ Hz, $J_2 = 18.0$ Hz), 3.34 (1H, *dd*, $J_1 = 4.4$, $J_2 = 18.0$ Hz), 1.21 (3H, *t*, $J = 7.2$ Hz); ^{13}C -NMR (100 MHz, CDCl_3 , δ / ppm): 197.0, 171.7, 160.5, 136.9, 136.2, 133.5, 128.7, 128.1, 122.3, 114.6, 61.3, 55.4, 45.8, 40.8, 14.1; MS (ESI): m/z 367 [$\text{M} + \text{Na}$] $^+$.

Ethyl 2-(1H-benzotriazol-1-yl)-4-oxo-4-phenylbutanoate (5a). New compound. Yield: 92 %; white solid; m.p. 95–97 °C; ¹H-NMR (400 MHz, CDCl₃, δ / ppm): 8.07 (1H, *d*, *J* = 8.4 Hz), 7.99 (2H, *d*, *J* = 8.0 Hz), 7.73 (1H, *d*, *J* = 8.4 Hz), 7.62–7.54 (2H, *m*), 7.50–7.46 (2H, *m*), 7.42–7.39 (1H, *m*), 6.22 (1H, *t*, *J* = 7.2 Hz), 4.35 (1H, *dd*, *J*₁ = 6.0, *J*₂ = 18.0 Hz), 4.25–4.16 (3H, *m*), 1.17 (3H, *t*, *J* = 7.2 Hz); ¹³C-NMR (100 MHz, CDCl₃, δ / ppm): 195.4, 168.1, 145.9, 135.8, 133.9, 133.4, 128.8, 128.3, 127.9, 124.2, 120.1, 109.8, 62.6, 56.3, 39.9, 13.9; MS (ESI): *m/z* 324 [M + H]⁺; HRMS (ESI) Calcd. for C₁₈H₁₇N₃O₃ [M + H]⁺: 324.1343. Found: 324.1347.

Ethyl 2-(1H-benzotriazol-1-yl)-4-oxo-4-(p-tolyl)butanoate (5b). New compound. Yield: 90 %; white solid; m.p. 90–92 °C; ¹H-NMR (400 MHz, CDCl₃, δ / ppm): 8.06 (1H, *d*, *J* = 8.4 Hz), 7.88 (2H, *d*, *J* = 8.0 Hz), 7.73 (1H, *d*, *J* = 8.4 Hz), 7.53 (1H, *t*, *J* = 8.0 Hz), 7.39 (1H, *t*, *J* = 8.0 Hz), 7.25 (2H, *d*, *J* = 8.0 Hz), 6.21 (1H, *t*, *J* = 6.8 Hz), 4.31 (1H, *dd*, *J*₁ = 6.0 Hz, *J*₂ = 18.0 Hz), 4.23–4.13 (3H, *m*), 2.39 (3H, *s*), 1.15 (3H, *t*, *J* = 7.2 Hz); ¹³C-NMR (100 MHz, CDCl₃, δ / ppm): 195.0, 168.2, 145.9, 144.9, 133.5, 133.3, 129.5, 128.4, 127.9, 124.2, 120.1, 109.8, 62.6, 56.4, 39.8, 21.7, 13.9; MS (ESI): *m/z* 338 [M + H]⁺; HRMS (ESI) Calcd. for C₁₉H₁₉N₃O₃ [M + H]⁺: 338.1499. Found: 338.1505.

Benzyl 2-(1H-benzotriazol-1-yl)-4-oxo-4-(p-tolyl)butanoate (5c). New compound. Yield: 80 %; white solid; m.p. 99–101 °C; ¹H-NMR (400 MHz, CDCl₃, δ / ppm): 8.07 (1H, *d*, *J* = 8.4 Hz), 7.87 (2H, *d*, *J* = 8.0 Hz), 7.68 (1H, *d*, *J* = 8.4 Hz), 7.51 (1H, *t*, *J* = 7.2 Hz), 7.39 (1H, *t*, *J* = 7.6 Hz), 7.27–7.25 (5H, *m*), 7.13–7.11 (2H, *m*), 6.28 (1H, *t*, *J* = 6.4 Hz), 5.20–5.13 (2H, *m*), 4.31 (1H, *dd*, *J*₁ = 6.0 Hz, *J*₂ = 18.0 Hz), 4.20 (1H, *dd*, *J*₁ = 7.6 Hz, *J*₂ = 18.0 Hz), 2.41 (3H, *s*); ¹³C-NMR (100 MHz, CDCl₃, δ / ppm): 194.9, 168.1, 145.9, 144.9, 134.7, 133.5, 133.3, 129.5, 128.5, 128.4, 128.3, 128.0, 127.9, 124.2, 120.1, 109.8, 68.0, 56.4, 39.7, 21.7; MS (ESI): *m/z* 400 [M + H]⁺; HRMS (ESI) Calcd. for C₂₄H₂₁N₃O₃ [M + H]⁺: 400.1656. Found: 400.1651.

Benzyl 2-(1H-benzotriazol-1-yl)-4-(3,4-dimethylphenyl)-4-oxobutanoate (5d). New compound. Yield: 88 %; white solid; m.p. 135–137 °C; ¹H-NMR (400 MHz, CDCl₃, δ / ppm): 8.06 (1H, *d*, *J* = 8.4 Hz), 7.74–7.67 (3H, *m*), 7.50 (1H, *t*, *J* = 7.2 Hz), 7.37 (1H, *t*, *J* = 8.0 Hz), 7.26–7.12 (6H, *m*), 6.29 (1H, *t*, *J* = 6.0 Hz), 5.17 (2H, *s*), 4.34–4.15 (2H, *m*), 2.31 (3H, *s*), 2.29 (3H, *s*); ¹³C-NMR (100 MHz, CDCl₃, δ / ppm): 195.1, 168.1, 146.0, 143.5, 137.1, 134.8, 133.8, 133.5, 130.0, 129.4, 128.5, 128.4, 127.9, 127.8, 126.0, 124.1, 120.1, 109.8, 67.9, 56.5, 39.7, 20.0, 19.6; MS (ESI): *m/z* 414 [M + H]⁺; HRMS (ESI) Calcd. for C₂₅H₂₃N₃O₃ [M + H]⁺: 414.1812. Found: 414.1821.

Ethyl 2-(1H-benzotriazol-1-yl)-4-oxo-4-(4-phenoxyphenyl)butanoate (5e). New compound. Yield: 83 %; white solid; m.p. 128–130 °C; ¹H-NMR (400 MHz, CDCl₃, δ / ppm): 8.06 (1H, *d*, *J* = 8.4 Hz), 7.96 (2H, *d*, *J* = 8.8 Hz), 7.73 (1H, *d*, *J* = 8.4 Hz), 7.55 (1H, *t*, *J* = 8.0 Hz), 7.39 (3H, *t*, *J* = 7.6 Hz), 7.20 (1H, *t*,

7.6 Hz), 7.06 (2H, *d*, $J = 8.4$ Hz), 6.99 (2H, *d*, $J = 8.8$ Hz), 6.20 (1H, *t*, $J = 6.4$ Hz), 4.28 (1H, *dd*, $J_1 = 6.4$ Hz, $J_2 = 18.0$ Hz), 4.24–4.13 (3H, *m*), 1.15 (3H, *t*, $J = 7.2$ Hz); ^{13}C -NMR (100 MHz, CDCl_3 , δ / ppm): 193.9, 168.2, 162.7, 155.2, 145.9, 133.5, 130.6, 130.4, 130.1, 127.9, 124.9, 124.2, 120.3, 120.1, 117.4, 109.8, 62.6, 56.4, 39.6, 13.9; MS (ESI): m/z 416 $[\text{M} + \text{H}]^+$; HRMS (ESI) Calcd. for $\text{C}_{24}\text{H}_{21}\text{N}_3\text{O}_3$ $[\text{M} + \text{H}]^+$: 416.1605. Found: 416.1597.

Ethyl 2-(1H-benzotriazol-1-yl)-4-(4-chlorophenyl)-4-oxobutanoate (5f). New compound. Yield: 90 %; white solid; m.p. 105–107 °C; ^1H -NMR (400 MHz, CDCl_3 , δ / ppm): 8.08 (1H, *d*, $J = 8.4$ Hz), 7.95–7.93 (2H, *m*), 7.72 (1H, *d*, $J = 8.4$ Hz), 7.59–7.55 (1H, *m*), 7.48–7.45 (2H, *m*), 7.44–7.40 (1H, *m*), 6.18 (1H, *t*, $J = 6.4$ Hz), 4.32 (1H, *dd*, $J_1 = 6.4$ Hz, $J_2 = 18.0$ Hz), 4.25–4.14 (3H, *m*), 1.16 (3H, *t*, $J = 7.2$ Hz); ^{13}C -NMR (100 MHz, CDCl_3 , δ / ppm): 194.3, 168.0, 145.9, 140.5, 134.1, 133.4, 129.7, 129.2, 128.0, 124.3, 120.2, 109.7, 62.7, 56.2, 39.8, 13.9; MS (ESI): m/z 358 (^{35}Cl), 360 (^{37}Cl) $[\text{M} + \text{H}]^+$; HRMS (ESI) Calcd. for $\text{C}_{18}\text{H}_{16}\text{ClN}_3\text{O}_3$ $[\text{M} + \text{H}]^+$: 358.0953. Found: 358.0959.

Ethyl 2-(1H-benzotriazol-1-yl)-4-(furan-2-yl)-4-oxobutanoate (5g). New compound. Yield: 57 %; yellow solid; m.p. 91–93 °C; ^1H -NMR (400 MHz, CDCl_3 , δ / ppm): 8.04 (1H, *d*, $J = 8.4$ Hz), 7.68 (1H, *d*, $J = 8.0$ Hz), 7.59 (1H, *d*, $J = 0.8$ Hz), 7.53 (1H, *t*, $J = 7.2$ Hz), 7.38 (1H, *t*, $J = 7.2$ Hz), 7.26–7.25 (1H, *m*), 6.54–6.53 (1H, *m*), 6.17 (1H, *t*, $J = 7.2$ Hz), 4.22–4.02 (4H, *m*), 1.14 (3H, *t*, $J = 7.2$ Hz); ^{13}C -NMR (100 MHz, CDCl_3 , δ / ppm): 184.1, 167.9, 151.7, 147.2, 145.8, 133.4, 128.0, 124.3, 120.0, 118.4, 112.6, 109.8, 62.7, 55.8, 39.5, 13.9; MS (ESI): m/z 314 $[\text{M} + \text{H}]^+$; HRMS (ESI) Calcd. for $\text{C}_{16}\text{H}_{15}\text{N}_3\text{O}_4$ $[\text{M} + \text{H}]^+$: 314.1135. Found: 314.1131.

Ethyl 2-(1H-benzotriazol-1-yl)-4-oxopentanoate (5h). New compound. Yield: 62 %; yellow solid; m.p. 70–72 °C; ^1H -NMR (400 MHz, CDCl_3 , δ / ppm): 7.87 (2H, *dd*, $J_1 = 3.2$ Hz, $J_2 = 6.8$ Hz), 7.40 (2H, *dd*, $J_1 = 3.2$ Hz, $J_2 = 6.8$ Hz), 6.13 (1H, *t*, $J = 7.2$ Hz), 4.26–4.16 (2H, *m*), 3.72–3.60 (2H, *m*), 2.27 (3H, *s*), 1.20 (3H, *t*, $J = 6.8$ Hz); ^{13}C -NMR (100 MHz, CDCl_3 , δ / ppm): 203.4, 167.8, 144.4, 126.9, 118.3, 63.6, 62.7, 44.3, 30.1, 14.0; MS (ESI): m/z 262 $[\text{M} + \text{H}]^+$; HRMS (ESI) Calcd. for $\text{C}_{13}\text{H}_{15}\text{N}_3\text{O}_3$ $[\text{M} + \text{H}]^+$: 262.1186. Found: 262.1191.

REFERENCES

1. K. Gotoh, T. Yamamoto, M. Yoshimatsu, *Chem. Pharm. Bull.* **54** (2006) 1611
2. M. Yoshimatsu, M. Kawamoto, K. Gotoh, *Eur. J. Org. Chem.* (2005) 2884.



J. Serb. Chem. Soc. 77 (5) 589–597 (2012)
JSCS–4292

Synthesis and evaluation of some novel derivatives of 2-propoxybenzylideneisonicotinohydrazide for their potential antimicrobial activity

MANAV MALHOTRA¹, MANU ARORA², ABDUL SAMAD³, KAPENDRA SAHU⁴,
PRIYANKA PHOGAT⁵ and AAKASH DEEP^{6*}

¹Department of Pharmaceutical Chemistry, Meerut Institute of Engineering and Technology, Bypass Road-Baghat Crossing, Meerut-250005, Uttar Pradesh, India, ²Institute of Pharmacy and Emerging Sciences, Baddi University, Baddi-173205, India, ³Department of Pharmaceutical Chemistry, College of Pharmacy in Al-Kharj, King Saud University, Riyadh, Saudi Arabia, ⁴Department of Pharmaceutical Sciences, Rajiv Gandhi Technical University, Bhopal-462033, India, ⁵Department of Pharmaceutical Sciences, Hindu College of Pharmacy, Sonapat-131001, India and ⁶Department of Pharmaceutical Sciences, Maharshi Dayanand University, Rohtak-124001, India

(Received 10 March, revised 18 June 2011)

Abstract: A novel series of Mannich bases containing isoniazid were prepared. First, reaction of 2-propoxybenzaldehyde with isoniazid gave the corresponding hydrazone (**2a**). Subsequently, product **2a** after the Mannich reaction of aminomethylation with formaldehyde and secondary amines gave **2b–k**. The inhibitory potencies of the synthesized compounds were assayed *in vitro* against a panel of microorganisms and against the A549 human lung adenocarcinoma cell line. Compounds **2c** and **2k** displayed moderate to potent antimicrobial activity against all the tested strains and they also exhibited significant cytotoxicity in a dose-dependent manner with IC_{50} values ranging from 2.84 to 8.55 $\mu\text{g/mL}$ and 0.007–0.030 mM. The structures of the newly synthesized compounds were evaluated by elemental and spectral (IR, ¹H-NMR, ¹³C-NMR) methods. The results demonstrated the potential and importance of developing new Mannich bases which would be effective against resistant microbial strains and may be useful leads for anticancer drug development in the future.

Keywords: benzylidene; antimicrobial; cytotoxicity; Mannich bases; ¹H-NMR; ¹³C-NMR.

INTRODUCTION

The incidence of microbial infections has increased to startling levels worldwide in the last 25 years because of antimicrobial resistance. The hasty develop-

* Corresponding author. E-mail: aakashdeep82@gmail.com
doi: 10.2298/JSC110310170M

ment of resistance to existing antibacterial and antifungal drugs poses a major threat to public health and generates a serious challenge to the scientific community. The increasing number of immuno-compromised patients as a result of cancer chemotherapy, organ transplantation and HIV infection are the major factors contributing to this increase. Consequently, there is a vital need for the development of new antimicrobial agents having potent activity against the resistant microorganism.²⁻⁵ Hydrazones belong to the Schiff base family containing azomethine $-NHN=CH-$ protons and the hydrazone moiety is considered one of the privileged structural fragments in modern medicinal chemistry due to its broad pharmacological vistas. Among the important pharmacophores responsible for antimicrobial activity, the hydrazone group is still considered a viable lead structure for the synthesis of more efficacious and broad-spectrum antimicrobial agents. Some widely used antibacterial drugs, such as nitrofurazone, furazolidone and ftivazide, contain the hydrazone group. Furthermore, pharmacokinetic and cellular permeability of a drug can be increased by derivatization to a bioreversible form of this drug, namely hydrazone. It is believed that the hydrazone functional group increases the lipophilicity of the parent amine and amides, which results in an enhancement of absorption through biomembranes and it is this enhanced lipophilicity of hydrazones which enables them to cross bacterial and fungal membranes.^{6,7} Hydrazones are formed when hydrazines react with an aldehyde or a ketone under specific condition. Hydrazones have been reported to possess antimicrobial,^{8,9} antitubercular,^{10,11} antileprotic,¹² anticonvulsant,¹³ analgesic,¹⁴ anti-inflammatory,^{15,16} antiplatelet,¹⁷ anticancer^{18,19} and antiviral properties.²⁰

Inspired by the above facts and in continuation of an ongoing research program in the field of the synthesis and antimicrobial activity of medicinally important compounds,²¹⁻²⁴ the synthesis and antimicrobial activity of some novel derivatives of isoniazid are reported herein.

EXPERIMENTAL

Melting points of the synthesized compounds were determined in open-glass capillaries on a Stuart SMP10 melting point apparatus and are uncorrected. The purity of the compounds was checked by thin layer chromatography (TLC). Silica gel plates 0.25 mm, 60 GF₂₅₄, pre-coated sheets, obtained from Merck, Darmstadt (Germany), were used for the TLC and the spots were visualized by iodine vapor or ultraviolet light as visualizing agents. The infrared (IR) spectra were obtained on a Perkin-Elmer 1600 FTIR spectrometer in KBr pellets. The nuclear magnetic resonance (NMR) spectra were recorded in deuterated dimethyl sulfoxide (DMSO-*d*₆) solutions using tetramethylsilane as the internal reference. A Varian-Mercury 300 MHz spectrometer was used for recording the ¹H-NMR spectra while the ¹³C-NMR spectra were acquired on a Bruker Avance II 400 spectrometer. Elemental analyses were performed on an ECS 4010 elemental combustion system. The necessary chemicals were purchased from Loba Chemie, Fluka and Sigma-Aldrich.

Synthesis of 2-propoxybenzylideneisonicotinohydrazide.

A mixture of 2-propoxybenzaldehyde (1.64 g, 0.010 mol) and isoniazid (1.37 g, 0.010 mol) in 15 ml of super dry ethanol was refluxed for 5 h. Completion of the reaction was confirmed by thin layer chromatography (TLC). The reaction mixture was then poured into ice-cold water and the obtained precipitate was filtered and dried in oven at a low temperature. The product was recrystallized from absolute ethanol.

Synthesis of substituted Mannich bases (2b–k)

2-Propoxybenzylideneisonicotinohydrazide (**1**) (679 mg, 0.0024 mol), formaldehyde (0.10 ml, 0.0036 mol) and the required substituted secondary amine (0.0024 mol) were placed in 100 ml round-bottom flask to which 50 ml of super dry ethanol was added, the pH was adjusted to 4 with hydrochloric acid and the mixture was refluxed for 28–33 h. Completion of the reaction was confirmed by TLC. The reaction mixture was allowed to cool to room temperature and then diethyl ether was added. The reaction mixture was kept for 3–5 h in a refrigerator. The resulting solid was filtered off and washed with *n*-hexane. The products were recrystallized from absolute ethanol.

Antimicrobial evaluation

The synthesized compounds were evaluated for their *in vitro* antimicrobial activity against the Gram-positive bacteria *Staphylococcus aureus* (MTCC 96), *Bacillus subtilis* (MTCC 121), Gram-negative *Escherichia coli* (MTCC 40), *Pseudomonas aeruginosa* (MTCC 2453) and the fungal strains *Candida albicans* (MTCC 227) and *Aspergillus niger* (MTCC 8189). The antimicrobial activity was assessed by the serial two-fold dilution technique. Amoxicillin was used as the standard drug for the antibacterial activity and nystatin was used as the standard drug for the antifungal activity. All the compounds were dissolved in dimethyl sulfoxide (DMSO) to give a concentration of 100 $\mu\text{g mL}^{-1}$. Twofold dilutions of the test and standard compounds were prepared in double strength nutrient broth for bacteria (Indian Pharmacopoeia: peptone 10 g, meat extracts 10 g, sodium chloride 0.5 g, distilled water 1000 mL, and pH 7.2 \pm 0.2) or Sabouraud dextrose broth for fungi (Indian Pharmacopoeia)²⁵. The stock solutions were serially diluted to give concentrations of 50–0.78 $\mu\text{g mL}^{-1}$ in the respective nutrient broth. The inoculum size was approximately 10⁶ colony forming units (CFU) mL⁻¹. The tubes were incubated at 37 \pm 1 °C for 24 h (bacteria) and 25 °C for 7 d (*A. niger*) and 37 \pm 1 °C for 48 h (*C. albicans*). After incubation, the inoculated culture tubes were macroscopically examined for turbidity. The culture tube showing turbidity (lower concentration) and the culture tube showing no turbidity (higher concentration) gave the minimum inhibitory concentration (MIC) for the compound.

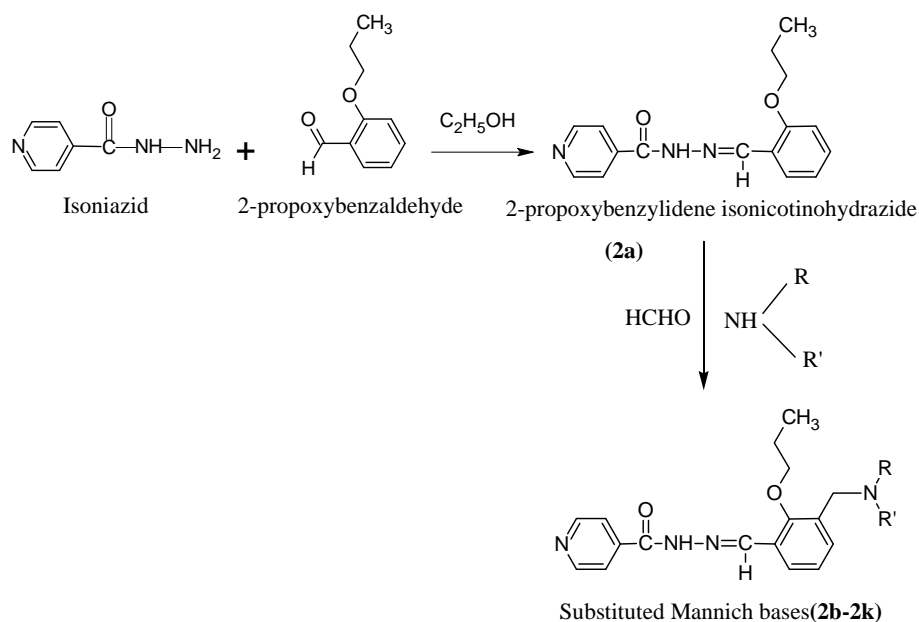
Cytotoxicity studies

The A549 (human lung adenocarcinoma) cell line was obtained from the National Centre for Cell Science, Pune, India. The cells were grown in Dulbecco's modified Eagle medium (DMEM) supplemented with 2 mmol L⁻¹ L-glutamine, 10 % fetal bovine serum (FBS), penicillin (50 IU mL⁻¹) and streptomycin (50 mg mL⁻¹) at a temperature of 37 °C in a humidified incubator with a 5 % CO₂ atmosphere. Gemcitabine, a well known anticancer drug, was used as the positive control for comparison.²⁶ The viability of the cells was assessed by the MTT 2-(5-dimethylthiazol-2-yl)-3,5-diphenyl-2H-tetrazolium bromide assay, which is based on the reduction of MTT by the mitochondrial dehydrogenase of intact cells to a purple formazan product.²⁷ Cells (1 \times 10⁴) were placed in a 96-well plate. After 24 h, they were treated with different concentrations (0–25 $\mu\text{g/mL}$) of the test compounds diluted appropriately with culture media for 48 h. Cells grown in media containing an equivalent amount of DMSO served

as the positive control and cells in medium without any supplementation were used as the negative control. After the treatment, the media containing the compounds were carefully removed. MTT in phosphate-buffered saline (PBS, 100 μL , 0.40 mg mL^{-1}) was added to each well and incubated in the dark for 4 h. Then DMSO (100 μL) was added to each well and kept in an incubator for 4 h for dissolution of the formed formazan crystals. The amount of formazan was determined by measuring the absorbance at 540 nm using an ELISA plate reader. The data are presented as percent post treatment recovery (% of live cells), whereas the absorbance from non-treated control cells was defined as 100 % live cells.

RESULT AND DISCUSSION

The synthesis of target compounds were carried as outlined in the Scheme 1. An equimolar quantity of 2-propoxybenzaldehyde and isoniazid in 15 ml of absolute ethanol was refluxed for 7 h to form acid hydrazone. The completion of reaction was confirmed by thin layer chromatography (TLC). Then 2-propoxybenzylideneisonicotinohydrazide along with formaldehyde and secondary amines was refluxed for 34–42 h in presence of 50 ml of super dry ethanol and the pH was adjusted to 4 with hydrochloric acid. The employed secondary amines are specified in Table I.



Scheme 1. General synthetic pathway for the formation of the title compounds.

The purity of the compounds was checked by TLC and they were characterized by elemental analysis and IR, ^1H - and ^{13}C -NMR spectroscopy. The results of the elemental analyses and the spectral data are given in the Supplementary data to this paper.

In general, the IR spectra of all compounds **2a–k** showed absorption band in the 3279–3255, 2978–2946, 2862–2835, 1677–1663, 1659–1641, 1581–1552, 1174–1125 and 1079–1038 cm^{-1} regions, conforming the presence of NH, CH, CH_2 , C=N, C=O, C=C and C–N, respectively. The structures of the prepared derivatives were confirmed by their $^1\text{H-NMR}$ spectrum based on the chemical shifts, multiplicities, and coupling constants. The spectra of most compounds showed the characteristic NH proton at δ 11.98–11.79 ppm, the proton of $-\text{N}=\text{C}-\text{H}$ at δ 8.79–8.21 ppm, the 4 protons of pyridine at around δ 8.86–7.46 ppm, the characteristic protons of benzylidene at δ 7.77–6.78 ppm, the 2 protons of $\text{Ar}-\text{O}-\text{CH}_2$ at δ 3.94–3.62 ppm and the 2 protons of $\text{Ar}-\text{CH}_2-\text{N}$ at δ 3.69–3.49 ppm. The $^{13}\text{C-NMR}$ spectra of most compounds had characteristic signals of C=O at around δ 163.91–163.18 ppm, of pyridine at δ 149.88–122.15 ppm, of the $-\text{N}=\text{C}-\text{H}$ group at δ 143.48–143.19 ppm, of benzylidene at δ 157.58–115.75 ppm and of $\text{Ar}-\text{O}-\text{CH}_2$ at δ 72.84–72.19 ppm and $\text{Ar}-\text{CH}_2-\text{N}$ at δ 55.89–45.59 ppm.

TABLE I. Structure and physical data of the synthesized Mannich bases

Compound	R	Molecular formulae	Yield, %	M.p., °C
2b	$-\text{N}(\text{CH}_3)_2$	$\text{C}_{19}\text{H}_{24}\text{N}_2\text{O}_2$	48	227–230
2c	$-\text{N}(\text{C}_2\text{H}_5)_2$	$\text{C}_{21}\text{H}_{28}\text{N}_4\text{O}_2$	45	235–238
2d	$-\text{N}(\text{C}_3\text{H}_7)_2$	$\text{C}_{23}\text{H}_{32}\text{N}_4\text{O}_2$	52	212–215
2e	$-\text{N}(\text{C}_4\text{H}_9)_2$	$\text{C}_{25}\text{H}_{36}\text{N}_4\text{O}_2$	43	218–221
2f	$-\text{N}(\text{C}_6\text{H}_5)_2$	$\text{C}_{29}\text{H}_{28}\text{N}_4\text{O}_2$	39	182–185
2g		$\text{C}_{22}\text{H}_{28}\text{N}_4\text{O}_2$	48	188–191
2h		$\text{C}_{21}\text{H}_{26}\text{N}_4\text{O}_2$	45	193–196
2i		$\text{C}_{21}\text{H}_{26}\text{N}_4\text{O}_3$	40	223–226
2j		$\text{C}_{21}\text{H}_{27}\text{N}_5\text{O}_2$	43	205–208
2k		$\text{C}_{22}\text{H}_{29}\text{N}_5\text{O}_2$	46	117–120

The compounds were evaluated for their antimicrobial properties in comparison the control antibacterial agent amoxicillin and antifungal agent nystatin.

The results of antibacterial screening, Table II, revealed that all the tested compounds showed moderate to good bacterial inhibition. Compounds **2c** and **2k** displayed excellent activity against the microbial strains. Compounds **2d**, **2h**, **2i**

TABLE II. Antimicrobial screening results ($MIC / \mu g mL^{-1}$) of the tested compounds

Compound	Gram-positive bacteria		Gram-negative bacteria		Fungal strain	
	<i>B. subtilis</i>	<i>S. aureus</i>	<i>P. aeruginosa</i>	<i>E. coli</i>	<i>C. albicans</i>	<i>A. nigar</i>
2a	25	12.5	12.5	6.25	25	12.5
2b	6.25	12.5	3.12	6.25	25	>100
2c	0.78	1.56	1.56	3.12	1.56	3.12
2d	3.12	12.5	6.25	25	12.5	12.5
2e	25	>100	12.5	6.25	3.12	12.5
2f	12.5	6.25	12.5	12.5	6.25	>100
2g	12.5	25	25	12.5	12.5	6.25
2h	6.25	25	12.5	6.25	12.5	25
2i	6.25	6.25	12.5	12.5	12.5	3.12
2j	6.25	12.5	6.25	12.5	12.5	6.25
2k	3.12	6.25	1.56	1.56	12.5	25
Amoxicillin	0.15	0.15	0.25	0.15	–	–
Nystatin	–	–	–	–	0.25	0.78

and **2j** showed moderate antibacterial activity. Of all the synthesized derivatives, compound **2a** was found to be the least active compound against most of bacterial strains. Concerning the antifungal activity of the tested compounds, only two fungal strains were selected, *C. albicans* and *A. niger*. The data of the antifungal screening, Table II, revealed that all the tested compounds showed moderate to good fungal inhibition as compared to standard drug nystatin. Among the derivatives, compound **2c** exhibited the highest antifungal activity against both fungal strains, while compounds **2e**, **2g** and **2j** showed moderate antifungal activity. Of all the synthesized derivatives, compound **2b** was found to be the least active compound against both fungal strains.

In addition, all the tested compounds demonstrated remarkable cytotoxicity against A549 lung cancer cell line, Table III. In particular, compounds **2c** and **2k** displayed significant inhibitory activity superior to that of the reference compound gemcitabine.

TABLE III. The cytotoxicity data against the A549 lung cancer cell line of the synthesized compounds

Compound	Cell death at various doses (in $\mu\text{g/mL}$), %					IC_{50}^a $\mu\text{g mL}^{-1}$	IC_{50} mM
	1	2	5	10	25		
2a	3.13	17.55	30.85	47.62	60.81	8.55	0.030
2b	4.19	18.13	31.18	48	61.28	8.12	0.023
2c	10.54	30.73	41.18	73.48	77.29	2.84	0.007
2d	9.12	23.26	36.55	69.84	71.39	4.18	0.010
2e	5.83	19.63	32.15	60.45	65.64	6.58	0.015
2f	4.15	18.25	31.52	51.13	62.81	7.73	0.016
2g	4.85	18.33	31.87	55.18	64.35	7.15	0.018
2h	9.15	21.35	34.16	66.65	70.19	5.18	0.014
2i	8.87	20.17	32.55	63.72	69.39	5.92	0.015
2j	8.22	19.77	32.12	61.15	66.29	6.29	0.016
2k	9.53	25.23	39.19	71.19	74.11	3.36	0.008
Gemcitabine	6.53	15.18	25.93	54.58	71.18	6.19	0.023

^aThe half maximal (50%) inhibitory concentration (IC) of a substance

CONCLUSIONS

In conclusion, the present paper describes the preparation and biological evaluation of a series of novel isoniazid derivatives. The synthesized compounds were characterized by suitable analytical techniques, *i.e.*, IR, ¹H-NMR, ¹³C-NMR and elemental analysis and the data obtained was in full agreement of the proposed structures. Among the synthesized derivatives, compound **2c** and **2k**, having a diethylamino and methylpiperazine moieties, were the most active compounds with significant biological activity. Based on preliminary antimicrobial and cytotoxicity results, it is supposed that both these compounds display antimicrobial and cytotoxicity activities through a non-specific mechanism of action or that they exert antimicrobial action due to their cytotoxicity activity. Taken together, the compounds reported in this paper could serve as potential leads for future studies and that further investigations are warranted to determine the mechanism of action of these molecules.

SUPPLEMENTARY MATERIAL

Analytical and spectral data of synthesized compounds are available electronically from <http://www.shd.org.rs/JSCS/>, or from the corresponding author on request.

ИЗВОД

СИНТЕЗА И ИСПИТИВАЊЕ АНТИМИКРОБНЕ АКТИВНОСТИ НЕКИХ НОВИХ
ДЕРИВАТА 2-ПРОПОКСИБЕНЗИЛИДЕН-ИЗОНИКОТИНОХИДРАЗИДА

MANAV MALHOTRA¹, MANU ARORA², ABDUL SAMAD³, KAPENDRA SAHU⁴,
PRIYANKA PHOGAT⁵ и AAKASH DEEP⁶

¹Department of Pharmaceutical Chemistry, Meerut Institute of Engineering and Technology, Bypass Road-Baghpat Crossing, Meerut-250005, Uttar Pradesh, India, ²Institute of Pharmacy and Emerging Sciences, Baddi University, Baddi-173205, India, ³Department of Pharmaceutical Chemistry, College of Pharmacy in Al-Kharj, King Saud University, Riyadh, Saudi Arabia, ⁴Department of Pharmaceutical Sciences, Rajiv Gandhi Technical University, Bhopal-462033, India, ⁵Department of Pharmaceutical Sciences, Hindu College of Pharmacy, Sonapat-131001 и ⁶Department of Pharmaceutical Sciences, Maharshi Dayanand University, Rohtak-124001, India

Синтетисана је серија нових Манихових база, деривата изонијазида. Прво је реакцијом 2-пропоксибензалдехида са изонијазидом добијен одговарајући хидразон (**2a**). Производ **2a** је у Маниховој реакцији аминометиловања формалдехидом и секундарним аминима дао производе (**2b–k**). Инхибиторна *in vitro* активност добијених једињења испитана је према панелу микроорганизама и А549 ћелијској линији аденокарцинома плућа. Деривати **2c** и **2k** имају умерену активност према микроорганизмима, и показују значајну цитотоксичност која зависи од примењене концентрације једињења. IC₅₀ вредности налазе се у опсегу 2,84–8,55 µg/mL и 0,007–0,030 mM. Структуре синтетисаних једињења одређене су на основу резултата елементарне анализе и спектралних података (IC, ¹H-NMR и ¹³C-NMR). Добијени резултати показују на значај развоја Манихових база, које могу бити активне према резистентним сојевима микроорганизама, и могу бити развијани као успешни модели за развој анти-туморских једињења.

(Примљено 10. марта, ревидирано 18. јуна 2011)

REFERENCES

1. M. Koca, S. Servi, C. Kirilimis, M. Ahmedzade, C. Kazaz, B. Ozbek, G. Otuk, *Eur. J. Med. Chem.* **40** (2005) 1351
2. C. Bonde, N. J. Gaikwad, *Bioorg. Med. Chem.* **12** (2004) 2151
3. D. Yu, G. Huiyuan, *Bioorg. Med. Chem. Lett.* **12** (2002) 857
4. S. D. Joshi, H. M. Vagdevi, V. P. Vaidya, G. S. Gadaginamath, *Eur. J. Med. Chem.* **43** (2008) 1989
5. S. Rollas, S. G. Kucukguzel, *Molecules.* **12** (2007) 1910
6. S. T. Murphy, H. L. Case, E. Ellsworth, S. Hagen, M. Husband, T. Jonnides, C. Limberakis, R. Marotti, A. M. Ottolini, M. Rauckhorst, J. Starr, M. Stier, C. Taylor, T. Zhu, A. Blasser, W. A. Denny, G. L. Lu, J. B. Smailic, F. Rivault, *Bioorg. Med. Chem. Lett.* **17** (2007) 2150
7. T. Scior, S. J. Garces-Eisele, *Curr. Med. Chem.* **13** (2006) 2205
8. S. Rollas, N. Gulerman, H. Edinz, *Farmaco* **57** (2002) 171
9. A. Imramovsky, S. Polanac, J. Vinsova, M. Kocevar, J. Jampitek, Z. Reckova, J. A. Kaustova, *Bioorg. Med. Chem.* **15** (2007) 4229
10. M. J. Hearn, M. H. Cynamon, M. F. Chen, R. Coppins, J. Davis, H. O. J. Kang, A. Noble, B. T. Sekine, M. S. Terrot, D. Trombino, M. Thai, E. R. Webster, R. Wilson, *Eur. J. Med. Chem.* **44** (2009) 4169
11. S. J. Gilani, S. A. Khan, N Siddiqui, *Bioorg. Med. Chem. Lett.* **20** (2010) 4762

12. F. R. Pavan, P. I. D. S. Maia, S. R. Leite, V. M. Deflon, A. A. Batista, D. N. Sato, S. G. Franzblau, C. Q. Leite, *Eur. J. Med. Chem.* **45** (2010) 1898
13. R. Sinha, U. V. S. Sara, R. L. Khosa, J. Stables, J. Jain, *Med. Chem. Res.* **20** (2011) 1499
14. U. Salgin-Goksen, N. Gokhan-Kelekci, O. Goktas, Y. Koysal, E. Kilic, S. Isik, G. Aktay, M. Ozalp, *Bioorg. Med. Chem.* **15** (2007) 5738
15. M. Malhotra, S. Sharma, A. Deep, *Med. Chem. Res.* **21** (2012) 1237
16. G. A. Silva, L. M. M. Costa, F. C. F. Brito, A. L. P. Miranda, E. J. Barreiro, C. A. M. Fraga, *Bioorg. Med. Chem.* **12** (2004) 3149
17. L. Savini, L. Chiasserini, V. Travagli, C. Pellerano, E. Novellino, S. Consentino, M. B. Pisano, *Eur. J. Med. Chem.* **39** (2004) 113
18. A. Bijev, *Lett. Drug Des. Discovery* **3** (2006) 506
19. C. Loncle, J. M. Brunel, N. Vidal, M. D. Herbomez, Y. Letourneux, *Eur. J. Med. Chem.* **39** (2004) 1067
20. M. T. Abdel-Aal, W. A. El-Sayed, E. H. El-Ashry, *Arch. Pharm. Chem. Life Sci.* **339** (2006) 656
21. A. Deep, S. Jain, P. C. Sharma, P. Verma, M. Kumar, C. P. Dora, *Acta Pol. Pharm.* **67** (2010) 255
22. A. Madhukar, N. Kannappan, A. Deep, P. Kumar, M. Kumar, P. Verma, *Int. J. ChemTech Res.* **1** (2009) 1376
23. M. Kumar, S. Jain, A. Deep, *Lat. Am. J. Pharm.* **30** (2010) 388
24. A. Deep, S. Jain, P. C. Sharma, S. K. Mittal, P. Phogat, M. Malhotra, *Arab. J. Chem.* (2011) doi: 10.1016/j.arabjc.2010.10.032
25. *Pharmacopoeia of India*, Vol. II, Ministry of Health Department, Government of India, New Delhi, 1996, p. A-88
26. R. H. Kenneth, P. J. Wedlund, R. M. Noone, G. R. Wilkinson, F. A. Greco, S. N. Wolff, *Cancer Res.* **44** (1984) 379
27. T. Mossman, *J. Immunol. Methods* **65** (1983) 55.



SUPPLEMENTARY MATERIAL TO
**Synthesis and evaluation of some novel derivatives of
2-propoxybenzylideneisonicotinohydrazide for their
potential antimicrobial activity**

MANAV MALHOTRA¹, MANU ARORA², ABDUL SAMAD³, KAPENDRA SAHU⁴,
PRIYANKA PHOGAT⁵ and AAKASH DEEP^{6*}

¹Department of Pharmaceutical Chemistry, Meerut Institute of Engineering and Technology, Bypass Road-Baghat Crossing, Meerut-250005, Uttar Pradesh, India, ²Institute of Pharmacy and Emerging Sciences, Baddi University, Baddi-173205, India, ³Department of Pharmaceutical Chemistry, College of Pharmacy in Al-Kharj, King Saud University, Riyadh, Saudi Arabia, ⁴Department of Pharmaceutical Sciences, Rajiv Gandhi Technical University, Bhopal-462033, India, ⁵Department of Pharmaceutical Sciences, Hindu College of Pharmacy, Sonapat-131001, India and ⁶Department of Pharmaceutical Sciences, Maharshi Dayanand University, Rohtak-124001, India

J. Serb. Chem. Soc. 77 (5) (2012) 589–597

ANALYTICAL AND SPECTRAL DATA OF THE SYNTHESIZED COMPOUNDS

N'-(2-Propoxybenzylidene)isonicotinohydrazide (**2a**). Yield 68 %; m.p. 201–204 °C; Anal. Calcd. for C₁₆H₁₇N₃O₂: C, 67.83; H, 6.05; N, 14.83 %. Found: C, 67.85; H, 6.09, N, 14.77 %; IR (KBr, cm⁻¹): 3264, 2948, 2859, 2839, 1667, 1655, 1557, 1125, 1075; ¹H-NMR (300 MHz, DMSO-*d*₆, δ / ppm): 11.98 (1H, *s*, –NH–N=), 8.86 (2H, *d*, *J* = 4.5 Hz, pyridine), 8.79 (1H, *s*, –N=C–H), 7.81 (2H, *d*, *J* = 4.2 Hz, pyridine), 7.73 (2H, *d*, *J* = 7.8 Hz, benzylidene), 7.37 (2H, *d*, *J* = 7.5 Hz, benzylidene), 3.89 (2H, *t*, *J* = 6.8 Hz, OCH₂), 1.69 (2H, *m*, CH₂), 1.18 (3H, *s*, CH₃); ¹³C-NMR (100 MHz, DMSO-*d*₆, δ / ppm): 163.62, 157.49, 149.86, 143.19, 139.82, 131.67, 129.84, 122.62, 120.67, 117.34, 114.53, 72.81, 25.27, 12.37.

N'-(3-((Dimethylamino)methyl)-2-propoxybenzylidene)isonicotinohydrazide (**2b**). Anal. Calcd. for C₁₉H₂₄N₄O₂: C, 67.04; H, 7.11; N, 16.46 %. Found: C 67.17, H 7.10, N 16.34 %; IR (KBr, cm⁻¹): 3265, 2978, 2862, 2843, 1675, 1654, 1559, 1135, 1068; ¹H-NMR (300 MHz, DMSO-*d*₆, δ / ppm): 11.85 (1H, *s*, –NH–N=), 8.64 (2H, *d*, *J* = 4.2 Hz, pyridine), 8.51 (1H, *s*, –N=C–H), 7.77 (2H, *d*, *J* = 3.8 Hz, pyridine), 7.58 (2H, *d*, *J* = 3.2 Hz, benzylidene), 7.28 (1H, *t*, benzylidene), 3.85 (2H, *t*, *J* = 6.2 Hz, OCH₂), 3.62 (2H, *s*, Ar–CH₂–N), 2.21 (6H, *s*, N–(CH₃)₂),

* Corresponding author. E-mail: aakashdeep82@gmail.com

1.89 (2H, *m*, CH₂), 1.15 (3H, *t*, *J* = 9.3 Hz, CH₃); ¹³C-NMR (100 MHz, DMSO-*d*₆, δ / ppm): 163.55, 157.51, 149.17, 143.45, 139.74, 132.17, 128.18, 122.53, 121.22, 120.44, 115.87, 72.47, 54.71, 46.22, 22.75, 12.87.

N'-(3-((Diethylamino)methyl)-2-propoxybenzylidene)isonicotinohydrazide (**2c**). Anal. Calcd. for C₂₁H₂₈N₄O₂: C, 68.45; H, 7.66; N, 15.21 %. Found: C, 68.35; H, 7.61; N, 15.36; IR (KBr, cm⁻¹): 3259, 2956, 2863, 2841, 1666, 1652, 1552, 1153, 1079; ¹H-NMR (300 MHz, DMSO-*d*₆, δ / ppm): 11.94 (1H, *s*, -NH-N=), 8.68 (2H, *d*, *J* = 4.5 Hz, pyridine), 8.54 (1H, *s*, -N=C-H), 7.64 (2H, *d*, *J* = 3.9 Hz, pyridine), 7.43 (2H, *d*, *J* = 3.2 Hz, benzylidene), 7.12 (1H, *t*, *J* = 7.8 Hz, benzylidene), 3.92 (2H, *t*, *J* = 6.5 Hz, OCH₂), 3.65 (2H, *s*, Ar-CH₂-N), 2.42 (4H, *m*, N-2(CH₂)), 1.89 (2H, *m*, CH₂), 1.08 (9H, *m*, 3CH₃); ¹³C-NMR (100 MHz, DMSO-*d*₆, δ / ppm): 163.18, 157.29, 149.88, 143.26, 139.77, 132.23, 128.66, 122.55, 121.12, 120.52, 116.78, 72.59, 52.77, 48.18, 22.37, 13.76, 12.91.

N'-(3-((Dipropylamino)methyl)-2-propoxybenzylidene)isonicotinohydrazide (**2d**). Anal. Calcd. for C₂₃H₃₂N₄O₂: C, 69.97; H, 8.13; N, 14.13 %. Found: C, 69.95; H, 8.10; N, 14.18 %; IR (KBr, cm⁻¹): 3259, 2956, 2863, 2841, 1666, 1652, 1552, 1152, 1079; ¹H-NMR (300 MHz, DMSO-*d*₆, δ / ppm): 11.79 (1H, *s*, -NH-N=), 8.78 (2H, *d*, *J* = 4.1 Hz, pyridine), 8.47 (1H, *s*, -N=C-H), 7.98 (2H, *d*, *J* = 3.8 Hz, pyridine), 7.35 (2H, *d*, *J* = 3.1 Hz, benzylidene), 7.17 (1H, *t*, *J* = 7.5 Hz, benzylidene), 3.92 (2H, *t*, *J* = 6.9 Hz, OCH₂), 3.68 (2H, *s*, Ar-CH₂-N), 2.54 (4H, *t*, N-2(CH₂)), 1.68 (6H, *m*, 3CH₂), 1.07 (9H, *m*, 3CH₃); ¹³C-NMR (100 MHz, DMSO-*d*₆, δ / ppm): 163.19, 157.38, 149.74, 143.19, 139.85, 132.17, 128.47, 122.48, 121.78, 119.89, 116.45, 72.23, 55.89, 51.73, 23.77, 21.75, 13.18, 12.89.

N'-(3-((Dibutylamino)methyl)-2-propoxybenzylidene)isonicotinohydrazide (**2e**). Anal. Calcd. for C₂₅H₃₆N₄O₂: C, 70.72; H, 8.55; N, 13.20 %. Found: C, 70.68; H, 8.64; N, 13.15 %; IR (KBr, cm⁻¹): 3269, 2967, 2858, 2843, 1663, 1658, 1561, 1174, 1058. ¹H-NMR (300 MHz, DMSO-*d*₆, δ / ppm): 11.85 (1H, *s*, -NH-N=), 8.72 (2H, *d*, *J* = 4.1 Hz, pyridine), 8.39 (1H, *s*, -N=C-H), 7.74 (2H, *d*, *J* = 3.9 Hz, pyridine), 7.31 (2H, *d*, *J* = 3.2 Hz, benzylidene), 7.15 (1H, *t*, *J* = 7.9 Hz, benzylidene), 3.49 (2H, *t*, *J* = 5.9 Hz, OCH₂), 3.62 (2H, *s*, Ar-CH₂-N), 2.35 (4H, *t*, N-2(CH₂)), 1.66 (10 H, *m*, 5CH₂), 1.04 (9H, *t*, 3CH₃); ¹³C-NMR (100 MHz, DMSO-*d*₆, δ / ppm): 163.14, 157.45, 149.54, 146.18, 143.27, 139.81, 131.93, 128.35, 122.85, 121.87, 120.74, 116.87, 72.38, 55.18, 52.81, 32.85, 20.25, 21.77, 14.18, 12.92.

N'-(3-((Diphenylamino)methyl)-2-propoxybenzylidene)isonicotinohydrazide (**2f**). Anal. Calcd. for C₂₉H₂₈N₄O₂: C, 74.98; H, 6.08; N, 12.06 %. Found: C, 74.91; H, 6.18; N, 12.03 %; IR (KBr, cm⁻¹): 3255, 2956, 2861, 2845, 1669, 1649, 1558, 1155, 1062; ¹H-NMR (300 MHz, DMSO-*d*₆, δ / ppm): 11.92 (1H, *s*, -NH-N=), 8.68 (2H, *d*, *J* = 4.2 Hz, pyridine), 8.27 (1H, *s*, -N=C-H), 7.59 (2H, *d*, *J* = 3.7 Hz, pyridine), 7.25–6.78 (13H, *m*, benzylidene), 3.84 (2H, *t*, *J* = 6.5 Hz,

OCH₂), 3.69 (2H, *s*, Ar-CH₂-N), 1.64 (2H, *m*, CH₂), 1.04 (9H, *t*, 3CH₃); ¹³C-NMR (100 MHz, DMSO-*d*₆, δ / ppm): 163.69, 155.28, 149.74, 143.29, 139.84, 129.75, 127.88, 122.76, 119.75, 118.72, 117.95, 116.84, 72.44, 45.59, 23.79, 12.76.

3-(Piperidin-1-ylmethyl)-N'-(2-propoxybenzylidene)isonicotinohydrazide (2g).
Anal. Calcd. for C₂₂H₂₈N₄O₂: C, 69.45; H, 7.42; N, 14.73 %. Found: C, 69.48; H, 7.47; N, 14.65 %; IR (KBr, cm⁻¹): 3268, 2968, 2862, 2843, 1667, 1644, 1569, 1168, 1072; ¹H-NMR (300 MHz, DMSO-*d*₆, δ / ppm): 11.89 (1H, *s*, -NH-N=), 8.64 (2H, *d*, *J* = 4.5 Hz, pyridine), 8.21 (1H, *s*, -N=C-H), 7.46 (2H, *d*, *J* = 4.2 Hz, pyridine), 7.54 (2H, *d*, *J* = 3.2 Hz, benzylidene), 7.18 (1H, *t*, *J* = 7.6 Hz, benzylidene), 3.85 (2H, *t*, *J* = 6.8 Hz, OCH₂), 3.62 (2H, *s*, Ar-CH₂-N), 2.62 (4H, *t*, N-2(CH₂), 1.74 (2H, *m*, CH₂), 1.52 (6H, *m*, 3CH₂), 1.06 (3H, *t*, *J* = 7.6 Hz, CH₃); ¹³C-NMR (100 MHz, DMSO-*d*₆, δ / ppm): 163.19, 157.28, 149.74, 146.73, 143.39, 139.48, 131.76, 128.39, 122.83, 121.55, 121.18, 120.29, 116.77, 72.42, 55.79, 52.34, 26.63, 24.37, 22.18, 12.44.

N'-(2-Propoxy-3-(pyrrolidin-1-ylmethyl)benzylidene)isonicotinohydrazide (2h).
Anal. Calcd. for C₂₁H₂₆N₄O₂: C, 68.83; H, 7.15; N, 15.29 %. Found: C, 68.71; H, 7.18; N, 15.38 %; IR (KBr, cm⁻¹): 3269, 2958, 2862, 2844, 1669, 1642, 1572, 1167, 1075; ¹H-NMR (300 MHz, DMSO-*d*₆, δ / ppm): 11.83 (1H, *s*, -NH-N=), 8.68 (2H, *d*, *J* = 4.3 Hz, pyridine), 8.43 (1H, *s*, -N=C-H), 7.85 (2H, *d*, *J* = 3.9 Hz, pyridine), 7.59 (2H, *d*, *J* = 3.2 Hz, benzylidene), 7.19 (1H, *t*, *J* = 7.6 Hz, benzylidene), 3.91 (2H, *t*, *J* = 6.9 Hz, OCH₂), 3.58 (2H, *s*, Ar-CH₂-N), 2.31 (4H, *t*, N-2(CH₂), pyrrolidine), 1.68–1.55 (6H, *m*, 3CH₂), 1.05 (3H, *t*, *J* = 9.3 Hz, CH₃); ¹³C-NMR (100 MHz, DMSO-*d*₆, δ / ppm): 163.55, 157.38, 149.69, 143.23, 139.27, 131.87, 128.39, 122.77, 121.57, 120.26, 116.76, 72.84, 58.89, 52.84, 26.67, 23.58, 12.76.

3-(Morpholinomethyl)-N'-(2-propoxybenzylidene)isonicotinohydrazide (2i).
Anal. Calcd. for C₂₁H₂₆N₄O₃: C, 65.95; H, 6.85; N, 14.65 %. Found: C, 65.85; H, 6.88; N, 14.72 %; IR (KBr, cm⁻¹): 3273, 2973, 2861, 2845, 1676, 1641, 1581, 1154, 1068; ¹H-NMR (300 MHz, DMSO-*d*₆, δ / ppm): 11.92 (1H, *s*, -NH-N=), 8.85 (2H, *d*, *J* = 4.2 Hz, pyridine), 8.46 (1H, *s*, -N=C-H), 7.79 (2H, *d*, *J* = 3.8 Hz, pyridine), 7.38 (2H, *d*, *J* = 3.1 Hz, benzylidene), 7.19 (1H, *t*, *J* = 7.5 Hz, benzylidene), 3.94 (2H, *t*, *J* = 6.3 Hz, OCH₂), 3.55 (2H, *s*, Ar-CH₂-N), 3.45 (4H, *t*, O-2(CH₂), morpholine), 2.31 (4H, *t*, N-2(CH₂), morpholine), 1.65 (2H, *m*, CH₂), 1.08 (3H, *t*, *J* = 8.9 Hz, CH₃); ¹³C-NMR (100 MHz, DMSO-*d*₆, δ / ppm): 163.81, 157.18, 149.81, 143.39, 139.75, 131.68, 128.39, 122.15, 121.59, 120.38, 116.78, 72.81, 67.47, 54.27, 52.66, 23.45, 12.35.

3-(Piperazin-1-ylmethyl)-N'-(2-propoxybenzylidene)isonicotinohydrazide (2j).
Anal. Calcd. for C₂₁H₂₇N₅O₂: C, 66.12; H, 7.13; N, 18.36 %. Found: C, 66.24; H, 7.05; N 18.32 %; IR (KBr, cm⁻¹): 3274, 2977, 2862, 2842, 1675, 1643, 1579, 1164, 1038; ¹H-NMR (300 MHz, DMSO-*d*₆, δ / ppm): 11.89 (1H, *s*, -NH-N=),

8.72 (2H, *d*, $J = 4.1$ Hz, pyridine), 8.35 (1H, *s*, $-\text{N}=\text{C}-\text{H}$), 7.69 (2H, *d*, $J = 3.7$ Hz, pyridine), 7.69 (2H, *d*, $J = 3.2$ Hz, benzylidene), 7.19 (1H, *t*, $J = 7.5$ Hz, benzylidene), 4.12 (1H, *s*, NH, D_2O exchangeable), 3.89 (2H, *m*, OCH_2), 3.65 (2H, *s*, $\text{Ar}-\text{CH}_2-\text{N}$), 2.68–2.48 (8H, *m*, 4CH_2 , piperazine), 1.68 (2H, *m*, CH_2), 1.05 (3H, *t*, $J = 8.8$ Hz, CH_3); ^{13}C -NMR (100 MHz, $\text{DMSO}-d_6$, δ / ppm): 163.58, 157.46, 149.12, 143.38, 139.48, 131.75, 128.35, 122.45, 121.62, 120.65, 116.58, 72.26, 55.69, 52.27, 47.35, 25.18, 12.18.

3-((4-Methylpiperazin-1-yl)methyl)- N' -(2-propoxybenzylidene)isonicotinohydrazide (**2k**). Anal. Calcd. for $\text{C}_{22}\text{H}_{29}\text{N}_5\text{O}_2$: C, 66.81; H, 7.39; N, 17.71 %. Found: C, 66.73; H, 7.43; N, 17.75 %. IR (KBr, cm^{-1}): 3269, 2946, 2852, 2835, 1674, 1659, 1552, 1129, 1078; ^1H -NMR (300 MHz, $\text{DMSO}-d_6$, δ / ppm): 11.95 (1H, *s*, $-\text{NH}-\text{N}=\text{C}$), 8.65 (2H, *d*, $J = 4.2$ Hz, pyridine), 8.24 (1H, *s*, $-\text{N}=\text{C}-\text{H}$), 7.83 (2H, *d*, $J = 3.7$ Hz, pyridine), 7.77 (2H, *d*, $J = 3.2$ Hz, benzylidene), 7.15 (1H, *t*, $J = 7.3$ Hz, benzylidene), 3.91 (2H, *t*, $J = 6.5$ Hz, OCH_2), 3.65 (2H, *s*, $\text{Ar}-\text{CH}_2-\text{N}$), 2.45 (8H, *m*, 4CH_2 , piperazine), 2.18 (3H, *s*, NCH_3 , piperazine), 1.84 (2H, *m*, CH_2), 1.05 (3H, *t*, $J = 9.1$ Hz, CH_3); ^{13}C -NMR (100 MHz, $\text{DMSO}-d_6$, δ / ppm): 163.91, 157.58, 149.51, 143.48, 139.64, 132.23, 128.25, 122.59, 121.29, 120.49, 115.75, 72.19, 55.18, 51.25, 49.37, 43.29, 23.18, 12.74.



Synthesis of 2-oxoazetidine derivatives of 2-aminothiazole and their biological activity

PUSHKAL SAMADHIYA*, RITU SHARMA, SANTOSH K. SRIVASTAVA
and SAVITRI D. SRIVASTAVA

Synthesis Organic Chemistry Laboratory, Department of Chemistry, Dr. H.S. Gour
University, Sagar, Madhya Pradesh-470003, India

(Received 5 January, revised 16 June 2011)

Abstract: A new series of 3-chloro-4-(substituted phenyl)-1-[[2-(2-thiazolylamino)ethyl]amino]-2-azetidinone, compounds **4a–m**, has been synthesized from 2-aminothiazole as the starting material. The structures of all the synthesized compounds were confirmed by chemical and spectral analyses, such as FTIR, ¹H-NMR and ¹³C-NMR spectroscopy. All the final synthesized compounds **4a–m** were screened for their antibacterial and antifungal activities against some selected bacteria and fungi and for their antitubercular activity against *Mycobacterium tuberculosis*, and their minimum inhibitory concentration (MIC) values were determined. The anti-inflammatory activities of the title compounds were screened using albino rats (either sex) and gave acceptable results.

Keywords: synthesis; 2-aminothiazole; azetidinone; antimicrobial; antitubercular; anti-inflammatory.

INTRODUCTION

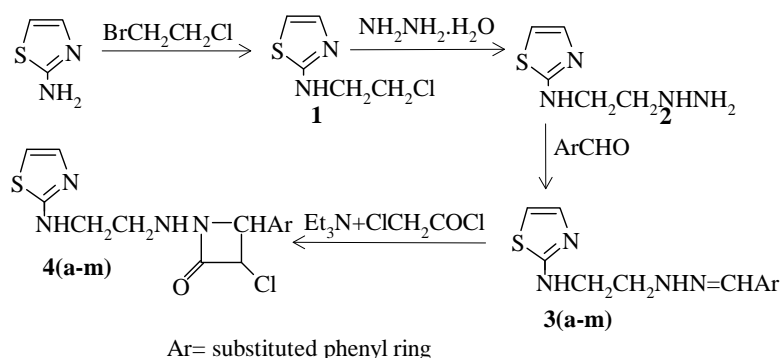
The azetidinone unit is a crucial structural feature of significant classes of antibiotics and its chemistry is very important to their biological activities, for instance, the penicillin and cephalosporin antibiotics possess *cis*- β -lactam units, whereas the thienamycins and trinemys have *trans*- β -lactam moieties. The effective synthesis of β -lactam became a desirable goal based on the discovery of penicillin and cephalosporin. Although most penicillin and cephalosporin related compounds are obtained by biosynthesis, chemical modification of intermediates for bioassay of the antibacterial activity of the resulting compounds has become of utmost importance because of the growing resistance of bacteria against penicillin- and cephalosporin-like compounds and the need for medicines with more specific antibacterial activity.^{1,2} The azetidinone derivatives have also been

* Corresponding author. E-mail: pushkalsamadhiya@rediffmail.com
doi: 10.2298/JSC110616002S

recognized as tumor necrosis factor-alpha (TNF-alpha) converting enzyme (TACE) inhibitors³ and agents with new biological activities, such as anticancer,⁴ anti-coccidial,⁵ cardiovascular,⁶ antiviral,⁷ mutagenic,⁸ anticonvulsant and anti-inflammatory.^{9,10} Condensed heterocyclic systems are of considerable interest not only because of their potential biological activity, but also because of their versatility as synthons in organic transformations.

The thiazole moiety is also an important component of the pharmacophores of a large number of molecules of medicinal significance and the evaluation of their biological activity, such as antiprotozoal,¹¹ antibacterial,¹² antifungal,^{13,14} antitubercular¹⁵ and anthelmintic,¹⁶ with emphasis on their potential medicinal applications, is desirable. Moreover, thiazole derivatives have attracted a great deal of interest due to their wide applications in the field of pharmaceuticals.

In the present study, a series of *N*-[2-(2-aminothiazolyl)ethyl]-4-(substituted phenyl)-3-chloro-2-oxo-1-iminoazetidines, compounds **4a–m**, was synthesized as shown in Scheme 1. The structure of all the synthesized compounds was elucidated by FTIR, ¹H-NMR, ¹³C-NMR, and chemical methods. All the final compounds **4a–m** were screened for their antibacterial, antifungal, antitubercular and anti-inflammatory activities.



Compound	Ar	Compound	Ar
3a and 4a	C ₆ H ₅	3h and 4h	4-NO ₂ C ₆ H ₄
3b and 4b	4-ClC ₆ H ₄	3i and 4i	3-NO ₂ C ₆ H ₄
3c and 4c	3-ClC ₆ H ₄	3j and 4j	2-NO ₂ C ₆ H ₄
3d and 4d	2-ClC ₆ H ₄	3k and 4k	4-CH ₃ OC ₆ H ₄
3e and 4e	4-BrC ₆ H ₄	3l and 4l	4-CH ₃ C ₆ H ₄
3f and 4f	3-BrC ₆ H ₄	3m and 4m	4-HOC ₆ H ₄
3g and 4g	2-BrC ₆ H ₄	–	–

Scheme 1. Synthesis of compounds **1–4**.

EXPERIMENTAL

Melting points were taken in open capillaries and are uncorrected. The progress of the reactions was monitored by silica gel-G coated TLC plates using MeOH:CHCl₃ (2:8) system.

The spot was visualized by exposing the dry plate to iodine vapors. The IR spectra were recorded in KBr discs on a Shimadzu 8201 PC FTIR spectrophotometer (ν_{\max} in cm^{-1}) and the $^1\text{H-NMR}$ and $^{13}\text{C-NMR}$ spectra were measured on a Bruker DRX-300 spectrometer in CDCl_3 at 300 and 75 MHz, respectively, using TMS as an internal standard. All chemical shifts are reported on δ scales. Elemental analyses were realized on a Carlo Erba-1108 analyzer. The analytical data of all the compounds were satisfactory. For column chromatographic purification of the products, Merck silica gel 60 (230–400 mesh) was used. The reagent grade chemicals were purchased from commercial sources and further purified before use.

Procedure for the synthesis of 2-[(2-chloroethyl)amino]thiazole, compound 1

2-Aminothiazole and 1-bromo-2-chloroethane (1:1 mole) were dissolved in methanol. The reaction mixture was continuously stirred on a magnetic stirrer at 30–35 °C for about 8 h. The product was filtered and purified by column chromatography. The purified product was dried in the oven at 45–50 °C for 8 h and recrystallized from ethanol to yield compound **1**.

Procedure for the synthesis of N-(2-hydrazinylethyl)-thiazolamine, compound 2

Compound **1** and hydrazine hydrate (1:1 mole) were dissolved in methanol at room temperature. The reaction mixture was continuously stirred on a magnetic stirrer at 30–35 °C for about 5 h. The product was filtered off and purified by column chromatography. The purified product was dried in an oven at 45–50 °C for 9 h and recrystallized from ethanol to yield compound **2**.

General procedure for the synthesis of substituted benzaldehyde, 2-[2-(thiazolylamino)ethyl]-hydrazone, compounds 3a–m

Compound **2** and an appropriate substituted benzaldehyde (1:1 mole) were dissolved in methanol and allowed to react. The reaction mixture was first continuously stirred on a magnetic stirrer at 30–35 °C for about 3–5 h and then kept on a steam bath at 75–90 °C for about 3–4 h. The products were filtered and cooled to room temperature. The filtered products were purified by column chromatography. The purified products were dried in an oven at 55–60 °C for 6–10 h and recrystallized from ethanol to yield compounds **3a–m**.

General procedure for the synthesis of 3-chloro-4-(substituted phenyl)-1-[2-(2-thiazolylamino)ethyl]amino}-2-azetidinone, compounds 4a–m

An appropriate compound **3a–m** and chloroacetyl chloride in the presence of Et_3N (1:1:1 mole ratio) were dissolved in methanol (50 ml) and allowed to react. The reaction mixture was first continuously stirred on a magnetic stirrer at 30–35 °C for about 3–4 h and then kept on a steam bath at 70–85 °C for about 3–5 h. The products were filtered and cooled to room temperature. The filtered products were purified by column chromatography. The purified products were dried in an oven at 60–65 °C for 4–8 h and recrystallized from ethanol to yield compounds **4a–m**, respectively.

Biological importance

The antibacterial, antifungal and antitubercular activities of compounds **4a–m** were assayed *in vitro* against selected bacteria: *Bacillus subtilis*, *Escherichia coli*, *Staphylococcus aureus* and *Klebsiella pneumoniae*, and fungi: *Aspergillus niger*, *A. flavus*, *Candida albicans* and *Fusarium oxysporum*, and *Mycobacterium tuberculosis* (H37Rv) strain. The minimal inhibitory concentration (MIC) values of compounds **4a–m** were determined using the filter paper disc diffusion method (antibacterial and antifungal activity) and the Lowenstein–Jensen (LJ) medium (conventional) method (antitubercular activity) at $100 \mu\text{g mL}^{-1}$ and lower concentrations. Streptomycin and griseofulvin, used as the standard for the antibacterial and antifungal

activity, respectively, showed MIC values in the range 1.25–3.25 $\mu\text{g mL}^{-1}$ for all the bacterial strain and 6.25–12.5 $\mu\text{g mL}^{-1}$ for all fungal strain. For the antitubercular activity, isoniazid and rifampicin were taken as standards (MIC range 1.25–2.50 $\mu\text{g mL}^{-1}$). All standards were also screened under similar condition for comparison.

Anti-inflammatory activity

The carageenan-induced rat paw edema method was employed for evaluating the anti-inflammatory activity of the compounds at a dose 50 mg kg^{-1} bw in albino rats (weighing 80–110 g, each group contained 5 animal) using phenylbutazone as the standard drug for comparison at a dose 30 mg kg^{-1} body weight. The rat paw edema was produced by the method of Winter *et al.*¹⁷ The percentage inhibition of inflammation was calculated by applying the Newbould formula.¹⁸

RESULTS AND DISCUSSION

3-Chloro-4-(substituted phenyl)-1-([2-(2-thiazolylamino)ethyl]amino)-2-azetidinone, compounds **4a–m**, were synthesized in four different steps. 2-Aminothiazole on reaction with $\text{Cl}(\text{CH}_2)_2\text{Br}$ at room temperature afforded 2-[(2-chloroethyl)amino]thiazole, compound **1**. The IR spectrum of compound **1** displayed absorptions at 1336 and 740 for (C–N) and (C–Cl), respectively, this clearly indicated the synthesis of compound **1**. Compound **1** on reaction with hydrazine hydrate at room temperature yielded *N*-(2-hydrazinylethyl)-2-thiazolamine, compound **2**. The IR spectrum of compound **2** showed absorptions for NH and NH_2 at 3378 and 3429 cm^{-1} , respectively, while the absorption for (C–Cl) in the IR spectrum of compound **1** had disappeared. The $^1\text{H-NMR}$ spectrum of **2** displayed signals at δ 7.63 and 5.56 ppm for NH and NH_2 , respectively. Compound **2** on further reaction with several selected substituted aromatic aldehydes produced substituted benzaldehyde, 2-[2-(thiazolylamino)ethyl]-hydrazone, compounds **3a–m**. The characteristic absorption for a Schiff base (N=CH) appeared in the range 1542–1579 cm^{-1} in the IR spectra of compounds **3a–m** and in the $^1\text{H-}$ and $^{13}\text{C-NMR}$ spectra signals appeared at δ 7.82–8.12 and δ 151.6–157.4 ppm, respectively. In the $^1\text{H-NMR}$, the broad signal of NH_2 present in the spectrum of compound **2** had disappeared. Compounds **3a–m** on treatment with ClCH_2COCl in the presence of Et_3N furnished the final products, compounds **4a–m**. In the IR spectra of compounds **4a–m**, the carbonyl group of the β -lactam ring showed a characteristic absorption in the range 1726–1752 cm^{-1} and the $^1\text{H-NMR}$ spectra of compounds **4a–m** showed two doublets for (N–CH) and (CH–Cl) in the range δ 4.72–4.98 and 4.13–4.28 ppm, respectively. In the $^{13}\text{C-NMR}$ spectra of compounds **4a–m**, three characteristic signals appeared for (N–CH), (CH–Cl) and (CO cyclic) in the δ ranges 60.8–65.7, 49.7–54.8 and 169.8–176.4 ppm, respectively. The IR absorption and $^1\text{H-}$ and $^{13}\text{C-NMR}$ signals of the N=CH group were absent. All these facts collectively suggest the successful synthesis of all the above compounds.

The analytic and spectral data of all the synthesized compounds are given in the supplementary material to this paper.

Biological testing

The results of all the described activities (antibacterial, antifungal, antitubercular and anti-inflammatory) are summarized in Tables I and II. The results of the antimicrobial screening data revealed that all the compounds **4a–m** showed considerable and varied activity against the selected microorganisms. The results shown in Tables I and II revealed that all the synthesized compounds **4a–m** have a structure activity relationship (SAR) because the activity of the compounds varied with substitution. The nitro group-containing compounds (**4h**, **4i** and **4j**) showed higher activity than the chloro (**4c** and **4d**), or bromo group containing compounds (**4e** and **4f**). The chloro and bromo derivatives also had a higher activity than the other rested compounds. Based on the SAR, it can be concluded that the activity of the compounds depends on electron withdrawing nature of the substituent groups. The sequence of the activity is the following: $\text{NO}_2 > \text{Cl} > \text{Br} > \text{OH} > > \text{OCH}_3 > \text{CH}_3$.

TABLE I. Antibacterial, antifungal and antitubercular activities of compounds **4a–m**. The MIC values of the standard streptomycin for all bacteria strains and griseofulvin for all fungi strains were in the range of 1.25–3.25 and 6.25–12.5 $\mu\text{g ml}^{-1}$, respectively. Isoniazid and rifampicin were used as standards, MIC values in the range of 1.25–2.50 $\mu\text{g ml}^{-1}$, for *M. tuberculosis*

Compd.	Antibacterial activity				Antifungal activity				Antitubercular activity
	<i>B. subtilis</i>	<i>E. coli</i>	<i>S. aureus</i>	<i>K. pneumoniae</i>	<i>A. niger</i>	<i>A. flavus</i>	<i>F. oxysporum</i>	<i>C. albicans</i>	<i>M. tuberculosis</i>
4a	12.5	>6.25	12.5	6.25	>25	>25	>25	>25	>12.5
4b	>3.25	6.25	3.25	>3.25	>25	>12.5	>25	>25	>2.50
4c	6.25	>3.25	6.25	3.25	>12.5	25	>12.5	>12.5	>2.50
4d	>3.25	6.25	3.25	6.25	>12.5	>25	>12.5	>12.5	2.50
4e	6.25	>3.25	3.25	>3.25	>12.5	25	25	>25	>2.50
4f	6.25	3.25	6.25	>3.25	>12.5	>12.5	>12.5	>12.5	>2.50
4g	>3.25	6.25	>3.25	6.25	25	>12.5	>12.5	25	6.25
4h	3.25	>3.25	3.25	3.25	25	>12.5	>12.5	>25	2.50
4i	3.25	3.25	>3.25	3.25	>12.5	>12.5	>12.5	>12.5	2.50
4j	3.25	>3.25	3.25	3.25	>12.5	>12.5	>12.5	>12.5	>2.50
4k	>12.5	6.25	>12.5	6.25	25	25	>25	>25	12.5
4l	>12.5	>12.5	>12.5	>12.5	>25	>25	>25	>25	>12.5
4m	>3.25	>3.25	>6.25	>6.25	>25	25	>12.5	>12.5	6.25

The investigation of antimicrobial (antibacterial, antifungal and antitubercular) data revealed that the compounds **4c**, **4d**, **4e**, **4f**, **4h**, **4i** and **4j** displayed high activity, the compounds **4b**, **4g** and **4m** showed moderate activity and the other compounds

showed low activity against all the strains compared with the standard drugs. In the anti-inflammatory activity test, compounds **4c**, **4d**, **4e**, **4f**, **4h**, **4i** and **4j** showed high activity while the other compounds displayed moderate to low activity.

TABLE II. Anti-inflammatory activity of compounds **4a–m**

Compound	Before carageenan administration (mean±SEM)	Total increase in paw volume after 5 h (mean±SEM)	Inhibition, %
4a	0.62±0.02	0.18±0.02	48.57
4b	0.65±0.02	0.16±0.02	54.29
4c	0.66±0.02	0.16±0.01	54.29
4d	0.64±0.02	0.17±0.02	51.43
4e	0.66±0.03	0.15±0.02	57.14
4f	0.67±0.02	0.14±0.01	60.00
4g	0.66±0.02	0.16±0.01	54.29
4h	0.65±0.03	0.14±0.01	60.00
4i	0.68±0.02	0.13±0.03	62.86
4j	0.67±0.03	0.12±0.02	65.71
4k	0.65±0.02	0.16±0.02	54.29
4l	0.64±0.02	0.18±0.02	48.57
4m	0.67±0.02	0.16±0.01	54.29
Control	0.68±0.02	0.35±0.01	–
Standard; pphenylbutazone	0.66±0.03	0.10±0.02	71.43

CONCLUSIONS

The research study reports the successful synthesis of compounds **1–4**. The antimicrobial and antitubercular activity of the newly synthesized compounds bearing a 2-azetidinone moiety revealed that all the tested compounds showed moderate to good antibacterial, antifungal and antitubercular activities against the selected microbial strains. The results of the anti-inflammatory activity testing also showed positive results. Some of the compounds displayed promising activities and are of interest for further transformations towards more potent derivatives.

SUPPLEMENTARY MATERIAL

Analytical and spectral data of synthesized compounds are available electronically from <http://www.shd.org.rs/JSCS/>, or from the corresponding author on request.

Acknowledgements. The authors are thankful to SAIF, Central Drugs Research Institute Lucknow (India) for providing the spectral and analytical data of the compounds. We are thankful to the Head, Department of Biotechnology, Dr. H. S. Gour, University, Sagar (India) for the antimicrobial (antibacterial and antifungal) activity determinations and to the Microcare Laboratory and the Tuberculosis Research Center Surat, Gujarat (India) for the antituberculosis activity results. We are also thankful to the Head, Department of Chemistry Dr. H. S. Gour, University, Sagar (India) for providing the facilities to carry out the work.

ИЗВОД

СИНТЕЗА И БИОЛОШКА АКТИВНОСТ 2-ОКСОАЗЕТИДИНСКИХ
ДЕРИВАТА 2-АМИНОТИАЗОЛА

PUSHKAL SAMADHIYA, RITU SHARMA, SANTOSH K. SRIVASTAVA и SAVITRI D. SRIVASTAVA

*Synthesis Organic Chemistry Laboratory, Department of Chemistry, Dr. H.S. Gour University, Sagar,
Madhya Pradesh-470003, India*

Синтетисана је серија нових деривата 3-хлоро-4-(супституисани фенил)-1-{{2-(тиазолиламино)етил}амино}-2-азетидинона, једињења **4a-m**, полазећи од 2-аминотиазола. Структура свих синтетисаних једињења потврђена је аналитичким и спектралним методама, ИС, ¹H-NMR и ¹³C-NMR спектроскопијом. Испитана је антибактеријска, антифунгална активност према одабраним хелијским линијама бактерија и гљива, као и антитуберкулозна активност према *Mycobacterium tuberculosis* синтетисаних једињења **4a-m**. Антиинфламаторна активност је испитана према албино пацовима. Резултати показују задовољавајућу активност тестираних једињења.

(Примљено 5. јануара, ревидирано 16. јуна 2011)

REFERENCES

1. A. Upadhyay, S. K. Srivastava, S. D. Srivastava, R. Yadav, *Proc. Natl. Acad. Sci. India* **80** (2010) 131
2. Y. Ikee, K. Hashimoto, M. Nakashima, K. Hayashi, S. Sano, M. Shiro, Y. Nagao, *Bioorg. Med. Chem. Lett.* **17** (2007) 942
3. B. G. Rao, U. K. Bandarage, T. Wang, J. H. Come, E. Perola, Y. W. S.-K, Tian, J. O. Saunders, *Bioorg. Med. Chem. Lett.* **17** (2007) 2250
4. B. K. Banik, I. Banik, F. F. Becker, *Bioorg. Med. Chem.* **13** (2005) 3611
5. G.-B. Liang, X. Qian, D. Feng, M. Fisher, T. Crumley, S. J. Darkin-Ratray, P. M. Dulski, A. Gurnett, P. S. Leavitt, P. A. Liberator, A. S. Misura, S. Samaras, T. Tamas, D. M. Schmatz, M. Wyvratta, T. Biftu, *Bioorg. Med. Chem. Lett.* **18** (2008) 2019
6. S. Takai, D. Jin, M. Muramatsu, Y. Okamoto, M. Miyazaki, *Pharmaco* **501** (2004) 1
7. W. W. Ogilvie, C. Yoakim, F. Do, B. Hache, L. Lagace, J. Naud, J. A. Omeara, R. Deziel, *Bioorg. Med. Chem.* **7** (1999) 1521
8. H. Valette, F. Dolle, M. Bottlaender, F. Hinnen, D. Marzin, *Nucl. Med. Biol.* **29** (2002) 849
9. P. Kohli, S. D. Srivastava, S. K. Srivastava, *J. Indian Chem. Soc.* **85** (2008) 326
10. S. K. Srivastava, S. Srivastava, S. D. Srivastava, *Indian J. Chem., Sect B* **38** (1999) 183
11. R. A. Tapia, Y. Prieto, F. Pautet, N. Walchshofer, H. Fillion, B. Fenet, M.-E. Sarciron, *Bioorg. Med. Chem.* **11** (2003) 3407
12. C.-H. Oh, H.-W. Cho, D. Baek, J.-H. Cho, *Eur. J. Med. Chem.* **37** (2002) 743; b) S. K. Bharti, G. Nath, R. Tilak, S. K. Singh, *Eur. J. Med. Chem.* **45** (2010) 651
13. L. Joshi, S. K. Srivastava, *J. Sci Ind. Res.* **60** (2001) 331
14. S. K. Sonwane, S. D., Srivastava, *Proc. Natl. Acad. Sci. India* **78** (2008) 129
15. G. V. Suresh Kumar, Y. Rajendraprasad, B. P. Mallikarjuna, S. M. Chandrashekar, C. Kistayya, *Eur. J. Med. Chem.* **45** (2010) 2063
16. R. Yadav, S. K. Srivastava, S. D. Srivastava, *Chem. Indian J.* **1** (2003) 95
17. C. A. Winter, E. A. Risley, G. W. Nuss, *Proc. Soc. Exp. Biol.* **111** (1962) 544
B. B. Newbould, *Brit J Pharmacol.* **21** (1963) 127.



SUPPLEMENTARY MATERIAL TO
**Synthesis of 2-oxo-azetidine derivatives of 2-amino thiazole
and their biological activity**

PUSHKAL SAMADHIYA*, RITU SHARMA, SANTOSH K. SRIVASTAVA
and SAVITRI D. SRIVASTAVA

*Synthesis Organic Chemistry Laboratory, Department of Chemistry, Dr. H.S. Gour
University, Sagar, Madhya Pradesh-470003, India*

J. Serb. Chem. Soc. 77 (5) (2012) 599–605

ANALYTICAL AND SPECTRAL DATA OF THE SYNTHESIZED COMPOUNDS

2-[(2-Chloroethyl)amino]thiazole (1). Yield: 56.0 g, 70 %; m.p. 66–70 °C; Anal. Calcd. for C₅H₇ClN₂S: C, 36.92; H, 4.33; N, 17.22 %. Found: C, 36.89; H, 4.30; N, 17.18 %; IR (KBr, cm⁻¹): 740 (C–Cl), 878 (C–S), 1336 (N–CH₂), 1564 (C=C), 2888, 3086 (CH), 3388 (NH); ¹H-NMR (300 MHz, CDCl₃, δ / ppm): 3.42 (2H, *t*, *J* = 7.50 Hz, CH₂–Cl), 3.94 (2H, *m*, N–CH₂), 6.80 (1H, *d*, *J* = 4.70 Hz, C5–H of thiazole), 7.18 (1H, *d*, *J* = 4.70 Hz, C4–H of thiazole), 7.70 (1H, *s*, NH); ¹³C-NMR (75 MHz, CDCl₃, δ / ppm): 46.8 (CH₂–Cl), 56.1 (N–CH₂), 109.9 (C5 of thiazole), 139.9 (C4 of thiazole), 169.8 (C2 of thiazole).

N-(2-Hydrazinylethyl)-2-thiazolamine (2). Yield: 43.0 g, 80 %; m.p. 60–61 °C; Anal. Calcd. for C₅H₁₀N₄S: C, 37.95; H, 6.37; N, 20.26 %. Found: C, 37.91; H, 6.35; N, 20.22 %; IR (KBr, cm⁻¹): 878 (C–S), 1248 (C–N), 3378 (NH), 3429 (NH₂); ¹H-NMR (300 MHz, CDCl₃, δ / ppm): 3.32 (2H, *m*, CH₂–N), 3.89 (2H, *m*, N–CH₂), 5.56 (2H, *s*, NH₂), 6.76 (1H, *d*, *J* = 5.0 Hz, C5–H of thiazole), 7.15 (1H, *d*, *J* = 5.0 Hz, C4–H of thiazole), 7.63 (1H, *s*, NH), 7.72 (1H, *s*, NH); ¹³C-NMR (75 MHz, CDCl₃, δ / pm): 49.1 (CH₂–N), 54.7 (N–CH₂), 109.8 (C5 of thiazole), 138.7 (C4 of thiazole), 168.6 (C2 of thiazole); Mass (FAB).

Benzaldehyde 2-[2-(2-thiazolylamino)ethyl]-hydrazone (3a). Yield: 3.27 g, 60 %; m.p. 79–80 °C; Anal. Calcd. for C₁₂H₁₄N₄S: C, 58.51; H, 5.72; N, 22.74 %. Found: C, 58.45; H, 5.67; N, 22.70 %; IR (KBr, cm⁻¹): 3374 (NH), 1557 (N=CH); ¹H-NMR (300 MHz, CDCl₃, δ / ppm): 3.41 (2H, *m*, CH₂–N), 3.96 (2H, *m*, N–CH₂), 6.64 (1H, *d*, *J* = 4.95 Hz, C5–H of thiazole), 7.29 (1H, *d*, *J* = 4.95 Hz, C4–H of thiazole), 7.56 (1H, *s*, NH), 7.82 (1H, *s*, N=CH), 7.98 (1H,

* Corresponding author. E-mail: pushkalsamadhiya@rediffmail.com

s, NH), 6.40–7.11 (5H, *m*, Ar–H); ^{13}C -NMR (75 MHz, CDCl_3 , δ / ppm): 49.5 ($\text{CH}_2\text{-N}$), 55.4 (N-CH_2), 112.8 (C5 of thiazole), 141.5 (C4 of thiazole), 152.2 (N=CH), 170.1 (C2 of thiazole), 124.6, 127.8, 131.8, 137.8 (Ar).

4-Chlorobenzaldehyde 2-[2-(2-thiazolylamino)ethyl]hydrazone (3b). Yield: 4.23 g, 68 %; m.p. 80–83 °C; Anal. Calcd. for $\text{C}_{12}\text{H}_{13}\text{ClN}_4\text{S}$: C, 51.33; H, 4.66; N, 19.95 %. Found: C, 51.30; H, 4.62; N, 19.92 %; IR (KBr, cm^{-1}): 3378 (NH), 1569 (N=CH), 747 (C–Cl); ^1H -NMR (300 MHz, CDCl_3 , δ / ppm): 3.53 (2H, *m*, $\text{CH}_2\text{-N}$), 3.94 (2H, *m*, N-CH_2), 7.16 (1H, *d*, $J = 5.0$ Hz, C5–H of thiazole), 7.40 (1H, *d*, $J = 5.0$ Hz, C4–H of thiazole), 7.55 (1H, *s*, NH), 7.82 (1H, *s*, NH), 7.94 (1H, *s*, N=CH), 6.68–7.81 (4H, *m*, Ar–H); ^{13}C -NMR (75 MHz, CDCl_3 , δ / ppm): 49.4 ($\text{CH}_2\text{-N}$), 57.8 (N-CH_2), 115.8 (C5 of thiazole), 143.9 (C4 of thiazole), 155.6 (N=CH), 172.9 (C2 of thiazole), 125.5, 129.6, 134.9, 140.4 (Ar).

3-Chlorobenzaldehyde 2-[2-(2-thiazolylamino)ethyl]hydrazone (3c). Yield: 4.17 g, 67 %; m.p. 77–79 °C; Anal. Calcd. for $\text{C}_{12}\text{H}_{13}\text{ClN}_4\text{S}$: C, 51.33; H, 4.66; N, 19.95 %. Found: C, 51.28; H, 4.60; N, 19.90 %; IR (KBr, cm^{-1}): 745 (C–Cl), 1566 (N=CH), 3378 (NH); ^1H -NMR (300 MHz, CDCl_3 , δ / ppm): 3.51 (2H, *m*, $\text{CH}_2\text{-N}$), 3.96 (2H, *m*, N-CH_2), 7.17 (1H, *d*, $J = 5.10$ Hz, C5–H of thiazole), 7.31 (1H, *d*, $J = 5.10$ Hz, C4–H of thiazole), 7.65 (1H, *s*, NH), 7.85 (1H, *s*, NH), 7.92 (1H, *s*, N=CH), 7.10–7.82 (4H, *m*, Ar–H); ^{13}C -NMR (75 MHz, CDCl_3 , δ / ppm): 47.4 ($\text{CH}_2\text{-N}$), 57.5 (N-CH_2), 114 (C5 of thiazole), 142.8 (C4 of thiazole), 157.4 (N=CH), 171.5 (C2 of thiazole), 126.8, 128.7, 130.8, 132.6, 136.7, 137.8 (Ar).

2-Chlorobenzaldehyde 2-[2-(2-thiazolylamino)ethyl]hydrazone (3d). Yield: 4.0 g, 65 %; m.p. 77–78 °C; Anal. Calcd. for $\text{C}_{12}\text{H}_{13}\text{ClN}_4\text{S}$: C, 51.33; H, 4.66; N, 19.95 %. Found: C, 51.25; H, 4.61; N, 19.93 %; IR (KBr, cm^{-1}): 748 (C–Cl), 1560 (N=CH), 3375 (NH); ^1H -NMR (300 MHz, CDCl_3 , δ / ppm): 3.48 (2H, *m*, $\text{CH}_2\text{-N}$), 3.80 (2H, *m*, N-CH_2), 7.17 (1H, *d*, $J = 5.0$ Hz, C5–H of thiazole), 7.36 (1H, *d*, $J = 5.0$ Hz, C4–H of thiazole), 7.53 (1H, *s*, NH), 7.79 (1H, *s*, NH), 7.89 (1H, *s*, N=CH), 7.20–7.92 (4H, *m*, Ar–H); ^{13}C -NMR (75 MHz, CDCl_3 , δ / ppm): 48.6 ($\text{CH}_2\text{-N}$), 58.2 (N-CH_2), 112.9 (C5 of thiazole), 142.9 (C4 of thiazole), 154.6 (N=CH), 170.6 (C2 of thiazole), 126.8, 128.6, 128.9, 129.8, 132.7, 139.6 (Ar); Mass (FAB).

4-Bromobenzaldehyde 2-[2-(2-thiazolylamino)ethyl]hydrazone (3e). Yield: 4.96 g, 69 %; m.p. 80–81 °C; Anal. Calcd. for $\text{C}_{12}\text{H}_{13}\text{BrN}_4\text{S}$: C, 44.31; H, 4.02; N, 17.22 %. Found: C, 44.21; H, 3.96; N, 17.15 %; IR (KBr, cm^{-1}): 642 (C–Br), 1552 (N=CH), 3360 (NH); ^1H -NMR (300 MHz, CDCl_3 , δ / ppm): 3.49 (2H, *m*, $\text{CH}_2\text{-N}$), 3.76 (2H, *m*, N-CH_2), 7.09 (1H, *d*, $J = 5.0$ Hz, C5–H of thiazole), 7.28 (1H, *d*, $J = 5.0$ Hz, C4–H of thiazole), 7.59 (1H, *s*, NH), 7.75 (1H, *s*, NH), 7.94 (1H, *s*, N=CH) 7.39–7.68 (4H, *m*, Ar–H); ^{13}C -NMR (75 MHz, CDCl_3 , δ / ppm): 48.2 ($\text{CH}_2\text{-N}$), 56.5 (N-CH_2), 111.8 (C5 of thiazole), 140.9 (C4 of thiazole), 154.6 (N=CH), 169.9 (C2 of thiazole), 126.9, 129.8, 133.9, 137.8 (Ar).

3-Bromobenzaldehyde 2-[2-(2-thiazolylamino)ethyl]hydrazone (3f). Yield: 4.82 g, 67 %; m.p. 82–83 °C; Anal. Calcd. for C₁₂H₁₃BrN₄S: C, 44.31; H, 4.02; N, 17.22 %. Found: C, 44.23; H, 3.96; N, 17.16 %; IR (KBr, cm⁻¹): 636 (C–Br), 1568 (N=CH), 3369 (NH); ¹H-NMR (300 MHz, CDCl₃, δ / ppm): 3.50 (2H, *m*, CH₂–N), 3.98 (2H, *m*, N–CH₂), 7.10 (1H, *d*, *J* = 5.0 Hz, C5–H of thiazole), 7.30 (1H, *d*, *J* = 5.0 Hz, C4–H of thiazole), 7.55 (1H, *s*, NH), 7.73 (1H, *s*, NH), 7.92 (1H, *s*, N=CH), 7.23–7.90 (4H, *m*, Ar–H); ¹³C-NMR (75 MHz, CDCl₃, δ / ppm): 47.8 (N–CH₂), 59.4 (CH₂–N), 112.8 (C5 of thiazole), 141.6 (C4 of thiazole), 151.8 (N=CH), 172.8 (C2 of thiazole), 124.8, 126.9, 129.6, 131.8, 137.9, 141.8 (Ar).

2-Bromobenzaldehyde 2-[2-(2-thiazolylamino)ethyl]hydrazone (3g). Yield: 4.46 g, 62 %; m.p. 79–81 °C; Anal. Calcd. for C₁₂H₁₃BrN₄S: C, 44.31; H, 4.02; N, 17.22 %. Found: C, 44.20; H, 3.95; N, 17.18 %; IR (KBr, cm⁻¹): 632 (C–Br), 1573 (N=CH), 3374 (NH); ¹H-NMR (300 MHz, CDCl₃, δ / ppm): 3.31 (2H, *m*, CH₂–N), 3.77 (2H, *m*, N–CH₂), 7.12 (1H, *d*, *J* = 5.0 Hz, C5–H of thiazole), 7.32 (1H, *d*, *J* = 5.0 Hz, C4–H of thiazole), 7.49 (1H, *s*, NH), 7.85 (1H, *s*, NH), 8.01 (1H, *s*, N=CH), 7.31–7.63 (4H, *m*, Ar–H); ¹³C-NMR (75 MHz, CDCl₃, δ / ppm): 50.1 (CH₂–N), 59.4 (N–CH₂), 109.9 (C5 of thiazole), 140.2 (C4 of thiazole), 154.6 (N=CH), 171.8 (C2 of thiazole), 126., 128.8, 129.7, 131.8, 133.8, 141.8 (Ar).

4-Nitrobenzaldehyde 2-[2-(2-thiazolylamino)ethyl]hydrazone (3h). Yield: 4.19 g, 65 %; m.p. 84–86 °C; Anal. Calcd. for C₁₂H₁₃N₅O₂S: C, 49.47; H, 4.49; N, 24.03 %. Found: C, 49.42; H, 4.45; N, 24.00 %; IR (KBr, cm⁻¹): 852 (C–N), 1542 (N=O), 1575 (N=CH), 3379 (NH); ¹H-NMR (300 MHz, CDCl₃, δ / ppm): 3.59 (2H, *m*, CH₂–N), 3.94 (2H, *m*, N–CH₂), 7.14 (1H, *s*, NH), 7.22 (1H, *d*, *J* = 5.0 Hz, C5–H of thiazole), 7.41 (1H, *s*, NH), 7.52 (1H, *d*, *J* = 5.0 Hz, C4–H of thiazole), 8.12 (1H, *s*, N=CH), 7.32–7.91 (4H, *m*, Ar–H); ¹³C-NMR (75 MHz, CDCl₃, δ / ppm): 48.3 (CH₂–N), 58.3 (N–CH₂), 112.9 (C5 of thiazole), 141.6 (C4 of thiazole), 155.8 (N=CH), 171.5 (C2 of thiazole), 124.8, 129.7, 138.8, 147.6 (Ar).

3-Nitrobenzaldehyde 2-[2-(2-thiazolylamino)ethyl]hydrazone (3i). Yield: 4.38 g, 68 %; m.p. 85–87 °C; Anal. Calcd. for C₁₂H₁₃N₅SO₂: C, 49.47; H, 4.49; N, 24.03 %. Found: C, 49.40; H, 4.47; N, 23.98 %; IR (KBr, cm⁻¹): 3365 (NH), 1534 (N=O), 1579 (N=CH), 858 (C–N); ¹H-NMR (300 MHz, CDCl₃, δ / ppm): 3.26 (2H, *m*, CH₂–N), 3.92 (2H, *m*, N–CH₂), 7.08 (1H, *s*, NH), 7.17 (1H, *d*, *J* = 5.0 Hz, C5–H of thiazole), 7.42 (1H, *d*, *J* = 5.0 Hz, C4–H of thiazole), 7.72 (1H, *s*, NH), 7.92 (1H, *s*, N=CH), 7.21–7.86 (4H, *m*, Ar–H); ¹³C-NMR (75 MHz, CDCl₃, δ / ppm): 47.2 (CH₂–N), 57.8 (N–CH₂), 154.5 (N=CH), 171.6 (C2 of thiazole), 112.8 (C5 of thiazole), 140.6 (C4 of thiazole), 122.7, 125.5, 128.7, 133.8, 137.7, 150.8 (Ar).

2-Nitrobenzaldehyde 2-[2-(2-thiazolylamino)ethyl]hydrazone (3j). Yield: 4.20 g, 65 %; m.p. 80–81 °C; Anal. Calcd. for C₁₂H₁₃N₅O₂S: C, 49.47; H, 4.49; N, 24.03 %. Found: C, 49.43; H, 4.44; N, 23.97 %; IR (KBr, cm⁻¹): 852 (C–N), 1541 (N=O), 1578 (N=CH), 3359 (NH); ¹H-NMR (300 MHz, CDCl₃, δ / ppm): 3.35 (2H, *m*, CH₂–N), 3.96 (2H, *m*, N–CH₂), 7.15 (1H, *s*, NH), 7.18 (1H, *d*, *J* = 4.90 Hz, C5–H of thiazole), 7.36 (1H, *d*, *J* = 4.90 Hz, C4–H of thiazole), 7.53 (1H, *s*, NH), 8.12 (1H, *s*, N=CH), 7.26–7.99 (4H, *m*, Ar–H); ¹³C-NMR (75 MHz, CDCl₃, δ / ppm): 47.6 (CH₂–N), 57.4 (N–CH₂), 110.7 (C5 of thiazole), 139.6 (C4 of thiazole), 155.8 (N=CH), 171.8 (C2 of thiazole), 122.8, 125.8, 127.8, 133.6, 137.7, 149.6 (Ar).

4-Methoxybenzaldehyde 2-[2-(2-thiazolylamino)ethyl]hydrazone (3k). Yield: 3.91 g, 64 %; m.p. 73–74 °C; Anal. Calcd. for C₁₃H₁₆N₄OS: C, 56.49; H, 5.83; N, 20.27 %. Found: C, 56.40; H, 5.78; N, 20.22 %; IR (KBr, cm⁻¹): 1568 (N=CH), 2949 (OCH₃), 3361 (NH); ¹H-NMR (300 MHz, CDCl₃, δ / ppm): 3.28 (2H, *m*, CH₂–N), 3.52 (3H, *s*, OCH₃), 3.67 (2H, *m*, N–CH₂), 7.20 (1H, *d*, *J* = 4.95 Hz, C5–H of thiazole), 7.39 (1H, *d*, *J* = 4.95 Hz, C4–H of thiazole), 7.45 (1H, *s*, NH), 7.85 (1H, *s*, N=CH), 7.98 (1H, *s*, NH), 7.34–7.52 (4H, *m*, Ar–H); ¹³C-NMR (75 MHz, CDCl₃, δ / ppm): 46.6 (CH₂–N), 55.5 (N–CH₂), 54.7 (OCH₃), 110.1 (C5 of thiazole), 138.6 (C4 of thiazole), 154.7 (N=CH), 170.6 (C2 of thiazole), 114.8, 128.8, 130.7, 159.9 (Ar).

4-Methylbenzaldehyde 2-[2-(2-thiazolylamino)ethyl]hydrazone (3l). Yield: 3.45 g, 60 %; m.p. 66–67 °C; Anal. Calcd. for C₁₃H₁₆N₄S: C, 59.97; H, 6.19; N, 21.51 %. Found: C, 59.92; H, 6.15; N, 21.44 %; IR (KBr, cm⁻¹): 1545 (N=CH), 2914 (CH₃), 3348 (NH); ¹H-NMR (300 MHz, CDCl₃, δ / ppm): 3.32 (2H, *m*, CH₂–N), 2.62 (3H, *s*, CH₃), 3.82 (2H, *m*, N–CH₂), 6.87 (1H, *d*, *J* = 4.85 Hz, C5–H of thiazole), 7.25 (1H, *d*, *J* = 4.85 Hz, C4H of thiazole), 7.38 (1H, *s*, NH), 7.82 (1H, *s*, NH), 7.89 (1H, *s*, N=CH), 7.39–7.79 (4H, *m*, Ar–H); ¹³C-NMR (75 MHz, CDCl₃, δ / ppm): 24.9 (CH₃), 45.3 (CH₂–N), 54.7 (N–CH₂), 151.6 (N=CH), 171.5 (C2 of thiazole), 111.5 (C5 of thiazole), 140.4 (C4 of thiazole), 127.9, 129.8, 134.5, 139.8 (Ar).

4-Hydroxybenzaldehyde 2-[2-(2-thiazolylamino)ethyl]hydrazone (3m). Yield: 3.60 g, 62 %; m.p. 66–67 °C; Anal. Calcd. for C₁₂H₁₄N₄OS: C, 54.94; H, 5.37; N, 21.35 %. Found: C, 54.90; H, 5.32; N, 21.31 %; IR (KBr, cm⁻¹): 1565 (N=CH), 3388 (NH), 3477 (OH); ¹H-NMR (300 MHz, CDCl₃, δ / ppm): 3.37 (2H, *m*, CH₂–N), 3.89 (2H, *m*, N–CH₂), 4.12 (1H, *s*, OH), 7.12 (1H, *d*, *J* = 4.85 Hz, C5–H of thiazole), 7.35 (1H, *d*, *J* = 4.85 Hz, C4–H of thiazole), 7.42 (1H, *s*, NH), 7.76 (1H, *s*, NH), 8.06 (1H, *s*, N=CH), 7.32–7.79 (4H, *m*, Ar–H); ¹³C-NMR (75 MHz, CDCl₃, δ / ppm): 48.1 (CH₂–N), 57.6 (N–CH₂), 108.8 (C5 of thiazole), 138.9 (C4 of thiazole), 154.6 (N=CH), 169.8 (C2 of thiazole), 115.7, 126.6, 130.8, 154.9 (Ar).

3-Chloro-4-phenyl-1-[[2-(2-thiazolylamino)ethyl]amino]-2-azetidinone (4a). Yield: 2.44 g, 62 %; m.p. 78–80 °C; Anal. Calcd. for C₁₄H₁₅ClN₄OS: C, 52.08; H, 4.68; N, 17.35 %. Found: C, 52.02; H, 4.63; N, 17.31%; IR (KBr, cm⁻¹): 1337 (C–N), 2917 (CH–Cl), 1741 (CO, cyclic); ¹H-NMR (300 MHz, CDCl₃, δ / ppm): 3.30 (2H, *m*, CH₂–N), 3.90 (2H, *m*, N–CH₂), 4.26 (1H, *d*, *J* = 4.90 Hz, CH–Cl), 4.72 (1H, *d*, *J* = 4.90 Hz, N–CH), 7.15 (1H, *d*, *J* = 4.95 Hz, C5–H of thiazole), 7.23 (1H, *d*, *J* = 4.95 Hz, C4–H of thiazole), 7.35 (1H, *s*, NH), 7.70 (1H, *s*, NH), 6.85–7.72 (5H, *m*, Ar–H); ¹³C-NMR (75 MHz, CDCl₃, δ / ppm): 41.2 (CH₂–N), 50.6 (N–CH₂), 54.6 (CH–Cl), 62.7 (N–CH), 111.7 (C5 of thiazole), 139.8 (C4 of thiazole), 171.5 (C2 of thiazole), 173.7 (CO, cyclic), 124.6, 128.9, 132.8, 137.9 (Ar).

3-Chloro-4-(4-chlorophenyl)-1-[[2-(2-thiazolylamino)ethyl]amino]-2-azetidinone (4b). Yield: 3.54 g, 68 %; m.p. 80–82 °C; Anal. Calcd. for C₁₄H₁₄Cl₂N₄OS: C, 47.06; H, 3.94; N, 15.68 %. Found: C, 47.00; H, 3.91; N, 15.64 %; IR (KBr, cm⁻¹): 769 (C–Cl), 1342 (C–N), 1752 (CO, cyclic), 2921 (CH–Cl); ¹H-NMR (300 MHz, CDCl₃, δ / ppm): 3.36 (2H, *m*, CH₂–N), 3.94 (2H, *m*, N–CH₂), 4.21 (1H, *d*, *J* = 4.95 Hz, CH–Cl), 4.86 (1H, *d*, *J* = 4.95 Hz, N–CH), 7.12 (1H, *d*, *J* = 5.0 Hz, C5–H of thiazole), 7.29 (1H, *d*, *J* = 5.0 Hz, C4–H of thiazole), 7.45 (1H, *s*, NH), 7.86 (1H, *s*, NH), 6.86–7.72 (4H, *m*, Ar–H); ¹³C-NMR (75 MHz, CDCl₃, δ / ppm): 42.3 (CH₂–N), 51.1 (N–CH₂), 53.5 (CH–Cl), 63.8 (N–CH), 113.6 (C5 of thiazole), 142.8 (C4 of thiazole), 172.6 (C2 of thiazole), 176.2 (CO, cyclic), 127.8, 130.7, 136.4, 140.5 (Ar).

3-Chloro-4-(3-chlorophenyl)-1-[[2-(2-thiazolylamino)ethyl]amino]-2-azetidinone (4c). Yield: 3.30 g, 65 %; m.p. 78–79 °C; Anal. Calcd. for C₁₄H₁₄Cl₂N₄OS: C, 47.06; H, 3.94; N, 15.68 %. Found: C, 47.02; H, 3.85; N, 15.62 %; IR (KBr, cm⁻¹): 778 (C–Cl), 1345 (C–N), 1745 (C=O, cyclic), 2919 (CH–Cl); ¹H-NMR (300 MHz, CDCl₃, δ / ppm): 3.32 (2H, *m*, CH₂–N), 3.96 (2H, *m*, N–CH₂), 4.38 (1H, *d*, *J* = 5.05 Hz, CH–Cl), 4.86 (1H, *d*, *J* = 5.05 Hz, N–CH), 7.15 (1H, *d*, *J* = 4.90 Hz, C5–H of thiazole), 7.24 (1H, *d*, *J* = 4.90 Hz, C4–H of thiazole), 7.46 (1H, *s*, NH), 7.80 (1H, *s*, NH), 6.79–7.64 (4H, *m*, Ar–H); ¹³C-NMR (75 MHz, CDCl₃, δ / ppm): 41.8 (CH₂–N), 51.9 (N–CH₂), 54.8 (CH–Cl), 65.7 (N–CH), 112.8 (C5 of thiazole), 142.4 (C4 of thiazole), 172.6 (C2 of thiazole), 175.5 (CO, cyclic), 126.8, 128.9, 129.7, 132.7, 135.6, 139.6 (Ar).

3-Chloro-4-(2-chlorophenyl)-1-[[2-(2-thiazolylamino)ethyl]amino]-2-azetidinone (4d). Yield: 3.18 g, 66 %; m.p. 74–75 °C; Anal. Calcd. for C₁₄H₁₄Cl₂N₄OS: C, 47.06; H, 3.94; N, 15.68 %. Found: C, 47.00; H, 3.89; N, 15.64 %; IR (KBr, cm⁻¹): 778 (C–Cl), 1339 (C–N), 1750 (C=O, cyclic), 2925 (CH–Cl); ¹H-NMR (300 MHz, CDCl₃, δ / ppm): 3.36 (2H, *m*, CH₂–N), 3.94 (2H, *m*, N–CH₂), 4.33 (1H, *d*, *J* = 5.0 Hz, CH–Cl), 4.86 (1H, *d*, *J* = 5.0 Hz, N–CH), 7.12 (1H, *d*, *J* = 4.85 Hz, C5–H of thiazole), 7.27 (1H, *d*, *J* = 4.85 Hz, C4–H of thiazole), 7.43 (1H, *s*, NH), 7.82 (1H, *s*, NH), 6.81–7.62 (4H, *m*, Ar–H); ¹³C-NMR

(75 MHz, CDCl₃, δ / ppm): 43.4 (CH₂-N), 52.9 (N-CH₂), 53.8 (CH-Cl), 63.4 (N-CH), 112.6 (C5 of thiazole), 141.7 (C4 of thiazole), 172.6 (C2 of thiazole), 174.2 (CO, cyclic), 126.4, 128.4, 129.5, 130.8, 133.9, 137.8 (Ar).

4-(4-Bromophenyl)3-chloro-1-[[2-(2-thiazolylamino)ethyl]amino]-2-azetidione (4e). Yield: 3.50 g, 60 %; m.p. 83–84 °C; Anal. Calcd. for C₁₄H₁₄BrClN₄O₂S: C, 41.85; H, 3.51; N, 13.94 %. Found: C, 41.82; H, 3.45; N, 13.90 %; IR (KBr, cm⁻¹): 572 (C-Br), 1310 (C-N), 1748 (CO cyclic), 2896 (CH-Cl); ¹H-NMR (300 MHz, CDCl₃, δ / ppm): 3.33 (2H, *m*, CH₂-N), 3.95 (2H, *m*, N-CH₂), 4.30 (1H, *d*, *J* = 5.0 Hz, CH-Cl), 4.92 (1H, *d*, *J* = 5.0 Hz, N-CH), 7.14 (1H, *d*, *J* = 4.95 Hz, C5-H of thiazole), 7.32 (1H, *d*, *J* = 4.95 Hz, C4-H of thiazole), 7.46 (1H, *s*, NH), 7.88 (1H, *s*, NH), 7.35–7.95 (4H, *m*, Ar-H); ¹³C-NMR (75 MHz, CDCl₃, δ / ppm): 43.0 (CH₂-N), 52.1 (N-CH₂), 53.6 (CH-Cl), 62.7 (N-CH), 112.6 (C5 of thiazole), 140.9 (C4 of thiazole), 171.2 (C2 of thiazole), 171.9 (CO, cyclic), 122.5, 128.8, 134.7, 137.8 (Ar).

4-(3-Bromophenyl)3-chloro-1-[[2-(2-thiazolylamino)ethyl]amino]-2-azetidione (4f). Yield: 3.60 g, 65 %; m.p. 81–82 °C; Anal. Calcd. for C₁₄H₁₄BrClN₄O₂S: C, 41.85; H, 3.51; N, 13.94 %. Found: C, 41.82; H, 3.48; N, 13.91 %; IR (KBr, cm⁻¹): 578 (C-Br), 1328 (C-N), 1744 (CO, cyclic), 2892 (CH-Cl); ¹H-NMR (300 MHz, CDCl₃, δ / ppm): 3.29 (2H, *m*, CH₂-N), 3.91 (2H, *m*, N-CH₂), 4.29 (1H, *d*, *J* = 5.10 Hz, CH-Cl), 4.97 (1H, *d*, *J* = 5.10 Hz, N-CH), 7.00 (1H, *d*, *J* = 4.90 Hz, C5-H of thiazole), 7.30 (1H, *d*, *J* = 4.90 Hz, C4-H of thiazole), 7.39 (1H, *s*, NH), 7.91 (1H, *s*, NH), 7.31–7.92 (4H, *m*, Ar-H); ¹³C-NMR (75 MHz, CDCl₃, δ / ppm): 42.5 (CH₂-N), 51.9 (N-CH₂), 52.7 (CH-Cl), 621.9 (N-CH), 112.6 (C5 of thiazole), 141.7 (C4 of thiazole), 171.9 (C2 of thiazole), 175.3 (CO, cyclic), 123.5, 125.6, 129.8, 130.7, 132.8, 139.2 (Ar).

4-(2-Bromophenyl)3-chloro-1-[[2-(2-thiazolylamino)ethyl]amino]-2-azetidione (4g). Yield: 3.30 g, 64 %; m.p. 80–81 °C; Anal. Calcd. for C₁₄H₁₄BrClN₄O₂S: C, 41.85; H, 3.51; N, 13.94 %. Found: C, 41.80; H, 3.50; N, 13.92 %; IR (KBr, cm⁻¹): 569 (C-Br), 1329 (C-N), 1750 (CO, cyclic), 2888 (CH-Cl); ¹H-NMR (300 MHz, CDCl₃, δ / ppm): 3.33 (2H, *m*, CH₂-N), 3.97 (2H, *m*, N-CH₂), 4.34 (1H, *d*, *J* = 5.10 Hz, CH-Cl), 4.95 (1H, *d*, *J* = 5.10 Hz, N-CH), 7.97 (1H, *d*, *J* = 4.90 Hz, C5-H of thiazole), 7.29 (1H, *d*, *J* = 4.90 Hz, C4-H of thiazole), 7.48 (1H, *s*, NH), 7.94 (1H, *s*, NH), 7.27–7.84 (4H, *m*, Ar-H); ¹³C-NMR (75 MHz, CDCl₃, δ / ppm): 42.4 (CH₂-N), 51.7 (N-CH₂), 51.7 (CH-Cl), 61.9 (N-CH), 111.8 (C5 of thiazole), 140.8 (C4 of thiazole), 170.8 (C2 of thiazole), 174.5 (CO, cyclic), 121.4, 125.7, 127.9, 131.3, 133.4, 142.6 (Ar).

3-Chloro-4-(4-nitrophenyl)-1-[[2-(2-thiazolylamino)ethyl]amino]-2-azetidione (4h). Yield: 3.40 g, 68 %; m.p. 88–90 °C; Anal. Calcd. for C₁₄H₁₄ClN₅O₃S: C, 45.71; H, 3.83; N, 19.04 %. Found: C, 45.66; H, 3.80; N, 19.00 %; IR (KBr, cm⁻¹): 878 (C-NO), 1548 (NO₂), 1744 (CO, cyclic), 2927 (CH-Cl); ¹H-NMR (300 MHz, CDCl₃, δ / ppm): 3.34 (2H, *m*, CH₂-N), 3.96 (2H,

m, N-CH₂), 4.30 (1H, *d*, *J* = 4.85 Hz, CH-Cl), 4.93 (1H, *d*, *J* = 5.10 Hz, N-CH), 7.30 (1H, *d*, *J* = 4.80 Hz, C4-H of thiazole), 7.81 (1H, *d*, *J* = 4.80 Hz, C5-H of thiazole), 7.45 (1H, *s*, NH), 7.87 (1H, *s*, NH), 7.13–7.71 (4H, *m*, Ar-H); ¹³C-NMR (75 MHz, CDCl₃, δ / ppm): 43.1 (CH₂-N), 52.6 (N-CH₂), 51.3 (CH-Cl), 64.8 (N-CH), 112.8 (C5 of thiazole), 140.9 (C4 of thiazole), 170.4 (C2 of thiazole), 171.3 (CO, cyclic), 125.7, 127.8, 137.9, 147.8 (Ar).

3-Chloro-4-(3-nitrophenyl)-1-[[2-(2-thiazolylamino)ethyl]amino]-2-azetidione (4i). Yield: 3.37 g, 65 %; m.p. 86–87 °C; Anal. Calcd. for C₁₄H₁₄ClN₅O₃S: C, 45.71; H, 3.83; N, 19.04 %. Found: C, 45.66; H, 3.80; N, 19.02 %; IR (KBr, cm⁻¹): 869 (C-NO), 1549 (NO₂), 1741 (CO, cyclic), 2924 (CH-Cl); ¹H-NMR (300 MHz, CDCl₃, δ / ppm): 3.35 (2H, *m*, CH₂-N), 3.98 (2H, *m*, N-CH₂), 4.37 (1H, *d*, *J* = 5.0 Hz, CH-Cl), 4.92 (1H, *d*, *J* = 5.0 Hz, N-CH), 6.94 (1H, *d*, *J* = 4.85 Hz, C5-H of thiazole), 7.20 (1H, *d*, *J* = 4.85 Hz, C4-H of thiazole), 7.46 (1H, *s*, NH), 7.83 (1H, *s*, NH), 7.16–7.79 (4H, *m*, Ar-H); ¹³C-NMR (75 MHz, CDCl₃, δ / ppm): 43.1 (CH₂-N), 53.7 (N-CH₂), 54 (CH-Cl), 62.8 (N-CH), 112.6 (C5 of thiazole), 141.2 (C4 of thiazole), 171.3 (C2 of thiazole), 172.3 (CO, cyclic), 120.5, 123.9, 128.6, 138.4, 139.6, 149.8 (Ar).

3-Chloro-4-(2-nitrophenyl)-1-[[2-(2-thiazolylamino)ethyl]amino]-2-azetidione (4j). Yield: 3.34 g, 61 %; m.p. 73–74 °C; Anal. Calcd. for C₁₄H₁₄ClN₅O₃S: C, 45.71; H, 3.83; N, 19.04 %. Found: C, 45.63; H, 3.79; N, 18.96 %; IR (KBr, cm⁻¹): 879 (C-NO), 1548 (NO₂), 1740 (CO, cyclic), 2923 (CH-Cl); ¹H-NMR (300 MHz, CDCl₃, δ / ppm): 3.30 (2H, *m*, CH₂-N), 3.97 (2H, *m*, N-CH₂), 4.30 (1H, *d*, *J* = 5.10 Hz, CH-Cl), 4.94 (1H, *d*, *J* = 5.10 Hz, N-CH), 6.90 (1H, *d*, *J* = 4.85 Hz, C5-H of thiazole), 7.22 (1H, *d*, *J* = 4.85 Hz, C4-H of thiazole), 7.49 (1H, *s*, NH), 7.89 (1H, *s*, NH), 7.05–7.71 (4H, *m*, Ar-H); ¹³C-NMR (75 MHz, CDCl₃, δ / ppm): 43.4 (CH₂-N), 53.4 (N-CH₂), 52.6 (CH-Cl), 63.8 (N-CH), 112.3 (C5 of thiazole), 140.7 (C4 of thiazole), 171.8 (C2 of thiazole), 173.2 (CO, cyclic), 123.8, 127.9, 129.8, 132.8, 135.9, 145.8 (Ar).

3-Chloro-4-(4-methoxyphenyl)-1-[[2-(2-thiazolylamino)ethyl]amino]-2-azetidione (4k). Yield: 2.75 g, 60 %; m.p. 72–74 °C; Anal. Calcd. for C₁₅H₁₇ClN₄O₂S: C, 51.06; H, 4.85; N, 15.87 %. Found: C, 51.00; H, 4.80; N, 15.82 %; IR (KBr, cm⁻¹): 1160 (C-O), 1323 (N-C), 1726 (CO, cyclic), 2890 (CH-Cl); ¹H-NMR (300 MHz, CDCl₃, δ / ppm): 3.29 (2H, *m*, CH₂-N), 3.95 (2H, *m*, N-CH₂), 3.60 (3H, *s*, OCH₃), 4.21 (1H, *d*, *J* = 5.15 Hz, CH-Cl), 4.79 (1H, *d*, *J* = 5.15 Hz, N-CH), 6.92 (1H, *d*, *J* = 4.95 Hz, C5-H of thiazole), 7.27 (1H, *d*, *J* = 4.95 Hz, C4-H of thiazole), 7.44 (1H, *s*, NH), 7.80 (1H, *s*, NH), 7.26–7.92 (4H, *m*, Ar-H); ¹³C-NMR (75 MHz, CDCl₃, δ / ppm): 40.9 (CH₂-N), 50.8 (N-CH₂), 50.7 (CH-Cl), 54.3 (OCH₃), 61.4 (N-CH), 111.6 (C5 of thiazole), 139.8 (C4 of thiazole), 169.7 (C₂ of thiazole), 171.5 (CO, cyclic), 113.4, 127.2, 131.7, 160.2 (Ar).

3-Chloro-4-(4-methylphenyl)-1-[[2-(2-thiazolylamino)ethyl]amino]-2-azetidione (4l). Yield: 2.30 g, 56 %; m.p. 69–70 °C; Anal. Calcd. for C₁₅H₁₇ClN₄OS: C, 53.48; H, 5.08; N, 16.63 %. Found: C, 53.43; H, 5.05; N, 16.60 %; IR (KBr, cm⁻¹): 1742 (CO, cyclic), 2880 (CH–Cl), 2928 (CH₃); ¹H-NMR (300 MHz, CDCl₃, δ / ppm): 2.61 (3H, *s*, CH₃), 3.32 (2H, *m*, CH₂–N), 3.94 (2H, *m*, N–CH₂), 4.13 (1H, *d*, *J* = 5.05 Hz, CH–Cl), 4.72 (1H, *d*, *J* = 5.05 Hz, N–CH), 6.80 (1H, *d*, *J* = 4.90 Hz, C5–H of thiazole), 7.18 (1H, *d*, *J* = 4.90 Hz, C4–H of thiazole), 7.36 (1H, *s*, NH), 7.82 (1H, *s*, NH), 7.28–7.98 (4H, *m*, Ar–H); ¹³C-NMR (75 MHz, CDCl₃, δ / ppm): 24.8 (CH₃), 40.1 (CH₂–N), 50.0 (N–CH₂), 49.7 (CH–Cl), 60.8 (N–CH), 111.6 (C5 of thiazole), 138.7 (C4 of thiazole), 169.8 (CO, cyclic), 170.5 (C2 of thiazole), 126.8, 129.5, 134.8, 137.7 (Ar).

3-Chloro-4-(4-hydroxyphenyl)-1-[[2-(2-thiazolylamino)ethyl]amino]-2-azetidione (4m). Yield: 2.65 g, 64 %; m.p. 65–67 °C; Anal. Calcd. for C₁₄H₁₅ClN₄O₂S: C, 49.62; H, 4.46; N, 16.53 %. Found: C, 49.55; H, 4.41; N, 16.50 %; IR (KBr, cm⁻¹): 1750 (CO, cyclic), 2925 (CH–Cl), 3462 (OH); ¹H-NMR (300 MHz, CDCl₃, δ / ppm): 4.18 (1H, *s*, OH), 3.35 (2H, *m*, CH₂–N), 3.98 (2H, *m*, N–CH₂), 4.28 (1H, *d*, *J* = 5.10 Hz, CH–Cl), 4.98 (1H, *d*, *J* = 5.10 Hz, N–CH), 6.92 (1H, *d*, *J* = 4.85 Hz, C5–H of thiazole), 7.32 (1H, *d*, *J* = 4.85 Hz, C4–H of thiazole), 7.39 (1H, *s*, NH), 7.85 (1H, *s*, NH), 7.09–8.12 (4H, *m*, Ar–H); ¹³C-NMR (75 MHz, CDCl₃, δ / ppm): 41.5 (CH₂–N), 51.8 (N–CH₂), 53.6 (CH–Cl), 63.9 (N–CH), 112.6 (C5 of thiazole), 139.8 (C4 of thiazole), 169.8 (C2 of thiazole), 176.4 (CO, cyclic), 113.8, 122.9, 138.8, 153.8 (Ar).



Isolation of complexes formed between insulin-like growth factor-binding protein-3 and transferrin from human serum

GORAN MILJUŠ^{*#}, MIOMIR PETROVIĆ and OLGICA NEDIĆ[#]

*Institute for the Application of Nuclear Energy – INEP, University of Belgrade,
Banatska 31b, 11080 Belgrade – Zemun, Serbia*

(Received 31 August, revised 7 December 2011)

Abstract: Insulin-like growth factors (IGFs) play an important role in the regulation of cell growth, differentiation and metabolism. The amount of free, biologically active IGFs is regulated by the IGF-binding proteins (IGFBPs). IGFBP-3 is the most abundant binding protein and it is known to interact with other circulating proteins, including transferrin (Tf). In order to elucidate the possible role of IGF/IGFBP-3 in the metabolism of iron, it is necessary to isolate IGFBP-3/Tf complexes. Several affinity-based techniques were employed. The results showed that only the double immunoprecipitation method with anti-Tf and anti-IGFBP-3 antibodies selectively separated the complexes from other molecular forms, such as monomers, oligomers or fragments of IGFBP-3 and Tf. The isolated complexes can now be used to investigate the relationship between IGF/IGFBP-3 and iron, both in structural and metabolic terms.

Keywords: IGFBP-3; transferrin; complex; isolation.

INTRODUCTION

Insulin-like growth factors (IGF-I and IGF-II), together with six IGF-binding proteins (IGFBP-1 to IGFBP-6), two IGF receptors (IGF-1R and IGF-2R) and insulin and its receptor (IR), comprise a complex system that plays an important role in the regulation of cell growth, differentiation and metabolism.^{1,2} The pivotal role in the regulation of the IGF action have the IGFBPs. The most abundant in circulation is IGFBP-3.³ It forms ternary complexes (150 kea) with IGF and an acid labile subunit (ALES).⁴ The ternary complexes cannot cross the vascular barrier and they are assumed to be an IGF reservoir, releasing free, biologically active IGF upon mitogenic and/or metabolic request of the organism. IGFBP-3 is, in its native form, a glycoprotein (40–45 kDa), synthesized in the liver parenchymal cells.⁵ Besides its ability to bind and regulate the activity of IGFs, it was

* Corresponding author. E-mail: goranm@inep.co.rs

Serbian Chemical Society member.

doi: 10.2298/JSC110831211M

also reported that IGFBP-3 has IGF-independent actions, *via* nuclear IGFBP-3 receptors,⁶ and it may bind to other molecules, of which transferrin is one.⁷

Transferrin (Tf) is a glycoprotein (70–80 kDa) functioning as the main iron transporter.⁸ Regulation of the iron distribution in the organism affects the formation of hemoglobin, the functionality of enzymes (having iron as a cofactor) and redox processes.⁹

Since the IGF/IGFBP-3 axis promotes anabolic reactions, it would be important to investigate its possible role in iron metabolism and the significance of the formation of the IGFBP-3/Tf complex. In order to do so, the first step is to isolate the complexes from other molecular forms of either IGFBP-3 or Tf, and other blood constituents. In this work several approaches based on affinity interactions were tested.

EXPERIMENTAL

Serum samples

Serum samples were obtained from healthy individuals. All samples were taken from venous blood 12 h after fasting. The sera were kept frozen at -20°C until used. This study was approved by the local ethical committee in the Institute for the Application of Nuclear Energy.

Immobilised metal-affinity chromatography (IMAC)

Iminodiacetic acid–agarose (IDA) was purchased from Sigma–Aldrich (Steinheim, Germany). A column was packed with 1 mL of gel and washed with distilled water. In order to saturate the column with ferric ions, 1.0 mL of 0.10 mol L^{-1} ferric chloride solution was applied. Unbound ions were washed with 5 mL of distilled water and 5 mL of 0.1 % acetic acid. Equilibration of the column was realized with dilution buffer: 0.05 mol L^{-1} MES (2-(*N*-morpholino)ethanesulphonic acid)/ 0.5 mol L^{-1} NaCl buffer pH 5.5.¹⁰ Samples (100 μL of sera diluted in 900 μL of dilution buffer) were applied to column and circulated for 1 h to ensure maximal binding. Unbound material was washed out with 5 mL of MES buffer. Elution of the bound molecules was performed using 8 mL of 0.2 mol L^{-1} phosphate buffer (PB) pH 8.0. The column was regenerated using 10 mL of 0.1 mol L^{-1} borate/ 1.0 mol L^{-1} NaCl buffer pH 10.0 and 10 mL of distilled water, followed by saturation with ferric chloride. The collected fractions were analysed by electrophoresis and immunoblotting.

Immunoaffinity chromatography (IgY-C)

An IgY-12 column (1.2 mL of microbeads) was purchased from Beckman Coulter (Fullerton, USA, Proteomelab IgY-12 High Capacity Proteome Partitioning Kit). According to the manufacturer's description, the matrix with immobilised antibodies enables the binding of the 12 most abundant proteins from human plasma: albumin, IgG, IgA, IgM, α 1-anti-trypsin, haptoglobin, fibrinogen, orosomucoid, α ₂M, HDL (apo A-I and apo A-II) and Tf. Samples were prepared by diluting 20 μL of sera with 480 μL of dilution buffer: 10 mmol L^{-1} Tris (tris(hydroxymethyl)aminomethane)–HCl/ 1.0 mol L^{-1} NaCl buffer pH 7.4, and incubated for 15 min at room temperature using a rotator.¹¹ Separation of the unbound proteins was performed by centrifugation for 30 s at $2000\times g$, followed by washing the column three times with dilution buffer. The bound proteins were eluted with 500 μL of elution buffer: 0.1 mol L^{-1} glycine–HCl, pH 2.5, for 3 min at room temperature using a rotator, separated from gel by centrifugation and immediately neutralised with 50 μL of 1 mol L^{-1} Tris–HCl buffer pH 8.0.

The elution was repeated three times. The column was neutralised with 500 μL of 2 mol L^{-1} Tris-HCl buffer pH 8.0 and washed with dilution buffer prior to the next chromatographic cycle. The collected fractions were analysed by electrophoresis and immunoblotting.

Lectin affinity chromatography (LAC)

Eleven agarose-immobilised lectins, purchased from Vector Laboratories (Burlingame, CA, USA), were packed in columns: SNA (*Sambucus nigra* agglutinin), LCA (*Lens culinaris* agglutinin), Con A (lectin from *Canavalia ensiformis*), PHA-E (*Phaseolus vulgaris* erythroagglutinin), PHA-L (*Phaseolus vulgaris* leucoagglutinin), RCA-I (*Ricinus communis* agglutinin I), WGA (wheat germ agglutinin), succinylated WGA, ECL (*Erythrina cristagalli* lectin), MAL (*Maackia amurensis* lectin) and UEA (*Ulex europaeus* agglutinin). All buffers and hapten sugars were prepared following procedures recommended by the producer. The exact composition of each buffer was published elsewhere.¹² Serum samples (100 μL) diluted in 900 μL of the corresponding buffers were circulated through columns for 1 h. Unbound material was washed out with 20 mL of the dilution buffers. The elution of bound glycoproteins was performed with 7 mL of hapten sugar (0.2–0.5 mol L^{-1} , as suggested by the producer) in 0.1 M acetic acid, pH 3.0. The PHA-E and PHA-L columns were eluted using a 0.1 mol L^{-1} acetic acid solution. The collected fractions were immediately neutralised using 2 mol L^{-1} Tris-HCl buffer pH 8.9, dialysed against distilled water overnight at 4 °C and analysed by electrophoresis and immunoblotting.

Immuno-electrophoresis (IEP)

Immuno-electrophoresis (IEP) was performed in a standard manner.¹³ Serum samples (5 μL) were applied in sample wells, and antibodies in channels (100 μL): polyclonal anti-Tf antibodies (INEP, Belgrade, Serbia), and polyclonal anti-IGFBP3 antibodies (DSL, Webster, TX, USA). The samples were incubated with antibodies in a humid chamber for 24 h at room temperature, to allow immunoprecipitation to occur.

Co-immunoprecipitation (Co-IP)

Immunoprecipitation of protein complexes was performed using Pierce® Co-Immunoprecipitation Kit (Pierce Biotechnology, Rockford, IL, USA). Following the manufacturer's instructions, AminoLink® Plus Coupling Resin (50 μL of 50 % slurry) was loaded into spin columns and 5 μg of anti-IGFBP-3 antibodies (Santa Cruz Biotechnology, Santa Cruz, CA, USA) or 10 μg of anti-Tf antibodies (INEP, Belgrade, Serbia) were immobilised. Serum samples (10 μL) were diluted in 190 μL of the buffer: 2.5 mmol L^{-1} Tris/0.15 mol L^{-1} NaCl/1.0 mmol L^{-1} EDTA/1% NP-40/5 % glycerol, pH 7.4 and incubated overnight at 4 °C with a resin having immobilised anti-Tf antibodies. Separation of the unbound proteins was performed by centrifugation for 30 s at 2000 $\times g$, followed by washing the column three times with dilution buffer. The bound proteins were eluted with 110 μL of the elution buffer pH 2.8 (provided within the Kit), separated by centrifugation and immediately neutralised with 2 μL of 2 mol L^{-1} Tris-HCl buffer, pH 8.9. Specifically eluted anti-Tf immunoreactive proteins were further incubated with a resin having immobilised anti-IGFBP-3 antibodies, overnight at 4 °C. The removal of the unbound and the elution of the bound proteins followed the same procedure as previously. The collected fractions were analysed by electrophoresis, dot and immunoblotting.

Electrophoresis, dot and Western immunoblotting (WIB)

Protein fractions obtained by IMAC, IgY-C, LAC, and Co-IP were subjected to denaturing non-reducing sodium dodecyl sulphate/polyacrylamide gel electrophoresis (SDS-PAGE) using 10 % gels.¹⁴ The separated proteins were transferred to a nitrocellulose membrane and stained with Ponceau S.

The WIB procedure was performed using goat polyclonal anti-IGFBP-3 (DSL, Webster, TX, USA) and sheep polyclonal anti-Tf (INEP, Belgrade, Serbia) primary antibodies, followed by anti-goat secondary antibodies coupled to horseradish peroxidase (Biosource, Camarillo, CA, USA). The immunoreactive proteins were visualised with an enhanced chemiluminescence (ECL) reagent kit (Pierce, Minneapolis, MN, USA).¹⁴ Molecular mass markers were obtained from BioRad Laboratories (Hemel Hempstead, UK). Recombinant IGFBP-3 (29 kDa, DSL, Webster, TX, USA) and Tf (INEP, Belgrade, Serbia) were used as protein markers.

The presence of IGFBP-3/Tf complexes was also confirmed by dot blotting, employing anti-IGFBP-3 and anti-Tf antibodies.

Ligand-binding assay

An in-house made matrix, CNBr-activated Sepharose 4B,^{15,16} was used to immobilise sheep anti-Tf antibodies (INEP, Belgrade, Serbia). This immunoaffinity resin was employed to test the ability of IGFBP-3 complexed to Tf to bind the ligand.

Serum samples (100 μ L) were incubated with ¹²⁵I-labelled IGF-II (¹²⁵I-IGF-II, 300 000 cpm) at 4 °C overnight, loaded onto a column packed with immunoaffinity resin and recirculated for 1 h. The column was left with the sample at 4 °C overnight and the next day, the sample was recirculated for a further 1 h. The unbound proteins were washed out with the dilution buffer: 0.05 mol L⁻¹ PBS/0.15 mol L⁻¹ NaCl, pH 7.2, and elution of the bound fraction was performed using the elution buffer: 0.1 mol L⁻¹ glycine/HCl, pH 3.7. Fractions were immediately neutralised with 2 mol L⁻¹ Tris-HCl buffer pH 8.9. The radioactivity and the A₂₈₀ of the collected fractions were measured.

Ultrafiltration

Protein fractions containing IGFBP-3/Tf complexes were subjected to ultrafiltration, in order to concentrate samples and remove small proteins. Microcon YM-50 filters were used (Millipore Corporation, Billerica, USA).

RESULTS AND DISCUSSION

In order to isolate IGFBP-3/Tf complexes from human serum, several affinity-based techniques were employed. As IGFBP-3 and Tf are glycosylated^{17,18} and IGFBP-3 is also phosphorylated,³ methods based on the following interactions were applied: metal ion–amino acid or phosphate residue,¹⁹ lectin–saccharide moiety^{20–22} and antigen–antibody.²³

In the IMAC method, all IGFBP-3 (Fig. 1A) and Tf (Fig. 1B) immunoreactive species were bound to the matrix: native IGFBP-3 (doublet at \approx 45 kDa), an IGFBP-3 fragment (\approx 30 kDa),²⁴ oligomeric/complexed forms of IGFBP-3 (>80 kDa), as well as Tf (70–80 kDa) and complexes of Tf (>100 kDa).

In the IgY-C method,²⁵ the immobilised antibodies recognised and bound complexes of IGFBP-3 (>100 kDa), whereas native and fragmented IGFBP-3 species remained among the unbound proteins (Fig. 2A). There were also IGFBP-3 immunoreactive bands at \approx 45 kDa and \approx 70 kDa, which might have originated from dissociated complexes. Immunoblotting with anti-Tf antibodies (Fig. 2B) indicated binding of native Tf, a Tf fragment (\approx 40 kDa)²⁶ and Tf complexes. In the IgY-unbound fraction, anti-Tf antibodies recognised a protein at \approx 70 kDa (Fig. 2B). It is known that Tf exists in several glycoforms²⁷ and the results of this

experiment suggested that the antibodies immobilised on the IgY-C matrix were unable to bind the Tf isoform that was less glycosylated.

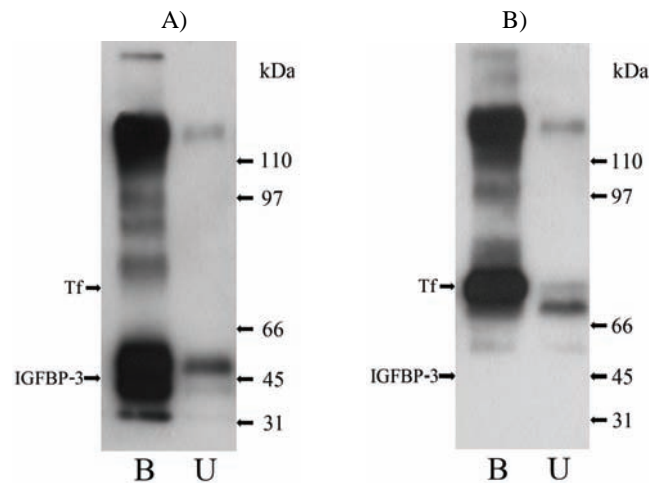


Fig. 1. Immunoblotting of the bound (B) and unbound (U) fractions of serum samples obtained after IMAC with A) anti-IGFBP-3 and B) anti-Tf antibodies. The positions of the IGFBP-3 monomer and Tf are indicated on the left side, whereas the positions of the molecular mass markers are indicated on the right side.

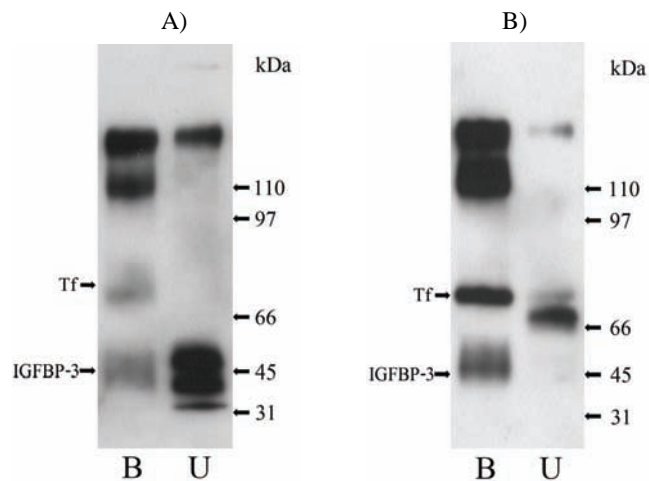


Fig. 2. Immunoblotting of the bound (B) and unbound (U) fractions of serum samples obtained after IgY-C with A) anti-IGFBP-3 and B) anti-Tf antibodies.

The positions of the IGFBP-3 monomer and Tf are indicated on the left side, whereas the positions of the molecular mass markers are indicated on the right side.

Lectins are established as an important analytical tool in glycoproteomics. As both IGFBP-3 and Tf are glycoproteins, the LAC method was the next me-

thod of choice. The lectins used in this experiment were those that are known to interact with serum glycoproteins.^{28,29} Of the eleven lectins that were employed in the LAC method, only six (PHA-E, RCA-I, Con A, WGA, SNA and LCA) bound native IGFBP-3 at ≈ 45 kDa (Fig. 3A) and five of them (except LCA) bound Tf at ≈ 80 kDa (Fig. 3B). Beside monomer forms (and in some cases fragments), higher molecular mass proteins that were both IGFBP-3 and Tf immunoreactive were not detected (except at the start). The tested lectins were, therefore, unable to bind IGFBP-3/Tf complexes.

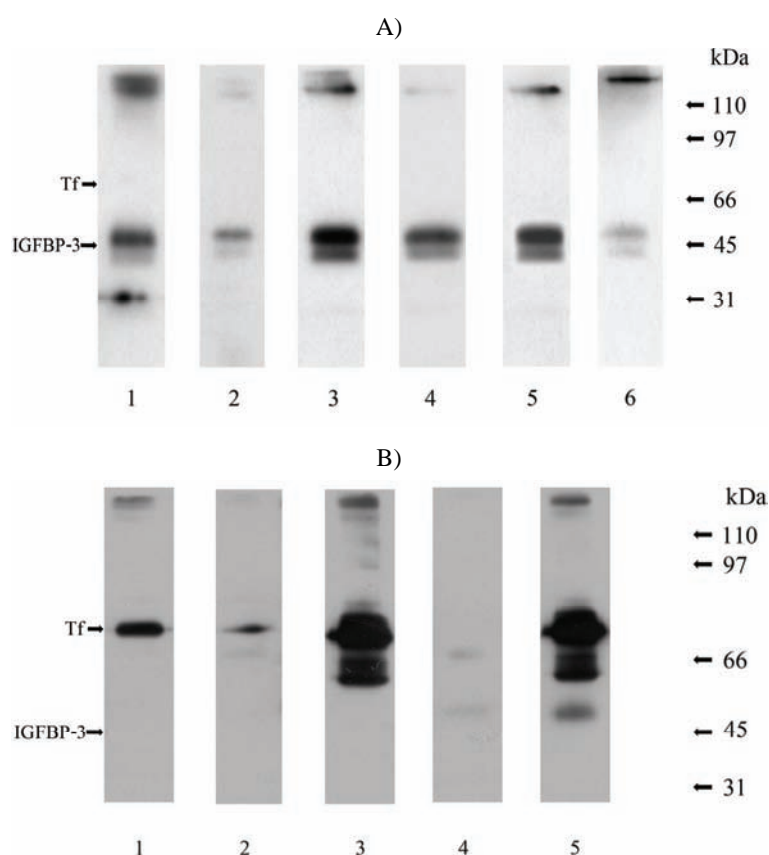
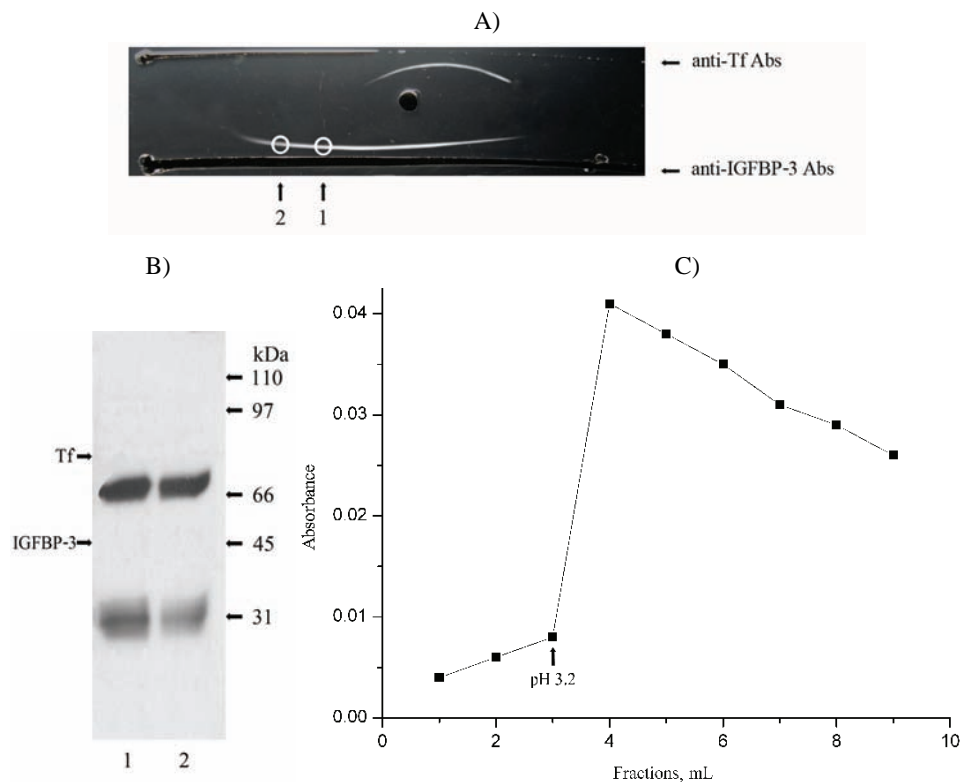


Fig. 3. Immunoblotting of the bound fractions of serum samples obtained after LAC with A) anti-IGFBP-3 and B) anti-Tf antibodies. The presented samples were eluted from: PHA-E-agarose (lane 1), RCA-I-agarose (lane 2), Con A-agarose (lane 3), WGA-agarose (lane 4), SNA-agarose (lane 5) and LCA-agarose (lane 6). The positions of the IGFBP-3 monomer and Tf are indicated on the left side, whereas the positions of the molecular mass markers are indicated on the right side.

To summarise the above results, none of the applied affinity-chromatography methods was able to selectively recognise IGFBP-3/Tf complexes and sepa-

rate them from the monomeric, oligomeric and fragmented forms of IGFBP-3 and Tf. As IgY-C seemed the most promising tool, other immunochemical techniques were tested for the isolation of the complexes: immunoelectrophoresis, preparative immunoaffinity chromatography and the immunoprecipitation method.³⁰

In the IEP method, the idea was to analyse immunoprecipitated proteins. The IGFBP-3/Tf complexes were expected to travel at a rate different to those of their subunits. Since the concentration of Tf in serum³¹ is much greater than the concentration of IGFBP-3,³² the search for complexes was performed in the region where free Tf was not expected to be found, but where the reaction with anti-IGFBP-3 antibodies was positive. Two samples (Fig. 4A, spots 1 and 2), from the immunoprecipitating line formed by the interaction of serum with anti-IGFBP-3 antibodies were analysed. Immunoblotting with anti-IGFBP-3 antibodies revealed that an IGFBP-3 fragment and, probably, a dimer (≈ 70 kDa), were the only immunoreactive species in this part of the immunoprecipitated line (Fig. 4B). No band at the expected molecular mass of the IGFBP-3/Tf complexes (≈ 110 kDa) was observed.



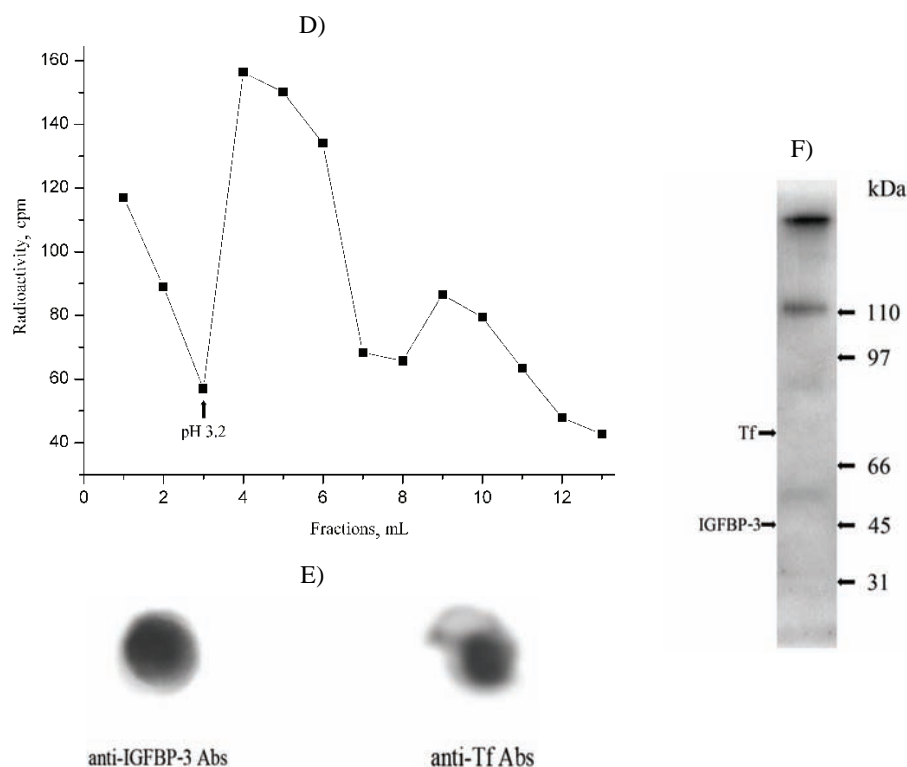


Fig. 4. A) IEP of a serum sample, with applied antibodies indicated on the right side; selected spots from the immunoprecipitating line (1 and 2) were subjected to B) immunoblotting with anti-IGFBP-3 antibodies; C) in preparative immunoaffinity chromatography, the amount of the eluted proteins (A_{280}) was measured. D) In preparative immunoaffinity chromatography, radioactivity of the eluted ligand-binding IGFBP-3/Tf complexes (cpm) was measured; E) dot blot and F) Western immunoblotting with anti-IGFBP-3 and anti-Tf antibodies of the isolated IGFBP-3/Tf complexes after co-immunoprecipitation. The positions of the IGFBP-3 monomer and Tf are indicated on the left side, whereas the positions of the molecular mass markers are indicated on the right side.

Preparative immunoaffinity chromatography is widely appreciated for the isolation and purification of immunoreactive species.³³ Since the commercial IgY matrix was able to bind IGFBP-3/Tf complexes, a matrix for the isolation of the anti-Tf antibody reactive molecules was prepared in-house, using CNBr activated resin.³⁴ The antibodies were coupled directly. The amount of bound immunoreactive proteins was, unfortunately, very small (Fig. 4C, A_{280}), probably due to an improper orientation of the antibodies. The yield of the bound proteins could possibly be improved by using spacer molecules, such as carbodiimide,³⁴ or protein A³⁵ in order to immobilise the antibodies *via* their C-terminal ends and leave their N-terminal, antigen-binding sites, free.³⁶ The same experiment was re-

peated with serum samples pre-incubated with ^{125}I -IGF-II. Radioactivity measurement (Fig. 4D, cpm) demonstrated that a certain amount of ^{125}I -IGF-II was bound to the immobilised anti-Tf antibodies, suggesting that IGFBP-3 in the IGFBP-3/Tf complexes retains its ability to bind ligand.

Finally, a co-immunoprecipitation method was employed, using a commercial activated resin to immobilise separately anti-IGFBP-3 and anti-Tf antibodies. The immunoprecipitation method is among the most specific techniques to isolate a target protein with the least amount of contaminating substances. In this study, a double immunoprecipitation was performed. Samples were allowed to interact with the immobilised anti-Tf antibodies in the first step and, after elution of the bound proteins, this fraction was allowed to interact with anti-IGFBP-3 antibodies. Due to the high affinity of antigen-antibody interactions, the elution necessitated the employment of rather harsh experimental conditions (pH 2.8). In order to test whether the IGFBP-3/Tf complexes had survived such conditions, their existence was investigated by dot blotting (Fig. 4E). The result demonstrated that complexes mostly resisted dissociation. The proteins that were eluted after the second step contained almost exclusively IGFBP-3/Tf complexes (Fig. 4F). Fragments (≈ 30 kDa) were present in minor amounts and they were completely removed by ultrafiltration.

CONCLUSION

Isolation of the IGFBP-3/Tf complexes from human serum was achieved by using an immunoaffinity method, whereas metal- and lectin-affinity techniques were unsuccessful. Among several immunochemical approaches, only the double immunoprecipitation method selectively separated the complexes from other molecular forms, such as monomers, oligomers or fragments of IGFBP-3 and Tf. A further study of the relationship between IGFBP-3, Tf and Tf saturation with iron is expected to elucidate the possible role of IGF/IGFBP-3 in iron metabolism.

Acknowledgement. This work was supported by the Ministry of Education and Science of the Republic of Serbia, Grant No. 173042.

ИЗВОД

ИЗОЛОВАЊЕ КОМПЛЕКСА ФОРМИРАНОГ ИЗМЕЂУ ВЕЗУЈУЋЕГ ПРОТЕИНА ЗА ИНСУЛИНУ СЛИЧНЕ ФАКТОРЕ РАСТА 3 И ТРАНСФЕРИНА ИЗ ХУМАНОГ СЕРУМА

ГОРАН МИЉУШ, МИОМИР ПЕТРОВИЋ И ОЛГИЦА НЕДИЋ

*Институт за примену нуклеарне енергије – ИНЕП, Универзитет у Београду,
Банатска 316, 11080 Београд-Земун*

Инсулину слични фактори раста (IGF) имају важну улогу у расту ћелија, њиховој диференцијацији и метаболизму. Количину слободног, биолошки активног IGF регулишу IGF везујући протеини (IGFBP). IGFBP-3 је присутан у највећој количини и има способност да интерагује са другим протеинима из циркулације, укључујући трансферин (Tf). Да би се утврдила могућа улога IGF/IGFBP-3 у метаболизму гвожђа, неопходно је изоловати ком-

плекс IGFBP-3/Tf. У овој студији је примењено неколико техника заснованих на афинитетним интеракцијама. Резултати су показали да само метода двоструке имунопреципитације са анти-Tf, а затим са анти-IGFBP-3 антителима, селективно одваја комплексе од осталих молекулских форми, као што су мономери, олигомери или фрагменти IGFBP-3 и Tf. Овако изоловани комплекс се може даље анализирати у циљу утврђивања односа између IGF/IGFBP-3 и гвожђа, у структурном и метаболичком смислу.

(Примљено 31. августа, ревидирано 7. децембра 2011)

REFERENCES

1. M. Annunziata, R. Granata, E. Ghigo, *Acta Diabetol.* **48** (2011) 1
2. D. Le Roith, *Exp. Diab. Res.* **4** (2003) 205
3. S. M. Firth, R. C. Baxter, *Endocr. Rev.* **23** (2002) 824
4. R. C. Baxter, J. L. Martin, V. A. Beniac, *J. Biol. Chem.* **264** (1989) 11843
5. E. Arany, S. Afford, A. J. Strain, P. J. Winwood, M. J. P. Arthur, D. J. Hill, *J. Clin. Endocrinol. Metab.* **79** (1994) 1871
6. K. W. Lee, B. Liu, L. Ma, H. Li, P. Bang, H. P. Koeffler, P. Cohen, *J. Biol. Chem.* **279** (2004) 469
7. S. A. Weinzimer, T. B. Gibson, P. F. Collet-Solberg, A. Khare, B. Liu, P. Cohen, *J. Clin. Endocrinol. Metab.* **86** (2001) 1806
8. P. Aisen, C. Enns, M. Wessling-Resnick, *Int. J. Biochem. Cell. Biol.* **33** (2001) 940
9. P. T. Gomme, K. B. McCann, *Drug Discov. Today* **10** (2005) 276
10. M. Machida, H. Kosako, K. Shirakabe, M. Kobayashi, M. Ushiyama, J. Inagawa, J. Hirano, T. Nakano, Y. Bando, E. Nishida, S. Hattori, *FEBS J.* **274** (2007) 1576
11. O. Nedić, R. Masnikosa, *J. Chromatogr., B* **877** (2009) 743
12. R. Masnikosa, O. Nedić, I. Baričević, D. Lagundžin, *Biochimie* **92** (2010) 97
13. I. Roitt, J. Brostoff, D. Male, *Immunology*, Mosby, London, UK, 1996, p. 406
14. O. Nedić, R. Masnikosa, *Metab. Clin. Exp.* **57** (2008) 658
15. T. Korpela, K. Kurkijärvi, *Anal. Biochem.* **104** (1980) 150
16. B. J. Ryan, C. Ó'Fágáin, *BMC Biotechnol.* **7** (2007) 1
17. H. R. Bergen, J. M. Lacey, J. F. O'Brien, S. Naylor, *Anal. Biochem.* **296** (2001) 122
18. S. M. Firth, R. C. Baxter, *J. Endocrinol.* **160** (1999) 379
19. N. Imam-Sghiouar, R. Joubert-Caron, M. Caron, *Amino Acids* **28** (2005) 105
20. X. Wei, L. Li, *Briefings Funct. Genomics Proteomics* **8** (2008) 104
21. H. Geyer, R. Geyer, *Biochem. Biophys. Acta Proteins Proteomics* **1764** (2006) 1853
22. J. Zhao, D. M. Simeone, D. Heidt, M. A. Anderson, D. M. Lubman, *J. Proteome Res.* **5** (2006) 1792
23. J. M. McDowell, *Plant Immunity*, Humana Press, Blackburg, VA, 2011, p. 295
24. M. M. Weber, G. Spöttl, C. Gössl, D. Engelhart, *J. Clin. Endocrinol. Metab.* **84** (1999) 1679
25. L. Huang, X. Fang, *Methods Mol. Cell Biol.* **425** (2008) 41
26. D. Grenier, V. Goulet, B. Britigan, K. Nakayama, *Infect. Immun.* **72** (2004) 4351
27. V. Sanz-Nebot, E. Balaguer, F. Benavente, C. Neusüß, J. Barbosa, *Electrophoresis* **28** (2007) 1949
28. S. Miyamoto, *Curr. Opin. Mol. Ther.* **8** (2006) 507
29. M. V. Novotny, M. Madera, B. Mann, Y. Mechref, *J. Sep. Sci.* **31** (2008) 2722

30. J. A. P. Bons, E. C. H. J. Michielsen, D. de Boer, F. G. Bouwman, J. Jaeken, M. P. van Dieijen-Visser, M. E. Rubio-Gozalbo, W. K. W. H. Wodzig, *Clin. Chem. Acta* **387** (2008) 59
31. G. de Jong, J. P. van Dijk, H. G. van Eijk, *Clin. Chim. Acta* **190** (1990) 1
32. A. Juul, *Growth Horm. IGF Res.* **13** (2003) 113
33. I. Roy, K. Mondal, M. N. Gupta, *J. Chromatogr., B* **849** (2007) 32
34. W. Xu, Y. Luo, K. Huang, A. Deng, B. Zhai, H. Zhao, Y. Li, Z. Liang, *Afr. J. Food Sci.* **1** (2007) 24
35. M. Tichá, Z. Kučerová, J. Frýdlová, *J. Chromatogr., B* **800** (2004) 109
36. L. J. Lee, H. He, Y. Yuan, *Biotechnol. Bioeng.* **102** (2009) 891.



Composition and antimicrobial activity of the essential oil from *Galatella linosyris* (L.) Rchb. f. (Asteraceae)

DEJAN GOĐEVAC^{1*}, LJUBODRAG VUJISIĆ², IVAN VUČKOVIĆ², VLATKA VAJS¹,
MARINA SOKOVIĆ³, PETAR D. MARIN^{4#} and VELE TEŠEVIĆ²

¹Institute of Chemistry, Technology and Metallurgy, Njegoševa 12, University of Belgrade, 11000 Belgrade, Serbia, ²Faculty of Chemistry, University of Belgrade, Studentski trg 16, P. O. Box 158, 11000 Belgrade, Serbia, ³Institute for Biological Research “Siniša Stanković”, University of Belgrade, Bulevar despota Stefana 142, 11000 Belgrade, Serbia and ⁴Faculty of Biology, University of Belgrade, Institute of Botany and Botanical Garden “Jevremovac”, Studentski trg 16, 11000 Belgrade, Serbia

(Received 15 September, revised 15 December 2011)

Abstract: An investigation of the chemical composition and antimicrobial activity of the essential oil of *Galatella linosyris* is presented. The chemical analysis (GC/MS, NMR) showed that sabinene (40 %), β -pinene (35.5 %), α -pinene (4.5 %), limonene (4 %), γ -muurolene (4 %), and (*E*)-caryophyllene (3.3 %) were dominant components in this oil. Microdilution assays were used to evaluate the minimum inhibitory concentration (*MIC*) and the minimum bactericidal/fungicidal concentrations (*MBC/MFC*). *G. linosyris* essential oil exhibited better antibacterial activity against some of the tested bacteria than anti-fungal activity.

Keywords: *Galatella linosyris*; essential oil; antimicrobial activity; GC/MS; NMR.

INTRODUCTION

Galatella linosyris (L.) Rchb. f. (Bas. *Chrysocoma linosyris* L.; Syn. *Aster linosyris* (L.) Bernh.; *Linosyris vulgaris* Cass. Ex DC; *Crinitaria linosyris* (L.) Less.; *Crinitina linosyris* (L.) Soják), is a member of the Asteraceae (Compositae) family, distributed from the middle, southern and eastern part of Europe to southern Scandinavia in the North, extending locally northwards to England, and also in Central Russia.^{1,2} This species, known as goldilocks aster, is a perennial herb with a decumbent to erect stem, 10–70 cm high. The leaves are lanceolate, sessile, and often glandular-punctate above. The capitula are small and grouped

* Corresponding author. E-mail: dgodjev@chem.bg.ac.rs

Serbian Chemical Society member.

doi: 10.2298/JSC110915213G

in dense corymbs. It grows on sunny rocks and stony slopes, on dry grasslands and cliffs, on calcareous soil.

G. linosyris has hitherto not been chemically investigated. From the plants of the *Galatella* genus, only the essential oil from *G. biflora* has been analyzed. The major components were α -pinene (34.7 %), (*E*)- β -ocimene (15.0 %), β -pinene (9.9 %), myrcene (7.4 %) and limonene (6.2 %).³

Based on the search for new alternatives for organic syntheses and natural biocontrol of bacteria and fungi, the objective of this study was to investigate the antibacterial and antifungal activity of the essential oil from *G. linosyris* against food poisoning and plant, animal and human pathogenic bacteria and fungi.

EXPERIMENTAL

Plant material

The plant material was collected in Deliblatska peščara, Serbia, during September 2010. A voucher specimen (BEOU16403) is deposited at the Herbarium of the Botanical Garden "Jevremovac," Faculty of Biology, University of Belgrade, Serbia.

Isolation of the essential oil

The air-dried plants (300 g) of *G. linosyris* were submitted for 3 h to water-distillation using a Clevenger apparatus. The obtained essential oil (1.2 mL) was stored at +4 °C until tested and analyzed. The qualitative and quantitative analyses of the oils were performed using nuclear magnetic resonance (NMR) spectroscopy, gas chromatography (GC) and GC coupled to mass spectroscopy (GC/MS).

GC and GC/MS

The GC and GC/MS analyses were performed on an Agilent 7890A GC equipped with a 5975C inert XL EI/CI mass selective detector (MSD) and a flame ionization detector (FID) connected by a capillary flow technology 2-way splitter with make-up. An HP-5MSI capillary column (30m \times 0.25mm \times 0.25 μ m) was used. The temperature of the GC oven was programmed from 60 °C to 300 °C at 3 °C min⁻¹ and held for 10 min. Helium was used as the carrier gas at 16.255 psi (constant pressure mode). The sample was analyzed in the splitless mode. The injection volume was 1 μ L. The FID temperature was 300 °C. The MS data was acquired in the EI mode, with a scan range 30–550 *m/z*; the source temperature was 230 °C and the quadrupole temperature was 150 °C. The solvent delay was 3 min.

NMR

The NMR spectra were acquired on a Bruker Avance DRX 500 MHz instrument with a 5 mm inverse detection probe, in CDCl₃ as the solvent, at 298 K. The spectra were referenced to tetramethylsilane (TMS), chemical shifts are given in δ (ppm), and coupling constants are reported in Hz. Two-dimensional experiments (COSY, HSQC, and HMBC) were recorded with standard Bruker pulse sequences.

Antibacterial activity

The following Gram-negative bacteria: *Escherichia coli* (ATCC 35210), *Pseudomonas aeruginosa* (ATCC 27853), *Salmonella typhimurium* (ATCC 13311), *Listeria monocytogenes* (NCTC 7973), *Enterobacter cloacae* (human isolate) and the following Gram-positive bacteria: *Bacillus cereus* (clinical isolate), *Micrococcus flavus* (ATCC 10240) and *Staphylococcus aureus* (ATCC 6538) were used.

The bacterial cell suspension was adjusted with sterile saline to a concentration of approximately 1.0×10^5 CFU (colony forming units) in a final volume of 100 μ L per well. The microplates were incubated for 24 and 48 h at 37 °C. The lowest concentrations without visible growth (under a binocular microscope) were defined as the minimum inhibition concentration (*MIC*) values. The minimum bactericidal concentration (*MBC*) values were determined by serial subcultivation of 2 μ L in microtitre plates containing 100 μ L of broth per well and further incubation for 24 and 48 h at 37 °C. The lowest concentration with no visible growth was defined as the *MBC*, respectively indicating 99.5 % killing of the original inoculum. Each experiment was repeated in triplicate. Streptomycin was used in the positive controls (1 mg mL⁻¹).

Antifungal activity

For the antifungal bioassays, the following fungi were used: *Aspergillus fumigatus* (plant isolate), *A. niger* (ATCC 6275), *A. versicolor* (ATCC 11730), *A. ochraceus* (ATCC 12066), *Penicillium funiculosum* (ATCC 36839), *P. ochrochloron* (ATCC 9112) and *Trichoderma viride* (IAM 5061).

The fungal spores were washed from the surface of agar plates with sterile 0.85 % saline containing 0.1 % Tween 80 (v/v). The spore suspension was adjusted with sterile saline to a spore concentration of approximately 1.0×10^5 in a final volume of 100 μ L per well. *MIC* determinations were performed by a serial dilution technique using 96-well microtiter plates. The essential oil was dissolved in 5 % DMSO solution containing 0.1 % Tween 80 (v/v) (1 mg mL⁻¹) and added into the broth medium with inoculum. The microplates were incubated for 72 h at 28 °C. The lowest concentrations without visible growth (at the binocular microscope level) were defined as *MIC* values. The minimum fungicidal concentration (*MFC*) values were determined by serial subcultivation of 2 μ L into microtiter plates containing 100 μ L of broth per well and further incubation for 72 h at 28 °C. The lowest concentration with no visible growth was defined as the *MFC* indicating 99.5 % killing of the original inoculum. The commercial fungicide ketoconazole was used as positive controls (0.60–25 μ g mL⁻¹).

The optical density of each well was measured at a wavelength of 655 nm using a Microplate manager 4.0 (Bio-Rad Laboratories) and compared with the corresponding blank and positive control. An aqueous solution of 3 % INT color *p*-iodonitrotetrazolium violet (2-(4-iodophenyl)-3-(4-nitrophenyl)-5-phenyltetrazolium chloride; Sigma) was added to each well and stored for another 3 h for incubation at 37 °C (for bacteria) and 28 °C (for fungi). Changes in color from yellow to a pinkish were indicative that there was no antimicrobial activity of tested oils, whereas no changes in color after 3 h indicated antimicrobial activity of the tested oil. Each experiment was repeated in triplicate.

RESULTS AND DISCUSSION

The components of the oil were identified by comparison of their mass spectra to those from Adams, Wiley 7, and NIST05 libraries. The identification was confirmed by the retention time lock (RTL) method and the RTL Adams database. For quantification purpose, area percent data registered by the FID were used. GC and GCMS analyses showed a total of 18 compounds in the essential oil of *G. linosyris* (Table I). The dominant compounds were sabinene (40 %) and β -pinene (35.5 %), followed by α -pinene (4.5 %), limonene (4 %), γ -muurolene (4 %) and (*E*)-caryophyllene (3.3 %). The chemical composition of the essential

oil from *G. linosyris* was similar to that of *G. biflora*,³ only differences in the component distribution were registered.

TABLE I. Chemical composition of *G. linosyris* essential oil (MIC and MBC in $\mu\text{g mL}^{-1}$)

Compound	Retention time, min	RI	%
α -Thujene	5.622	910	0.24
α -Pinene	5.807	918	4.46
Sabinene	6.898	968	39.98
β -Pinene	7.011	973	35.46
Myrcene	7.400	990	0.77
Terpinene	8.265	1016	0.75
Limonene	8.676	1027	4.02
Z-Ocimene	8.994	1034	0.14
E-Ocimene	9.366	1044	0.64
γ -Terpinene	9.768	1054	1.24
Terpinolene	10.923	1086	0.20
Terpinylacetate	22.263	1351	0.14
β -Elemene	24.124	1393	0.97
E-Caryophyllene	25.298	1420	3.25
α -Humulene	26.764	1459	0.18
γ -Muuroolene	27.943	1483	3.98
γ -Patchoulene	28.603	1499	0.43
Premnaspirdiene	28.957	1508	0.63
Total			97.49

The identities of sabinene and α - and β -pinene were confirmed by 2D NMR analysis of the whole essential oil. Assignment of the ^1H - and ^{13}C -NMR signals was achieved by characteristic COSY, HSQC, and HMBC correlations (Figs. 1–3). The 2D techniques also enabled the resolution of the overlapped ^1H - and ^{13}C -NMR signals of each detected compound. The obtained chemical shifts were comparable to those from the literature.^{4,5}

Sabinene. ^1H -NMR (500 MHz, CDCl_3 , δ / ppm): 0.64 (2H, *d*, $J = 5.2$ Hz), 0.88 (3H, *d*, $J = 6.8$ Hz), 0.94 (3H, *d*, $J = 6.8$ Hz), 1.48 (1H, *sept*, $J = 6.8$ Hz), 1.58 (1H, *t*, $J = 5.2$ Hz), 1.70 (2H, *m*), 2.01 (1H, *m*), 2.14 (1H, *m*), 4.61 (1H, *m*), 4.80 (1H, *m*). ^{13}C -NMR (125 MHz, CDCl_3 , δ / ppm): 16.0, 19.6, 19.7, 27.4, 28.9, 30.1, 32.6, 37.5, 101.5, 154.4.

β -Pinene. ^1H -NMR (500 MHz, CDCl_3 , δ / ppm): 0.72 (3H, *s*), 1.23 (3H, *s*), 1.42 (1H, *d*, $J = 9.8$ Hz), 1.82 (2H, *m*), 1.97 (1H, *m*), 2.24 (1H, *m*), 2.31 (1H, *m*), 2.45 (1H, *t*, $J = 5.4$ Hz), 2.53 (1H, *m*), 4.55 (1H, *m*), 4.62 (1H, *m*). ^{13}C -NMR (125 MHz, CDCl_3 , δ / ppm): 21.8, 23.5, 23.5, 26.1, 26.9, 40.4, 51.7, 105.9, 152.2.

α -Pinene. ^1H -NMR (500 MHz, CDCl_3 , δ / ppm): 0.83 (3H, *s*), 1.26 (3H, *s*), 1.16 (1H, *d*, $J = 8.5$ Hz), 1.65 (3H, *m*), 1.93 (1H, *m*), 2.07 (1H, *m*), 2.17 (1H, *m*), 2.21 (1H, *m*), 2.33 (1H, *m*), 5.18 (1H, *t* of *sex*, $J = 3.0$; 1.5 Hz). ^{13}C -NMR (125 MHz, CDCl_3 , δ / ppm): 20.8, 23.0, 26.3, 31.3, 31.3, 38.1, 40.5, 47.0, 115.9, 144.4.

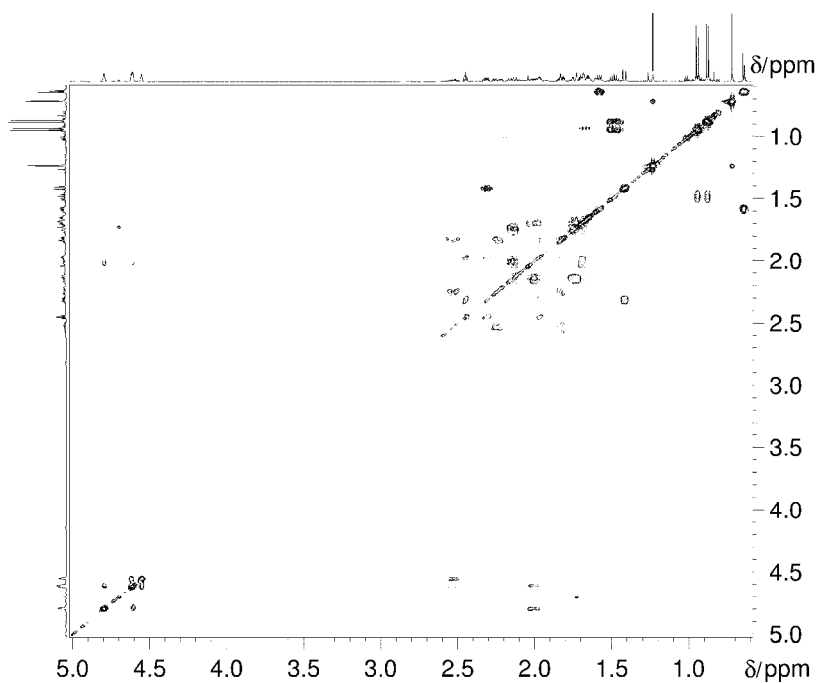


Fig. 1. COSY spectrum of *G. linosyris* essential oil.

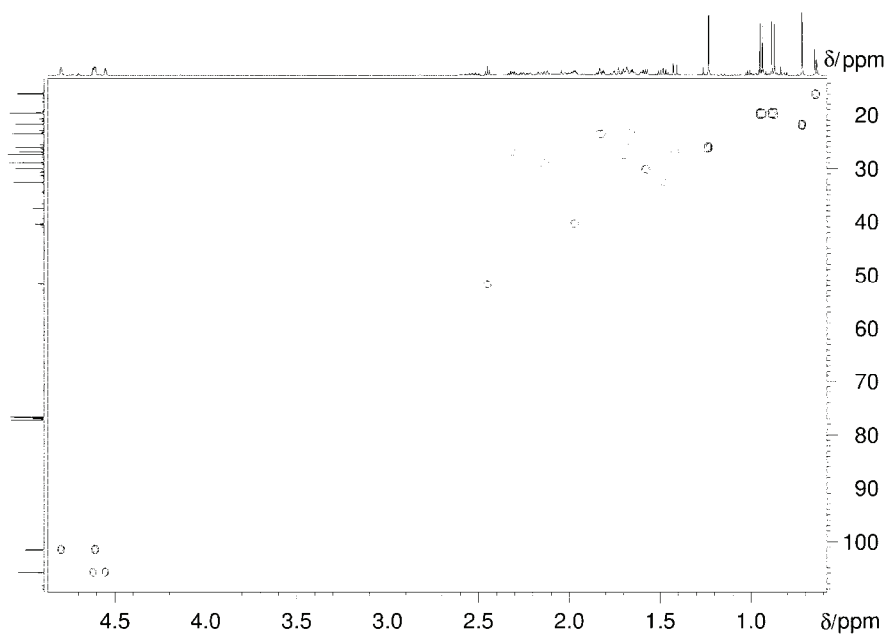


Fig. 2. HSQC spectrum of *G. linosyris* essential oil.

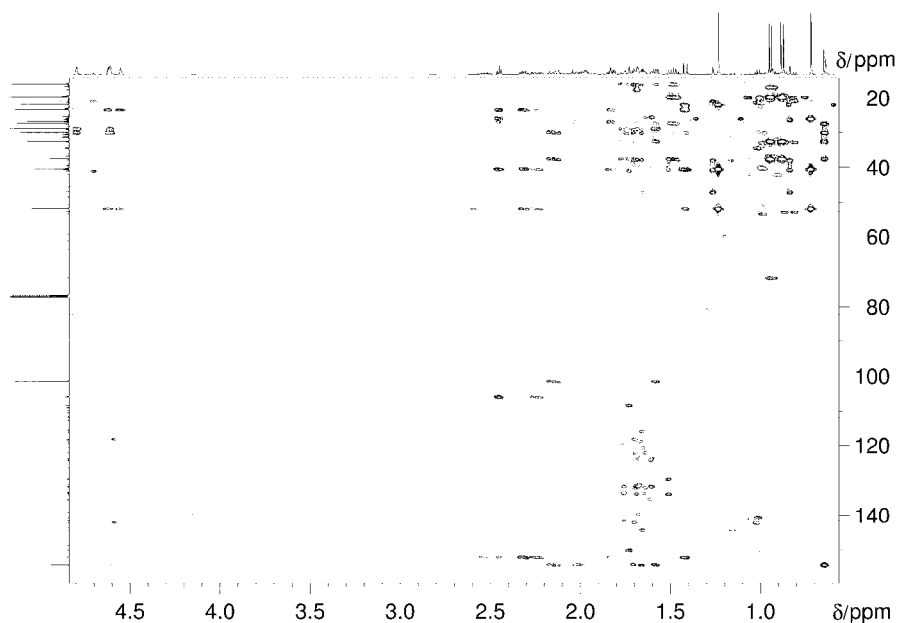


Fig. 3. HMBC spectrum of *G. linosyris* essential oil.

The results of the determination of the antibacterial and antifungal activity of the tested essential oil are given in Tables II and III, respectively. The bacteria were proved to be more sensitive than fungi to the effect of the essential oil.

TABLE II. Antibacterial activity of *G. linosyris* essential oil and streptomycin (*MIC* and *MBC* in $\mu\text{g mL}^{-1}$)

Bacterium	Concentration type	<i>G. linosyris</i>	Streptomycin ^a
<i>S. aureus</i>	<i>MIC</i>	–	3.13
	<i>MBC</i>	–	6.25
<i>B. cereus</i>	<i>MIC</i>	12.50	1.25
	<i>MBC</i>	25.00	2.50
<i>M. flavus</i>	<i>MIC</i>	–	0.63
	<i>MBC</i>	–	1.25
<i>L. monocytogenes</i>	<i>MIC</i>	–	12.50
	<i>MBC</i>	–	25.00
<i>P. aeruginosa</i>	<i>MIC</i>	6.00	1.60
	<i>MBC</i>	12.50	3.13
<i>E. cloacae</i>	<i>MIC</i>	–	0.63
	<i>MBC</i>	–	1.25
<i>S. typhimurium</i>	<i>MIC</i>	25.00	1.25
	<i>MBC</i>	50.00	2.50
<i>E. coli</i>	<i>MIC</i>	6.00	0.63
	<i>MBC</i>	25.00	1.25

^aStock solution 1 mg mL⁻¹

TABLE III. Antifungal activity of *G. linosyris* essential oil and ketoconazole (*MIC* and *MFC* in $\mu\text{g mL}^{-1}$)

Fungus	Concentration type	<i>G. linosyris</i>	Ketoconazole ^a
<i>A. versicolor</i>	<i>MIC</i>	25.00	0.63
	<i>MFC</i>	100.00	5.00
<i>A. ochraceus</i>	<i>MIC</i>	50.00	5.00
	<i>MFC</i>	100.00	25.00
<i>A. niger</i>	<i>MIC</i>	100.00	25.00
	<i>MFC</i>	200.00	25.00
<i>A. fumigatus</i>	<i>MIC</i>	25.00	2.50
	<i>MFC</i>	100.00	5.00
<i>P. ochrochloron</i>	<i>MIC</i>	25.00	5.00
	<i>MFC</i>	100.00	10.00
<i>P. funiculosum</i>	<i>MIC</i>	25.00	0.63
	<i>MFC</i>	150.00	1.25
<i>T. viride</i>	<i>MIC</i>	25.00	25.00
	<i>MFC</i>	200.00	–

^aStock solution 1 mg mL⁻¹

The oil exhibited *MIC* values against the tested bacteria in the concentration range 6.0–25.0 $\mu\text{g mL}^{-1}$, and *MBC* values in range of 12.5–50.0 $\mu\text{g mL}^{-1}$. The most sensitive bacteria was *P. aeruginosa* with an *MIC* of 6 $\mu\text{g mL}^{-1}$ and an *MBC* of 12.5 $\mu\text{g mL}^{-1}$, while *S. typhimurium* was only slightly sensitive with an *MIC* of 25.0 $\mu\text{g mL}^{-1}$ and an *MBC* of 50.0 $\mu\text{g mL}^{-1}$. The bacteria *S. aureus*, *M. flavus*, *L. monocytogenes* and *E. coli* were resistant to this oil. Streptomycin showed activity against the tested bacteria in the concentration range 0.63–25.0 $\mu\text{g mL}^{-1}$.

The essential oil from *G. linosyris* possessed antifungal activity with *MIC* values in the range 25.0–100.0 $\mu\text{g mL}^{-1}$ and *MFC* values in the range 100.0–200.0 $\mu\text{g mL}^{-1}$ (Table III). The commercial preparation of the fungicidal agent, ketoconazole showed *MIC* values in the range 0.63–25.0 $\mu\text{g mL}^{-1}$ and *MFC* values in the range of 1.25–25.0 $\mu\text{g mL}^{-1}$ (Table III).

From the chemical analysis of this oil, it can be seen that hydrocarbons were the dominant components (approx. 80 %). Hydrocarbons tend to be relatively inactive regardless of their structural type, and this inactivity is closely related to their limited hydrogen bonding capacity and water solubility. This suggested that the components present in great proportions were responsible for a large share of the total activity.

From the results given above, it can be concluded that the studied essential oil expressed antimicrobial activity. The antifungal activity was slightly lower in comparison to the antibacterial effect against certain bacteria. The oil exhibited lower antimicrobial activity than did the used commercial antimicrobial agents. The growth of tested microorganism responded differently to the essential oil,

which indicates that different components may have different modes of action or that the metabolism of some microorganisms is better able to overcome the effect of the oil or adapt to it.

The obtained results clearly demonstrate that the tested oil presents potential for medical procedures and for the food, cosmetics and pharmaceutical industries.

Acknowledgement. This study is financially supported by the Ministry of Education and Science of the Republic of Serbia, Project Nos. 173032, 173029, and 172053.

ИЗВОД

САСТАВ И АНТИМИКРОБНА АКТИВНОСТ ЕТАРСКОГ УЉА ИЗ
Galatella linosyris (L.) Rchb. f. (ASTERACEAE)

ДЕЈАН ГОЂЕВАЦ¹, ЉУБОДРАГ ВУЈИСИЋ², ИВАН ВУЧКОВИЋ², ВЛАТКА ВАЈС¹, МАРИНА СОКОВИЋ³,
ПЕТАР Д. МАРИН⁴ и ВЕЛЕ ТЕШЕВИЋ²

¹Институт за хемију, технологију и металургију, Њевошева 12, Универзитет у Београду, 11000 Београд,
²Хемијски факултет, Универзитет у Београду, Студентски тврџ 16, б.бр. 158, 11000 Београд, ³Институт за
биолошка истраживања „Синиша Спанковић“, Универзитет у Београду, Булевар десетог Септембра 142,
11000 Београд и ⁴Биолошки факултет, Универзитет у Београду, Институт за бојанику и
Бојаничка базила „Јевремовац“, Студентски тврџ 16, 11000 Београд

У овом раду је приказано испитивање хемијског састава и антимикробне активности етарског уља биљне врсте *Galatella linosyris*. Хемијском анализом (GC-MS и NMR) је утврђено да су главни састојци овог етарског уља сабинен (40 %), β -пинен (35,5 %), α -пинен (4,5 %), лимонен (4 %), γ -мууролен (4 %) и (*E*)-кариофилен (3,3 %). За процену минималне инхибиторне концентрације (MIC) и минималне бактерицидне/фунгицидне концентрације (MBC/MFC) коришћени су тестови микроразблажења. Етарско уље *G. linosyris* је показало бољу антибактеријску него антифунгалну активност.

(Примљено 15. септембра, ревидирано 15. децембра 2011)

REFERENCES

1. H. Merxmüller, A. Schreiber, in *Flora Europea*, Vol. 4, T. G. Tutin, V. H. Heywood, N. A. Burges, D. M. Moore, D. H. Valentine, S. M. Walters, D. A. Webb, Eds., Cambridge University Press, Cambridge, UK, 1976, p. 112
2. W. Greuter, in *Med-Checklist: A critical inventory of vascular plants of the circum-Mediterranean countries*, Vol. 2, W. Greuter, E. von Raab-Straube, Eds., OPTIMA Secretariat, Palermo, Med-Checklist Trust of OPTIMA, Geneva, Euro+Med Plantbase Secretariat, Berlin, 2008, pp. 225–227
3. W. Letchamo, E. A. Korolyuk, A. V. Tkachev, *J. Essent. Oil Res.* **16** (2004) 141
4. S. Araki, T. Shimizu, P. S. Johar, S. J. Jin, Y. Butsugan, *J. Org. Chem.* **56** (1991) 2538
5. A. Guerrini, G. Sacchetti, M. Muzzoli, R. G. Moreno, A. Medici, E. Besco, R. Bruni, *J. Agr. Food Chem.* **54** (2006) 7778.



J. Serb. Chem. Soc. 77 (5) 627–637 (2012)
JSCS–4296

Physico-chemical and biological studies of Cu(II), Co(II) and Ni(II) complexes of an N₄ coordinating ligand derived from the Schiff base of diacetyl with ethylenediamine and benzoic acid

NETRA PAL SINGH* and ABHAY NANDA SRIVASTAVA

Department of Chemistry, Meerut College, Meerut-250001, India

(Received 12 April, revised 28 August 2011)

Abstract: Mononuclear metal complexes of the type [ML₁]Cl₂ (where, M = Cu(II), Co(II) or Ni(II) and L₁ = ligand) were synthesized by the reaction of a new N₄ coordinating ligand, *N,N'*-{(1,2-dimethylethanediylidene)bis[nitrilo(2,1-ethanediy)]}bis[benzamide] derived from the Schiff base of diacetyl with ethylenediamine and benzoic acid, and the corresponding hydrated metal chloride salts. The metal complexes were characterized by elemental analysis, melting point determination, molar conductance and magnetic moment measurements, IR, UV–Vis, ¹H- and ¹³C-NMR, and ESR spectroscopy. The ligand and all the metal complexes were stable in the solid state at room temperature. From the analytical and spectroscopic investigations, the stoichiometry of the complexes was found to be 1:1 (metal:ligand). Based on the electronic spectra and magnetic moment data, the metal complexes had a square planar geometry. The molar conductance values show the 1:2 electrolytic nature of the metal complexes. A cyclic voltammetric study of the Cu(II) metal complex has also performed, which showed one electron quasi-reversible reduction around –0.92 to –1.10 V. *In vitro* biological activities of the ligand and metal complexes was checked against two bacteria *Bacillus subtilis* and *Escherichia coli* and two fungi *Aspergillus niger* and *A. flavus* which showed the antibacterial and antifungal properties of the ligand and its metal complexes.

Keywords: mononuclear Cu(II), Co(II) and Ni(II) complexes; square planar geometry; antibacterial and antifungal properties.

INTRODUCTION

Metallo-drugs became an interesting research area after the discovery of cis-platin.¹ Since then, many complexes have been synthesized and tested on a number of biological systems. New areas of research, which mainly focused on the specific synthesis of highly functional metal-based drug complexes have drawn considerable attention. Some transition metals are essential for the normal func-

* Corresponding author. E-mail: netrapal_chem@yahoo.com
doi: 10.2298/JSC110412148S

tion of living organisms. Schiff bases and their complexes have a variety of applications in biological, clinical, analytical and pharmacological areas.^{2,3} When ligands coordinate to transition metals, it is believed that the selectivity towards certain biological systems is improved.⁴⁻⁷ The enormous interest in the field of coordination chemistry of transition metal ions with Schiff bases is due to use of these compounds as biological models, as oxygen carriers and as drugs.^{8,9} Recently synthesized Cu(II), Ni(II), Co(II), Zn(II) and Fe(III) complexes show the current interest of researchers in the field of coordination chemistry of these metal ions.^{10,11} *N*-Coordinating ligands and their transition metal complexes have been found to possess important catalytic as well as biological activity.¹²⁻¹⁴ Some other transition metal complexes have also been synthesized recently which show good biological activities *viz.* antibacterial, antifungal, toxicity, DNA interaction and antitumour.¹⁵⁻²¹ In view of the importance of metal complexes, herein the preparation and characterization of Cu(II), Ni(II) and Co(II) metal complexes of a new N₄ coordinating ligand derived from the Schiff base of diacetyl with ethylenediamine and benzoic acid are reported. The synthesized compounds were characterized by various analytical and spectral studies, such as elemental analysis, magnetic moment and molar conductance measurements, and IR, UV-Vis, NMR and ESR spectroscopy. *In vitro* antibacterial and antifungal activities of the synthesized compounds against some specific bacteria (*viz.* *Bacillus subtilis* and *Escherichia coli*) and fungi (*viz.* *Aspirtgillus niger* and *A. flavus*) were also studied.

EXPERIMENTAL

All chemicals were of A.R. grade. MeOH, EtOH, *n*-BuOH, diethyl ether and the metal salts were purchased from Qualigens. Diacetyl was purchased from Aldrich. Ethylenediamine and benzoic acid were purchased from CDH. All chemicals were used as obtained without further purification. Elemental analysis (C, H, N) was performed using a Carlo Erba 1106 elemental analyzer. Metals and chlorides were determined volumetrically²² and gravimetrically,²³ respectively. The IR spectra were recorded using KBr discs (4000–400 cm⁻¹) on a Shimadzu 8300 IR spectrophotometer. The electronic absorption spectra in the 200–900 nm range were obtained in dimethylformamide (DMF) (1.0×10⁻⁴ M) on a Systronic UV-Vis spectrophotometer. The molar conductance measurements were performed in dimethyl sulphoxide (DMSO) (≈10⁻³ M) at room temperature using a Jenway Model 4070 conductivity meter. The magnetic moment measurements were realized by the Gouy method using Hg[Co(SCN)₄] as the calibrant. The ¹H- and ¹³C-NMR spectra were recorded at room temperature in DMSO-*d*₆ (≈1.0×10⁻³ M) on a Bruker AC 700L NMR spectrometer with reference to TMS (tetramethylsilane). Chemical shifts are reported on the δ scale. The electrochemical behaviour of the Cu(II) complex was investigated in acetonitrile solution on a CH620A electrochemical analyzer using a platinum electrode. Tetraethylammonium perchlorate (0.4 M) was used as the supporting electrolyte and the potentials are referenced to the saturated calomel electrode (SCE) without junction correction. The cyclic voltammogram was recorded at a scan rate of 50 mV s⁻¹ with *iR* compensation. The ESR spectrum of the Cu(II) complex was recorded in

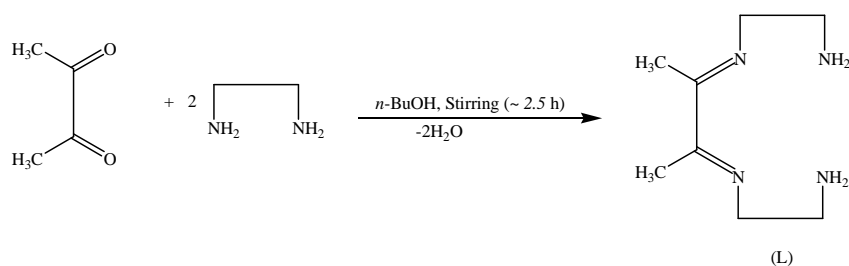
acetonitrile solution at room temperature on an E-112 ESR spectrophotometer employing 2,2-diphenyl-1-picrylhydrazyl (DPPH) as the *g*-marker.

Synthesis of the ligand (L_1)

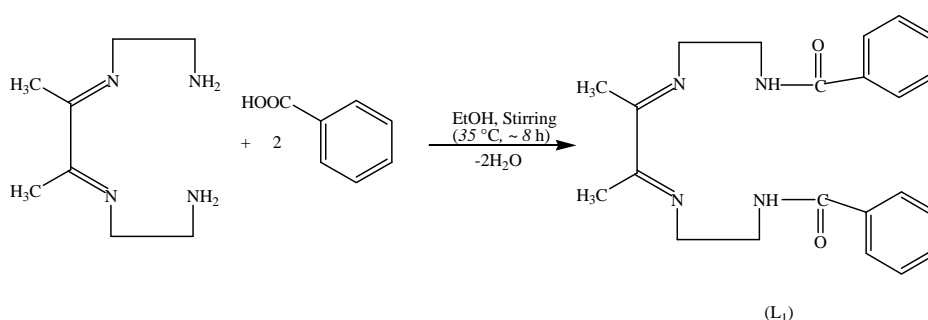
A diacetyl (0.44 ml, 5 mmol) solution in 20 ml of *n*-BuOH was added to ethylenediamine (0.67 ml, 10 mmol) and stirred for ≈ 2.5 h. The formed white solid (*N,N'*-(1,2-dimethylethanediyldene)bis[1,2-ethanediamine] (L)) was filtered off, washed with water and diethyl ether and dried in a vacuum desiccator. A solution of L (0.85 g, 5 mmol) in 30 ml of EtOH was added to a benzoic acid (1.22 g, 10 mmol) solution in 20 ml of EtOH and stirred at 35 °C for ≈ 8 h and cooled to room temperature. The precipitated ligand *N,N'*-{(1,2-dimethylethanediyldene)bis[nitrilo(2,1-ethanediy)]}bis[benzamide] (L_1) was filtered, washed with diethyl ether and dried in a vacuum desiccator over anhydrous calcium chloride (Scheme 1).

Yield: 76 %; m.p. 104 °C; colour: yellow. Anal. Calcd. for $C_{22}H_{26}N_4O_2$ (FW: 378.45): C, 69.85; H, 6.92; N, 14.80 %. Found: C, 69.80; H, 6.94; N, 14.85 %.

Step I:



Step II:

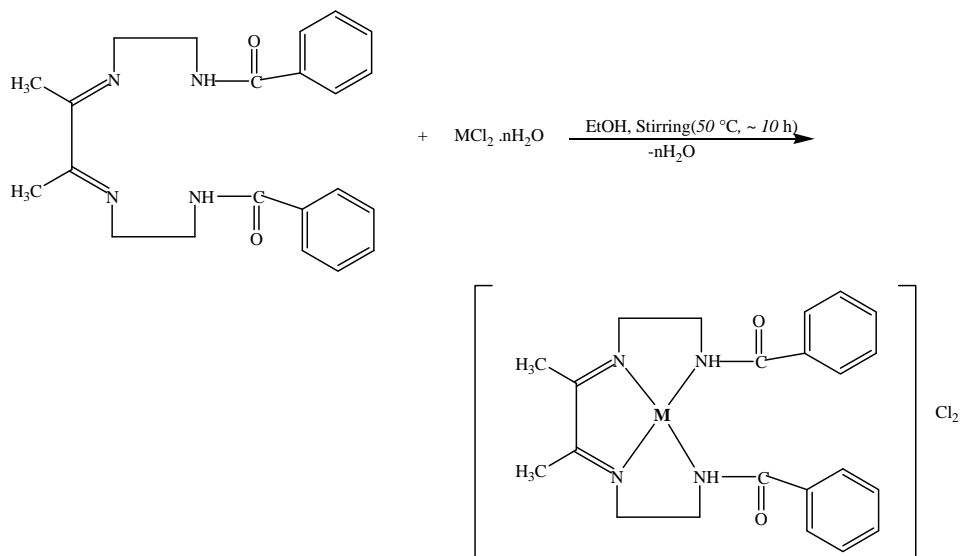


Scheme 1. Synthesis of the ligand L_1 .

Synthesis of the metal complexes

A solution of 1.0 mmol of hydrated metal chloride salt ($CuCl_2 \cdot 2H_2O$ (0.17 g), $NiCl_2 \cdot 6H_2O$ (0.23 g) and $CoCl_2 \cdot 6H_2O$ (0.23 g)) in 15 ml EtOH was added to an ethanolic

solution of L_1 (0.38 g, 1.0 mmol) and stirred at 50 °C for ≈ 10 h and cooled in refrigerator overnight. Coloured products of the metal complexes were obtained which were filtered off, washed with methanol, ethanol and diethyl ether and dried in a vacuum desiccator over anhydrous calcium chloride (Scheme 2).



Scheme 2. Synthesis of the metal complexes $[ML_1]Cl_2$.

In vitro antibacterial and antifungal studies

The antibacterial and antifungal study of the newly synthesized ligand (L_1) and all the metal complexes were realised *in vitro* by reported methods.²⁴ A stock solution (1 mg ml^{-1}) of the test chemical was prepared by dissolving 10 mg of the test chemical in 10 ml of DMSO. The stock solution was suitably diluted with sterilized distilled water to obtain 500 and $100 \mu\text{g ml}^{-1}$ solutions. A control for each dilution was prepared by diluting 10 ml of solvent instead of stock solution with sterilized distilled water. All compounds were evaluated for their *in vitro* antibacterial activity against *Bacillus subtilis* and *Escherichia coli* and antifungal activity against *Aspigoillus niger* and *A. flavus* by the agar-well diffusion method. The bacteria were inoculated into Nutrient Broth (Difco) and incubated for 30 h and the studied fungi were incubated in Malt Extract Broth (Difco) for 54 h. In the agar-well diffusion method, Müller Hinton Agar (Oxoid) for the bacteria and Malt Extract Broth (Difco) for the fungi, sterilized in a flask and cooled to ≈ 48 °C, were distributed (20 ml) in sterilized petri dishes after injecting 0.01 ml of a culture of a bacterium or fungus, prepared as mentioned above, and allowed to solidify. The dilution plate method was used to enumerate the microorganism (10^5 bacteria per ml and fungi 10^3 – 10^4 per ml) for 24 h. Wells were dug in the culture plates using a sterilized cork borer (7 mm diameter). The compounds dissolved in DMSO were added (0.2 μl) to these wells. The Petri dishes were left at 4 °C for 2 h and then the plates were incubated at 30 °C for the bacteria (24–28 h) or at 25 °C for the fungi (78 h). Subsequently, the diameters of the inhibition zones formed on the medium were evaluated in millimetres. The bio-

logical activity data of all the compounds are expressed as the % inhibition over the control. The percent inhibition was calculated using the formula:

$$\text{Inhibition level} = 100(C - T) / C$$

where C is the diameter of the microbial colony in the control plate and T is the diameter of the microbial colony in the tested plate after same incubation period.

RESULTS AND DISCUSSION

The newly synthesized ligand and its metal complexes are stable at room temperature in the solid state. The ligand is soluble in common organic solvents whereas the metal complexes are soluble in DMF and DMSO.

Condensation of N,N' -(1,2-dimethylethanediyldiene)bis[1,2-ethanediamine] and benzoic acid readily gives the corresponding ligand L_1 , which is easily identified by its IR, $^1\text{H-NMR}$ and $^{13}\text{C-NMR}$ spectra. The metal complexes of general formula $[\text{ML}_1]\text{Cl}_2$ of Cu(II), Co(II) and Ni(II) were prepared by stirring a mixture of corresponding hydrated metal chloride with the title ligand at a ratio of 1:1. Square planar geometry is proposed for all complexes.

Analytical data for the complexes

$[\text{CuL}_1]\text{Cl}_2$ (1). Yield: 64 %; m.p. 222 °C. Colour: brown. Anal. Calcd. for $\text{C}_{22}\text{H}_{26}\text{Cl}_2\text{CuN}_4\text{O}_2$ (FW 512.90): C, 50.51; H, 5.11; N, 10.92; Cu, 12.39; Cl, 13.82 %. Found: C, 51.48; H, 5.07; N, 10.90; Cu, 12.37; Cl, 13.80 %.

$[\text{CoL}_1]\text{Cl}_2$ (2). Yield: 61 %; m.p. 212 °C. Colour: light brown. Anal. Calcd. for $\text{C}_{22}\text{H}_{26}\text{Cl}_2\text{CoN}_4\text{O}_2$ (FW 508.30): C, 51.98; H, 5.15; N, 11.02; Co, 11.60; Cl, 13.95 %. Found: C, 51.96; H, 5.12; N, 11.08; Co, 11.58; Cl, 13.92 %.

$[\text{NiL}_1]\text{Cl}_2$ (3). Yield: 67 %; m.p. 198 °C. Colour: reddish brown. Anal. Calcd. for $\text{C}_{22}\text{H}_{26}\text{Cl}_2\text{N}_4\text{NiO}_2$ (FW 508.07): C, 51.00; H, 5.16; N, 11.03; Cu, 11.56; Cl, 13.94 %. Found: C, 51.05; H, 5.12; N, 11.08; Cu, 11.54; Cl, 13.91 %.

The analytical data are in good agreement with the proposed stoichiometry of the complexes.

IR spectra

The IR spectral data of ligand and metal complexes are given in Table I. The IR spectrum of the ligand shows a sharp band at 1576 cm^{-1} , which shows the presence of $\nu(\text{C}=\text{N})$ vibrations.²³ There is no peak of free $-\text{NH}_2$ groups in the IR spectrum of ligand, which indicates the formation of the proposed ligand. In the IR spectra of metal complexes, the $\nu(\text{C}=\text{N})$ band is shifted to $1598\text{--}1626\text{ cm}^{-1}$, which shows the coordination of $(\text{C}=\text{N})$.²⁵⁻²⁹ The new band which appeared in the range $460\text{--}466\text{ cm}^{-1}$ may be assigned $\nu(\text{M}-\text{N})$ vibrations.³⁰ A band in the range of 1762 cm^{-1} in the spectra of the ligand and all the metal complexes show that the $\text{C}=\text{O}$ group did not participate in the coordination. In the IR spectra of L_1 , the sharp medium band at 3300 cm^{-1} is assigned to $\nu(\text{N}-\text{H})$ stretching vibrations. This band is shifted to lower wave numbers in the spectra of Cu(II),

Co(II) and Ni(II), *i.e.*, to 3208, 3200 and 3196 cm^{-1} , respectively, which indicates the coordination of the ($-\text{N}-\text{H}$) nitrogen.^{31,32}

TABLE I. IR spectral data (ν / cm^{-1}) of the ligand and its metal complexes. All spectra were recorded using KBr discs in the range 4000–400 cm^{-1}

Compound	$\nu(-\text{N}-\text{H})$	$\nu(\text{C}=\text{O})$	$\nu(\text{C}=\text{N})$	$\nu(\text{M}-\text{N})$
L_1	3300	1762	1576	–
$[\text{CuL}_1]\text{Cl}_2$	3208	1765	1598	460
$[\text{CoL}_1]\text{Cl}_2$	3200	1763	1626	462
$[\text{NiL}_1]\text{Cl}_2$	3196	1765	1610	466

Electronic absorption spectra

The electronic absorption data of the metal complexes were obtained in DMF. The absorption region and band assignments of the complexes are given in Table II. The UV–Vis spectra of the Cu(II) complex showed an absorption band at 487 nm, which was assigned to the ${}^2\text{B}_{1g} \rightarrow {}^2\text{A}_{1g}$ transition characteristic of square planar Cu(II) complexes. The Co(II) complex exhibited an absorption band at 510 nm, which was assigned to the ${}^1\text{A}_{1g} \rightarrow {}^1\text{B}_{1g}$ transition characteristic of square planar Co(II) complexes. The Ni(II) complex showed absorption bands at 512 nm and 633 nm, which were assigned to ${}^1\text{A}_{1g} \rightarrow {}^1\text{A}_{2g}$ and ${}^1\text{A}_{1g} \rightarrow {}^1\text{B}_{1g}$ transitions, respectively, characteristics of square planar Ni(II) complexes. These obtained spectral values are comparable with those of many similar reported metal complexes.^{33–36}

TABLE II. Electronic spectral data and magnetic moment values of the metal complexes. All electronic absorption spectra were measured in DMF ($\approx 1.0 \times 10^{-4}$ M) and magnetic moment values were measured at room temperature using $\text{Hg}[\text{Co}(\text{SCN})_4]$ as the calibrant

Compound	$\lambda_{\text{max}} / \text{nm}$	Assignments	$\mu_{\text{eff}} / \mu_{\text{B}}$
$[\text{CuL}_1]\text{Cl}_2$	240	INCT	1.76
	380	INCT	
	487	${}^2\text{B}_{1g} \rightarrow {}^2\text{A}_{1g}$	
$[\text{CoL}_1]\text{Cl}_2$	242	INCT	3.62
	378	INCT	
	510	${}^1\text{A}_{1g} \rightarrow {}^1\text{B}_{1g}$	
$[\text{NiL}_1]\text{Cl}_2$	238	INCT	Diamagnetic
	370	INCT	
	512	${}^1\text{A}_{1g} \rightarrow {}^1\text{A}_{2g}$	
	633	${}^1\text{A}_{1g} \rightarrow {}^1\text{B}_{1g}$	

${}^1\text{H}$ - and ${}^{13}\text{C}$ -NMR spectra

The ${}^1\text{H}$ - and ${}^{13}\text{C}$ -NMR spectral data of the ligand and the Ni(II) complex were obtained in $\text{DMSO}-d_6$ and the results are given in Table III. In the ${}^1\text{H}$ -NMR spectrum of ligand, no signal corresponding to primary amine proton was observed, which suggests the formation of the ligand. In the ${}^1\text{H}$ -NMR spectrum of

Ni(II) complex, the signal of the signal of ($\text{H}_3\text{C}-\text{C}=\text{N}$) protons and ($-\text{N}-\text{H}$) proton shifted compared to the free ligand, suggesting coordination through azomethine and ($-\text{N}-\text{H}$) nitrogen atoms.³¹

TABLE III. ^1H - and ^{13}C -NMR spectral data of the ligand and its Ni(II) complex. All spectra were measured in $\text{DMSO}-d_6$ ($\approx 1.0 \times 10^{-3}$ M) at room temperature with reference to TMS (tetramethylsilane)

Compound	^1H -NMR (δ / ppm)	^{13}C -NMR (δ / ppm)
L_1	1.62 (6H, <i>s</i> , 2 =C-CH ₃), 3.58 (4H, <i>t</i> , 2 =N-CH ₂), 3.84 (4H, <i>m</i> , 2 -N-CH ₂), 7.16–7.35 (10H, <i>m</i> , Ar), 9.68 (2H, <i>s</i> , <i>br</i> , 2 -NH)	10.13 (C-9, C-11), 46.20 (C-6, C-13), 97.13 (C-7, C-12), 116.42 (C-4, C-15), 117.63 (C-(2, 2'), C-(17, 17')), 119.82 (C-(3, 3'), C-(16, 16')), 122.07 (C-1, C-18), 160.40 (C-8, C-10), 165.28 (C-5, C-14)
$[\text{NiL}_1]\text{Cl}_2$	1.11 (6H, <i>s</i> , 2 =C-CH ₃), 3.46 (4H, <i>t</i> , 2 =N-CH ₂), 3.83 (4H, <i>m</i> , 2 -N-CH ₂), 7.06–7.25 (10H, <i>m</i> , Ar), 9.01 (2H, <i>s</i> , <i>br</i> , 2 -NH)	10.06 (C-9, C-11), 44.60 (C-6, C-13), 96.94 (C-7, C-12), 116.41 (C-4, C-15), 117.61 (C-(2, 2'), C-(17, 17')), 119.81 [C-(3, 3'), C-(16, 16')], 122.11 [C-1, C-18), 157.80 (C-8, C-10), 165.26 (C-5, C-14)

In the ^{13}C NMR spectrum of Ni(II) complex, change in the chemical shift values compared to the free ligand, show coordination through nitrogen atom of azomethine and ($-\text{NH}$) group. On the other hand, no change in the chemical shift value of carbon of carbonyl group moiety indicates that oxygen atom of this group did not participate in the coordination. Thus, ^1H and ^{13}C NMR spectral data support proposed structure (Fig. 1) of ligand and metal complex and as well coordination behaviour of ligand.³¹

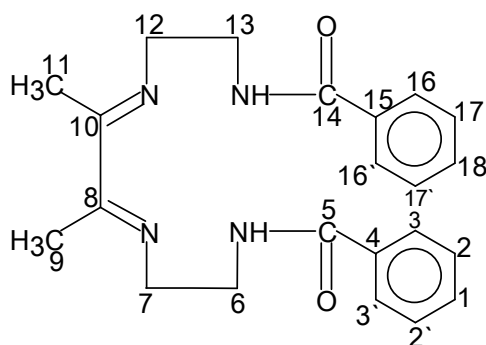


Fig. 1. Numbering of the C-atoms in the ligand (L_1).

Molar conductance measurements

The molar conductance (Λ_M) values of all the metal complexes were measured in DMSO and the obtained values (8.4 , 5.2 and $9.8 \Omega^{-1} \text{cm}^2 \text{mol}^{-1}$ for complexes **1**, **2** and **3**, respectively) show their 1:2 electrolyte nature.³⁷

Magnetic moment measurements

Magnetic moments of metal complexes were measured at room temperature and the effective magnetic (μ_{eff}) values of the complexes are given in Table II. The magnetic moment of Cu(II) complex is $1.76 \mu_{\text{B}}$, which corresponds to a single unpaired electron of the d^9 -system of square planar Cu(II).³⁸ The magnetic moment of the Co(II) complex is $3.62 \mu_{\text{B}}$, which corresponds to square planar geometry of Co(II). The Ni(II) complex is diamagnetic.

ESR spectrum of the Cu(II) metal complex

The ESR spectrum of the Cu(II) complex shows four lines due to hyperfine splitting with nuclear hyperfine $3/2$. For Cu(II) complex, the observed g_{\parallel} value was 2.31 while the g_{\perp} value was 2.02. The relation $g_{\parallel} > g_{\perp}$ is typical for Cu(II) having one unpaired electron in a $d_{x^2-y^2}$ orbital.³⁹ The g_{av} value, calculated according to the relation $= 1/3 (g_{\parallel} + 2g_{\perp})$, was found to be 2.12. A $\langle g \rangle$ value less than 2.3 indicates a square planer geometry around Cu(II).⁴⁰

Cyclic voltammetric study of the Cu(II) complex

The electrochemical properties of Cu(II) complex were studied by cyclic voltammetry in acetonitrile solution vs. SCE. The cyclic voltammogram of Cu(II) complex was recorded in the potential range 0 to -1.4 V. The voltammogram shows one quasi-reversible reduction wave at a negative potential in the range -0.90 to -1.04 V, which was assigned to Cu(II) to Cu(I) reduction.

In vitro antibacterial and antifungal activity

The *in vitro* antimicrobial activities of the newly synthesized ligand and metal complexes were determined against the bacteria *B. subtilis* and *E. coli* and the fungi *A. niger* and *A. flavus* and the results are summarized in Table IV. The values indicate that all complexes have higher antimicrobial activity than the free ligand. Of the tested metal complexes, the Co(II) metal complex shows the highest biological activity against all microbes. Such increased activity of the metal

TABLE IV. *In vitro* antibacterial and antifungal activity data of the ligand and the metal complexes (inhibition level, %). The agar well diffusion technique was used to evaluate the antibacterial and antifungal activity of the synthesized compounds

Compound	$c / \mu\text{g ml}^{-1}$	<i>B. subtilis</i>	<i>E. coli</i>	<i>A. niger</i>	<i>A. flavus</i>
L_1	100	40	51	62	65
	500	48	58	74	78
$[\text{Cu}L_1]\text{Cl}_2$	100	48	54	71	72
	500	53	55	83	85
$[\text{Co}L_1]\text{Cl}_2$	100	52	73	82	80
	500	61	82	89	86
$[\text{Ni}L_1]\text{Cl}_2$	100	46	59	69	70
	500	52	64	77	79

chelates can be explained based on chelation theory. On chelation, the polarity of the metal ion will be reduced largely due to overlap of the ligand orbital and the partial sharing of the positive charge of the metal ion with the donor groups. Furthermore, it increases the delocalization of the π -electrons over the whole chelate ring, which enhances the penetration of the complexes into the lipid membranes and the blocking of the metal binding sites in the enzymes of the microorganisms. These complexes also disturb the respiration process of the cell and thus block the synthesis of proteins, which restricts further growth of microorganisms.⁴¹

CONCLUSIONS

The newly synthesized N_4 coordinating ligand was used to prepare Cu(II), Co(II) and Ni(II) complexes. The ligand and all the metal complexes were characterized by various physico-chemical methods. The data obtained from these studies were in good agreement with the proposed structure and composition of the ligand and the metal complexes. Square planar geometry was confirmed for the metal complexes by electronic absorption spectroscopy, ESR spectroscopy [Cu(II)] and the magnetic moment values. Molar conductance values showed the 1:2 electrolyte nature of all the metal complexes. The electrochemical behaviour of the Cu(II) complex was studied and the results showed a one electron quasi-reversible reduction of the Cu(II) to Cu(I). *In vitro* antibacterial and antifungal studies showed that metal complexes were more biologically active than the free ligand. The [CoL₁]Cl₂ complex showed the highest antibacterial and antifungal activity against all the studied bacterial and fungal strains.

Acknowledgements. The authors are thankful to ACBR, Delhi for providing the spectral data, IIT-Delhi for the NMR spectra, CDRI, Lucknow for providing the elemental analysis data and SARC, Meerut for the biological activity results. The authors are also thankful to the authorities of Meerut College, Meerut for providing the necessary research facilities.

ИЗВОД

ФИЗИЧКО-ХЕМИЈСКА И БИОЛОШКА ИСПИТИВАЊА Cu(II), Co(II) И Ni(II) КОМПЛЕКСА СА N_4 -ТИПОМ ЛИГАНАДА КОЈИ СУ ДОБИЈЕНИ ИЗ ШИФОВЕ БАЗЕ ДИАЦЕТИЛА СА ЕТИЛЕНДИАМИНОМ И БЕНЗОЕВЕ КИСЕЛИНЕ

NETRA PAL SINGH и ABHAY NANDA SRIVASTAVA

Department of Chemistry, Meerut College, Meerut-250001, India

Полазећи од новог лиганда N_4 -типа N,N' -{(1,2-диметилетандиилиден)бис[нитрило(2,1-етандиил)]}бис[бензамида] који је изведен из шифове базе диацетила са етилендиамином у и бензоеве киселине и хидратисане хлоридне соли јона метала синтетизовани су мононуклеарни комплекси опште формуле [ML₁]Cl₂ (M = Cu(II), Co(II) или Ni(II); L₁ = лиганд). Комплекси су окарактерисани помоћу елементарне микроанализе, одређивања њихових тачки топљења, моларне проводљивости и магнетних момената, као и спектроскопских IR, UV-Vis, ¹H- и ¹³C-NMR и ESR мерења. Лиганд и одговарајући комплекси су стабилни на собној температури у чврстом стању. На основу аналитичких и спектроскопских резултата закључено

је да су у комплексима лиганд и јон метала координовани у 1:1 молском односу. На бази електронских спектра и вредности магнетног момента закључено је да испитивани комплекси имају квадратно-планарну геометрију. Вредности за моларну проводљивост показују да су комплекси електролити типа 1:2. Циклично-волтаметријска испитивања за одговарајући Cu(II) комплекс показују једноелектронску квазиреверзибилну редукцију на $-0,92$ до $-1,10$ V. Нађено је да лиганд и одговарајући комплекси показују одређену антибактеријску и антифунгалну активност при *in vitro* испитивањима на две врсте бактерија, *Bacillus subtilis* и *Escherichia coli*, и гљива *Aspiggillus niger* и *A. flavus*.

(Примљено 12. априла, ревидирано 28. августа 2011)

REFERENCES

1. M. C. Orving, J. Abrams, *Chem. Rev.* **99** (1999) 2201
2. T. Hitoshi, N. Tamao, A. Hideyuki, F. Manabu, M. Takayuki, *Polyhedron* **16** (1997) 3787
3. T. Punniamurthy, S. J. S. Kalra, J. Iqbal, *Tetrahedron Lett.* **36** (1995) 8497
4. A. Tavman, N. M. Agh-Atabay, S. Güner, F. Gücin, B. Dülger, *Transition Met. Chem.* **32** (2007) 172
5. P. G. Ramappa, K. G. Somasekharappa, *J. Inorg. Biochem.* **55** (1994) 13
6. A. Tavman, N. M. Agh-Atabay, A. Neshat, F. Gücin, B. Dülger, D. Hacı, *Transition Met. Chem.* **31** (2006) 194
7. Q. Zhou, P. Yang, *Inorg. Chim. Acta* **359** (2006) 1200
8. R. K. Parashar, R. C. Sharma, A. Kumar, G. Mohan, *Inorg. Chim. Acta* **151** (1988) 201
9. K. S. Suslick, T. J. Reinert, *J. Chem. Educ.* **62** (1985) 974
10. M. D. Revenco, O. V. Palamarcuic, P. N. Bourosh, J. Lipkowski, M. Gdaniec, Y. A. Simonov, R. Clerac, *Inorg. Chim. Acta* **368** (2011) 157
11. A. Alagha, L. Parthasrathi, D. Gaynor, H. M. Bunz, Z. A. Starikova, E. Farkas, E. C. O. Brien, M. J. Gil, K. B. Nolan, *Inorg. Chim. Acta* **368** (2011) 58
12. R. K. O. Sigel, H. Sigel, *J. Am. Chem. Soc.* **119** (1997) 744
13. B. Song, R. K. O. Sigel, H. Sigel, *Chem. Eur. J.* **3** (1997) 29
14. H. Sigel, *Chem. Soc. Rev.* **22** (1993) 255
15. S. Tabassum, N. P. Singh, J. Mussarat, *Synth. React. Inorg. Met.-Org. Chem.* **31** (2001) 1803
16. M. Palil, R. Hunoor, K. Gudasi, *Eur. J. Med. Chem.* **45** (2010) 2981
17. K. Singh, D. Pal, *J. Serb. Chem. Soc.* **75** (2010) 917
18. S. Chandra, M. Tyagi, S. Agarwal, *J. Serb. Chem. Soc.* **75** (2010) 935
19. S. Tabassum, G. C. Sharma, F. Arjmand, A. Azam, *Nanotechnology* **21** (2010) 195102
20. N. P. Singh, A. N. Srivastava, *Int. J. Chem. Environ. Pharm. Res.* **1** (2010) 27
21. N. P. Singh, A. N. Srivastava, *E-J. Chem.* **8** (2010) 809
22. C. N. Reilley, R. W. Schmidt, F. A. Sadek, *J. Chem. Educ.* **36** (1959) 619
23. A. I. Vogel, *A Text Book of Quantitative Inorganic Analysis*, Longmans, London, 1961, p. 433
24. A. K. Sadna, Y. Mirza, A. R. Aneja, O. Prakash, *Eur. J. Med. Chem.* **38** (2003) 533
25. M. S. Deshpande, A. S. Kumbhar, *J. Chem. Sci.* **117** (2005) 153
26. R. C. Maurya, J. Chourasia, P. Sharma, *Indian J. Chem., A* **47** (2008) 517
27. M. Sonmez, M. Sekerci, *Pol. J. Chem.* **76** (2002) 907
28. M. Sonmez, A. Levent, M. Sekerci, *Synth. React. Inorg. Met.-Org. Chem.* **33** (2003) 1747
29. M. Sonmez, A. Levent, M. Sekerci, *J. Coord. Chem.* **30** (2004) 655

30. M. Tumer, N. Deligonul, A. Golcu, E. Akgum, M. Dolaz, H. Demirelli, M. Digrak, *Transition Met. Chem.* **31** (2006) 1
31. R. M. Silverstein, C. G. Bassler, T. C. Morrill, *Spectrometric Identification of Organic Compounds*, 3rd ed., Wiley, New York, 1974, p. 108
32. J. Pons, A. Chadghan, J. Casabo, A. Alvarez-Larena, J. F. Piniella, J. Ros, *Polyhedron* **20** (2001) 2531
33. L. N. Sharda, M. C. Ganorkar, *Indian J. Chem., Sect A* **27** (1988) 617
34. D. V. Warad, C. D. Satish, V. H. Kulkarni, C. S. Bajgur, *Indian J. Chem., Sect A* **39** (2000) 415
35. R. L. Farmer, F. L. Urbach, *Inorg. Chem.* **13** (1974) 587
36. A. B. P. Lever, *Inorganic Electronic Spectroscopy*, 2nd ed., Elsevier, New York 1968
37. W. J. Geray, *Coord. Chem. Rev.* **7** (1971) 81
38. J. D. Crane, D. E. Fenton, J. M. Latour, A. J. Smith, *J. Chem. Soc., Dalton Trans.* (1991) 2279
39. J. C. Duff, *J. Chem. Soc.* (1941) 547
40. E. Billing, R. W. William, I. Bernol, H. B. Grey, *Inorg. Chem.* **3** (1964) 663
41. N. Dharmaraj, P. Viswanathamurthi, K. Natarajan, *Transition Met. Chem.* **26** (2002) 105.



J. Serb. Chem. Soc. 77 (5) 639–650 (2012)
JSCS–4297

A quantitative structure–activity relationship study on histamine receptor antagonists using the genetic algorithm–multi-parameter linear regression method

MARYAM ADIMI¹, MAHMOUD SALIMI², MEHDI NEKOEI^{3*},
ESLAM POURBASHEER⁴ and ABOLGHASEM BEHESHTI⁴

¹Chemical Engineering Department, Faculty of Engineering, Islamic Azad University – Farahan Branch, Farmahin, Iran, ²Chemical Engineering Department, Faculty of Engineering, Islamic Azad University – Arak Branch, Arak, Iran, ³Department of Chemistry, Shahrood branch, Islamic Azad University, Shahrood, Iran and ⁴Center of Excellence in Electrochemistry, Faculty of Chemistry, University of Tehran, P. O. Box 14155-6455, Tehran, Iran

(Received 4 August 2011)

Abstract: A quantitative structure activity relationship (QSAR) model has been generated for predicting the antagonist potency of biphenyl derivatives as human histamine (H3) receptors. The molecular structures of the compounds were numerically represented by various kinds of molecular descriptors. The whole data set was divided into training and test sets. A genetic algorithm based multiple linear regression was used to select the most statistically effective descriptors. The final QSAR model ($N = 24$, $R^2 = 0.916$, $F = 51.771$, $Q^2_{\text{LOO}} = 0.872$, $Q^2_{\text{LGO}} = 0.847$, $Q^2_{\text{BOOT}} = 0.857$) was fully validated employing the leave-one-out (LOO) cross-validation approach, Fischer statistics (F), the Y -randomization test, and predictions based on the test data set. The test set presented an external prediction power of $R^2_{\text{test}} = 0.855$. In conclusion, the generated QSAR model could be used as a valuable tool for designing similar groups of new antagonists of histamine (H3) receptors.

Keywords: QSAR; genetic algorithm; multiple linear regression; biphenyl derivatives; histamine (H3) receptors.

INTRODUCTION

Alzheimer's disease is the most common form of neurodegenerative dementia.¹ It accounts for approximately 50–60 % of the overall cases of dementia among individuals over the age of 65 years.² Unfortunately, the therapeutic options for Alzheimer's disease are limited. No true disease-modifying therapies are known and at best, physicians can only hope to alleviate with symptomatic

* Corresponding author. E-mail: nekoei_m1@yahoo.com; m_nekoei1356@yahoo.com
doi: 10.2298/JSC110804205A

treatments the cognitive deficits that characterize this disease. One of the most frequently prescribed anti-Alzheimer's drugs are the histamine H3 receptor antagonists. Histamine is a biogenic amine that influences a wide range of pathophysiological processes through the activation of different G protein-coupled receptors (GPCRs).³ The histamine H3 receptor was identified in 1983 and was initially described as an autoreceptor, mainly expressed in the central nervous system (CNS), regulating histamine biosynthesis and release from histaminergic neurons.⁴ The high density of H3 receptors in different CNS areas and their influence on the release of a large variety of neurotransmitters encouraged wide pharmacological investigations on their physiological role and the quest for potential therapeutic applications of H3-antagonists in the treatment of various CNS diseases.^{5,6}

Recently, some classes of H3-antagonists have been described that are endowed with additional pharmacological properties that may synergistically potentiate their therapeutic efficacy in the treatment of disorders related to neurotransmitter deficits, such as Alzheimer's disease. Although there are several experimental methods available for screening the estrogenic activity of chemicals (*e.g.*, *in vivo* and *in vitro* assay tests), which have been performed using receptors and other biological material of human, rat, mouse, and calf origin at least,⁷ they are costly, time-consuming, and can potentially produce toxic side products from the experimental methods used today. An efficient way to obtain a complete data set without the necessity of performing expensive laboratory experiments is the application of quantitative structure activity relationship (QSAR) techniques. A QSAR model describes a mathematical relationship between structural attribute(s) and activity of a set of chemicals. The potential promise of using QSAR models for the screening of chemical databases or virtual libraries before their synthesis appears equally attractive for chemical manufacturers, pharmaceutical companies, and government agencies, particularly in times of shrinking resources.⁸ The main aim of the present work was to establish a new QSAR model for predicting the antagonist potency of biphenyl derivatives as histamine (H3) receptors by a genetic algorithm–multiple linear regression (GA–MLR) technique. In addition, several possible approaches for QSAR model validation are described, including the leave-one-out (LOO), leave-group-out (LGO), cross-validation, external test set and the *Y*-randomization test approaches.

MATERIALS AND METHODS

Data set

The 30 studied biphenyl derivatives and the corresponding antagonist potency (pK_B) at human histamine H3-receptors (hH3) were collected from the literature.⁹ The chemical structures and activity data (pK_B) for the complete set of compounds are presented in Table I. The data set was randomly divided into two subsets: the training set containing 24 compounds (80 %) and the test set containing 6 compounds (20 %). The training set was used to build a regression model, while the test set was used to evaluate the predictive ability of the obtained model.

TABLE I. Experimental and predicted antagonist potency of biphenyl derivatives at H3 receptors (pK_B) by the GA-MLR technique

$$R_1-(CH_2)_n-\text{C}_6\text{H}_4-\text{C}_6\text{H}_4-(CH_2)_m-R_2$$

No.	<i>n</i>	<i>m</i>	R ₁	R ₂	Exp.	Predicted
1	1	2			9.28	9.33
2	1	1	-N(C ₃ H ₇) ₂		6.96	7.24
3	1	1			8.16	8.02
4	1	2			8.82	8.67
5	1	1			8.77	8.38
6	1	1	-N(CH ₃) ₂		8.17	8.11
7	1	1	H	-N-(C ₅ H ₁₁)	6.51	6.52
8	1	1			6.19	6.44
9	1	1			7.68	7.55
10	1	1			7.67	7.87
11	1	1			6.7	6.69
12	1	1			9.19	8.76
13	1	1			8.48	8.16
14	1	1			7.77	7.83
15	1	1			7.27	7.22

TABLE I. Continued

$\text{R}_1-(\text{CH}_2)_n-\text{C}_6\text{H}_4-\text{C}_6\text{H}_4-(\text{CH}_2)_m-\text{R}_2$						
No.	n	m	R ₁	R ₂	Exp.	Predicted
16	1	1		$-\text{N}(\text{CH}_3)_2$	8.92	9.25
17	1	1		$-\text{N}(\text{C}_2\text{H}_5)_2$	8.9	9.13
18	1	1		$-\text{N}(\text{C}_3\text{H}_7)_2$	8.18	8.41
19	1	1			7.98	8.19
20	1	1			7.86	7.38
21	1	1			8.03	8.12
22	1	1			7.46	7.76
23	2	2			8.5	8.59
24	2	2			8.17	7.95
25^a	1	1	$-\text{N}(\text{C}_2\text{H}_5)_2$	$-\text{N}(\text{C}_2\text{H}_5)_2$	8.96	8.32
26^a	1	1	$-\text{N}(\text{C}_3\text{H}_7)_2$	$-\text{N}(\text{C}_3\text{H}_7)_2$	7.8	7.26
27^a	1	1			6.54	6.86
28^a	1	1			7.27	7.41
29^a	1	1			8.64	8.57
30^a	2	2	$-\text{N}(\text{CH}_3)_2$	$-\text{N}(\text{CH}_3)_2$	8.06	7.91

^aTest set*Descriptors calculation*

To obtain a QSAR model, compounds are often represented by molecular descriptors. The numerical representation (often-called molecular descriptor) of the chemical structure is the most important factor affecting the quality of a QSAR model. The calculation process of the molecular descriptors employed in the present investigation is described as below: all molecules were entered into HyperChem¹⁰ and pre-optimized using MM+ molecular mecha-

nics force field. A more precise optimization has been realized with the semi-empirical AM1 method. The molecular structures were optimized using the Polak–Ribiere algorithm until the root mean square gradient was 0.01. Then, 1481 theoretical molecular descriptors were calculated in the DRAGON program,¹¹ including a) 0D-constitutional descriptors, b) 1D-functional groups, atom centered fragments, c) 2D-topological descriptors, walk and path counts, connectivity index, information index, various auto-correlations from the molecular graph, edge adjacency indices, descriptors of the Burden eigenvalues, topological charge indices, eigenvalues-based indices, d) 3D-Randic molecular profiles, geometrical descriptors, Weighted Holistic Invariant Molecular descriptors (WHIMs), Geometry, Topology and Atom-Weights Assembly (GETAWAY) descriptors, e) charge descriptors and f) molecular properties (calculated from models, together with some empirical descriptors). The list and meaning of the molecular descriptors can be found from the DRAGON package, and the calculation procedure is explained in detail in the literature.¹² The theoretical descriptors were reduced by the following procedures: first, descriptors that were constant were eliminated. Second, to decrease the redundancy existing in the descriptors, the correlations of the descriptors with each other and with the pK_B values of the molecules were additionally examined, whereby collinear descriptors ($R > 0.9$) were detected. Among the collinear descriptors, the one having the highest correlation with pK_B was retained, and the others were removed from the data matrix.

Genetic algorithm (GA)

The genetic algorithm (GA) developed by Holland *et al.*¹³ is a stochastic optimization technique that mimics selection in nature and has proved itself to be a very effective tool in QSAR studies with many merits.^{14–17} The distinctive aspect of a GA is that it investigates many possible solutions simultaneously, each of which explores different regions in parameter space.¹⁸ The first step is to create a population of N individuals. Each individual encodes the same number of randomly chosen descriptors. The fitness of each individual in this generation is determined. In the second step, a fraction of the children of the next generation is produced by crossover (crossover children) and the rest by mutation (mutation children) from the parents based on their scaled fitness scores. A new offspring contains characteristics from two or one of its parents. In this study, GA and MLR were combined to build a QSAR model. The fitness score used herein was the leave-one-out (LOO) cross-validated correlation coefficient (Q^2).

Model validation and applicability domain

A good fit alone does not guarantee that the model is useful for prediction purposes. Some kind of validation is necessary to test how stable the model is and how well it predicts. In the current work, several statistic terms, such as correlation coefficient (R^2), leave-one-out (LOO) cross-validated Q^2 , root mean squared error ($RMSE$), were used to assess the internal predictive ability of the proposed models.

Another validation technique is the bootstrap technique.¹⁹ By this technique, validation is performed by randomly generating training sets with sample repetitions and then evaluating the predicted responses of the samples not included in the training set. The bootstrapping was repeated 5000 times for each validated model.

In addition, Y -scrambling techniques were employed to exclude the possibility of chance correlation and to check for reliability and robustness by permutation testing. Multi-collinearity between the selected descriptors was detected by calculating their variation inflation factors (VIF), which can be calculated as follows:

$$VIF = \frac{1}{1 - r^2} \quad (1)$$

where r is the correlation coefficient of the multiple regression between one variable and the others in the model. If VIF equals 1.0, no intercorrelation exists for each variable; if VIF falls into the range 1.0–5.0, the related model is acceptable; and if VIF is larger than 10.0, the related model is unstable and recheck is necessary.²⁰ To examine the relative importance as well as the contribution of each descriptor in the model, the value of the mean effect (MF) was calculated for each descriptor. This calculation was performed using the equation:

$$MF_j = \frac{\beta_j \sum_{i=1}^n d_{ij}}{\sum_j \beta_j \sum_i^n d_{ij}} \quad (2)$$

where MF_j represents the mean effect for the considered descriptor j , β_j is the coefficient of the descriptor j , d_{ij} stands for the value of the target descriptors for each molecule and m is the descriptors number in the model. The MF value indicates the relative importance of a descriptor, compared with the other descriptors in the model. Its sign exhibits the variation direction in the values of the activities resulting from an increase (or a reduction) of this descriptor value.

The Williams plot, a plot of the standardized residuals *vs.* the leverage, was exploited to visualize the applicability domain.²¹ The leverage indicates the distance of a compound from the centroid of X . The leverage of a compound in the original variable space is defined as:²²

$$h_i = x_i^T (X^T X)^{-1} x_i \quad (3)$$

where x_i is the descriptor vector of the considered compound and X is the descriptor matrix derived from the descriptor values of the training set. The warning leverage (h^*) is defined as:²³

$$h^* = 3(p+1)/n \quad (4)$$

where n is the number of training compounds and p is the number of predictor variables. A compound with $h_i > h^*$ seriously influences the regression performance, but it does not appear to be an outlier because its standardized residual may be small, even though it has been excluded from the applicability domain. Moreover, a value of 3 for a standardized residual is commonly used as a cut-off value for accepting predictions, because points that lie ± 3 standardized residual from the mean cover 99 % of the normally distributed data.²⁴ Thus, the leverage and the standardized residual were combined for the characterization of the applicability domain.

RESULTS AND DISCUSSION

The total data set was divided into a training set of 24 compounds to develop the models and a test set of 6 compounds. In order to select the training and test sets, the range of the activity values of both the training set and test set should be covered from the lowest to the highest. The two sets are indicated in Table I. After splitting the data set into a training set and a test set, the next step was to select the main factors that were the most important for the antagonist potency of the biphenyl derivatives. The genetic algorithm was performed to select descriptors correlated to the activity based on the training set samples and various models with various numbers of descriptors were obtained. To select the optimum number of descriptors, the influence of the number of the descriptors was investi-

gated for one to six descriptors. The influence of the number of descriptors on the coefficients of determination (R^2), the adjusted R^2 (R^2_{adj}),²⁵ the standard deviation (s), and the coefficient of the leave one out cross-validation (Q^2) for the training set are shown in Fig. 1.

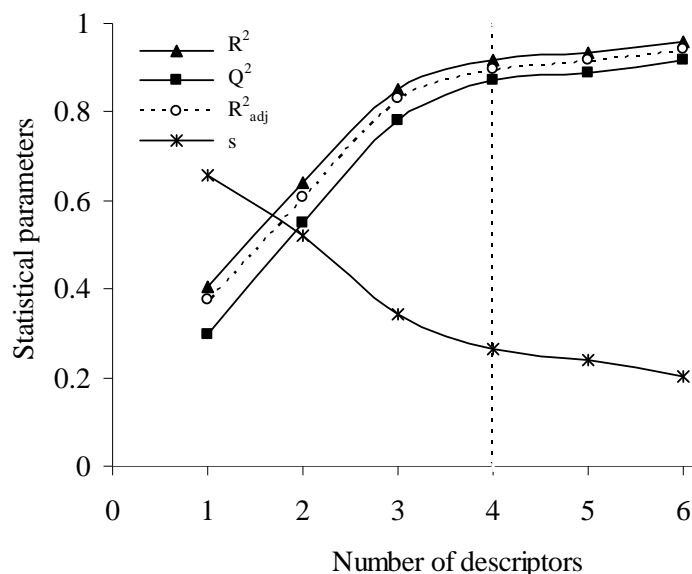


Fig. 1. Influence of the number of descriptors on the statistical parameters.

As can be seen, the models with 5 and 6 descriptors did not improve significantly the statistics of the model; it was determined that the optimum subset size had been achieved with a maximum 4 descriptors. The four most significant descriptors according to the GA-MLR algorithm are given in Table II. The genetic algorithm-MLR analysis led to the derivation of one model, with four variables, which is described by the following equation:

$$pK_B = -11.023 (\pm 1.602) + 1.042 (\pm 0.131) IDDE + 4.085 (\pm 0.813) MATS3v + 0.688 (\pm 0.089) GATS2e + 24.364 (\pm 2.687) RARS \quad (5)$$

$$N_{train} = 24, R^2_{train} = 0.916, F = 51.771, RMSE_{train} = 0.0482, Q^2_{LOO} = 0.872$$

$$Q^2_{LGO} = 0.847, Q^2_{BOOT} = 0.857, R^2_{test} = 0.855, RMSE_{test} = 0.1537$$

In this equation, N is the number of compounds, R^2 is the squared correlation coefficient, Q^2_{LOO} , Q^2_{LGO} and Q^2_{BOOT} are the squared cross-validation coefficients for leave one out, leave group out and bootstrapping, respectively, $RMSE$ is the root mean square error and F is the Fisher F statistic. The figures in parentheses are the standard deviations.

Then, the built model was used to predict the test set data. The prediction results are given in Table I. The predicted values of pK_B for the compounds in

the training and test sets using Eq. (1) are plotted *vs.* the experimental values in Fig. 2. As can be seen, the predicted values of pK_B are in good agreement with those of the experimental values.

TABLE II. The linear model based on the four parameters selected by genetic algorithm method (*VIF* – variation inflation factor)

Descriptor	Chemical meaning	Coefficient	Mean effect	<i>VIF</i>
Constant	Intercept	-11.023	-	-
IDDE	Mean information content on the distance degree equality topological descriptors	1.042	0.202	1.227
MATS3v	Moran autocorrelation - lag 3 / weighted by atomic van der Waals volumes 2D autocorrelations	4.085	-0.020	1.301
GATS2e	Geary autocorrelation – lag 2 / weighted by atomic Sanderson electronegativities 2D autocorrelations	0.688	0.122	1.527
RARS	R matrix average row sum GETAWAY descriptors	24.364	0.696	1.307

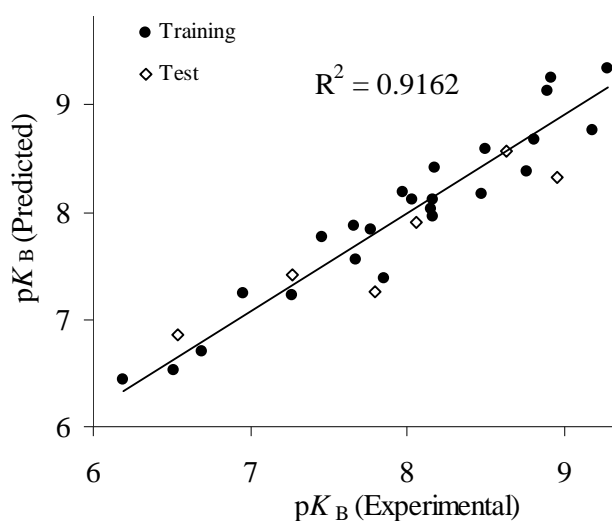


Fig. 2. Predicted *vs.* experimental antagonist potency (pK_B) by the GA-MLR methodology.

The chemical meaning and the mean effect (*MF*) of selected descriptors are given in Table II. In addition, the multi-collinearity between the above six descriptors was detected by calculating their variation inflation factors (*VIF*), which are also given in Table II. As can be seen from this table, most variables have *VIF* values of less than 5, indicating that the obtained model has obvious statistical significance. The real usefulness of QSAR models is not just their ability to reproduce known data, verified by their fitting power (R^2), but more importantly,

their possibility of predictive application. For this reason, the model obtained was validated using Leave-One-Out (LOO) and Leave-Group-Out (LGO) cross-validation process. For LOO cross-validation, a data point is removed from the set and the model is recalculated. The predicted activity for that point is then compared to its actual value. This is repeated until each data point has been omitted once. For LGO, 20 % of the data points are removed from the dataset and the model is refitted; the predicted values for those points are then compared to their experimental values. Again, this is repeated until each data point has been omitted once. The internal predictive ability of the model was also verified using the bootstrap Q^2_{BOOT} procedure, as is strongly recommended for QSAR modeling. The robustness of the proposed model and its predictive ability was guaranteed by the high value of Q^2_{BOOT} based on the bootstrapping being repeated 5000 times.

The cross-validation parameters are shown by Eq. (1). The cross-validation results confirmed that the obtained regression model has a good internal and external predictive power. In addition, in order to assess the robustness of the model, the Y -randomization test was applied in this contribution.⁸ The dependent variable vector (pK_B) was randomly shuffled and a new QSAR model was developed using the original independent variable matrix. The new QSAR models (after several repetitions) are expected to have low R^2 and Q^2_{LOO} values. If the opposite is the case, then an acceptable QSAR model cannot be obtained for the specific modeling method and data. The results of Y -randomization tests are shown in Table III. The applicability domain of this model was also evaluated by leverage analysis expressed as a Williams plot (Fig. 3), in which the standardized residuals and the leverage values (h) were plotted. From this figure, it is obvious that there are no chemicals with a leverage higher than the warning h^* value of 0.625. Additionally, for all the compounds in the training and test sets, their standardized residuals were smaller than three standard deviation units (3δ), which means a coverage of more than 99 % of the training compounds. Thus, there are no outliers for the developed QSAR model (GA-MLR). Consequently, this GA-MLR approach currently constitutes the most accurate method for predicting the antagonist potency of biphenyl derivatives as histamine (H3) receptors.

Molecular descriptor interpretations

By interpreting the descriptors contained in the model, it is possible to gain some insight into the factors that are related to the antagonist potency of biphenyl derivatives. For this reason, an acceptable interpretation of the QSAR results is provided below.

The molecular descriptors selected by the genetic algorithm are listed in Table II. IDDE (mean information content on the distance degree equality) is one of the topological descriptors that appear in the model. The mean information content derives from the pruning partition of acyclic graphs. The mean information content on atomic composition is the mean value of the total information

content. As is apparent from Table II, the IDDE mean effect has a positive sign, which indicate that antagonist potency of histamine (H3) receptors is directly related to this descriptor. Therefore, increasing the value of this descriptor leads to an increase in antagonist potency (pK_B value).

TABLE III. R^2_{train} and Q^2_{LOO} values after several Y -randomization tests

Iteration	R^2_{train}	Q^2_{LOO}
1	0.269	0.019
2	0.137	0.067
3	0.117	0.124
4	0.040	0.392
5	0.265	0.003
6	0.070	0.199
7	0.271	0.040
8	0.188	0.002
9	0.200	0.005
10	0.160	0.004

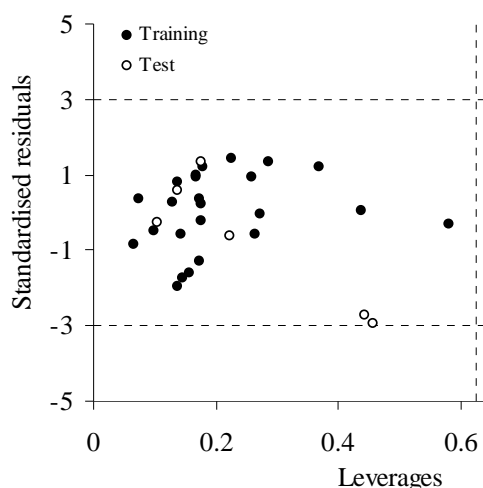


Fig. 3. Williams plot of the GA-MLR model. The training and test set samples are labeled differently. The dashed lines are the 3δ limit and the warning value of hat ($h^* = 0.625$) Compounds with high h values are numbered as in Table I.

MATS3v (Moran autocorrelation – lag 3 / weighted by atomic van der Waals volumes) is the second descriptor appearing in the model. It is one of the 2D autocorrelations descriptors. In this descriptor, the Geary coefficient is a distance-type function, the function is any physicochemical property calculated for each atom of the molecule, such as atomic mass, polarizability, *etc.*¹² Thus, the molecule atoms represent a set of discrete points in space and the atomic property is the function evaluated at these points. The physicochemical property in this case is the atomic van der Waals volumes. The MATS3v mean effect displays a negative sign, which indicates that the pK_B value is inversely related to this descriptor. Hence, it was concluded that by increasing the molecular volume the value of this descriptor increased, causing a reduction in the pK_B value.

The third descriptor is GATS2e (Geary autocorrelation – lag 2 / weighted by atomic Sanderson electronegativities), which is one of the 2D autocorrelations descriptors. The physico-chemical property in this case is atomic Sanderson electronegativities. The MATS3v mean effect displays a positive sign, which indicates that the pK_B value is directly related to this descriptor. Hence, by increasing the atomic Sanderson electronegativities, the value of this descriptor increases, causing an increasing in the pK_B value.

The final descriptor is RARS (R matrix average row sum) that belong to the GETAWAY descriptors. The GETAWAY (GEometry, Topology, and Atom-Weights Assembly) descriptors have been recently proposed as chemical structure descriptors derived from a new representation of molecular structure, the Molecular Influence Matrix (MIM).¹² The RARS descriptor has the highest mean effect value with a positive sign. It can be concluded that RARS displays a great effect in the model and the value of this descriptor is directly related to antagonist potency of histamine (H3) receptors.

CONCLUSIONS

In this work, an accurate and validated QSAR model using the GA-MLR method was developed for predicting the antagonist potency of biphenyl derivatives as histamine (H3) receptors. The proposed model has good stability, robustness and predictive ability, which were verified by internal validation (cross-validation by LOO, LGO, Bootstrap, and Y-scrambling) and external validation. The results indicate that the constructed QSAR model is more accurate and could be useful to understand the QSAR of biphenyl compounds as histamine (H3) receptors. The proposed model could identify and provide some insight into which structural features are related to the antagonist potency of biphenyl derivatives.

ИЗВОД

QSAR СТУДИЈА АНТАГОНИСТА ХИСТАМИН (H3) РЕЦЕПТОРА ПРИМЕНОМ ГЕНЕТИЧКИХ АЛГОРИТАМА И ВИШЕПАРАМЕТАРСКЕ ЛИНЕАРНЕ РЕГРЕСИЈЕ

MARYAM ADIMI¹, MAHMOUD SALIMI² и MEHDI NEKOEI³

¹Chemical Engineering Department, Faculty of Engineering, Islamic Azad University – Farahan Branch, Farahan, Iran, ²Chemical Engineering Department, Faculty of Engineering, Islamic Azad University – Arak Branch, Arak, Iran и ³Department of Chemistry, Shahrood branch, Islamic Azad University, Shahrood, Iran

Направљен је квантитативни модел за релацију између структуре и активитета (QSAR) за предвиђање антагонистичког учинка деривате бифенила на хумане хистамин (H3) рецепторе. Молекулска структура једињења нумерички је репрезентована различитим молекулским дескрипторима. Скуп података подељен је на тренинг сет и тест сет. Примењени су генетички алгоритми засновани на вишеструкој линеарној регресији и помоћу њих су изабрани статистички најефектнији дескриптори. Коначни QSAR модел ($N = 24$, $R^2 = 0,916$, $F = 51,771$, $Q^2_{LOO} = 0,872$, $Q^2_{LGO} = 0,847$ и $Q^2_{BOOT} = 0,857$) је у потпуности проверен стандардним статистичким поступцима. Тест сет поседује спољашњу моћ предвиђања од $R^2_{test} =$

= 0,855. У закључку, генерисани QSAR модел се може употребити као средство за дизајнирање нових антагониста хистаминских (H3) рецептора.

(Примљено 4. августа 2011)

REFERENCES

1. I. Dorronsoro, A. Castro; A. Martinez, *Expert. Opin. Ther. Patents* **13** (2003) 1725
2. D. Knopman, *Clin. Neuropharmacol.* **26** (2003) 314
3. M. E. Parsons, C. R. Ganellin, *J. Pharmacol.* **147** (2006) S127
4. J.-M. Arrang, M. Garbarg, J.-C. Schwartz, *Nature (London)* **302** (1983) 832
5. R. Leurs, R. A. Bakker, H. Timmerman, I. J. P. de Esch, *Nat. Rev. Drug Discov.* **4** (2005) 107
6. M. Wijtmans, R. Leurs, I. de Esch, *Expert Opin. Invest. Drugs* **16** (2007) 967
7. D. L. Hill, *The Biochemistry and Physiology of Tetrahymena*, 1st ed., Academic Press, New York, USA, 1972
8. A. Tropsha, P. Gramatica, V. K. Gombar, *QSAR Comb. Sci.* **22** (2003) 69
9. G. Morini, M. Comini, M. Rivara, S. Rivara, F. Bordi, P. V. Plazzi, L. Flammini, F. Saccani, S. Bertoni, V. Ballabeni, E. Barocelli, *Bioorgan. Med. Chem.* **16** (2008) 9911
10. HyperChem Release 7, HyperCube, Inc., <http://www.hyper.com>
11. R. Todeschini, Milano Chemometrics and QSPR Group, <http://www.disat.unimib.it/chm>
12. R. Todeschini, V. Consonni, *Handbook of Molecular Descriptors*, Wiley-VCH, Weinheim, Germany, 2000
13. J. H. Holland, in *Adaptation in natural and artificial systems*, University of Michigan, Ann Arbor, MI, 1975
14. D. Rogers, A. J. Hopfinger, *J. Chem. Inf. Comput. Sci.* **34** (1994) 854
15. A. Habibi-Yangjeh, E. Pourbasheer, M. Danandeh-Jenagharad, *Bull. Korean. Chem. Soc.* **29** (2008) 833
16. A. Habibi-Yangjeh, E. Pourbasheer, M. Danandeh-Jenagharad, *Monatsh. Chem.* **139** (2008) 1423
17. A. Habibi-Yangjeh, E. Pourbasheer, M. Danandeh-Jenagharad, *Monatsh. Chem.* **140** (2009) 15
18. H. M. Cartwright, *Applications of artificial intelligence in chemistry*. Oxford University Press, Oxford, 1993
19. R. Wehrens, H. Putter, L. M. C. Buydens, *Chemom. Intell. Lab. Systems* **54** (2002) 35
20. V. K. Agrawal, P. V. Khadikar, *Bioorg. Med. Chem.* **9** (2001) 3035
21. OECD, Guidance Document on the Validation of (Quantitative) Structure–Activity Relationships [(Q)SAR] Models, Organisation for Economic Co-operation and Development, Paris, France, 2007
22. T. I. Netzeva, A. P. Worth, T. Aldenberg, R. Benigni, M. T. D. Cronin, P. Gramatica, J. S. Jaworska, S. Kahn, G. Klopman, C. A. Marchant, G. Myatt, N. Nikolova-Jeliazkova, G. Y. Patlewicz, R. Perkins, D. W. Roberts, T. W. Schultz, D. T. Stanton, J. J. M. van de Sandt, W. Tong, G. Veith, C. Yang, *Altern. Lab. Anim.* **33** (2005) 155
23. L. Eriksson, J. Jaworska, A. P. Worth, M. T. D. Cronin, R. M. McDowell, P. Gramatica, *Environ. Health Persp.* **111** (2003) 1361
24. J. S. Jaworska, J. N. Nikolova, T. Aldenberg, *Altern. Lab. Anim.* **33** (2005) 445
25. C. Hansch, J. Taylor, P. Sammes, *Comprehensive Medicinal Chemistry: The Rational Design, Mechanistic Study & Therapeutic Application of Chemical Compounds*, Vol. 6, Pergamon: New York, 1990, p. 1.



Effect of electrolysis parameters on the morphologies of copper powders obtained at high current densities

GÖKHAN ORHAN* and GIZEM GÜZZEY GEZGIN

Istanbul University, Faculty of Engineering, Metallurgical and Materials Engineering Department, 34320 Istanbul, Turkey

(Received 27 June, revised 20 October 2011)

Abstract: The effects of copper ion concentrations and electrolyte temperature on the morphologies and on the apparent densities of electrolytic copper powders deposited at high current densities under galvanostatic control were examined. These parameters were evaluated by the current efficiency of hydrogen evolution. In addition, scanning electron microscopy was employed for analyzing the morphology of the copper powders. It was found that the morphology was dependent on the copper ion concentration and electrolyte temperature under same current density (CD) conditions. At 150 mA cm⁻² and a potential of 1000±20 mV (vs. SCE), porous and disperse copper powders were obtained at low concentrations of Cu ions (0.120 M Cu²⁺ in 0.50 M H₂SO₄). Under these conditions, a high rate of hydrogen evolution occurred parallel to copper electrodeposition. The morphology was changed from porous, disperse and cauliflower-like to coral-like, shrub-like and stalk-stock-like morphology with increasing Cu ion concentrations from 0.120, through 0.155, 0.315 and 0.475 to 0.630 M Cu²⁺ in 0.5 M H₂SO₄, respectively, at the same CD. Similarly, with increasing temperature, the powder morphology and the apparent density changed. The apparent density values of the copper powders were suitable for many powder metallurgy applications.

Keywords: electrolytic copper powder; apparent density; hydrogen evolution; scanning electron microscopy (SEM).

INTRODUCTION

Copper powder is widely used in electronics and powder metallurgy and it can be produced by a number of methods. There are four main commercially available methods: electrochemical, reduction of copper oxide, chemical precipitation and atomization. The shape, size and other physical properties of copper powders strongly depend on the manufacturing technique.^{1–3}

* Corresponding author. E-mail: gorhan@istanbul.edu.tr
doi: 10.2298/JSC110627196O

Electrolysis is an economic processing method that requires low capital investment, energy consumption and operational costs. Since this method enables the production of metal powder of high purity, it has the advantages of good green strength and low oxygen content compared to the other alternative powder production technologies. Another significant feature of this method is that it allows for the production of powders with a wide range of apparent densities ($0.4\text{--}4.0\text{ g cm}^{-3}$).⁴

An electrolytic metal powder represents disperse electrodeposits removed from the electrode by tapping or some other similar manner. In potentiostatic systems, disperse copper deposits are obtained at overpotentials on the plateau of the limiting current density, as well as at higher ones (at the end of this plateau). The copper electrodeposition process occurs simultaneously with the hydrogen evolution reaction. In galvanostatic systems, electrodeposition of copper has the tendency to form powders when current densities larger than the limiting diffusion current density are used (or overpotentials outside the plateau of the limiting diffusion current density).^{2,5–8} In addition, increasing the overpotential or current density leads to the formation of more dispersed deposits characterized by decreased particle size. The only real difference lies in the morphology of the powder particles obtained by potentiostatic and galvanostatic deposition, *i.e.*, particles obtained by galvanostatic deposition are less dendritic than those obtained by potentiostatic deposition, because the overpotential at the end of the deposition is less negative than in the latter case.⁶

The most important properties of a metal powder are its specific surface area, apparent density, flowability and particle grain size and distribution.⁵ These properties, which are typically known as decisive properties, characterize the behavior of a metal powder. The morphologies of copper powder particles correlated with the apparent density and flowability have been reported by Pavlović *et al.*⁹ and Popov *et al.*^{10,11} It can be seen from these investigations that the more dendritic is the structure of the powder particles, the lower is the apparent density of the copper powder. Popov *et al.*¹⁰ also proposed a method for the determination of the critical apparent density which permits the free flow of electrodeposited copper powders. The apparent density or volumetric mass is defined as the mass per unit volume and can also be determined experimentally. The powder particles from the same fraction of different powders occupy approximately the same volume, but, depending on the structure of the metallic copper, exhibit different apparent densities.

Many investigators studied the electrodeposition of copper deposits from acidic sulfate solutions by potentiostatic or galvanostatic methods. The morphologies of copper deposits obtained at overpotentials belonging to the plateau of the diffusion limiting current density and larger overpotentials were investigated. The results showed that the morphologies and the properties of the copper de-

posits were strongly dependent on parameters such as overpotential, quantity of evolved hydrogen,^{5,7,8} current density,^{3,12,13} concentrations of copper ions^{3,14} and H₂SO₄^{15,16} and temperature of the solution.^{3,17}

The aim of this study was to produce copper powders from acid sulfate solutions by means of electrolysis using a conventional electrolysis cell with scraper that provides faster ionic movement due to the convective diffusion at the electrode–electrolyte interface. The morphologies of the copper powders and their apparent densities were investigated as a function of current density, copper ion concentration and temperature of the electrolyte.

EXPERIMENTAL

Electrodeposition of the copper powders onto vertical flat cathode with a scraper was performed in a laboratory-scale electrolysis cell. A stainless steel cathode with an area of 30 cm² (2 cm×15 cm) and two lead anodes were used. The surface of the cathodes was ground and polished prior to each experiment. The total electrolyte volume was 3.5 dm³. One of the most important technological problems faced in electrolysis is the continuity of the process due to changes in the size of the cathode. In the designed cell, the metal powder produced is removed from the cathode surface by two scrapers, which leads to the accumulation of the powder at the bottom of the cell. Thus, the cathode size is kept constant and the problem of the continuous increasing of cathode surface area is solved. It is important to note that the cathode-scraper was positioned at a distance of 1 mm from the surface of the cathode and a scraper speed of 10 cycles per min was used in all the experiments.

Doubly distilled water and analytical grade chemicals were used for the preparation of the solution for the electrodeposition of copper. The electrolyte circulation rate was kept constant at 1.0 dm³ min⁻¹. In the experiments, electrolytic copper powder was galvanostatically deposited from the following solutions:

- a) 0.120 M Cu²⁺ (solution I),
- b) 0.155 M Cu²⁺ (solution II),
- c) 0.315 M Cu²⁺ (solution III),
- d) 0.475 M Cu²⁺ (solution IV) and
- e) 0.630 M Cu²⁺ (solution V),

all in 0.5 M H₂SO₄.

Following the electrolysis, the obtained powder was washed several times with distilled water. Then, in order to prevent oxidation, the powder was rinsed with ethanol and dried at 95 °C in a drying train under vacuum. The current density vs. voltage curve was measured using linear sweep voltammetry (Gamry Instrument PCA 750). For the majority of the experiments, the potential was swept from 0 to -1200 mV vs. standard calomel electrode (SCE). All the potentials in the paper are given with respect to SCE. The employed scan rate was 0.5 mV s⁻¹.

The powder particles were characterized using a scanning electron microscope (JEOL JSM 5600). The concentration of copper ions in the electrolyte before and after the electrodeposition was measured by inductively coupled plasma atomic emission spectroscopy (ICP). Using these data and the Faraday Law, the current efficiencies of the copper electrodepositions were determined. Assuming that the only electrochemical processes on the cathode were Cu deposition and H₂ evolution and ignoring current losses, the hydrogen evolution efficiency was calculated. The apparent densities of copper powder were measured by a 2 cm³ minimized Arnold meter.

RESULTS AND DISCUSSION

The polarization curves for copper electrodeposition from solutions I, III and V are shown in Fig. 1, from which it can be seen that the beginning of the plateau of the limiting diffusion current density was rapidly shifted to lower electrodeposition potentials with decreasing concentration of Cu ions. The range of potentials belonging to the plateau of the limiting diffusion current density for solutions I, III and V were 140–840 mV, 240–900 mV and 380–1020 mV, respectively. It is known that the hydrogen evolution reaction accompanies copper electrodeposition at high overpotentials and the significant hydrogen evolution occurred at the cathode surface at the potentials more negative than –840, –900 and –1020 mV for solutions I, III and V, respectively.

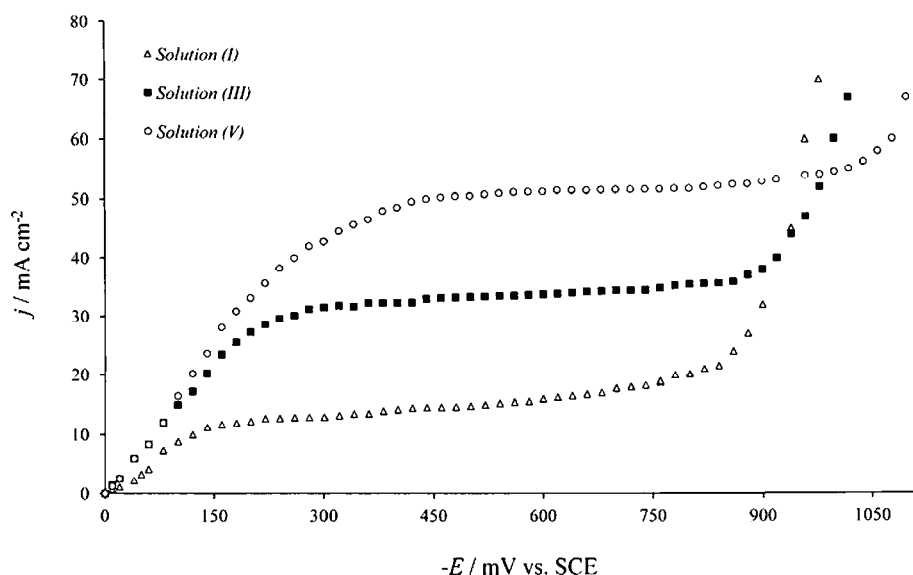


Fig. 1. Polarization curves for the cathodic process of copper deposition from solutions I, III and V.

The cathode polarization *vs.* time curves, which were obtained by repeated experiments run under galvanostatic conditions, are displayed in Fig. 2. The cathode potential on the electrode surface shifted towards more negative values with decreasing Cu ions concentrations in the electrolyte. On the other hand, during the electrodeposition process, the potential values fluctuated with the amplitude by approximately ± 20 mV. Since the cathode surface was scraped at a distance of approximately 1 mm from its surface, the dendrite lengths and the related surface area remained relatively constant, and thus the potential curves can be considered to have a smooth character. At a CD of 150 mA cm^{-2} , the

potential values were approximately 1000, 700, 600 and 400 mV for solutions I and III–V, respectively.

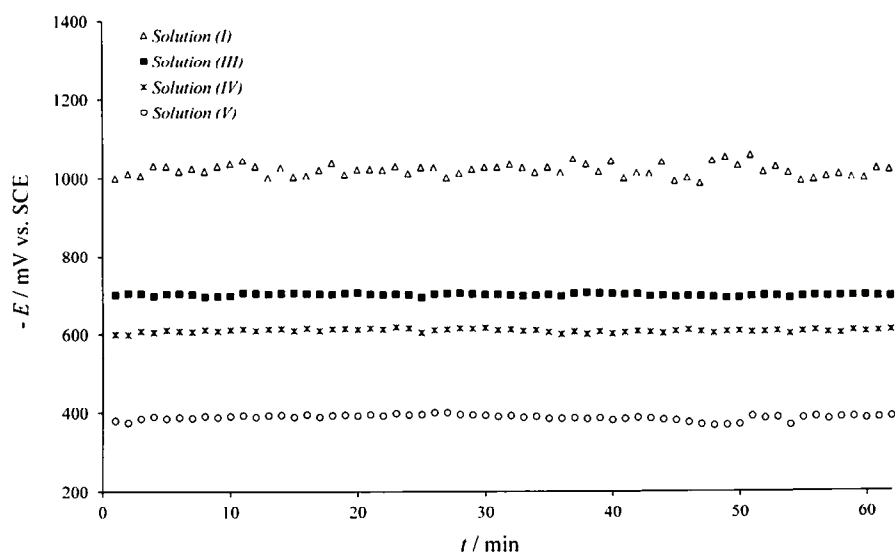


Fig. 2. Cathodic polarization value vs. time of copper deposition from solutions I and III–V.

The effect of current density on the morphology of electrolytic copper powder and on the properties of the copper powder was investigated at CD values of 150 and 200 mA cm⁻² and with different Cu ions concentrations at 30 °C.

The results obtained from solution I are shown in Fig. 3. Figures 3a and 3b show the morphologies of the copper powder obtained at 150 mA cm⁻². From Fig. 3a, it can be seen that a very disperse structure was formed at a CD of 150 mA cm⁻². The formed particles consisted of small cauliflower-like agglomerates of copper grains (Fig. 3b). Similar morphologies of the powder particles were obtained at a CD of 200 mA cm⁻² (Figs. 3c and 3d), which can be explained by the fact that both particles were formed under conditions of vigorous hydrogen evolution. It can be concluded that both types of powder particles consisted of agglomerates of copper grains. The only difference lay in the size of the individual copper grains of which these agglomerates were constituted. The estimated average size of copper grains in Fig. 3b is about 850±100 nm while it is about 400±100 nm in Fig. 3d. The nucleation rate and the grain size depend on the CD; thus, the grain size is considerably decreased at 200 mA cm⁻². According to Popov,⁶ the deposits obtained at low CDs grew from a small number of nuclei. However, with the increasing CD, the number of growth sites increased and the grain size of the deposit decreased. This is in good agreement with the fact that particles obtained at the low CD (Figs. 3a and 3b) were less branched and denser than those obtained at the higher CD (Figs. 3c and 3d). The increase of dispersity

and the decrease in grain size are the result of both the increased nucleation rate and the intensification of the hydrogen evolution reaction with increasing CD.

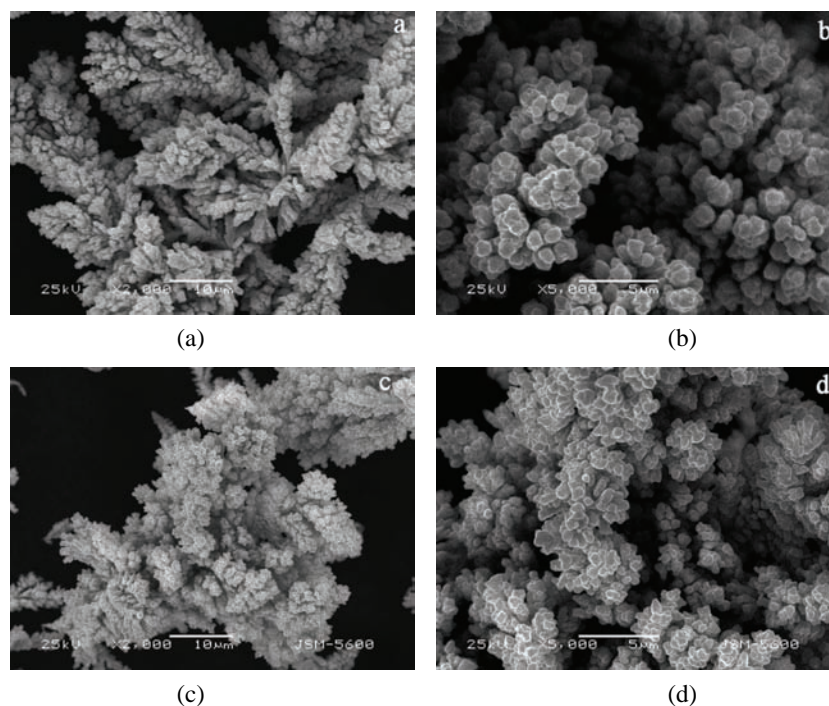


Fig. 3. SEM Photomicrographs of copper powder particles obtained from solution I at current densities of: 150 (a and b) and 200 mA cm⁻² (c and d).

The morphologies of copper powders obtained from solution II at CDs of 150 and 200 mA cm⁻² are shown in Fig. 4. From Figs. 4a and 4c, it may be seen that the powder particles were coral-like and consisted of small cauliflower-like agglomerates of copper grains. On the other hand, it can be said that the agglomerated copper particles were globular at the high CD (Fig. 4d). The one directional growth of the powder particles can be clearly seen in Fig. 4.

As can be seen from Fig. 5, the copper powder particles obtained from solution III at both current density values had a denser deposit structure and consisted of agglomerated copper grains. At higher magnifications, it can be easily seen that the shape of these grains could be characterized as globular (Figs. 5b and 5d). The copper deposit obtained from this solution at both CDs had a cauliflower-like structure. However, the size of the cauliflower-like particles increased with increasing copper ion concentration. Furthermore, the tendency of single directional growth can be clearly seen, which is similar to the deposits obtained from solution II.

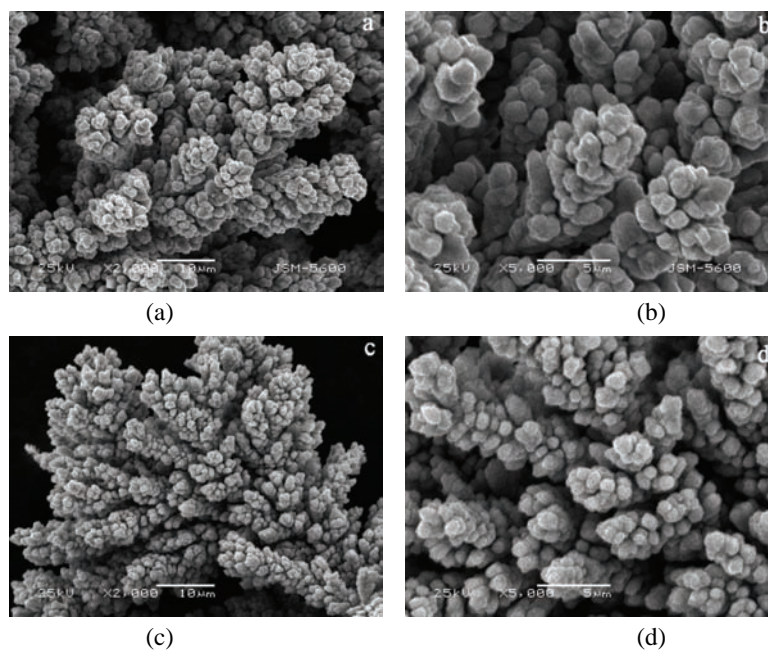


Fig. 4. SEM Photomicrographs of copper powder particles obtained from solution II at current densities of: 150 (a and b) and 200 mA cm⁻² (c and d).

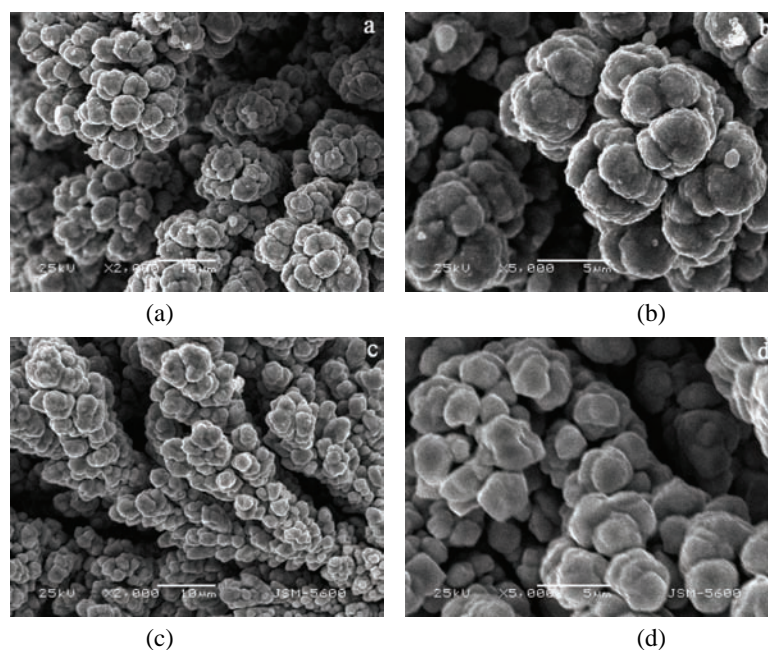


Fig. 5. SEM Photomicrographs of copper powder particles obtained from solution III at current densities of: 150 (a and b) and 200 mA cm⁻² (c and d).

The shrub-like morphology of the copper obtained from Solution IV at CDs of 150 and 200 mA cm^{-2} can be seen in Fig. 6. This structure consisted of bunched copper grains (Fig. 6a). Copper powder morphology and size at both CDs from this electrolyte are the same. It can be concluded that the upper surface of this structure has porous character (Fig. 6b). It is important to note that the bunches were observed at higher magnifications.

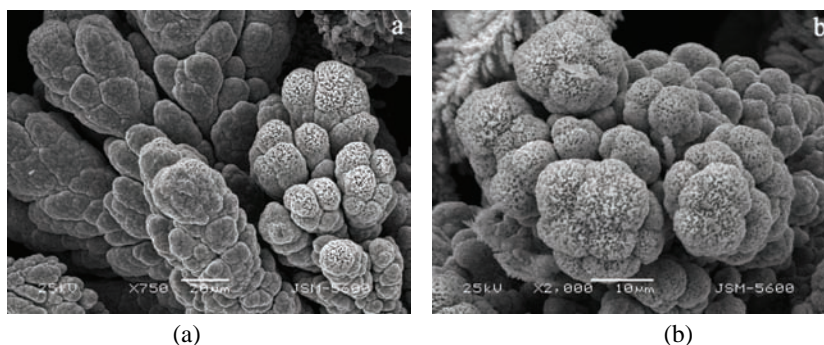


Fig. 6. SEM Photomicrographs of copper powder particles obtained from solution IV at current densities of: 150 (a) and 200 mA cm^{-2} (b).

It can be seen from Fig. 7 that a denser deposit of the copper powder particles was obtained from solution V at 150 mA cm^{-2} , which consisted of agglomerated copper grains. The shape of these grains can be characterized as course.

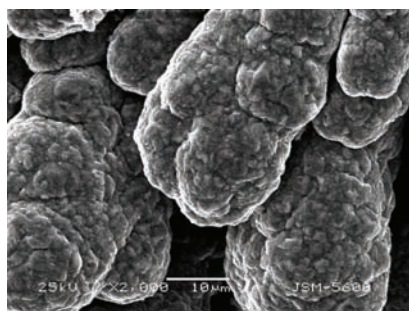


Fig. 7. SEM Photomicrograph of copper powder particles obtained from solution V at 150 mA cm^{-2} .

The average current efficiencies for the hydrogen evolution reaction at 30 °C for various CDs and Cu concentrations are given in Table I. It can be seen that hydrogen evolution efficiency decreased with increasing Cu ion concentration and increased with increasing CD. The current efficiency of hydrogen evolution obtained from solution I at 150 mA cm^{-2} was 24.4 %, while it was 28.6 % at 200 mA cm^{-2} . This value decreased with the increasing Cu ion concentration at both CDs and became zero for solution V. The current efficiency value of zero for hydrogen evolution indicates that all the current in the system was consumed for copper electrodeposition. Thus, according to Nikolić,^{7,10} an average current effi-

ciency of hydrogen evolution of 30 % is sufficient to cause mixing of the solution in the near-electrode layer while simultaneously decreasing the diffusion layer thickness and increasing the limiting diffusion current density. Due to the change in the hydrodynamic conditions caused by vigorous hydrogen evolution, the morphologies of the deposits become similar to those obtained at some lower overpotential, before the initiation of dendritic growth.⁵ This clearly explains the cauliflower-like shape of the powders obtained in this work.

TABLE I. The values of the average current efficiencies of hydrogen evolution, in dependence on the copper ion concentration and current density

Cu ²⁺ concentration, mol dm ⁻³	Hydrogen evolution efficiency, %	
	150 mA cm ⁻²	200 mA cm ⁻²
0.120	24.4	28.6
0.155	12.5	13.2
0.315	3.8	4.5
0.475	0.6	0.8
0.630	0	0

The copper ion concentration and the CD are significantly important parameters determining the limiting current density; thus, they determine the morphology and size of electrolytic copper powders. According to Levich, in metal electrodeposition under natural convection, the limiting current density (i_L) varies with concentration as:¹⁴

$$i_L \approx c_0^{1.25} \quad (1)$$

where c_0 is concentration of Cu ions.

According to Eq. (1), the limiting current density increases with the increasing concentration of Cu ions. Finally, with increasing limiting current density, the morphologies of copper powder at higher copper ion concentrations were similar to those obtained at lower CDs, despite working at a higher CD. In other words, when the copper concentrations are high, the working CD actually stays below the limiting diffusion current density.

The change in the morphologies of the electrolytic copper powder with concentration of copper ions in solution under galvanostatic control can be seen in Figs. 3a, 4a, 5a, 6a and 7 for a CD of 150 mA cm⁻² or in Figs. 3c, 4c, 5c and 6c for a CD of 200 mA cm⁻². The morphologies changed to cauliflower-like, coral-like, shrub-like, and stalk-stock-like morphology with increasing of Cu ion concentrations from 0.120, through 0.15, 0.315 and 0.475, to 0.630 M Cu²⁺ in 0.5 M H₂SO₄, respectively, at the same CD. The particle size variation depending on the applied CD was in good agreement with the nucleation rate and nuclei growth rate. With increasing CD, the grain size will be finer and may lead to an increase in the dispersity of copper deposits, because the nucleation rate is greater than nuclei growth rate.^{3,5,7,18}

The apparent densities for the copper powder obtained at 150 and 200 mA cm⁻² for various copper concentrations under standard conditions are given in Table II, from which it can be seen that the properties of the powder changed with the applied CD. This can be explained as follows: the decrease in the size of the grains with increasing of CD or with decreasing Cu ion concentrations leads to an increase in the specific surface area of the powder. It is known that an increase in the specific surface area of a powder results in a decrease in the apparent density.^{3,5,9,11} As can be seen in Table II, the obtained results are in accordance with the surface area–apparent density relation. While the apparent density values varied from 0.68 to 3.38 g cm⁻³ with increasing Cu ion concentration at 150 mA cm⁻², the apparent density varied between 0.58–3.43 g cm⁻³ at a CD of 200 mA cm⁻².

TABLE II. Apparent density of the copper powder obtained at different CDs and Cu concentrations at 30 °C

Cu ²⁺ concentration, mol dm ⁻³	Apparent density, g cm ⁻³	
	150 mA cm ⁻²	200 mA cm ⁻²
0.120	0.68	0.58
0.155	0.88	0.66
0.315	1.11	1.62
0.475	3.10	2.57
0.630	3.38	3.43

To understand the effect of electrolyte temperature on the Cu powder morphology and apparent density, the powders obtained from solution II were investigated. The morphologies of electrolytic copper powder particulates obtained from solution II at a CD of 150 mA cm⁻² at 45 and 60 °C are shown in Fig. 8. It can be stated that powder particles obtained at all three temperatures (30, 45 and 60 °C) were branched structures and the branches consisted of agglomerated copper grains (Figs. 4a, 8a and 8c). The variation of the morphology with increasing temperature can be clearly observed at higher magnifications. The surface properties of the powders obtained at 45 and 60 °C differ from the velvety structure of the powder obtained at 30 °C. It is well known that an increase in the specific surface area of a powder means a decrease in the apparent density. The apparent densities of powders obtained at an electrolyte temperature of 30, 45 and 60 °C were 0.88, 0.65, and 0.38 g cm⁻³, respectively. As expected, a decrease in the apparent density with increasing surface area was observed. The morphology of copper powder particles obtained at 200 mA cm⁻² CD from solution II at 60 °C is shown in Fig. 9. It can be seen from 30 (Figs. 4c and 4d) and 60 °C (Fig. 9) that the powder particles are sponge-like. It can also be seen that copper particles have globular structure.

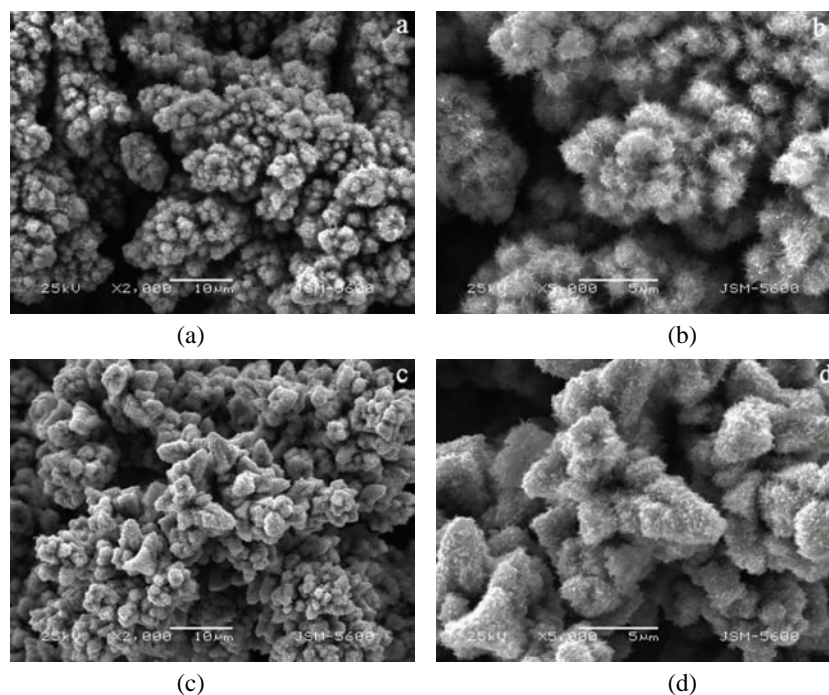


Fig. 8. SEM Photomicrographs of copper powder particles obtained from solution II at temperatures of: 45 (a and b) and 60 °C (c and d) at 150 mA cm⁻².

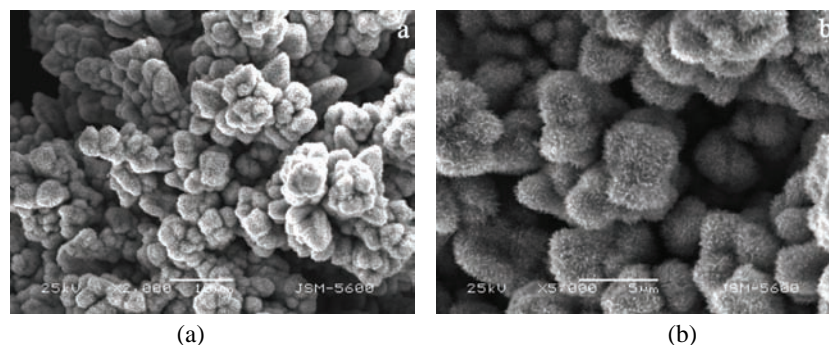


Fig. 9. SEM Photomicrographs of copper powder particles obtained from solution II at a temperature of 60 °C at 200 mA cm⁻².

The powder obtained at 200 mA cm⁻² from solution II and at 60 °C is had the same velvety structure as the powder obtained at 150 mA cm⁻² and at 45 and 60 °C. The apparent density values of the powders obtained at 30 and 60 °C under the same experimental conditions were 0.66 and 0.42 g cm⁻³, respectively. These are in good agreement with the morphologies of the respective copper powders.

In the experiments in which the electrolyte temperature was 30 °C, the average current efficiency of the hydrogen evolution was 12.5 % in solution II at a CD of 150 mA cm⁻², while at 45 and 60 °C, the average current efficiencies of hydrogen evolution were 25.5 and 38.2 %, respectively. On the other hand, the average current efficiency of hydrogen evolution in solution II at a CD of 200 mA cm⁻² and at 30 °C was 13.2 %. When the temperature was increased to 60 °C, the average current efficiency of hydrogen evolution increased to 41.1 % in the same solution.

All powders that were obtained from solutions I–III at a CD of 150 or 200 mA cm⁻² and at temperatures 30–60 °C consisted of agglomerates of copper grains. The size of the grains in these agglomerates was a function of the CD (*i.e.*, of the overpotential), Cu ion concentration, temperature and quantity of evolved hydrogen. The decrease in the mean size of the grains was related to the increasing quantity of evolved hydrogen.

SEM Images of powders obtained in the absence of the scraper are shown in Fig. 10. In this case, the surface area of the electrode continues to enlarge, which leads to a decreasing current density. The powder obtained under these conditions does not have a homogenous structure. The powder structure was comprised of agglomerated copper grains, which grew extremely like the cauliflower-like grains (Fig. 10a). These powders seem to be a mixture of powders with different grain structures because of the surface, which could not remain constant due to the absence of the scraper. The denser-like deposit structure obtained from solutions IV and V as seen in Part A and the cauliflower-like structure obtained from solution II as seen in Part B of Fig. 10b simultaneously co-existed.

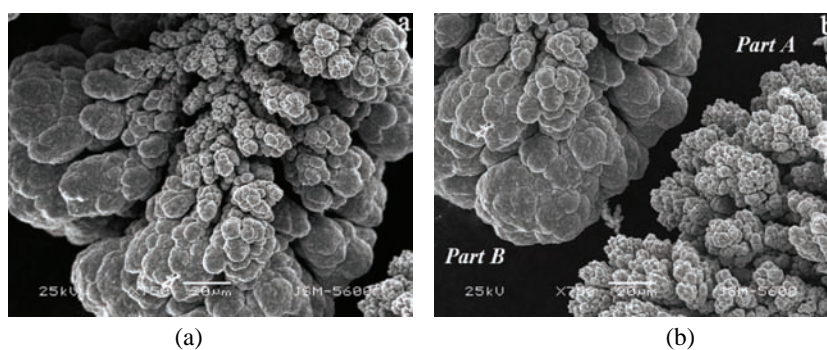


Fig. 10. SEM Photomicrographs of copper powder particles obtained from solution II at 150 mA cm⁻² without a scraper.

CONCLUSION

The effect of different Cu ion concentrations, temperature and current density on the morphology and apparent density of copper powders obtained at high

CDs were examined. The concentration of H_2SO_4 and the scraper speed were kept constant. The following conclusions may be deduced.

The morphologies of the disperse and porous copper powders from solutions I and II were small cauliflower-like agglomerates of copper grains at current density values of 150 and 200 mA cm^{-2} . It is important to note that the powders from solution II were denser than those from solution I. Thus, this structure can be called coral-like. The particles from solution III were also in cauliflower-like form at CDs values of 150 and 200 mA cm^{-2} . In solution IV, the particles were shrub-like in form at both applied CDs and finally a stalk–stock-like form were found in solution V at a CD of 150 mA cm^{-2} under the same working conditions. The morphologies of the copper powder obtained at the applied CDs, *i.e.*, overpotentials, were in accordance with the position of the CD on the polarization curve. In other words, the morphologies of the copper powders were correlated with the hydrogen evolution rates. The cauliflower-like structure was the main characteristic of deposits obtained at high CDs and high overpotentials, belonging to the limiting diffusion current density plateau, at which the hydrogen evolution rate was high. However, when the hydrogen evolution rate was lower, the morphologies changed from small cauliflower-like agglomerates of copper grains to sponge-like, shrub-like or stalk–stock-like shape.

Temperature also has a significant influence on the copper powder morphology along with current density and copper ion concentration. The velvety structure of the powders obtained at 45 and 60 °C, which is different to that formed at 30 °C, is noteworthy. This structure resulted in an increase in the surface area and, consequently, a decreased apparent density.

The apparent density values of the copper powder also changed with respect to their morphologies. The smaller the cauliflower-like structure of the powder particulates, the lower was the apparent density of the copper powder. Therefore, the apparent densities of copper powders can be controlled by changing the electrolysis parameters. Depending on the electrolysis parameters, such as CD, Cu ion concentration and temperature, the apparent densities of copper powders were within the range 0.38 and 3.43 g cm^{-3} .

Moreover, the importance of the employment of a scraper is dominantly seen in this work. It allows for a homogenous powder production. In addition, pre-determined particles of copper-plated electrodes can be obtained on the surface.

Acknowledgement. The authors would like to thank the Scientific and Technological Research Council of Turkey (TUBITAK), which supported this work as part of the TUBITAK Project No. 105M137.

ИЗВОД

ЕФЕКТИ ПАРАМЕТАРА ЕЛЕКТРОЛИЗЕ НА МОРФОЛОГИЈУ БАКАРНОГ ПРАХА
ДОБИЈЕНОГ ПРИ ВИСОКИМ ГУСТИНАМА СТРУЈЕ

GÖKHAN ORHAN и GIZEM GÜZEY GEZGIN

*Istanbul University, Faculty of Engineering, Metallurgical and Materials Engineering
Department, 34320 Istanbul, Turkey*

Испитиван је утицај концентрације јона бабра и температуре електролита на морфологију и привидну густину бакарног праха добијеног у галваностатском режиму при високим густинама струје. Ови параметри су одређени искоришћењем струје издвајања водоника при таложењу бабра. Поред тога, морфологија бакарног праха је анализирана и скенирајућом електронском микроскопијом. Нађено је да морфологија прахова добијених при истој густини струје зависи од концентрације јона бабра у електролиту и температуре електролита. Таложењем при густини струје 150 mA cm^{-2} и потенцијалу $-1000 \pm 20 \text{ mV}$ (према ЗКЕ) из електролита који је садржао $0,120 \text{ M Cu}^{2+}$ и $0,50 \text{ M H}_2\text{SO}_4$ добијен је порозан и дисперзан прах бабра. Под тим условима паралелно са таложењем бабра интензивно се издваја водоник. Са повећањем концентрације јона Cu^{2+} од $0,120, 0,155, 0,315, 0,475$ до $0,630 \text{ M}$ при истој густини струје, запажена је промена морфологије праха од порозне, дисперзне и облика сличних карфиолу до морфологије која подсећа на корале, жбунове и стабљике. Повећање температуре такође утиче на морфологију и привидну густину бакарног праха. Вредности привидне густине прахова таложених током овог испитивања показују да су они погодни за примену у разним областима металургије.

(Примљено 27. јуна, ревидирано 20. октобра 2011)

REFERENCES

1. A. Agrawal, S. Kumari, D. Bagchi, V. Kumar, B. D. Pandey, *Hydrometallurgy* **84** (2006) 218
2. M. G. Pavlović, K. I. Popov, <http://electrochem.cwru.edu/encycl/art-p04-metalpowder.htm>, 2005
3. G. Orhan, G. Harçi, *Powder Technol.* **201** (2010) 57
4. M. G. Pavlović, Lj. J. Pavlović, I. D. Doroslovački, N. D. Nikolić, *Hydrometallurgy* **73** (2004) 155
5. N. D. Nikolić, Lj. J. Pavlović, M. G. Pavlović, K. I. Popov, *Powder Technol.* **185** (2008) 195
6. K. I. Popov, S. S. Djokić, B. N. Grgur, *Fundamental Aspects of Electrometallurgy*, Kluwer Academic/Plenum Publishers, New York, USA, 2002
7. N. D. Nikolić, K. I. Popov, Lj. J. Pavlović, M. G. Pavlović, *Surf. Coat. Technol.* **201** (2006) 560
8. N. D. Nikolić, K. I. Popov, Lj. J. Pavlović, M. G. Pavlović, *J. Electroanal. Chem.* **588** (2006) 88
9. M. G. Pavlović, Lj. J. Pavlović, E. R. Ivanović, V. Radmilović, K. I. Popov, *J. Serb. Chem. Soc.* **66** (2001) 923
10. K. I. Popov, S. B. Krstić, M. G. Pavlović, *J. Serb. Chem. Soc.* **68** (2003) 511
11. K. I. Popov, S. B. Krstić, M. C. Obradović, M. G. Pavlović, Lj. J. Pavlović, E. R. Ivanović, *J. Serb. Chem. Soc.* **69** (2004) 43
12. R. Walker, S. J. Duncan, *Surf. Technol.* **23** (1984) 301
13. A. Agrawal, S. Kumari, D. Bagchi, V. Kumar, B. D. Pandey, *Miner. Eng.* **20** (2007) 95

14. N. D. Nikolić, K. I. Popov, Lj. J. Pavlović, M. G. Pavlović, *Sensors* **7** (2007) 1
15. N. D. Nikolić, G. Branković, M. G. Pavlović, K. I. Popov, *J. Electroanal. Chem.* **621** (2008) 13
16. N. D. Nikolić, Lj. J. Pavlović, S. B. Krstić, M. G. Pavlović, K. I. Popov, *Chem. Eng. Sci.* **63** (2008) 2824
17. N. D. Nikolić, Lj. J. Pavlović, M. G. Pavlović, K. I. Popov, *J. Serb. Chem. Soc.* **72** (2007) 1369
18. N. D. Nikolić, K. I. Popov, Lj. J. Pavlović, M. G. Pavlović, *J. Solid State Electrochem.* **11** (2007) 667.



J. Serb. Chem. Soc. 77 (5) 667–683 (2012)
JSCS–4299

Different behaviour of 3-nitrotyrosine and tyrosine toward perfluorinated reagents suitable for the one-step preparation of volatile derivatives

RADMILA PAVLOVIĆ^{1,2*}, PIER ANTONIO BIONDI³, LUCA MARIA CHIESA³,
NATAŠA TRUTIĆ², MIRJANA ABRAMOVIĆ² and ENZO SANTANIELLO¹

¹Department of Medicine, Surgery and Dentistry, School of Medicine c/o S. Paolo Hospital, Università degli Studi di Milano, Italy, ²Department of Chemistry, Medical Faculty, University of Niš, Serbia and ³Department of Veterinary Sciences and Technologies for Food Safety, Faculty of Veterinary Medicine, Università degli Studi di Milano, Italy

(Received 4 March 2011, revised 10 January 2012)

Abstract: With the view of developing a gas-chromatographic (GC) determination of the 3-nitrotyrosine (NY)/tyrosine (Y) ratio as a marker of nitro-oxidative stress, different reagents were tested with the objective of obtaining a single volatile fluorinated product for each amino acid in a one-step derivatisation procedure. The heptafluorobutyric anhydride (HFBA)/heptafluorobutanol (HFBOH) mixture proved unsuccessful for the simultaneous analysis of NY and Y. The reaction with different chloroformates, isobutyl chloroformate (*i*BuCF) and ethyl chloroformate (EtCF) in the presence of different perfluorinated alcohols, such as trifluoroethanol (TFEOH) and HFBOH, was investigated. A combination EtCF/fluorinated alcohols yielded derivatives of NY and Y as single peaks suitable for the GC determination of the NY/Y ratio. The different behaviours of the two amino acids in the employed reaction mixtures and the parameters influencing the results are discussed.

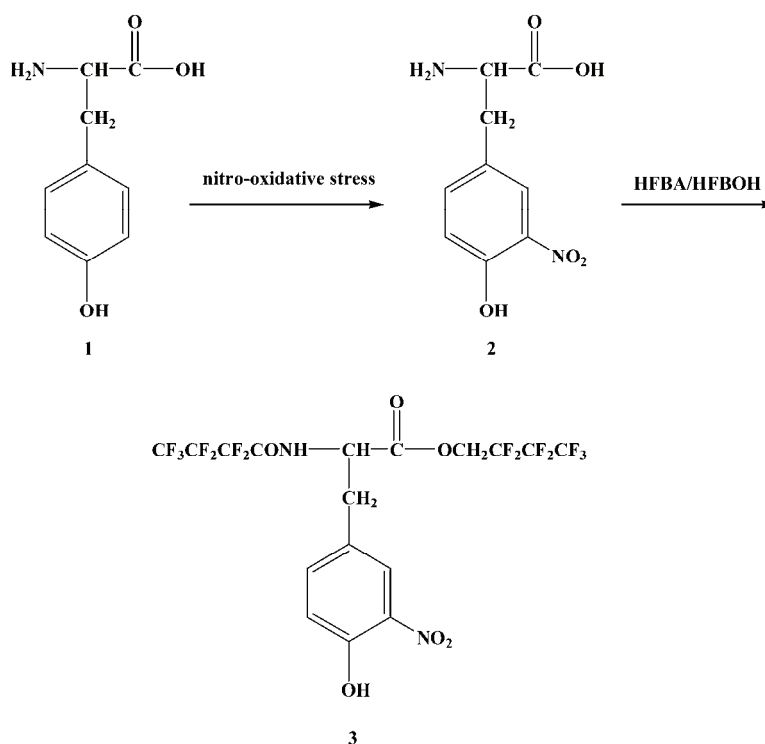
Keywords: perfluorinated derivatives; tyrosine; 3-nitrotyrosine; GC–MS.

INTRODUCTION

Nitration of tyrosine Y (**1**) (Scheme 1), under particular conditions that are generally termed “nitro-oxidative stress”, may impair cell function by altering the protein conformation, solubility and susceptibility to aggregation, and could be responsible for increased protein degradation. This is especially relevant if enzymes of patho-physiological significance are involved.^{1–3} 3-Nitrotyrosine (NY, **2**) is formed under the above conditions and, therefore, its detection and quanti-

* Corresponding author. E-mail: radmila.pavlovic@medfak.ni.ac.rs
doi: 10.2298/JSC110304003P

fication has been used as an indicator of the nitro-oxidative stress in biological systems.^{4–10}



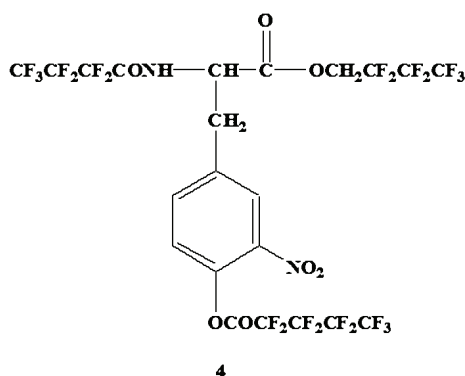
Scheme 1. Nitration of Y and structure of the derivative obtained from NY by treatment with a HFBA/HFBOH mixture.

Recently, the preparation of derivative (3), obtained with a heptafluorobutyric anhydride (HFBA)/heptafluorobutanol (HFBOH) mixture, was described for the evaluation of the NY content in the plasma of human volunteers by gas chromatography with an electron capture detector (GC–ECD).¹¹ This method was considered as a significant contribution to 3-nitrotyrosine quantification.¹²

In the above paper,¹¹ a combination of HFBA/HFBOH was selected in order to prepare in a one-step procedure a derivative with the highest possible content of fluorine atoms, since GC–ECD sensitivity is strongly influenced by the fluorine content of the derivative to be analyzed*.¹³

* Another procedure has been reported for the preparation of a volatile derivative for GC/negative chemical ionization (NCI) MS/MS analysis containing fourteen fluorine atoms.¹⁴ However, it should be mentioned that this derivative was obtained in three steps, which included the reduction of NY to the corresponding amino derivative and the use of trimethylsilyl diazomethane for the methylation step.

During the experimental work, several conditions were tried in order to achieve the formation of the tris-substituted derivative **4** (Scheme 2), but with no success. This could be explained by the presence of an electron-withdrawing group at position 3 in NY that should significantly influence the reactivity of the phenolic OH and, consequently, the chemical properties of the NY derivatives that could be prepared.



Scheme 2. Structure of NY heptafluorobutyl ester reacted with HFBA at both amino and phenol moieties.

The main aim of the present work was to propose a one-step procedure suitable for obtaining volatile derivatives for the simultaneous determination of Y and NY as a useful approach to evaluate protein nitro-oxidative stress. Major efforts were related to the possibility of obtaining the same fluorinated derivative for both compounds, taking into account the different reactivity of NY and Y under the derivatisation conditions.

All procedures described in the present paper were realised on the micromolar scale under conditions that should simulate the analysis of biological samples. Due to potential application as an analytical method, special attention was devoted to the achievement of the completeness of the derivatisation in a simple, one-step procedure to give a single product. After performing preliminary studies with the GC–FID analytical technique, all structures of the obtained derivatives were identified by MS analysis and the fragmentation spectra are presented herein as proof of the chemical structures.

MATERIALS AND METHODS

Chemicals

Y (**1**) and NY (**2**) were purchased from Sigma–Aldrich Italia, as well as derivatisation reagents (trifluoroacetic anhydride (TFAA), heptafluorobutyric anhydride (HFBA), ethyl chloroformate (EtCF), *iso*-butyl chloroformate (*i*BuCF) 2,2,2-trifluoroethanol (TFEOH), heptafluorobutanol (HFBOH), ethanol (EtOH), *iso*-butanol (*i*BuOH), *N,O*-bis(trimethylsilyl) trifluoroacetamide (BSTFA) and *N*-methyl-*N*-(*t*-butyldimethylsilyl)trifluoroacetamide (MTBSTFA)).

Preparation of N-perfluoroacyl perfluoroalkyl esters and their silyl derivatives

Y and NY were derivatised by conversion to their *N*- or *N,O*-perfluoroacyl perfluoroalkyl esters according to a previously reported procedure.¹⁵ Briefly, the two derivatising agents (50 μL perfluoroalcohol and 100 μL of perfluoroalkyl anhydride) were added to the dry amino acids (0.1 μmol each) and heated at 80 $^{\circ}\text{C}$ for 30 min. The alcohols used in the present experiments were TFEOH and HFBOH, while the anhydrides were TFAA and HFBA. Excess reagents were removed under a stream of nitrogen and the residues were dissolved in ethyl acetate. The organic extract was both directly injected or treated with 100 μL of BSTFA or MTBSTFA and heated at 80 $^{\circ}\text{C}$ for 30 min. After cooling to room temperature, 1 μL of the resulting mixture was injected into the GC–MS system.

Preparation of N(O)-alkoxycarbonyl alkyl esters

Y and NY were derivatised to their N(O)-alkoxycarbonyl alkyl esters and analyzed following the protocol previously described by Husek¹⁶ and modified by Wang *et al.*¹⁷ In brief, amino acids (0.10 μmol each) were dissolved 100 μL of H_2O and treated with 100 μL of alcohol/pyridine in a volume ratio 80:20. The alcohols used in the present experiments were: EtOH, *i*BuOH, TFEOH and HFBOH. Then 12.5 μL of EtCF or *i*BuCF were added and mixed by shaking gently for 30s. The derivatives were extracted with 150 μL of hexane containing 2 % chloroformate. A 1 μL aliquot was taken from the organic layer and injected.

GC–FID

A Trace GC Ultra (Thermo) (Milan, Italy) fitted with an FID was used in the control experiments. This chromatograph was equipped with a capillary column Optima 1701 (15 $\text{m} \times 0.25$ mm, 0.25 μm) (Macherey-Nagel, Duren, Germany). The temperatures of the injector and detector were 250 and 280 $^{\circ}\text{C}$, respectively. The split injection technique was used with a 1:10 ratio. The column temperature was programmed from 140 to 290 $^{\circ}\text{C}$ at 10 $^{\circ}\text{C} \text{ min}^{-1}$. Helium at a flow rate of 0.9 $\text{ml} \text{ min}^{-1}$ was used as the carrier gas.

GC/MS

GC/MS Analyses were performed on a 5972A mass selective detector interfaced to a 5890 gas chromatograph (Agilent, Milano, Italy). The instrument was operated in the electron ionisation (EI) mode with an electron energy of 70 eV. The GC separation was accomplished on a HP-5 MS (30 $\text{m} \times 0.25$ mm, 0.25 μm) column. The transfer line temperature was 310 $^{\circ}\text{C}$ and the injector temperature was set at 300 $^{\circ}\text{C}$. The injector was operated in the splitless mode. The column temperature was held at 50 $^{\circ}\text{C}$ for 5 min, then programmed to increase at a rate of 20 $^{\circ}\text{C} \text{ min}^{-1}$ to 300 $^{\circ}\text{C}$ and finally held for 15 min at the end temperature.

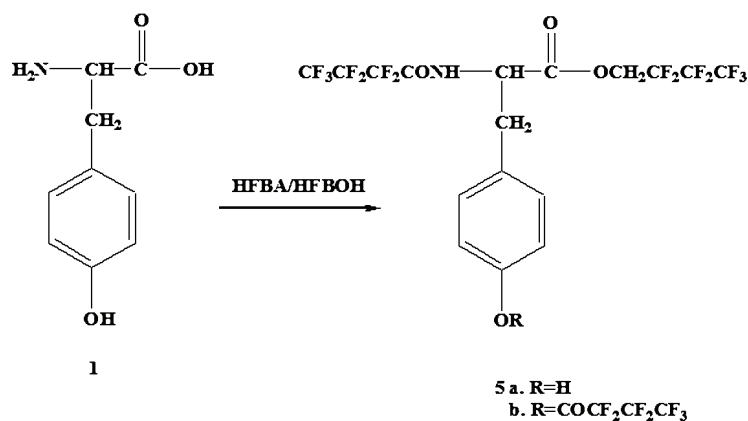
RESULTS AND DISCUSSION

As the objective of this work was the simultaneous derivatisation of Y and NY, the optimal reaction conditions (80 $^{\circ}\text{C}$, 30 min) that afforded the NY bis-derivative **3** with a HFBA/HFBOH mixture in a previous study¹¹ were repeated on the parent proteinogenic amino acid Y. However, the reaction of Y afforded a mixture of tris- and bis-derivatives (Scheme 3, compounds **5a** and **5b**) as shown in Fig. 1.

As a possible explanation of these results, it should be considered that a strong electron-withdrawing group, such as a nitro group, increases the acidity of the phenolic hydroxyl moiety. Consequently, the intermediate *O*-heptafluoro bu-

tanoate could be more susceptible to *in situ* hydrolysis, constantly producing free OH. Interestingly, an internal hydrogen bond between the phenolic OH and the nitro group in NY¹⁸ could lower the OH reactivity.

Since a reliable, quantitative analysis is generally based on unique peaks of the analytes, the simultaneous determination of Y and NY would not be possible using the HFBA/HFBOH mixture.



Scheme 3. Derivatisation of tyrosine by the perfluoroacylation/perfluoroesterification procedure.

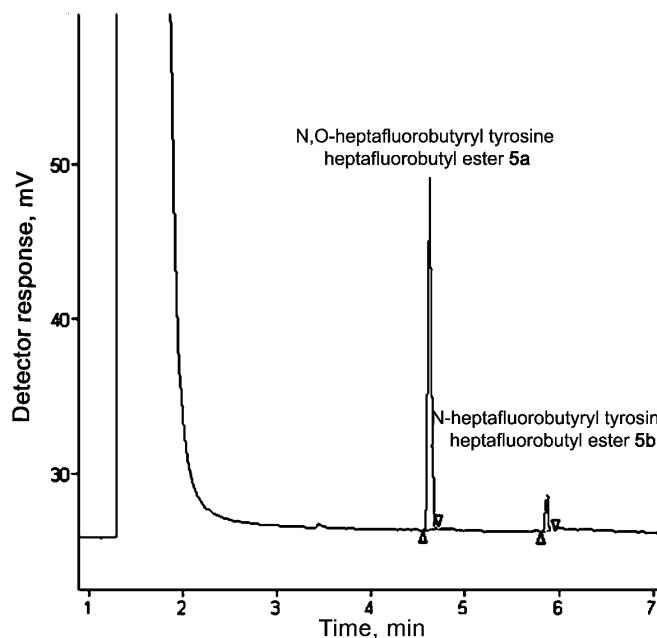
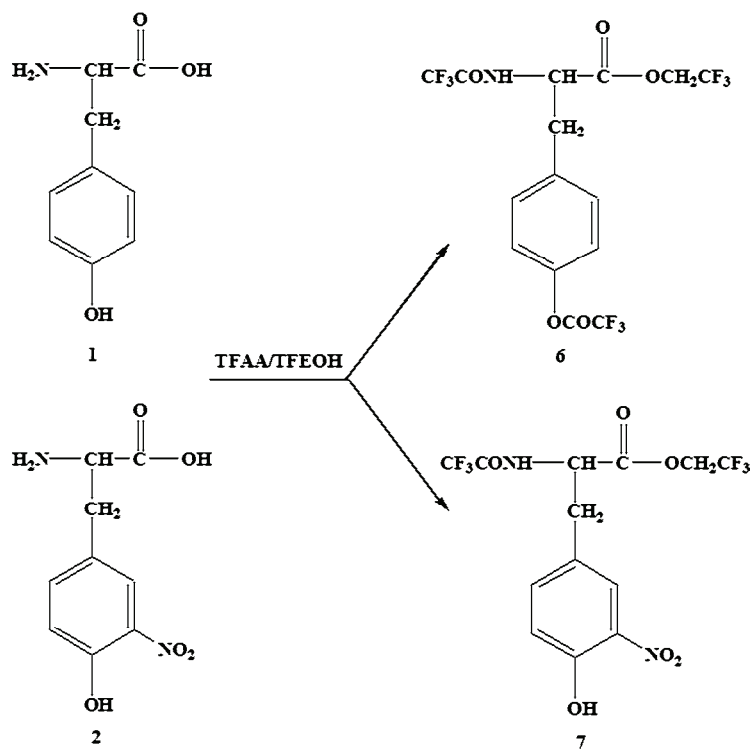


Fig. 1. GC-FID Chromatogram of the products obtained by treatment of Y with HFBA and HFBOH, tris- (first peak) and bis-substituted (second peak) derivatives.

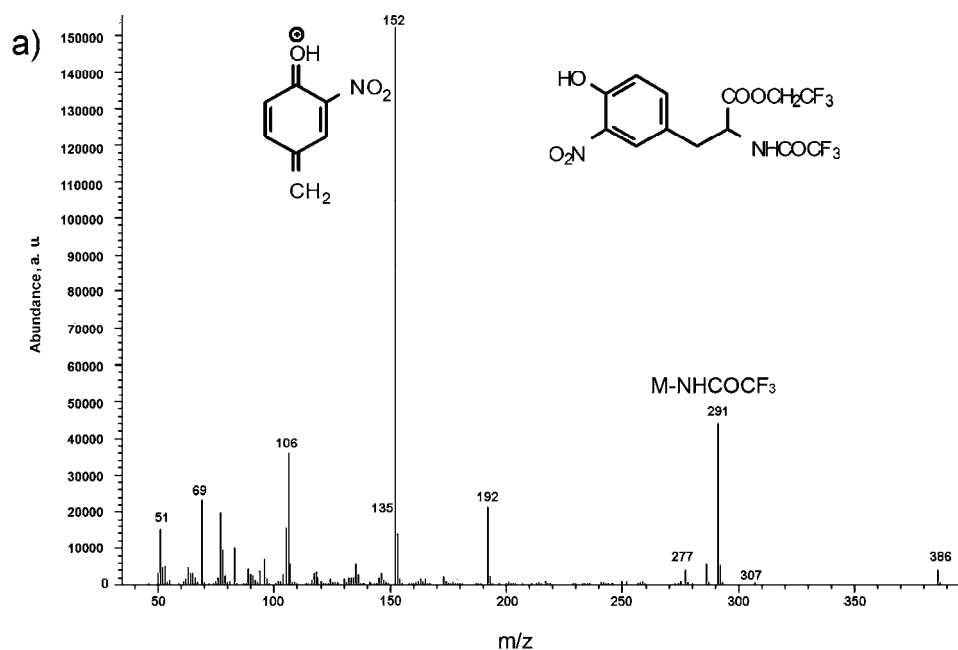
Therefore, the derivatives obtained using the TFAA/TFEOH combination were examined. Both Y and NY afforded unique products, but while Y gave the tris-derivative **6**, NY afforded only the bis-derivative with a free phenolic OH (Scheme 4, compound **7**). The mass spectrometric data of the obtained derivatives are given in Table I. Some results are in the agreement with previously reported information,^{19,20} while those regarding **5b** are presented here for the first time. In particular, the fragmentation pattern of the NY derivatives was especially investigated. The main peak for both derivatives was the 4-methylene-2-nitro-cyclohexa-2,5-dienylidene-oxonium cation (3-nitro-4-hydroxybenzyl cation) ($m/z = 152$). Important ions were present in both fluorinated derivatives **7** (Fig. 2a) and **3**, such as the ones originating from the cleavage of the C–C bond next to the ester group, with the formation of peaks at $m/z = 277$ (M–127) for the TFAA–TFEOH derivative and $m/z = 377$ (M–227) for the one obtained with HFBA–HFBOH. Moreover, other peaks in both cases were derived from the fragment produced by the loss of CF_3CONH_2 , $m/z = 291$ (M–113) for the TFAA–TFEOH derivative or $\text{CF}_3(\text{CF}_2)_2\text{CONH}_2$, $m/z = 391$ (M–213) for the one obtained from HFBA–HFBOH.



Scheme 4. Derivatization of 3-nitrotyrosine by the perfluoroacylation/perfluoroesterification procedure.

TABLE I. Characteristic ion peaks in the mass spectra of *N*,(*O*)-perfluoroacyl perfluoroalkyl tyrosine and 3-nitrotyrosine esters

Amino acid	Anhydride/alcohol	Derivative	<i>m/z</i>	Main peak, <i>m/z</i>	Characteristic peaks, <i>m/z</i>
Tyrosine	TFAA/TFEOH	<i>N</i> , <i>O</i> -trifluoroacetyl tyrosine trifluorethyl ester 6	455 ^a	203	231, 243, 328, 342
	HFBA/HFBOH	<i>N</i> , <i>O</i> -heptafluorobutyryl tyrosine heptafluorobutyl ester 5a	755 ^a	542	275, 303, 343
		<i>N</i> -heptafluorobutyryl tyrosine heptafluorobutyl ester 5b	559	107	332, 346
3-Nitrotyrosine	TFAA/TFEOH	<i>N</i> -trifluoroacetyl 3-nitrotyrosine trifluorethyl ester 7	404 ^a	152	106, 277, 291, 386
	HFBA/HFBOH	<i>N</i> -heptafluorobutyryl 3-nitrotyrosine heptafluorobutyl ester 3	604	152	106, 377, 391

^aNo molecular ion identifiedFig. 2. Mass spectra of NY, *N*-trifluoroacetyl trifluorethyl ester and its silyl derivatives:
a) compound **6**.

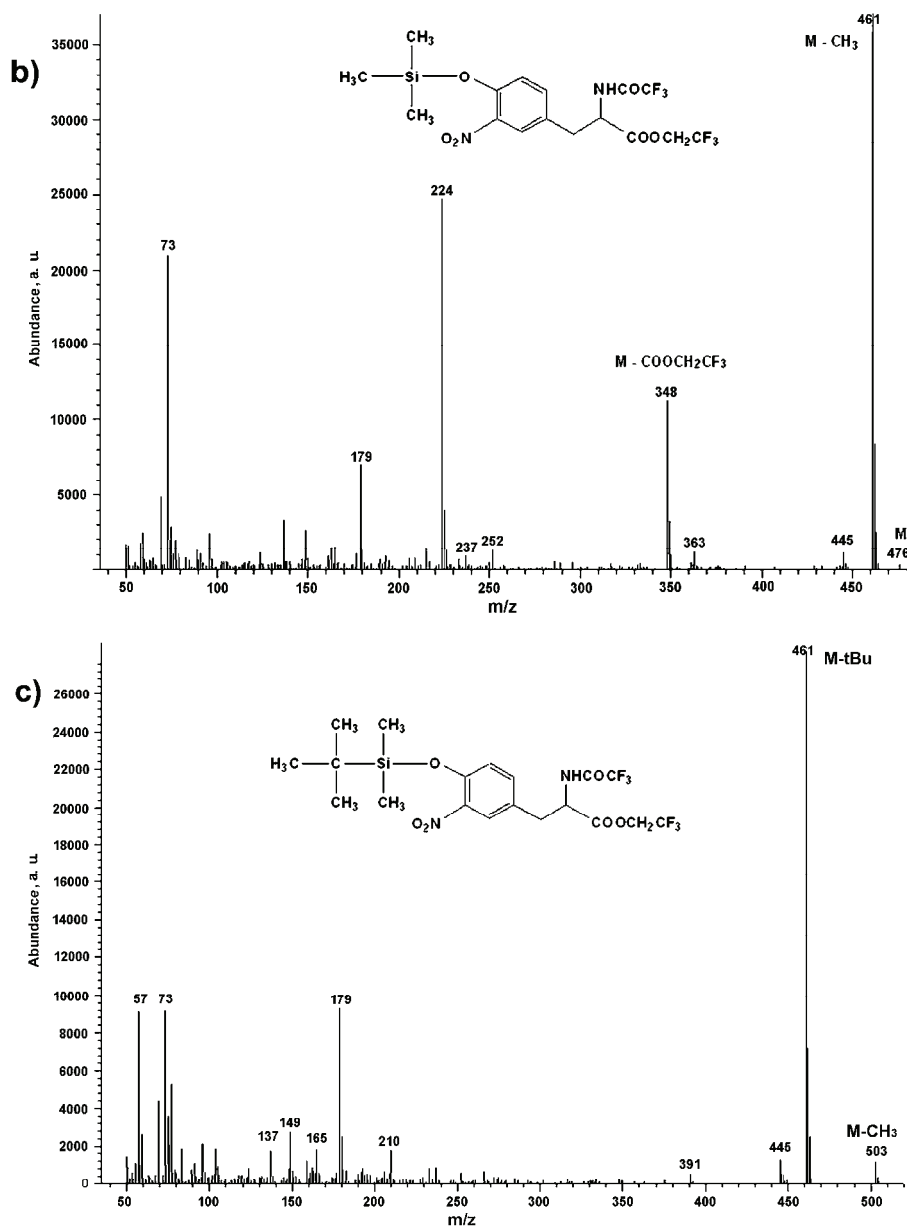
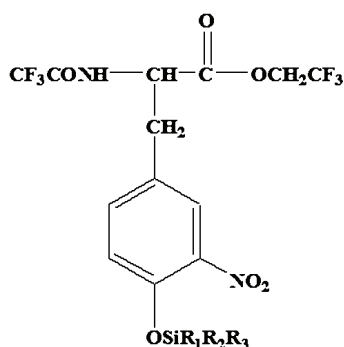


Fig. 2. (Continued) Mass spectra of NY, *N*-trifluoroacetyl trifluorethyl ester and its silyl derivatives: b) compound **8a** and c) compound **8b**.

Moreover, additional studies are reported that were performed during a reappraisal of the NY protocol.¹¹ Namely, it was observed that after numerous injections of standard and biological samples into the same column, the peak

shape of the NY derivatives showed an increasing tailing. It was reasoned that the presence of the free phenolic group could influence the reliability of the analytical procedure, as already observed for other 2-nitrophenols.²¹ In order to demonstrate that a derivative of NY with a protected phenolic OH is more suitable for gas-chromatographic analysis, silylation of compound **7** with different silylating agents was performed. Trimethylsilyl (TMS) and *t*-butyldimethylsilyl (TBDMS) derivatives **8a** and **8b** were prepared (Scheme 5) and the corresponding MS data are given in Table II and shown in Figs. 2b and 2c. It is of interest to observe that this derivatisation technique offers the advantage of a sufficient abundance of high molecular mass fragments that should facilitate the identification of the compound.



8 a. $R_1=R_2=R_3=CH_3$
8 b. $R_1=R_2=CH_3, R_3=tBu$

Scheme 5. Structures of the silyl derivatives of NY previously reacted with TFA/TFEHOH mixture.

TABLE II. Characteristic ion peaks in the mass spectra of NY silyl derivatives of N-trifluoroethyl esters

Derivative	<i>m/z</i>	Main peak, <i>m/z</i>	Characteristic peaks, <i>m/z</i>
TMS derivate of NY	473	461	179, 224, 348
<i>N</i> -trifluoroacetyl trifluoroethyl ester (8a)			
TBDMS derivate of NY	518 ^a	461	179, 210, 445, 503
<i>N</i> -trifluoroacetyl trifluoroethyl ester (8b)			

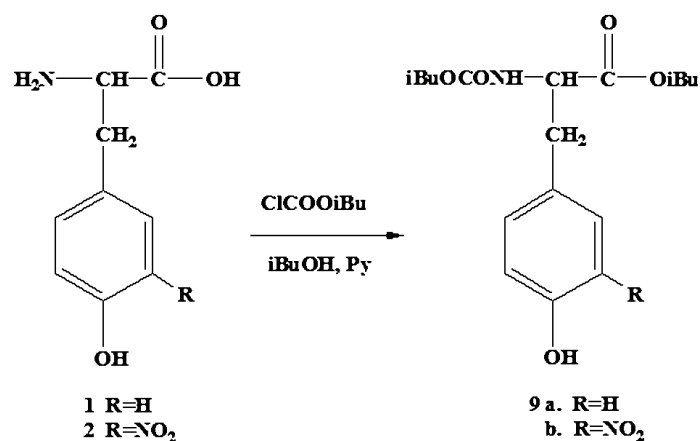
^aNo molecular ion identified

GC analysis of the silyl derivatives **8a** and **8b** showed that, as opposed to derivatives **3** and **7**, the peaks remained constantly sharp after many injections onto the same column; thus confirming that a tris-derivative of NY would be highly desirable.

In any event, the impossibility of obtaining the same derivatives for both NY and Y by an anhydride/alcohol mixture, led to the exploration for alternative methods. The Husek method^{16,22} is a validated procedure for proteinogenic amino acids that offers distinct advantages due to its simplicity and rapidity. According

to this procedure, aqueous solutions of practically all natural amino acids react with alkyl chloroformates and alcohols in pyridine to form *N(O)*-alkoxycarbonyl alkyl esters suitable for GC analysis. A combination of alkyl chloroformates and fluoroalkanols has already been used for amino acids analysis,^{17,15,23–26} but, to the best of our knowledge, has not been exploited for the purpose of NY determination. In accordance with previous studies,¹⁷ the reaction of the carboxylic group with a chloroformate and an alcohol leads to the formation of an ester, the alkyl moiety of which is provided by the alcohol. The same reaction with an amine group leads to an *N*-alkoxycarbonyl derivative bearing the alkyl group of the chloroformate. In the case of an amino acid, such as Y or NY, tris-substituted *N,O*-alkoxycarbonyl derivatives are possible, due to the presence of the phenolic OH. The main experiments in this work were addressed to the study of the different behaviour of NY with respect to Y, of which some Husek derivatives have already been reported. The purpose was the careful monitoring of the influence of the nitro group on the outcome of the derivatisation procedures performed with different commercial chloroformate reagents and perfluoroalcohols.

Among *N(O,S)* alkoxycarbonyl alkyl esters of amino acids, isobutoxycarbonyl isobutyl esters can be considered as an optimal solution to start with, from the viewpoint of both sensitivity and stability.²⁵ Therefore, the classical combination *i*BuCF/*i*BuOH and bis-substituted derivatives of Y and NY was first investigated and *N*-*iso*-butoxycarbonyl *iso*-butyl esters **9a** and **9b** were exclusively obtained (Scheme 6). This result is in line with previously reported data for Y.^{25,26}

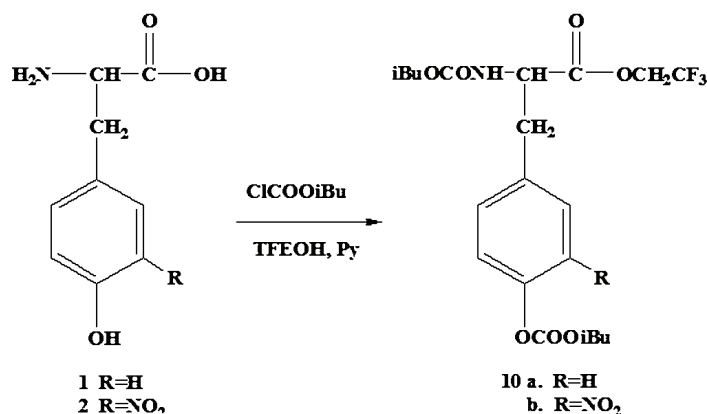


Scheme 6. Derivatisation of tyrosine and 3-nitrotyrosine by isobutyl chloroformate/isobutanol combinations.

In this case, the reaction did not occur at the phenolic OH of either Y or NY, which could be due to the presence of the apolar alcohol *i*BuOH in the reaction mixture. This may affect some chemico–physical parameters of the derivatisation

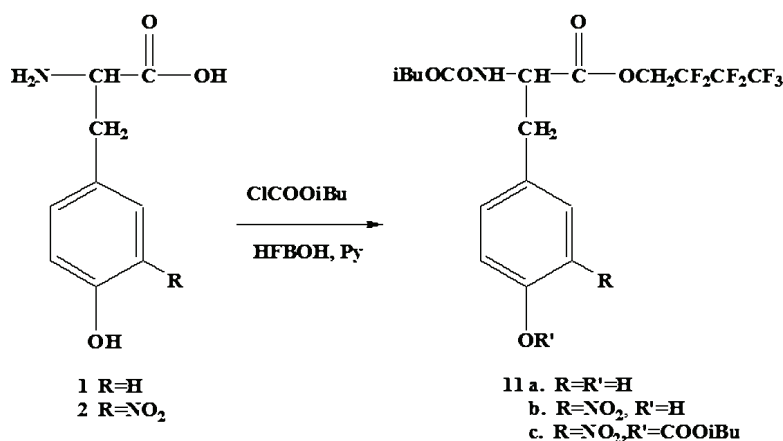
medium, with the effect of decreasing the reactivity of the phenolic OH toward chloroformate.

Being as the aim was to prepare volatile fluorinated derivatives, TFEOH was initially selected as the perfluoroalcohol in the Huseck procedure. The combination *i*BuCF/TFEOH afforded the tris-substituted derivative as the single product for both Y and NY (Scheme 7, compounds **10a** and **10b**).



Scheme 7. Derivatization of tyrosine and 3-nitrotyrosine by isobutyl chloroformate/TFEOH combinations.

In a subsequent experiment, HFBOH was tested (Scheme 8). The encouraging result obtained with TFEOH was not confirmed by the combination of *i*BuCF with the less hydrophilic HFBOH. In fact, Y afforded the trisubstituted derivative **11a** as a single product, whereas NY afforded two products (bis- and trisubstituted **11b** and **11c**), as shown in Fig. 3. As the efficiency of the deri-



Scheme 8. Derivatization of tyrosine and 3-nitrotyrosine by isobutyl chloroformate/HFBOH combinations.

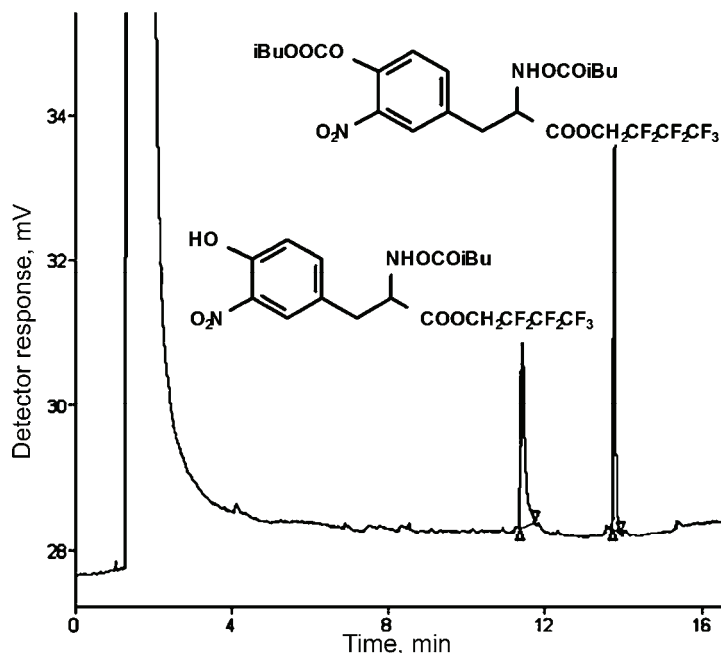


Fig. 3. GC-FID Chromatogram of NY derivatives obtained by treatment with *i*BuCF and HFBOH.

vatation procedure may be attributed to different experimental conditions, an attempt was made to eliminate the double products obtained with the *i*BuCF/HFBOH combination by varying the reaction time and the amounts of chloroformate, pyridine and alcohol in the reaction mixture. These changes, however, did not completely lead to a single product. One possible explanation can be related to the low solubility of *i*BuCF in the mixture H₂O/HFBOH/pyridine that might cause incomplete derivatisation of NY. In this context, the high polarity of NY,²⁷ which renders this amino acid more hydrophilic than tyrosine itself, may also have contributed to the incomplete derivatisation of NY when the *i*BuCF/HFBOH combination was applied.

MS analysis of the derivatives obtained with *i*BuCF was used for the identification of the products. In Table III, the most significant peaks in the mass spectra of derivatives are listed. The EI spectra could be interpreted with reference to that reported by Wang *et al.*¹⁷ and Sobolevsky *et al.*²⁵ for tyrosine.

As a general comment, using *i*BuCF only in combination with TFEOH afforded a single tris-substituted derivative product for NY and Y (compounds **10a** and **10b**). Although, the fluorine content was low, this result evidences that it is possible to obtain tris-substituted products for both Y and NY by a suitable combination of alkyl chloroformates and alcohols.

TABLE III. Characteristic ion peaks in the mass spectra of *N*-isobutoxycarbonyl(per-fluoro)alkyl esters of tyrosine and 3-nitrotyrosine

Amino acid	Chloroformate/alcohol	Derivative	<i>m/z</i>	Main peak, <i>m/z</i>	Characteristic peaks, <i>m/z</i>
Tyrosine	<i>i</i> BuCF/ <i>i</i> BuOH	<i>N</i> -isobutoxycarbonyl isobutyl ester 9a	337	107	164, 220, 320
	<i>i</i> BuCF/TFEOH	<i>N,O</i> -di-isobutoxycarbonyl trifluoroethyl ester 10a	463 ^a	107	207, 235, 246, 390
	<i>i</i> BuCF/HFBOH	<i>N,O</i> -di-isobutoxycarbonyl heptafluorbutyl ester 11a	563	107	57, 207, 256, 346
3-Nitrotyrosine	<i>i</i> BuCF/ <i>i</i> BuOH	<i>N</i> -isobutoxycarbonyl isobutyl ester 9b	382 ^a	57	137, 152, 209, 280
	<i>i</i> BuCF/TFEOH	<i>N,O</i> -di-isobutoxycarbonyl trifluoroethyl ester 10b	508	57	135, 152, 156, 291, 334, 435
	<i>i</i> BuCF/HFBOH	<i>N</i> -isobutoxycarbonyl heptafluorbutyl ester 11b	508	152	57, 234, 256, 281, 391, 434
		<i>N,O</i> -isobutoxycarbonyl heptafluorbutyl ester 11c	608 ^a	152	57, 106, 256, 391, 462, 490, 508, 535

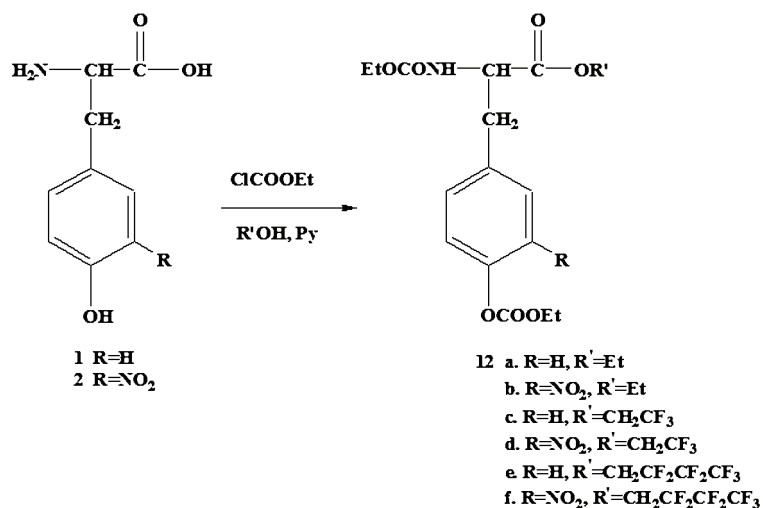
^aNo molecular ion identified

This prompted the study of other combinations of reagents, and ethyl chloroformate (EtCF) was selected, which, although less stable than *i*BuCF, has already been used in combination with different alcohols for Y derivatisation.^{17,19,23} The combination EtCF/EtOH that gave the tris-substituted derivative **12a** with Y²⁸ was tested with NY. The non-proteinogenic amino acid NY also afforded the *N,O*-diethoxycarbonyl ethyl ester **12b** (Scheme 9).

It was gratifying to observe that both NY and Y reacted also with TFEOH or HFBOH in the presence of EtCF and pyridine to give always the tris-derivatives (compounds **12c–f**).

The MS spectra of the derivatives obtained with EtCF are collected in Table IV, in which the molecular ions and the most characteristic fragments of the mass spectra of derivatives **12a–f** are presented. The mass fragmentation pattern of the NY tris-substituted derivative (**12f**) is shown in Fig. 4.

The results obtained with EtCF and fluorinated alcohols open several analytical perspectives, since it has been demonstrated that by a suitable selection of alkyl chloroformates and alcohols, NY and Y can be determined in the same run, affording the corresponding tris-substituted derivative. This opens a new opportunity for the determination of their ratio as nitro-oxidative marker.



Scheme 9. Derivatisation of tyrosine and 3-nitrotyrosine by ethyl chloroformate/ethanol or perfluoro alcohols combinations.

TABLE IV. Characteristic ion peaks in the mass spectra of *N,O*-diethoxycarbonyl (perfluoro)alkyl esters of tyrosine and 3-nitrotyrosine

Amino acid	Chloroformate/alcohol	Derivative	<i>m/z</i>	Main peak, <i>m/z</i>	Characteristic peaks, <i>m/z</i>
Tyrosine	EtCF/EtOH	<i>N,O</i> -diethoxycarbonyl ethyl ester 12a	353	107	135, 192, 264, 280
	EtCF/TFEOH	<i>N,O</i> -diethoxycarbonyl trifluoroethyl ester 12c	407	107	135, 179, 246, 280, 318
	EtCF/HFBOH	<i>N,O</i> -diethoxycarbonyl heptafluorbutyl ester 12e	507	107	135, 179, 280, 346, 434
3-Nitrotyrosine	EtCF/ EtOH	<i>N,O</i> -diethoxycarbonyl ethyl ester 12b	398	102	106, 135, 152, 174, 237, 265, 235
	EtCF/TFEOH	<i>N,O</i> -diethoxycarbonyl trifluoroethyl ester 12d	452	152	106, 135, 228, 291, 325, 362
	EtCF/HFBOH	<i>N,O</i> -diethoxycarbonyl heptafluorbutyl ester 12f	552	152	135, 256, 391, 462

CONCLUSIONS

Several one-step preparations of fluorinated derivatives of Y and NY, which would be suitable for GC analysis, were investigated. The simultaneous determination of Y and NY could constitute a new, useful method for the evaluation of the nitro-oxidative stress of proteins; in this regard, the optimal derivatisation method should afford only a single product in a one-step procedure

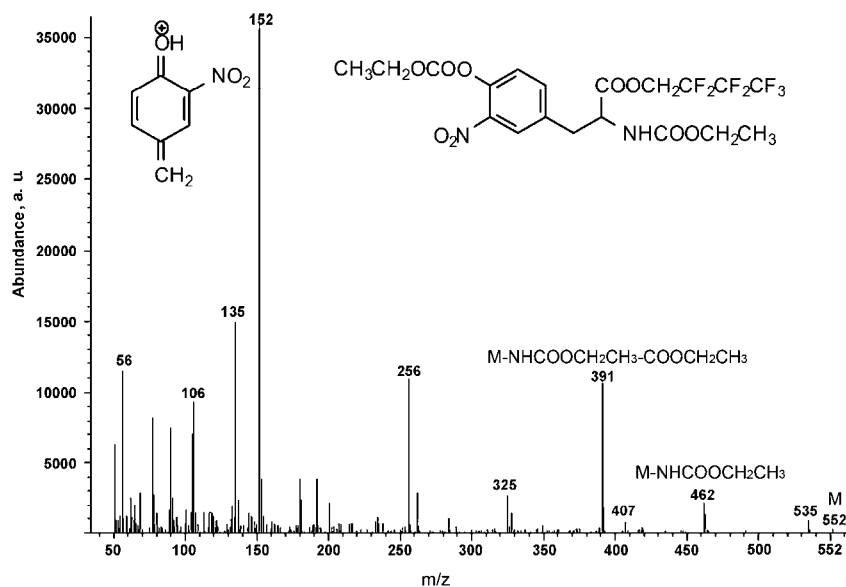


Fig. 4. Mass spectrum of the *N,O*-diethoxycarbonyl heptafluorobutyl ester derivative of NY (compound **12f**).

with both amino acids. Actually, in addition to inductive effect reasons, the presence of an *ortho*-nitro group causes different availability of the phenolic OH when bulky reagents are used, while small reagents are not influenced to the same extent by groups located near the phenolic OH. In addition, the structure of the alcohol appears to represent a critical parameter that could influence different reaction courses with NY and Y. The chloroformate/perfluoroalcohol procedure was evaluated by GC-FID and all the derivatives were identified by MS analysis. The best results were obtained with *i*BuCF/TFE OH and EtCF/HFBOH combinations. The *N,O*-diethoxycarbonyl heptafluorobutyl ester derivative **12f** is a trisubstituted product endowed with good GC characteristics. This derivative can be obtained in a single derivatisation step and could, therefore, be proposed as a suitable derivative for the simultaneous determination of Y and NY by GC analysis coupled to detectors sensitive to the presence of atoms with a high electron affinity, such as MS used in the negative ion chemical ionisation (NICI) mode.

Finally, the information presented herein could be useful from the viewpoint of exploiting the potential availability of perfluoroalkylchloroformates recently reported by Husek *et al.*²⁹ The use of this reagent could allow the introduction of a consistent number of fluorine atoms into the *N,O*-dialkoxycarbonyl part of the final derivative.

Acknowledgements. We thank University of Milan for a PhD studentship to R. P. and the financial support from the Italian Ministry for Education, University and Research, General

12. D. Tsikas, *Chromatographia* **70** (2009) 1767
13. C. F. Poole, *J. High Res. Chromatogr.* **5** (1982) 454
14. A. S. Soderling, H. Ryberg, A. Gabrielsson, M. Lärstad, K. Torén, S. Niari, K. Caidahl, *J. Mass Spectrom.* **38** (2003) 1187
15. M. G. Zampolli, D. Meunier, R. Sternberg, F. Raulin, C. Szopa, M. C. Pietrogrande, F. Dondi, *Chirality* **18** (2006) 279
16. P. Husek, *J. Chromatogr., A* **552** (1991) 289
17. J. Wang, Z. H. Huang, D. A. Gage, J. T. Watson, *J. Chromatogr., A* **663** (1994) 71
18. V. De Filippis, R. Frasson, A. Fontana, *Protein Sci.* **5** (2006) 976
19. D. Yi, B. A. Ingelse, M. W. Duncan, G. A. Smythe, *J. Am. Soc. Mass Spectrom.* **11** (2000) 578
20. M. G. Zampolli, G. Basaglia, F. Dondi, R. Sternberg, C. Szopa, M. C. Pietrogrande, *J. Chromatogr., A* **1150** (2007) 162
21. D. Puig, D. Barcelo, *Trends Anal. Chem.* **15** (1996) 362
22. P. Husek, *J. Chromatogr., B* **717** (1998) 57
23. S. Casal, M. B. Oliveira, M. A. Ferreira, *J. Chromatogr., A* **866** (2000) 221
24. J. Pietzsch, S. Kopprasch, R. Bergmann, *Rapid Commun. Mass Spectrom.* **17** (2003) 767
25. T. G. Sobolevsky, A. Revelsky, I. Revelsky, B. Miller, V. Oriedo, *Eur. J. Mass Spectrom.* **8** (2002) 447
26. T. G. Sobolevsky, A. Revelsky, B. Miller, V. Oriedo, S. Chernetsova, I. Revelsky, *J. Chromatogr., B* **800** (2004) 101
27. S. Erkoç, F. Erkoç, A. Sepici-Dincel, *Amino Acids* **38** (2010) 319
28. Z. H. Huang, J. Wang, D. A. Gage, J. T. Watson, C. C. Sweeley, P. Husek, *J. Chromatogr.* **635** (1993) 271
29. P. Husek, P. Simek, P. Hartvich, H. Zahradnickova, *J. Chromatogr., A* **1186** (2008) 391.



J. Serb. Chem. Soc. 77 (5) 685–697 (2012)
JSCS–4300

Modified polyacrylamide-supported chlorochromate as a new polymeric oxidizing agent

BAHMAN TAMAMI*, ROGHAYEH HEIRAN and ELHAM RIAZI MONTAZER

Department of Chemistry, Shiraz University, Shiraz-71454, Iran

(Received 31 January, revised 21 December 2011)

Abstract: Modified polyacrylamide-supported chlorochromate was synthesized and used as a versatile and efficient oxidizing agent for the oxidation of various organic compounds, such as hydroxyl compounds, silylethers, oximes, thiols, and others. Over oxidation of the products (aldehydes to carboxylic acids) was not observed with this oxidizing agent. The oxidant was insoluble in the oxidation media and the chromium(VI) ions remained firmly bound to the insoluble polymeric support after the oxidation reaction. The mild reaction condition, easy work-up, short reaction times, regenerability of the reagent and its easy preparation and handling are among the advantages of this new polymeric chlorochromate reagent.

Keywords: chromium(VI) oxidant; modified polyacrylamide; polymeric oxidizing agent; chlorochromate.

INTRODUCTION

During the past years, there have been several important advances in the field of organic synthesis; the use of polymer-supported reagents is one of them.¹ Polymeric reagents can be defined as functionalized polymers used in stoichiometric amounts in one-step processes to transform low-molecular-weight substrates into products.² They have been investigated widely and a very large range of reactions can be realized using such reagents.³ The most important benefits of these reagents over their soluble counterparts are simple filtration procedures, ease of separation from the reaction mixture, selectivity and low toxicity.⁴ These reagents have been developed for use in simple reactions, such as oxidation, reduction, condensation, acylation, alkylation, halogenation, the Wittig reaction, *etc.*⁵

Chromium(VI)-based oxidizing reagents have been extensively used in organic synthesis.⁶ Among these, pyridinium chlorochromate (PCC),⁷ prolinium chlorochromate,⁸ caffenilium chlorochromate,⁹ tetrahexylammonium chlorochro-

*Corresponding author. E-mail: tamami@chem.susc.ac.ir
doi: 10.2298/JSC110131216T

mate,¹⁰ 2,6-dicarboxypyridinium chlorochromate,^{11,12} and tributylammonium chlorochromate¹³ are a number of oxidizing agents based on chlorochromate that have been reported.

Numerous heterogeneous polymer-supported oxidizing agents with different functionalities have been reported in the literature that offers some advantages over their more traditional soluble counterparts. Among these, polymer-bound metallic oxidants and especially polymer-supported chromium(VI) reagents have received considerable attention.¹⁴ Heterogeneous polymeric reagents such as poly[vinyl(pyridinium chlorochromate)] and dichromate,^{15,16} poly(*n*-butyl-4-vinylpyridinium)dichromate,¹⁷ poly(4-vinylpyridinium nitrate),¹⁸ poly(*N*-vinylpyrrolidone)-hydrotribromide,¹⁹ poly(*n*-butyl-4-vinylpyridinium)periodate, iodate and bromate,²⁰ polystyrene supported *t*-butylchromates²¹ and poly[vinyl (pyrrolidonium chlorochromates)]²² are among those reported in the literature.

In continuation of our interest on modified polyacrylamides,^{23–26} the synthesis and use of a modified polyacrylamide-supported chlorochromate as new polymeric oxidizing agent for the oxidation of various organic compounds, such as hydroxyl compounds, oximes, silylethers, thiols and some other compounds, are described herein.

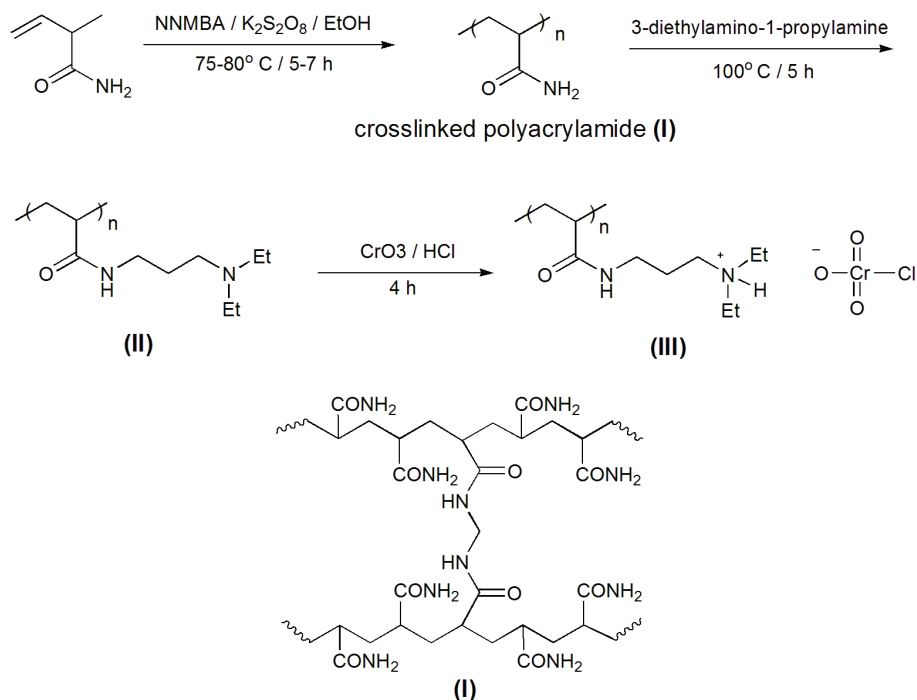
EXPERIMENTAL

Chemicals were purchased either from Merck or Fluka, or were synthesized in the laboratory. Acrylamide and the cross-linking agent, *N,N'*-methylene bisacrylamide (NNMBA), were commercial products obtained from Merck. Trimethylsilyl ethers were prepared by a reported procedure.²⁷ All products were characterized by comparison of their IR and/or ¹H-NMR spectra and physical data with those of authentic samples. All yields refer to the isolated products.

The purity determination of the substrates and products and monitoring of the reaction were accomplished by thin layer chromatography (TLC) on silica gel polygram SIL/UV 254 plates. The FTIR spectra were run on a Shimadzu FTIR-8300 spectrophotometer. The ¹H-NMR (250 MHz) and ¹³C-NMR (62.5 MHz) were recorded on a Bruker Advanced DPX instrument. Melting points were recorded on a Büchi B-545 apparatus (Switzerland) in open capillary tubes.

Preparation of different cross-linked polyacrylamides (I)

Cross-linked polyacrylamide (Scheme 1) was synthesized by the free-radical precipitation polymerization technique using *N,N'*-methylene bisacrylamide (NNMBA) as a cross-linking agent.^{26,28} As an example for the preparation of 5 % cross-linked polyacrylamide, acrylamide (5.00 g, 69.0 mmol) and (NNMBA) (0.56 g, 3.6 mmol) were dissolved in ethanol (40 mL). Potassium persulfate (0.017 g, 0.070 mmol) was added as an initiator and the mixture was heated at 75–80 °C under stirring for 7 h. The polymer was collected by filtration, washed several times with ethanol and dried under vacuum at 50 °C. A white powder was obtained in almost quantitative yield. The same procedure was repeated for the preparation of 2, 10, 15 and 20 % cross-linked polyacrylamides using 0.22, 1.18, 1.85 and 2.66 g of NNMBA, respectively.



Scheme 1. Cross-linked polyacrylamide synthesis route.

Incorporation of (3-diethylamino-1-propylamine) function onto cross-linked polyacrylamide

In a round bottomed flask, excess 3-diethylamino-1-propylamine (35 mL) was added to 5 % cross-linked polyacrylamide **(I)** (5.00 g). The reaction mixture was stirred at room temperature to allow complete swelling of the polymer by the diamine. The reaction mixture was then heated at 100 °C for 5 h. The aminated gel was filtered and washed with sodium chloride solution (0.1 M) many times; it was then washed with water and ethanol. The product was dried under vacuum at 60 °C to give the aminated resin **(II)** in 42 % yield (7.25 g).

Incorporation of chlorochromate function onto the aminated cross-linked polymer

In a round bottomed flask, chromium trioxide (4.50 g, 45.0 mmol) was added to aminated cross-linked polymer **(II)** (5.00 g) suspended in HCl (50 mL, 1 M). The mixture was stirred in an ice bath for 4 h and filtered. The brown beads were filtered off and washed extensively with acetone until the filtrate was clear. The resin was then dried under vacuum (60 °C, 5 h) in the presence of CaCl₂ to give a stable brown powder **(III)**. The capacity of this resin was determined by the iodometric titration method to be 1.64 mmol CrO₃ g⁻¹ polymeric reagent, which was in agreement with the value of 1.58 obtained by the atomic absorption technique.²⁹

Determination of capacity of 5 % cross-linked polymer (III) by atomic absorption technique

A series of standards containing 0.00, 0.90, 1.50, 3.00, 4.50, 6.00, 7.50, 9.00 ppm of CrO₃ (with respect to Cr) were prepared in water and their atomic absorptions were determined (Fig. 1). To a solution of potassium hydroxide (0.40 g) in water (10 mL) was added polymeric reagent **(III)** (0.08 g), which was then stirred for 12 h. The mixture was filtered and

washed with distilled water several times. Activated carbon black was added to the combined filtrates and the mixture was stirred for 20 min at 40 °C. Then, the mixture was filtered and washed with distilled water. The solution of the combined filtrates was diluted to 500 mL in a volumetric flask; then 10 mL of this solution was diluted to 250 mL. Atomic absorption spectroscopy of the final solution with respect to chromium gave an absorbance value of 1.014 using the calibration curve (Fig. 1). The capacity of the reagent was determined to be 1.58 mmol of CrO₃ per gram of the reagent.

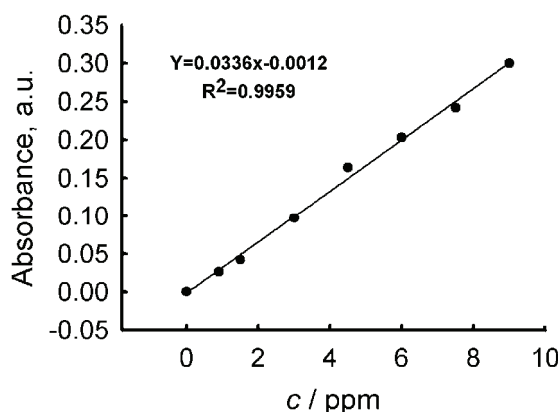


Fig. 1. Calibration curve for the atomic absorption spectroscopy method.

General procedure for the oxidation of organic compounds with the 5 % cross-linked polymer (III)

In a round bottomed flask (25 mL), a mixture of the organic compound (1.00 mmol) and polymeric reagent (III) (2.00–4.00 mmol, based on the molar ratio of oxidant to substrate) in cyclohexane or *n*-hexane (10 mL) was stirred at room temperature for an appropriate time. The progress of the reaction was followed by TLC. When the reaction was completed, the resin was filtered off and washed twice with solvent. Evaporation of the combined filtrates afforded pure products (in the few cases when the reaction did not go to completion, the crude product was purified on a silica gel plate with an appropriate eluent).

Regeneration of the 5 % cross-linked polymer (III)

The spent polymeric reagents obtained from different oxidation reactions were combined and washed thoroughly with CH₂Cl₂ to remove any residual soluble organic substrate or product; then it was washed with HCl (1 M) until the filtrate was colorless, neutralized with NaOH (1 M), washed with water and acetone and finally vacuum dried. The polymer (10.00 g) was suspended in HCl (100 mL, 1 M) for 0.5–1.0 h, chromium trioxide (9.00 g) added and the mixture stirred for 4.0 h at 0 °C. It was filtered and washed with acetone until the filtrate was clear. The obtained polymer was dried under vacuum (50 °C) in the presence of CaCl₂ overnight. The capacities of the regenerated resins were determined as described previously.

RESULTS AND DISCUSSION

Copolymers of acrylamide with NNMBA as a cross-linking agent (2, 5, 10, 15 and 20 %) were prepared by free-radical precipitation polymerization using potassium persulfate as the initiator (Scheme 1). White polymers were obtained as irregularly-shaped amorphous particles. The IR spectra of the polymers showed

characteristic absorptions of amide (N–H), and carbonyl groups at 3421 and 1666 cm^{-1} , respectively (Fig. 2).

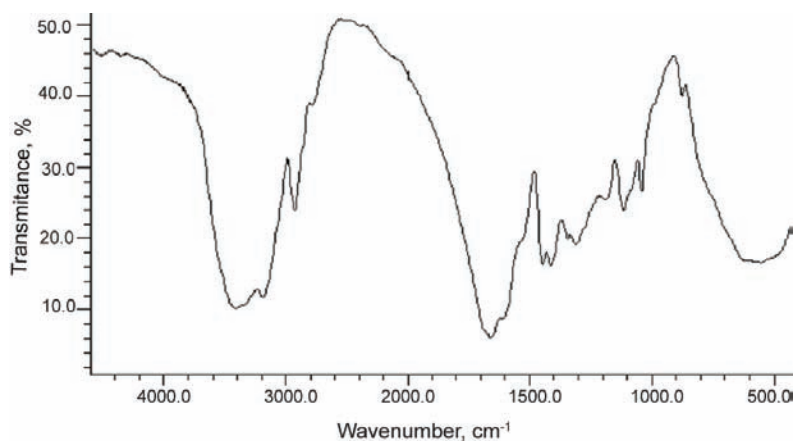


Fig. 2. FTIR spectrum of **I**.

Poly[*N*-3-(diethylamino)propyl] acrylamides (**II**) with different degrees of cross-linking were prepared by transamidation reaction of excess 3-diethylamino-1-propylamine with the polyacrylamides having different degrees of cross-linking (Scheme 1). The amino polymer exhibited strong absorption bands at 3202 and 3329 cm^{-1} (N–H stretching), 1655 cm^{-1} (C=O amide stretching) and 1528 cm^{-1} (N–H amide bending) (Fig. 3). The average amine value (4.70 mmol amine g^{-1} of polymer) was calculated by the back acid–base titration method. It was noticed that as the proportion of the cross linking agent increased, the capacity of the polymer decreased because of the highly cross-linked network structure.

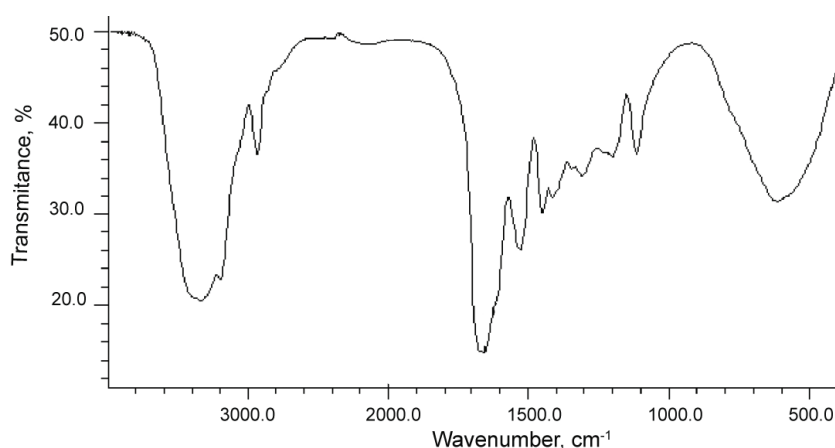


Fig. 3. FTIR spectrum of **II**.

Polymeric oxidizing agents containing chlorochromate (**III**) were prepared very easily by addition of chromium(VI) oxide to a suspension of the cross-linked poly[*N*-3-(diethylamino)propyl] acrylamides in dilute HCl (Scheme 1). The presence of the chlorochromate anion in the oxidizing agents was confirmed by their IR spectra, showing bands at 945 and 769 cm^{-1} , which are characteristic peaks for the chromate anion (Fig. 4). Capacity of the polymeric oxidizing agent (5 % cross-linked) was measured easily by titration with an appropriate reducing agent ($\text{S}_2\text{O}_3^{2-}$) and by atomic absorption spectroscopy. The obtained values were 1.64 and 1.58 $\text{mmol Cr(VI) g}^{-1}$ polymeric reagent, respectively.

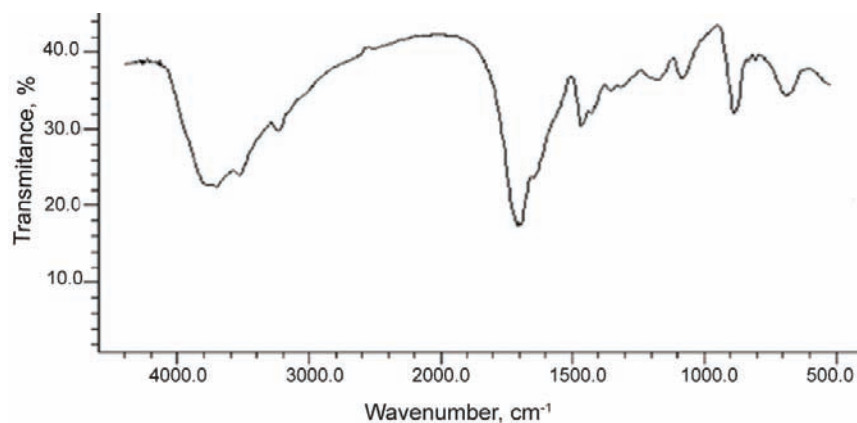


Fig. 4. FTIR spectrum of **III**.

As a model, the oxidation reaction of benzyl alcohol with the polymeric reagents having different percentage crosslinking was performed in cyclohexane at room temperature (Table I). The best results were obtained using the gel-like 2 % cross-linked polymer, which was difficult to handle however; thus the 5 % cross-linked sample was chosen for the general study, due to its better stability.

TABLE I. Oxidation of benzyl alcohol with polymer **III** of different degrees of cross-linking in cyclohexane (molar ratio of polymeric oxidant to substrate was 2:1; wet polymer was used; conversion in all cases was 100 %)

Entry	Content of III in polymer %	Average capacity of polymer mmol g^{-1}	Time, h
1	2	1.80	2.5
2	5	1.64	3.0
3	10	1.10	4.0
4	15	1.04	4.5
5	20	0.81	5.0

The choice of solvent in organic reactions using polymeric reagents is extremely important. A solvent should be chosen in which the insoluble polymeric

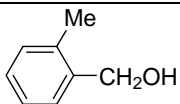
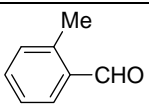
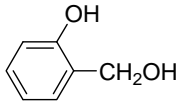
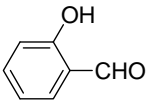
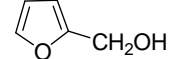
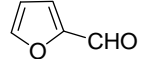
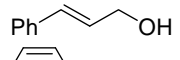
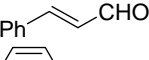
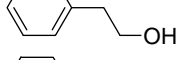
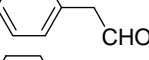
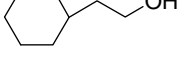
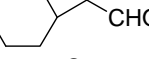
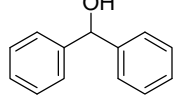
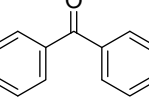
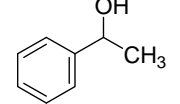
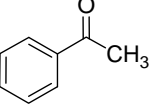
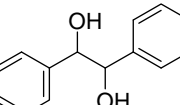
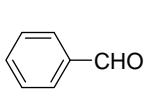
oxidizing agent swells well. The effect of solvent on the oxidation reaction showed that less polar solvents gave the best results. For the oxidation reaction, cyclohexane and *n*-hexane were the best solvents compared to toluene, ethyl acetate, CH₃CN, THF, CHCl₃ and H₂O. This is probably due to the higher compatibility of these two solvents with the polymeric reagent and the substrates. The polymeric oxidant was insoluble in the reaction media and the chromium ions remained firmly bound to the insoluble polymer support after the oxidation reaction, which was confirmed by atomic absorption spectroscopy (chromium ions were not observed in reaction solvent after filtration). This advantage is one of the advantages of this polymeric reagent over monomeric chromium(VI)-based oxidants.

The generality of this polymeric oxidant was tested for different alcohols (Table II) and other functionalities (Table III). The oxidant was capable to convert primary and secondary alcohols to their corresponding aldehydes and ketones. Over-oxidation of the products to carboxylic acids was not observed. Electron donating groups increased the rate of conversion. Aliphatic alcohols had a low yield so the oxidant could oxidize selectively benzylic alcohols in the presence of aliphatic alcohols.

TABLE II. Oxidation of benzylic alcohols with 5 % cross-linked polymer **III** (these reactions were carried out in cyclohexane at r.t.; wet polymer was used; molar ratio of polymeric oxidant to substrate was 2:1)

Entry	Substrate	Product	Time, h	Yield, %
1			3	90
2			6	80
3			6	70
4			10	45
5			4	90
6			4	85
7			4	92

TABLE II. Continued

Entry	Substrate	Product	Time, h	Yield, %
8			5.5	85
9			5	92
10			5	95
11			12	80
12			20	85
13			10	40
14			3.5	90
15			3	95
16 ^a			3	93

^aMolar ratio of polymeric oxidant to substrate was 3:1

Aldoximes, ketoximes, and silylethers were oxidized to their corresponding aldehydes and ketones without over-oxidation in good to high yields. Deoxygenation of oximes required a long reaction time compared to the oxidation of alcohols. The oxidation of thiols to their corresponding disulfides was performed easily by this polymeric reagent. The oxidation of *p*-hydroquinone, benzylamine, and benzoin were also investigated.

The oxidant was not able to oxidize α -hydroxyl carboxylic acids, toluene, naphthalene, epoxides and sulfides. Hence, hydroxyl compounds, oximes, silylethers and thiols can be selectively oxidized in the presence of these functional groups.

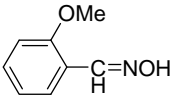
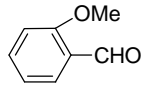
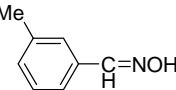
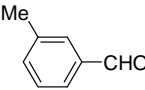
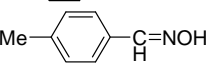
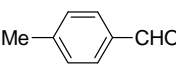
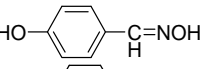
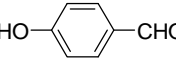
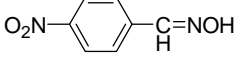
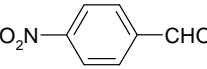
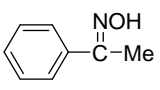
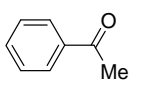
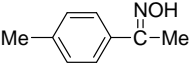
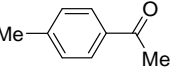
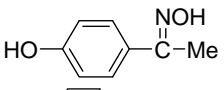
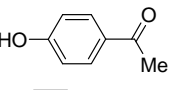
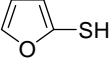
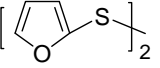
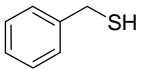
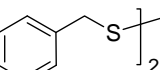
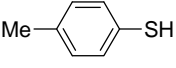
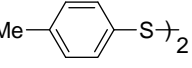
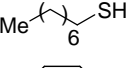
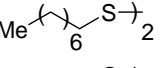
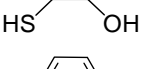
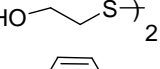
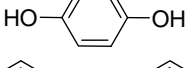
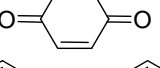
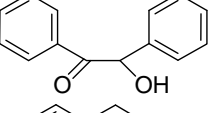
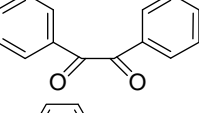
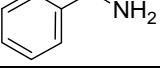
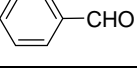
Regenerability and reuse of the spent polymeric reagent is one of the main advantages in the use of this polymeric reagent. The reagent could be recycled at least three times (Table IV). There was a small decrease in the capacity of the

resins after each regeneration, which might have been caused by mechanical degradation of the polymeric reagent.²² This polymeric reagent can be stored several months without loss of its activity.

TABLE III. Oxidation of other organic compounds with 5 % cross-linked polymer (III); these reactions were realized in cyclohexane at room temperature; wet polymer was used

Entry	Substrate	Product	Time, h	Yield, %
1 ^a			4.5	93
2 ^a			4.0	90
3 ^a			4.5	82
4 ^a			5.5	95
5 ^a			7.0	90
6 ^a			7.0	93
7 ^a			5.0	90
8 ^a			6.0	85
9 ^a			5.0	73
10 ^a			5.0	78
11 ^b			10.0	90
12 ^b			8.0	75

TABLE III. Continued

Entry	Substrate	Product	Time, h	Yield, %
13 ^b			9.0	78
14 ^b			11.0	75
15 ^b			10.0	82
16 ^b			8.0	95
17 ^b			10.0	40
18 ^b			10.0	90
19 ^b			9.0	90
20 ^b			12.0	70
21 ^c			5.0	85
22 ^c			1.0	95
23 ^c			5/6	92
24 ^d			9.0	50
25 ^d			9.0	10
26 ^a			45/60	96
27 ^a			8.0	60
28 ^a			5.0	75

^aMolar ratio of polymeric oxidant to substrate was 2:1; ^bMolar ratio of polymeric oxidant to substrate was 4:1 and reactions were realized in *n*-hexane at r.t.; ^cMolar ratio of polymeric oxidant to substrate was 3:1; ^d% conversion and molar ratio of polymeric oxidant to substrate was 3:1

TABLE IV. Capacity of the polymeric reagent after regeneration

Number of regenerations	Capacity of polymer, mmol g ⁻¹
1	1.30
2	1.15
3	0.92

A comparison of the efficiency of the presented polymeric reagent (**III**) with a number of other reported polymeric oxidants based on chromium(VI) is given in Table V. The polymeric reagent (**III**) is more efficient in the oxidation of 1-phenylethanol than most of the other reagents.

TABLE V. Comparison of the efficiency of **III** with those of different chromium(VI)-based polymeric oxidants in the oxidation of 1-phenylethanol

Entry	Oxidizing agent	Time, h	Molar ratio	Yield, %
1 ^a	III	3	2/1 (r.t)	95
2 ^a	ref. 15	3.5	4.5/1 (reflux)	69 ^d
3 ^a	ref. 16	5	1.1/1 (reflux)	89 ^d
		24	1.1/1 (reflux)	>99 ^d
4 ^a	ref. 17	12.5	2/1 (reflux)	91
5 ^b	ref. 22	44	5/1 (reflux)	96
6 ^c	ref. 30	25/60	1/1 (reflux)	95

^aReactions were realized in cyclohexane; ^b reaction was realized in chloroform; ^c reaction was realized in toluene; ^d% conversion

CONCLUSIONS

In conclusion, this modified polyacrylamide-supported chlorochromate is a useful oxidant for the oxidation of different organic compounds, such as hydroxyl compounds, silylethers, oximes, thiols, *etc.* Over oxidation of the products was not observed with this oxidizing agent. It was able to oxidize the aforementioned functional groups in the presence of α -hydroxyacids, benzylic acids, epoxides, sulfides, aldehydes and double bonds. The handling and use of this heterogeneous reagent is environmentally safer than its monomeric soluble counterparts. The mild reaction conditions, stability, selectivity, good to excellent yields of the products, simple recovery of the reaction products and regenerability of the reagent make this heterogeneous polymeric oxidizing agent useful in organic synthesis. The reagent can be stored for months without any loss in its activity.

Acknowledgments. We gratefully acknowledge the partial supported of this study by the Shiraz University Research Council.

ИЗВОД

ПОЛИАКРИЛАМИД МОДИФИКОВАН ДИЕТИЛПРОПИЛАМОНИЈУМ-ХЛОП-ХРОМАТОМ – НОВИ ПОЛИМЕРНИ ОКСИДАЦИОНИ АГЕНС

BAHMAN TAMAMI, ROGHAYE HEIRAN и ELHAM RIAZI MONTAZER

Department of Chemistry, Shiraz University, Shiraz-71454, Iran

Полимерни носач, на бази умреженог полиакриламида, модификован диетилпропил-амонијум-хлорхроматом, показао се као веома ефикасан реагенс за оксидацију различитих органских једињења: алкохола, силелетра, оксима, тиола, итд. У реакцијама оксидације алкохола, производи оксидације су били алдехиди или кетони, и није се одвијала даља оксидација алдехида у карбоксилне киселине. Оксидациони агенс је нерастворан у реакционој средини, а хром(VI) јони остају везани за полимерну матрицу и након реакције оксидације. Предности овог новог полимерног оксидационог реагенса, диетилпропиламонијум-хлорхромата, су: благи реакциони услови, једноставан начин и кратко време извођења реакције оксидације, као и једноставна и лака регенерација реагенса.

(Примљено 31. јануара, ревидирано 21. децембра 2011)

REFERENCES

1. A. McKillop, D. W. Young, *Synthesis* **1979** (1979) 401
2. A. Akelah, A. Moet, *Functionalized Polymers and their Applications*, Thomson Press India, New Delhi, 1990, p. 79
3. D. C. Sherington, P. Hodge, *Synthesis and Separation Using Functional Polymers*, Wiley, New York, 1988, p. 45
4. A. Akelah, D. C. Sherington, *Chem. Rev.* **81** (1981) 557
5. D. C. Sherington, P. Hodge, *Synthesis and Separation Using Functional Polymers*, Wiley, New York, 1988, p. 75
6. W. J. Mijs, C. R. H. I. de Jonge, *Organic Synthesis by Oxidation with Metal Compounds*, Plenum Press, New York, 1986, p.119
7. G. Buchi, B. Egger, *J. Org. Chem.* **36** (1971) 2021
8. M. Mamaghani, F. Shirini, F. Parsa, *Russ. J. Org. Chem.* **38** (2002) 1113
9. F. Shirini, I. Mohammadpoor-Baltork, Z. Hejazi, P. Heravi, *Bull. Korean Chem. Soc.* **24** (2003) 517
10. B. Koohestani, Z. Javanshir, S. H. Ghammamy, K. H. Mehrani, H. Afrand, L. Saghatforoush, *J. Mex. Chem. Soc.* **52** (2008) 116
11. M. Tajbakhsh, R. Hosseinzadeh, M. Yazdani-Niaki, *J. Chem. Res.* **2002** (2002) 508
12. R. Hosseinzadeh, M. Tajbakhsh, M. Yazdani-Niaki, *Tetrahedron Lett.* **43** (2002) 9413
13. S. H. Ghammamy, M. Mazareey, *J. Serb. Chem. Soc.* **70** (2005) 687
14. D. H. Drewry, D. M. Coe, S. Poon, *Med. Res. Rev.* **19** (1999) 97
15. J. M. J. Frechet, J. Warnock, M. J. Farral, *J. Org. Chem.* **43** (1978) 2618
16. J. M. J. Frechet, P. Darling, M. J. Farral, *J. Org. Chem.* **46** (1981) 1728
17. B. Tamami, A. R. Kiasat, *Iran. Polym. J.* **6** (1997) 273
18. A. Ghorbani-Choghamarani, S. Sardari, *J. Sulfur Chem.* **32** (2011) 63
19. E. P. Koshy, J. Zacharias, V. N. R. Pillai, *React. Funct. Polym.* **66** (2006) 845
20. B. Tamami, K. Parvanak-Borujeny, M. M. Khakzad, *Iran. Polym. J.* **12** (2003) 4, 331
21. K. Geethakumari, K. Sreekumar, *React. Funct. Polym.* **42** (1999) 11
22. J. Zacharias, E. P. Koshy, V. N. R. Pillai, *React. Funct. Polym.* **56** (2003) 159

23. B. Tamami, H. Mahdavi, *Tetrahedron Lett.* **42** (2001) 8721
24. B. Tamami, M. Kolahdoozan, *Tetrahedron Lett.* **42** (2004) 1535
25. B. Tamami, A. Fadavi, *Catal. Commun.* **6** (2005) 747
26. B. Tamami, S. Ghasemi, *J. Iran. Chem. Soc.* **5** (2008) S26
27. B. Karimi, B. Golshani, *J. Org. Chem.* **65** (2000) 7228
28. B. Tamami, S. Ghasemi, *Appl. Catal., A* **393** (2011) 242
29. D. A. Skoog, D. M. West, *Fundamentals of Analytical Chemistry*, 4th ed., Saunders College, Philadelphia, PA, 1982, p. 582
30. B. Tamami, N. Goudarzian, *Eur. Polym. J.* **28** (1992) 1035.



J. Serb. Chem. Soc. 77 (5) 699–714 (2012)
JSCS–4301

The influence of shaped TiO₂ nanofillers on the thermal properties of poly(vinyl alcohol)

MARIJA B. RADOIČIĆ¹, ZORAN V. ŠAPONJIĆ^{1*},
MILENA T. MARINOVIĆ-CINCOVIĆ¹, SCOTT P. AHRENKIEL²,
NATAŠA M. BIBIĆ¹ and JOVAN M. NEDELJKOVIĆ¹

¹Vinča Institute of Nuclear Sciences, P.O. Box 522, 11001 Belgrade, Serbia and

²South Dakota School of Mines and Technology, Rapid City, SD, USA

(Received 31 March, revised 29 June 2011)

Abstract: Poly(vinyl alcohol)-based nanocomposites consisting of shaped TiO₂ nanocrystals (nanoparticles, nanotubes or nanorods) were synthesized by direct blending of the polymer and a solution of titania nanocrystals or powder. In order to elucidate the influence of the shape of the titania nanocrystals on thermal stability of the polymer matrix and particles interaction with poly(vinyl alcohol) (PVA) chains, structural and thermal characterizations of PVA/TiO₂ nanocomposites were performed. Faceted nanoparticles increased the thermal stability of the PVA matrix. Titania nanotubes and nanorods did not show any stabilizing effect on the polymer matrix under an argon atmosphere. The thermo-oxidative degradation temperature of PVA increased with addition of faceted TiO₂ nanoparticles. The thermo-oxidative stability of the PVA matrix was affected more by the presence of titania nanotubes and nanorods in comparison with its thermal stability under an inert atmosphere. The degree crystallinity ($X_c=32\%$) of the PVA matrix slightly decreased in the presence of the faceted TiO₂ nanoparticles in nanocomposite samples.

Keywords: nanocomposite materials; thermal properties; differential scanning calorimetry; thermogravimetric analysis; TiO₂; poly(vinyl alcohol).

INTRODUCTION

The usage of nanoparticles instead of sub-micron- or micron-sized particles as polymer fillers presents a new dimension in the development and application of this class of advanced materials.^{1,2} The main benefits of this type of composite materials are based on the large specific surface area of nanocrystals and their size and shape dependent properties, such as enhanced chemical reactivity and specific bindings. On the other hand, they are based on the desired properties of the polymer matrix, such as long-term stability, reprocessability, *etc.* Although

* Corresponding author. E-mail: saponjic@vinca.rs
doi: 10.2298/JSC110331161R

the individual features of both inorganic and organic constituents of nanocomposite are preserved, their synergy can produce completely novel functionalities. However, the resulting properties of nanocomposites are primarily the simple combination of the properties of all the constituents.

Nanocomposites possess several advantages, such as greater thermal stability, increased strength, enhanced electrical conductivity, improved flammability properties, *etc.* of polymer matrix. Much effort has been made to improve these properties by changing the size and shape as well as amount of applied nanoparticles. However, still not all the possibilities have been completely exploited.^{3–5}

The preparation methods of polymer nanocomposites are mainly based on *in situ* polymerization processes in the presence of nanoparticles and direct blending of a polymer solution, a polymer melt or emulsion with solutions of nanoparticles or nanoparticle powders.⁶

Poly(vinyl alcohol) (PVA) is a non-toxic and water-soluble synthetic polymer which has been predominantly utilized for biochemical and medical applications due to its excellent biocompatibility.^{7,8} Additionally, owing to its easy processability and optical transparency, semi-crystalline PVA is widely applied as a polymer matrix for the synthesis of nanocomposites by cost efficient and environmentally friendly direct blending methods.^{9–11}

Recent achievements in the synthesis of various metal–oxide nanoparticles of different chemical composition, size and shape opened up new possibilities for the preparation and design of polymer/metal oxide nanocomposites. Titanium dioxide (TiO₂) nanoparticles are of particular importance due to their potential applications in different fields, such as photocatalytic degradation of hazardous industrial byproducts or nanocrystalline solar cells.^{12,13} X-Ray absorption spectroscopic studies showed that the surface states in TiO₂ nanocrystallites ($d < 25$ nm) are characterized by coordinately unsaturated (penta-coordinated) Ti sites formed upon nanoparticle surface reconstruction.¹⁴ The existence of such unique surface structures of TiO₂ nanoparticles allows control of the surface chemistry in the direction of enhanced coupling of polymer chains and titania nanoparticles.

In this work, the direct blending method was applied for the synthesis of PVA/TiO₂ nanocomposites using differently shaped titania nanoparticles, such as faceted nanoparticles, nanotubes and nanorods as precursors. The size and shape of applied nanofillers were examined by transmission electron microscopy (TEM). The interaction between oxygen-containing groups within the polymer chains and surface hydroxyl groups of the titania nanoparticles was studied by Fourier transform infrared (FTIR) spectroscopy in the reflection mode. The influence of both the content and shape of the fillers on the overall polymer thermal stability in air and inert atmospheres, as well as the crystallization behavior of the PVA matrix was investigated by non-isothermal thermogravimetry (TGA) and differential scanning calorimetry (DSC) analysis.

EXPERIMENTAL

Materials

All chemicals (PVA ($M_w = 72,000 \text{ g mol}^{-1}$, hydrolysis degree min. 99 %), TiCl₄ (Merck), H₂SO₄ (Aldrich) and TiO₂ powder (Fluka) were reagent-grade and used without further purification. Milli-Q deionized water was used as a solvent. Air and argon gases were of high purity (99.5 %). An acid digestion bomb, model 4746 (Parr Instruments), was used for the synthesis of titania nanotubes and nanorods.

Synthesis of colloidal TiO₂ nanoparticles

Colloidal TiO₂ nanoparticles were prepared by the controlled hydrolysis of titanium tetrachloride.¹⁵ A solution of TiCl₄, cooled to $-20 \text{ }^\circ\text{C}$, was added drop-wise to cold water (at $4 \text{ }^\circ\text{C}$) under vigorous stirring and then held at this temperature for 30 min. The pH of the solution was between 0 and 1, depending on the TiCl₄ concentration. Slow growth of the particles was achieved by dialysis against water at $4 \text{ }^\circ\text{C}$ until the pH of the solution reached 3.5. The final concentration of TiO₂ colloidal solution (0.14 M) was determined from the concentration of the peroxide complex obtained after dissolution of the particles in concentrated H₂SO₄.¹⁶

Synthesis of TiO₂ nanotubes

Scrolled titania nanotubes were synthesized by the hydrothermal treatment (20 h/ $150 \text{ }^\circ\text{C}$) of TiO₂ powder (250 mg) dispersed in 10 ml of proton deficient aqueous solution (10 M NaOH) without shaking.¹⁷ After autoclaving, the ensuing powders were sequentially washed with an aqueous 0.1 M HCl solution and distilled water. This washing procedure was repeated until the water reached pH 7. Finally, the powder was separated from the washing solution by centrifugation. The synthesized nanotubes were dried at $70 \text{ }^\circ\text{C}$ until attainment of a constant mass.

Synthesis of TiO₂ nanorods

Rod shaped TiO₂ nanocrystals were prepared from the titania nanotubes in an additional hydrothermal treatment.¹⁸ Dry nanotubes (50 mg) were dispersed in 10 ml of distilled water (pH 7), transferred into a Teflon vessel and treated under saturated vapor pressure of water at $250 \text{ }^\circ\text{C}$ for 90 min. After autoclaving, the synthesized nanorods were dried at $70 \text{ }^\circ\text{C}$ to constant mass.

Synthesis of PVA/TiO₂ nanocomposites

The PVA/TiO₂ nanocomposites were synthesized from TiO₂ nanoparticles of different shapes and PVA. The polymer (1.5 mass %) was dissolved in boiling water and its concentration was kept constant in all synthesis. The content of THE inorganic phase (TiO₂) in each nanocomposite sample was 0.25 mass %. Direct mixing of the aqueous PVA solution with an adequate amount of colloidal TiO₂ solution or TiO₂ powder resulted in the formation of a stable and transparent PVA/TiO₂ (particles/tubes/rods) dispersion. The mixture was placed into a Petri dish and dried in a vacuum oven at $40 \text{ }^\circ\text{C}$ for 24 h. After solvent evaporation, transparent solid films were obtained. A neat PVA film, without the addition of the inorganic phase, was prepared in the same manner.

Characterization

The sizes and shapes of the used titania nanoparticles were determined by transmission electron microscopy (TEM) using a JEOL 100CX microscope operating at 100 kV. The morphology of the titania nanotubes was characterized by TEM using a Hitachi H-7000 FA mic-

roscope with a W filament at a high tension of up to 125 kV. The TEM samples were prepared by drop-wise addition of 6 μl of a dispersion of TiO_2 nanoparticles that had been subjected to 10 min of ultrasound treatment onto a holey carbon film supported on a copper grid. The specimen was air-dried overnight.

Fourier transform infrared (FTIR) spectra of neat PVA film and nanocomposite films were recorded in the attenuated total reflection mode (ATR) using a Nicolet 6700 FTIR Spectrometer (Thermo Scientific) at 2 cm^{-1} resolution, in the wavenumber range 500–4000 cm^{-1} .

The thermal characteristics of the neat PVA and nanocomposite samples were determined by thermogravimetric analysis (TGA) and differential scanning calorimetry (DSC). The non-isothermal thermogravimetric analysis was realized using a SETSYS Evolution 1750 thermogravimetry analyzer under dynamic argon or air atmospheres at flow rates of 20 and 16 ml min^{-1} , respectively. The heating rate in both cases was 10 $^\circ\text{C min}^{-1}$. The DSC measurements of the neat PVA and PVA/titania nanocomposites were performed on a DSC 151R SETARAM instrument in the temperature range from 30 to 250 $^\circ\text{C}$. The heating rate was 20 $^\circ\text{C min}^{-1}$. The sample weights were in the range 3–3.5 mg for both methods.

RESULTS AND DISCUSSION

Structural characterization of the PVA/TiO₂ nanocomposites

The shape and size distribution of the TiO_2 nanoparticles used for incorporation into the PVA matrix were estimated by TEM. A TEM image of faceted TiO_2 nanoparticles with an average dimension of about 5 nm is shown in Fig. 1. A selected area electron diffraction pattern (not presented) displayed very broad and diffuse diffraction rings, implying a mainly amorphous structure of the TiO_2 particles. Mainly amorphous structure of the TiO_2 nanoparticles or more precisely the existence of very small crystalline domains was expected due to applied synthetic procedure. Namely, the acidic hydrolysis of titanium tetrachloride occurred at a low temperature (4 $^\circ\text{C}$) and was not accompanied by post-synthetic heating of the obtained colloidal TiO_2 nanoparticles or annealing of the nanoparticles powder. Without additional thermal treatment, the degree of crystallinity of these TiO_2 nanoparticles is very low.

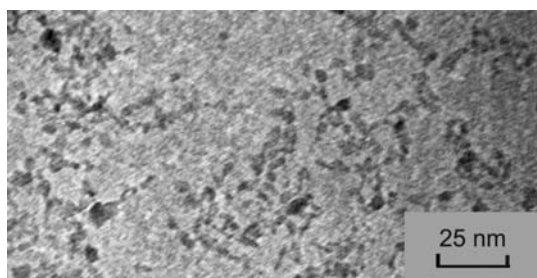
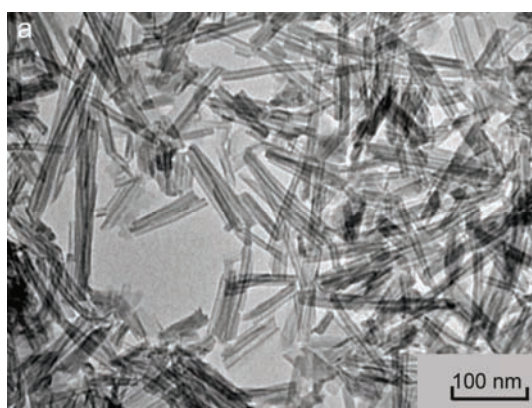


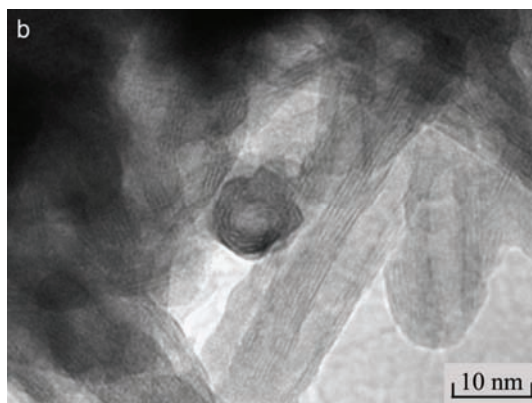
Fig. 1. TEM Image of faceted TiO_2 nanoparticles.

The typical morphology of the titania nanotubes is shown in the Fig. 2a. The conventional TEM image of the same region at a higher magnification, Fig. 2b,

reveals an open-ended multiwall morphology of the scrolled nanotubes. The uniform size distribution of nanotubes outer (approximately 10 nm) and inner (approximately 7 nm) diameters with lengths mainly in the range between 100 and 200 nm was confirmed by conventional TEM measurements. The inter-wall spacing is about 0.73 nm. From the structural point of view, the nanotubes are characterized by quasi-anatase, axially symmetric, distorted octahedral coordination of the Ti atoms with a large fraction of highly reactive five-coordinated sites ($\approx 40\%$) on the surface.¹⁹ These surface sites generally appear as a result of the accommodation of objects in the nanoscale regime for high curvature and surface reconstruction.¹⁹



(a)



(b)

Fig. 2. TEM Images of tube-like TiO₂ nanoparticles obtained at lower (a) and higher (b) magnification.

A TEM image of the TiO₂ rods is shown in Fig. 3. The presented agglomerate consists of prolate spheroids (rod-like crystallites) with diameters of around 50 nm and lengths in the range from 300 to 700 nm. In a previous study, the anatase crystal form of these rod-like TiO₂ nanoparticles was confirmed, as was

the appearance of spatially confined corner defect (under-coordinated) sites on their tips. The curvature of rods in these regions corresponds to the requested dimension ($d < 25$ nm).²⁰

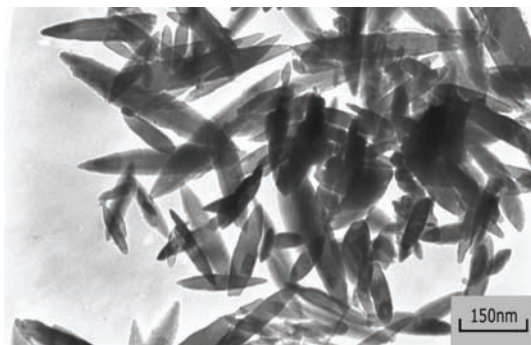


Fig. 3. TEM Image of rod-like TiO₂ nanoparticles.

The intensity of the interaction between a polymer matrix and similarly shaped nanofillers critically depends on the content and specific surface area of particles, *i.e.*, the inter-particle distance.²¹ In order to reveal the possible chemical bonding between the differently shaped TiO₂ nanoparticles and the PVA matrix, attenuated total reflection Fourier-transform infrared spectrometry was performed over the region 500–4000 cm⁻¹. The FTIR spectra of the three samples of PVA/TiO₂ (faceted, rods, tubes) nanocomposite films and the neat PVA film measured in the reflection mode are shown in Fig. 4. All characteristic bands corresponding to PVA can be observed in 500–4000 cm⁻¹ region of the blank PVA film. The symmetric C–C stretching vibration that is an indication of the presence of crystalline regions in PVA is characterized by a band at 1142 cm⁻¹ in each spectrum shown in Fig. 4.²² The slight decrease in the intensity of this band in the nanocomposite samples compared to the same band in the neat PVA sample confirms a decrease in the crystalline phase of the polymer. The presence of peaks at 1142 and 914 cm⁻¹ in all samples (neat PVA and nanocomposites) reveals the existence of the syndiotactic structure in the polymer chain.^{23,24} Taking into account the intensity ratio I_{sy} of the peaks at 914 and 830 cm⁻¹ for an evaluation of syndiotacticity level of the PVA, according to Abdelaziz *et al.*²⁵ and Tawansi *et al.*,²⁶ a slight decrease was observed only for the PVA/TiO₂ (tubes) nanocomposite sample. According to Naguro *et al.*,²⁷ who found a correlation between the increase in the syndiotacticity of PVA and density level of molecular packing in the polymer crystal, it could be assumed that the molecular packing of the PVA/TiO₂ (tubes) nanocomposite sample was denser, which enables stronger intermolecular hydrogen bonds and lower molecular motions, compared to the other samples with a similar percentage syndiotacticity. A comparison of IR spectra of the PVA matrix and PVA/TiO₂ nanocomposites revealed changes in the band positioned at 1322 cm⁻¹. This can be attributed to a coupling of the

O–H plane vibrations (stronger line at 1417 cm⁻¹) with C–H wagging vibrations. Therefore, the decrease in the intensity ratio of bands at 1417 and 1322 cm⁻¹ independently of the shape of TiO₂ nanoparticles implies the existence of a decoupling process between the mentioned vibrations due to interaction between the titania nanoparticles and the OH groups attached to the methane carbons of PVA.^{28,29}

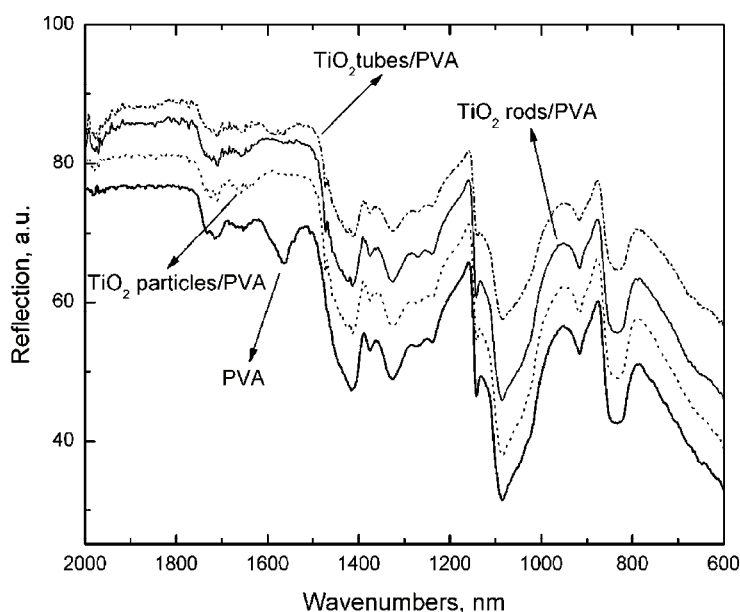


Fig. 4. FTIR Spectra of pure PVA, PVA/TiO₂ faceted particles, PVA/TiO₂ rods and PVA/TiO₂ tubes nanocomposite films.

The most distinct feature in the FTIR spectra of the PVA/TiO₂ nanocomposites was the disappearance of the transmission band at around 1570 cm⁻¹, in the spectra of the PVA/TiO₂ particles nanocomposite and the PVA/TiO₂ rods nanocomposite. A remarkable decrease in the intensity of the same band was also observed in the spectrum of the PVA/TiO₂ tubes nanocomposite. According to Krimm *et al.*, PVA may contain some C=O groups within the chain, assigned to β -diketone groups and, consequently, they suggested that the band of this group appears at 1590 cm⁻¹.³⁰ The decision to assign the shifted band at 1570 cm⁻¹ in neat PVA samples to β -diketone groups, most likely in the enol form, was additionally supported by the presence of band at 1710 cm⁻¹ associated to the stretching vibration of the C=O functionality.³¹ The carbonyl stretching vibration band is verification of the existence of residual vinyl acetate groups in partially hydrolyzed PVA.^{32,33} Taking into account the presence of OH groups on the surface of the titania nanocrystals, the possibility of hydrogen bond formation between

them and the β -diketone groups from the polymer chain could be an explanation for the decrease in intensity and disappearance of the band at 1570 cm^{-1} . The existence of such functionality within PVA chain imparts additional binding locations for TiO_2 nanoparticles.

Thermal properties of PVA/TiO₂ nanocomposites

The influence of the shape, and consequently the different surface areas, of the TiO_2 nanofillers on the thermal properties of the PVA matrix was examined by non-isothermal TGA and DSC. Their content in the nanocomposites was kept constant. The thermal and thermo-oxidative stability of the PVA/ TiO_2 nanocomposites were compared with the thermal and thermo-oxidative stability of neat PVA. The thermogravimetric (TG) and differential thermogravimetric (DTG) curves obtained under an inert atmosphere for the neat PVA and PVA loaded with differently shaped TiO_2 nanofillers are shown in Fig. 5. The temperature differences between the neat PVA and PVA/ TiO_2 nanocomposite samples at 50 % weight loss are listed in Fig. 5a.

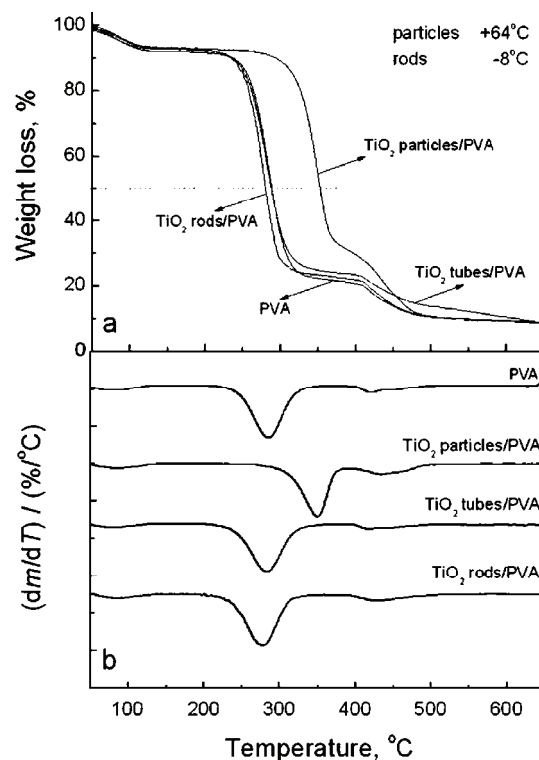


Fig. 5. a) TG and b) DTG curves of pure PVA, PVA/ TiO_2 faceted particles, PVA/ TiO_2 tubes and PVA/ TiO_2 rods nanocomposite samples obtained under an argon atmosphere.

The weight loss that emerges around $100\text{ }^\circ\text{C}$ is a consequence of loss of physically absorbed moisture and/or evaporation of trapped solvent.^{34,35} The

thermal degradation mechanism of the synthesized PVA/TiO₂ nanocomposites and neat PVA in an inert atmosphere mainly consists of two steps initiated by different modes. The first one appears in the range between 250 and 370 °C depending on the shape of particles incorporated into the nanocomposite. The dominant processes during this degradation stage are elimination of OH groups and chain-scission reactions.³⁶ The major decomposition products are polyenes generated from the dehydration reaction of the PVA chains. Using a highly-hydrolyzed PVA for synthesis of nanocomposite materials, Peng *et al.* confirmed the formation of two polyenes structures, conjugated and non-conjugated, during the first degradation process.³⁷ During the second degradation step that occurs between 400 and 480 °C depending on the particle shape, chain-scission and Diels–Alder intramolecular and intermolecular cyclization prevailed.³⁷

The thermal stability of the PVA/TiO₂ nanocomposites and neat PVA was compared at 50 % weight loss. The presence of shaped TiO₂ nanofillers within the polymer matrix did not affect the degradation mechanism itself, but it demonstrated a noticeable influence on the overall thermal stability of the polymer. The presence of faceted TiO₂ nanoparticles in the nanocomposite caused an increase in the thermal stability of the PVA matrix by 64 °C in an argon atmosphere. Generally, according to the barrier model, it was suggested that the improved thermal stability is due to the formation of polymeric–inorganic char on the surface of the polymer melt, which reduces mass and heat transfer.³⁸ It can be assumed that the faceted titania nanoparticles inhibited the degradation of the PVA matrix by decreasing the efficiency of OH group elimination and chain-scission reactions. The possible reason for the suppression of these reactions is the interaction of the faceted TiO₂ nanoparticles with the OH groups from the PVA chain. Such interactions may increase the energy barrier for OH group elimination reactions. An additional reason is the reduced mobility of the polymer chains in the presence of the faceted TiO₂ nanoparticles that induces a decrease of their collision frequency and suppresses chain transfer reactions. This type of physical constraint affects the reactions occurring within the second degradation step. It should be emphasized that the considerable increase of PVA thermal stability under a nitrogen atmosphere was achieved with a very low content of TiO₂ nanoparticles (0.25 mass %) in the nanocomposite. In a previous work, the ability of the same type of titania nanoparticles to increase the thermal stability of polystyrene to similar extent under a nitrogen atmosphere was demonstrated but with higher amount of TiO₂ (2 mass %) in the nanocomposite.³⁹

The addition of titania nanotubes into the polymer matrix did not have any influence on the thermal stability of the PVA under an inert atmosphere. The decomposition temperature of the PVA matrix (Fig. 5a) slightly decreased by ≈8 °C in the presence of the same amount of titania nanorods. Generally, titania nanotubes and nanorods do not exhibit stabilizing effect on a polymer matrix. It is

well known that polymer adsorption onto surfaces is dominated by a balance between the chain conformational entropy and polymer–substrate interactions.⁴⁰ Polymer–substrate interaction favors adsorption in a flat configuration with many contact points and thin layer formation. Titania nanorods and nanotubes separately can be considered as flat surfaces due to their length of a few hundred nanometers and thus, a stabilizing effect on the composite system through the formation of a polymer barrier layer failed. The obtained small decrease in the decomposition temperature of PVA (≈ 8 °C) in the presence of TiO₂ nanorods could be the consequence of increased localized heat conductivity in the nanocomposite sample.

The mechanism of the thermo-oxidative degradation of PVA is more complicated in comparison with that of degradation under an inert atmosphere. Thermo-oxidative degradation process of neat PVA occurs in five stages. The first one appears at around 100 °C and indicates the loss of physically adsorbed water.⁴¹ The partial dehydration of the PVA chains that generates polyene structures occurs in the temperature range between 230 and 300 °C.⁴² As a result of the decomposition of polyenes, macroradicals are formed. The polyene macroradicals form *cis*- and *trans*-derivatives. The later form polyconjugated aromatic structures due to intramolecular cyclization and condensation reactions according to the Diels–Alder mechanism in the temperature range between 300 and 400 °C.⁴² The fourth degradation step occurring between 400 and 480 °C is a consequence of cyclization and condensation processes of the polyaromatic structures. The final degradation step responsible for the destruction of the carbonized residue occurs between 480 and 600 °C.⁴²

The TG and DTG curves of neat PVA and the PVA/TiO₂ nanocomposites obtained under an air atmosphere are shown in Fig. 6.

As in the case under an inert atmosphere, the presence of TiO₂ nanofillers of different shapes in the PVA matrix did not significantly alter the degradation mechanism, but did affect the overall thermal stability. The evidenced noticeable overall increase in the thermal stability of the PVA matrix in the presence of the faceted nanoparticles is the consequence of increased temperatures of the following processes: generation of polyene structures ($\Delta T \approx 44$ °C), formation of polyconjugated aromatic structures ($\Delta T \approx 57$ °C), cyclization and the condensation of polyaromatic structures ($\Delta T \approx 9$ °C) and the destruction of carbonized residues ($\Delta T \approx 8$ °C).

The thermo–oxidative stability of the PVA matrix was more influenced by the presence of titania nanotubes and nanorods than its thermal stability in an inert atmosphere. According to the curves presented in Fig. 6b, it could be concluded that the presence of the nanotubes had inhibitory effects on the cyclization processes and on the condensation of polyaromatic structures ($\Delta T \approx 28$ °C) and destruction of the carbonized residues ($\Delta T \approx 53$ °C). In the sample of PVA/TiO₂

rods nanocomposite, only the final degradation step of the PVA matrix, the destruction of the carbonized residue, was shifted toward higher temperature by ≈ 25 °C compared to that of the neat PVA sample.

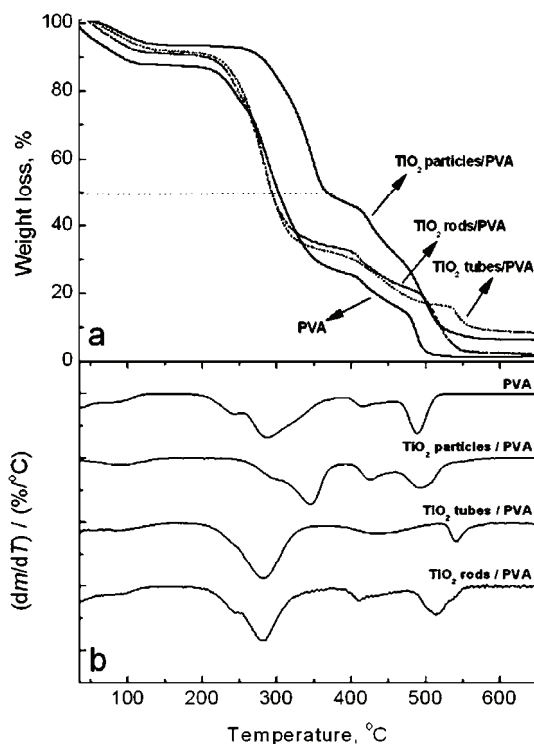


Fig. 6. a) TG and b) DTG curves of pure PVA, PVA/TiO₂ faceted particles, PVA/TiO₂ tubes and PVA/TiO₂ rods nanocomposite samples obtained under an air atmosphere.

Residues at 600 °C under both atmospheres (inert and air) were detected. It could be observed (Figs. 5a and 6a) that the residue in an inert atmosphere was larger than in an air atmosphere. Thomas *et al.* suggested that the large residue in an inert atmosphere could be expected since the pyrolyzation results in the formation of amorphous carbon.⁴³ The residue observed in an air atmosphere is a consequence of the effects of geometry on the degradation process.

PVA is a semi-crystalline polymer with a decomposition temperature close to its melting temperature.⁶ This fact complicates conclusions on the perfection of its crystallinity based on melting temperature measurements.

The DSC curves of the synthesized PVA/TiO₂ nanocomposites and of the corresponding neat PVA obtained during heating are shown in Fig. 7a. Two endothermic peaks in all samples are evident. The broad signals in the temperature range from 60 to 100 °C arose due to vaporization of physically adsorbed water.^{44,45} The peak that appears between 200 and 250 °C in the curves of the samples corresponds to the melting temperature (T_m). It should be stressed that

the melting temperature of the polymer matrix was not affected by the addition of the faceted TiO_2 nanoparticles, indicating a lack of their influence on the heat resistance in an inert atmosphere. The presence of titania nanotubes or titania nanorods in the PVA matrix slightly increased the melting temperature of the polymer by ≈ 2 and ≈ 3 °C, respectively. Such small rises in the melting temperature of the PVA/ TiO_2 tubes and PVA/ TiO_2 rods nanocomposites are likely due to a modification in the diffusion of volatiles in the polymer or simply to a different tortuosity of polymer chains depending on the particle shape.

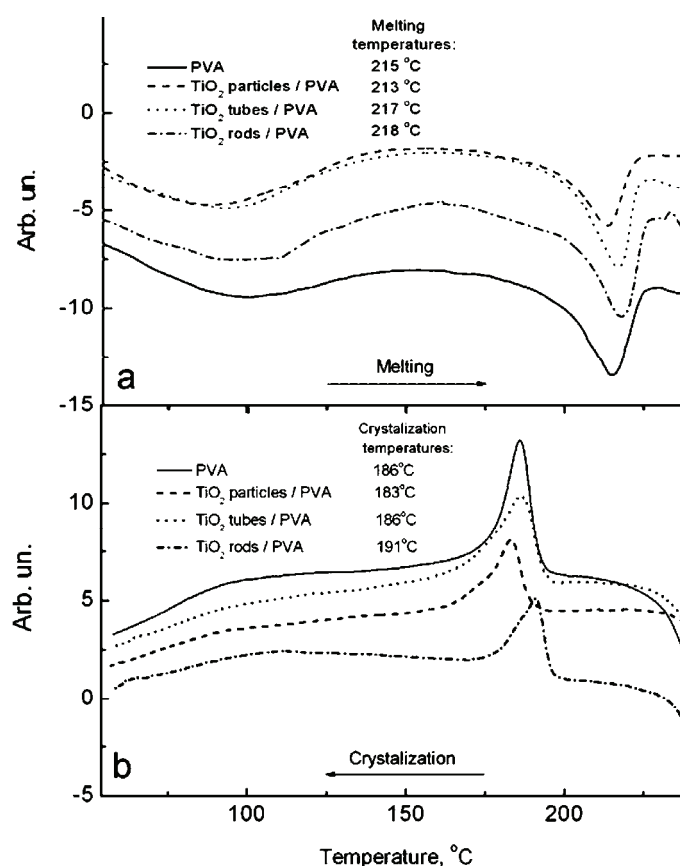


Fig. 7. DSC Curves of pure PVA, PVA/ TiO_2 nanoparticles, PVA/ TiO_2 tubes and PVA/ TiO_2 rods nanocomposite samples obtained under a nitrogen atmosphere in a) heating and b) cooling processes.

The DSC thermograms of the synthesized PVA/ TiO_2 nanocomposites and the neat PVA polymer obtained in cooling process are shown in Fig. 7b. It is clear that the titania nanorods induced the nucleation of the PVA matrix at an earlier stage, *i.e.*, at a higher temperature, during the cooling run, compared to the

neat PVA. The OH groups existing on the particle surface may act as nucleation sites together with the adequate morphology of the nanoparticles.^{6,46}

The geometry of the faceted TiO₂ nanoparticles present in the PVA matrix caused a slight delay of the onset of crystallization and, consequently, decreased the crystallization temperature of the nanocomposite ($T_c = 183$ °C). The presence of titania nanotubes did not affect the crystallization process at all ($T_c = 186$ °C).

The degree of crystallinity (X_c) of PVA in the presence of the shaped TiO₂ nanoparticles was calculated using the following equation:

$$X_c (\%) = 100(\Delta H_c / (1-f)\Delta H_m)$$

where ΔH_m is the enthalpy corresponding to the melting of a 100 % crystalline sample (138.6 J g^{-1}),⁴⁷ ΔH_c is the apparent enthalpy of crystallization corresponding to the nanocomposite sample and f is the weight fraction of TiO₂ nanoparticles in the PVA/TiO₂ nanocomposite.

The incorporation of faceted TiO₂ nanoparticles into the PVA matrix led to a slight decrease in the degree of crystallinity of PVA ($X_c = 32$ %) compared to neat PVA ($X_c = 38$ %) despite the excess of OH groups on the particles surface that may act as nucleation sites. The decrease in crystallinity, as well as the delay of the onset of crystallization, is likely caused by a reduction of the PVA chain mobility and by possible hydrogen bonding formation between the surface OH groups of the faceted TiO₂ nanoparticles and the PVA chain. According to DSC measurements, titania nanorods and nanotubes did not affect the degree of crystallinity of PVA in PVA/TiO₂ rods ($X_c = 39$ %) and PVA/TiO₂ tubes ($X_c = 38$ %) nanocomposites.

In general, the first step of any crystallization process is nucleation. When the critical size is attained, these nuclei become the centers for the growth of polymer crystalline phase. The overall crystallization rate is attributed to the contribution of both nucleation and growth rates. The rate of nucleation is higher as the temperature drops. The determining factor is the degree of supercooling $T_m - T_c$, which presents the difference between the melting point T_m and the temperature of crystallization T_c (crystallization at temperatures T_c below the melting point T_m).⁴⁸ The rate of crystal growth is mainly determined by the mobility of the polymer chains in the melt. Therefore, according to Ou *et al.*⁴⁹ and Krijgsman *et al.*,⁵⁰ the degree of supercooling is an indication of polymer crystallizability during a non-isothermal process. In other words the smaller the difference, ($T_m - T_c$), the higher the overall crystallization rate.

Analyzing the $T_m - T_c$ values for all the investigated samples, it could be noticed that incorporation of the shaped TiO₂ nanofillers into the PVA matrix did not significantly change the overall crystallization rate of the polymer. Such conclusion is based on the small differences in the degree of supercooling between the neat PVA ($T_m - T_c = 29$ °C) and PVA/TiO₂ particles ($T_m - T_c = 30$ °C), PVA/

/TiO₂ tubes ($T_m - T_c = 31$ °C) and PVA/TiO₂ rods ($T_m - T_c = 27$ °C) nanocomposites. According to obtained values of the T_c/T_m ratio, in the range from 0.86 to 0.88 for all samples, and the Mandelkern rule, the rates of crystallization processes in the PVA-based nanocomposites are relatively high.⁵¹

CONCLUSIONS

Three PVA/TiO₂ nanocomposite samples were synthesized by direct blending of PVA and differently shaped TiO₂ nanofillers (faceted nanoparticles, nanotubes or nanorods) as precursors. The interaction between PVA polymer chains and the surface of the titania nanofillers was confirmed by FTIR spectroscopy in the reflection mode. It was found that the same amount of TiO₂ nanofillers independent of the shape did not change the degradation mechanism of PVA in argon and air atmospheres. The faceted nanoparticles ($d \approx 5$ nm) increased the thermal stability of the PVA matrix by 64 °C under an inert atmosphere. The presence of TiO₂ nanotubes ($d = 10$ nm, $L < 200$ nm) and titania nanorods ($d \approx 50$ nm, $300 < L < 700$ nm) did not exhibit a stabilizing effect on the thermal properties of the polymer matrix under an argon atmosphere. The temperature of the thermo-oxidative degradation of PVA increased with addition of faceted TiO₂ nanoparticles. The presence of titania nanotubes had inhibitory effect only on the cyclization reactions and the condensation of the polyaromatic structure and destruction of the carbonized residues, which appeared at higher temperatures during the thermo-oxidative degradation of the PVA matrix. In the course of cooling, titania nanorods induced crystallization of PVA at a higher temperature. The degree of crystallinity of the polymer matrix in the presence of faceted TiO₂ nanoparticles decreased ($X_c = 32$ %) compared with the degree of crystallinity of the neat PVA ($X_c = 38$ %).

Acknowledgements. Financial support for this study was granted by the Ministry of Education and Science of the Republic of Serbia under Projects 172056 and 45020.

ИЗВОД

УТИЦАЈ ОБЛИКА ТИТАН-ДИОКСИДНИХ НАНОПУНИЛАЦА НА ТЕРМАЛНЕ КАРАКТЕРИСТИКЕ ПОЛИВИНИЛ-АЛКОХОЛА

МАРИЈА Б. РАДОИЧИЋ¹, ЗОРАН В. ШАПОЊИЋ¹, МИЛЕНА Т. МАРИНОВИЋ-ЦИНЦОВИЋ¹,
SCOTT P. АНРЕНКИЕЛ², НАТАША М. БИБИЋ¹ и ЈОВАН М. НЕДЕЉКОВИЋ¹

¹Институт за нуклеарне науке Винча, б. бр. 522, 11001 Београд и ²South Dakota School of
Mines and Technology, Rapid City, SD, USA

Наноконтрополи на бази поливинил-алкохола (PVA) и TiO₂ нанокристала различитих облика и величина (наночестице, нанотубе и наносапићи) синтетисани су методом директног мешања раствореног полимера (1,5 мас. %) и колоидних раствора/прахова нанокристала TiO₂ (0,25 мас. %). У циљу испитивања утицаја облика титан-диоксидних нанокристала на њихову интеракцију са PVA ланцима и термалну стабилност полимерне матрице, урађена је структурна и термална карактеризација PVA/TiO₂ наноконтрополи. Уочено је да иста коли-

чина TiO₂ нанокристала, независно od њиховог облика, не утиче на механизам деградације PVA како на ваздуху тако ни у атмосфери аргона. Наночестице TiO₂ ($d \approx 5$ nm) повећавају термалну стабилност PVA матрице за 64 °C, док титан-диоксидне нанотубе ($d = 10$ nm, $L < 200$ nm) и наноштапићи ($d \approx 50$ nm, $300 < L < 700$ nm) не показују стабилизациони утицај на полимерну матрицу у атмосфери аргона. Термо-оксидативна стабилност PVA расте са додатком TiO₂ наночестица. Приликом хлађења PVA/TiO₂ нанокомпозита, TiO₂ наноштапићи индукују кристализацију PVA на вишим температурама. Степен кристаличности PVA матрице је благо умањен у присуству наночестица TiO₂ у нанокомпозитном узорку ($X_c = 32$ %) у поређењу са степеном кристаличности чистог PVA ($X_c = 38$ %).

(Примљено 31. марта, ревидирано 29. јуна 2011)

REFERENCES

1. W. Caseri, *Macromol. Rapid Commun.* **21** (2000) 705
2. D. Y. Godovsky, *Adv. Polym. Sci.* **153** (2000) 163
3. E. Džunuzović, M. Marinović-Cincović, K. Jeremić, J. Vuković, J. Nedeljković, *Polym. Degrad. Stab.* **93** (2008) 77
4. J. Zheng, R. Ozisik, R. W. Siegel, *Polymer* **46** (2005) 10873
5. J. K. Pandey, K. R. Reddy, A. P. Kumar, R. P. Singh, *Polym. Degrad. Stab.* **88** (2005) 234
6. Z. Peng, D. Chen, *J. Polym. Sci., B* **44** (2006) 534
7. K. Yamamura, N. Kuranuki, M. Suzuki, T. Tanigami, S. Matsuzawa, *J. Appl. Polym. Sci.* **41** (1990) 2409
8. Y. Li, K. G. Neoh, E. T. Kan, *Polymer* **45** (2004) 8779
9. J. Kuljanin, M. I. Čomor, V. Djoković, J. M. Nedeljković, *Mater. Chem. Phys.* **95** (2006) 67
10. L. Liu, Z. Qi, X. Zhu, *J. Appl. Polym. Sci.* **71** (1999) 1133
11. J. Kuljanin-Jakovljević, Z. Stojanović, J. M. Nedeljković, *J. Mater. Sci.* **41** (2006) 5014
12. H. Gerischer, A. Heller, *J. Phys. Chem.* **95** (1991) 5261
13. G. J. Meyer, *J. Chem. Edu.* **74** (1997) 652
14. L. X. Chen, T. Rajh, Z. Wang, M. C. Thurnauer, *J. Phys. Chem., B* **101** (1997) 10688
15. T. Rajh, A. E. Ostafin, O. I. Mičić, D. M. Tiede, M. C. Thurnauer, *J. Phys. Chem.* **100** (1996) 4538
16. R. C. Thompson, *Inorg. Chem.* **23** (1984) 1794
17. T. Kasuga, M. Hiramatsu, A. Hoson, T. Sekino, K. Niihara, *Adv. Mater.* **11** (1999) 1307
18. N. M. Dimitrijević, Z. Šaponjić, B. M. Rabatic, O. G. Poluektov, T. Rajh, *J. Phys. Chem., C* **111** (2007) 14597
19. Z. Šaponjić, N. Dimitrijević, D. Tiede, A. Goshe, X. Zuo, L. Chen, A. Barnard, P. Zapol, L. Curtiss, T. Rajh, *Adv. Mater.* **17** (2005) 966
20. B. Rabatic, N. Dimitrijević, R. Cook, Z. Šaponjić, T. Rajh, *Adv. Mater.* **18** (2006) 1033
21. D. Šajinović, Z. Šaponjić, N. Cvjetičanin, M. Marinović-Cincović, J. Nedeljković, *Chem. Phys. Lett.* **329** (2000) 168
22. S. K. Mallapragada, N. A. Peppas, *J. Polym. Sci., B* **34** (1996) 1339
23. S. Rajendran, M. Sivakumar, R. Subadevi, *Mater. Lett.* **58** (2004) 641
24. S. Murahashi, H. Yūcki, T. Sano, U. Yonemura, H. Tadokoro, Y. Chatani, *J. Polym. Sci.* **62** (1962) 77
25. M. Abdelaziz, *J. Appl. Polym. Sci.* **94** (2004) 2178

26. A. Tawansi, H. M. Zidan, A. H. Oraby, M. E. Dorgham, *J. Phys., D* **31** (1998) 3428
27. M. Nagura, S. Matsuzawa, K. Yamaura, H. Ishikawa, *Polym. J.* **14** (1982) 69
28. Z. H. Mbhele, M. G. Salemane, C. G. van Sittert, J. M. Nedeljković, V. Djoković, A. S. Luyt, *Chem. Mater.* **15** (2003) 5019
29. B. Karthikeyan, *Physica B* **364** (2005) 328
30. S. Krimm, C. Y. Liang, G. B. B. M. Sutherland, *J. Polym. Sci.* **22** (1956) 227
31. G. Socrates, *Infrared and Raman characteristic group frequencies: Tables and Charts*, Wiley, New York, 2001 p. 115
32. S. M. Rabie, N. Abdel-Hakeem, M. A. Moharram, *J. Appl. Polym. Sci.* **38** (1989) 2269
33. P. Alexy, D. Kachova, M. Krsiak, D. Bakos, B. Simkova, *Polym. Degrad. Stab.* **78** (2002) 413
34. C. C. Yang, S. J. Chiu, K. T. Lee, W. C. Chien, C. T. Lin, C. A. Huang, *J. Power Sources* **184** (2008) 44
35. D. Lopez, I. Cendoya, F. Torres, J. Tejada, C. Mijangos, *J. Appl. Polym. Sci.* **82** (2001) 3215
36. J. W. Gilman, D. L. Vander Hart, T. Kashiwagi, *ACS Symp. Ser.* **599** (1994) 161
37. Z. Peng, L. X. Kong, *Polym. Degrad. Stab.* **92** (2007) 1061
38. A. N. Krklješ, M. T. Marinović-Cincović, Z. M. Kačarević-Popović, J. M. Nedeljković, *Thermochim. Acta* **460** (2007) 28
39. E. Džunuzović, V. Vodnik, K. Jeremić, J. M. Nedeljković, *Mater. Lett.* **63** (2009) 908
40. E. Tadd, A. Zeno, M. Zubris, N. Dan, R. Tannenbaum, *Macromolecules* **36** (2003) 6497
41. P. Budrugaec, *J. Therm. Anal. Cal.* **92** (2008) 291
42. A. Y. Shaulov, S. M. Lomakin, T. S. Zarkhina, A. D. Rakhimkulov, N. G. Shilkina, Y. B. Muravlev, A. A. Berlin, *Dokl. Phys. Chem.* **403** (2005) 154
43. P. S. Thomas, J. P. Guerbois, G. F. Russell, B. J. Briscoe, *J. Therm. Anal. Cal.* **64** (2001) 501
44. Q. Wu, J. Zhang, S. Sang, *J. Phys. Chem. Solids* **69** (2008) 2691
45. A. N. Krklješ, M. Marinović-Cincović, Z. Kačarević-Popović, J. M. Nedeljković, *Eur. Polym. J.* **43** (2007) 2171
46. W. B. Xu, P. S. He, *Polym. Eng. Sci.* **41** (2001) 1903
47. Z. Peng, L. X. Kong, S. D. Li, *Polymer* **46** (2005) 1949
48. A. Ram, *Fundamentals of polymer engineering*, Plenum Press, New York, 1997, p. 51
49. C. F. Ou, M. T. Ho, J. R. Lin, *J. Polym. Res.* **10** (2003) 127
50. J. Krijgsman, G. J. E. Biemond, R. J. Gaymans, *J. Appl. Polym. Sci.* **103** (2007) 512
51. M. M. Feldstein, G. A. Shandryuk, S. A. Kuptsov, N. A. Plate, *Polymer* **41** (2000) 5327.



J. Serb. Chem. Soc. 77 (5) 715 (2012)

Errata (printed version only)

Issue No. 4 (2012), Vol. 77, paper No. *JSCS-4280*:

– page 423, line 2 from above should read:

...activity and phenolic content of *Dodonaea viscosa* Jacq.

– back cover, line 12 from above should read:

...content of *Dodonaea viscosa* Jacq.